2016

ENHANCING THE STRENGTH PROPERTIES OF FLY ASH BY ADDING WASTE PRODUCTS

Alfred J. Susilo
University of Kentucky, alfredsusilo@aol.com
Digital Object Identifier: http://dx.doi.org/10.13023/ETD.2016.388

Recommended Citation

STUDENT AGREEMENT:

I represent that my thesis or dissertation and abstract are my original work. Proper attribution has been given to all outside sources. I understand that I am solely responsible for obtaining any needed copyright permissions. I have obtained needed written permission statement(s) from the owner(s) of each third-party copyrighted matter to be included in my work, allowing electronic distribution (if such use is not permitted by the fair use doctrine) which will be submitted to UKnowledge as Additional File.

I hereby grant to The University of Kentucky and its agents the irrevocable, non-exclusive, and royalty-free license to archive and make accessible my work in whole or in part in all forms of media, now or hereafter known. I agree that the document mentioned above may be made available immediately for worldwide access unless an embargo applies.

I retain all other ownership rights to the copyright of my work. I also retain the right to use in future works (such as articles or books) all or part of my work. I understand that I am free to register the copyright to my work.

REVIEW, APPROVAL AND ACCEPTANCE

The document mentioned above has been reviewed and accepted by the student's advisor, on behalf of the advisory committee, and by the Director of Graduate Studies (DGS), on behalf of the program; we verify that this is the final, approved version of the student's thesis including all changes required by the advisory committee. The undersigned agree to abide by the statements above.

Alfred J. Susilo, Student

Dr.. Michael E. Kalinski, Major Professor

Dr. Yi-Tin Wang, Director of Graduate Studies

ENHANCING THE STRENGTH PROPERTIES OF FLY ASH BY ADDING
WASTE PRODUCTS

_____

DISSERTATION

_____

A dissertation submitted in partial fulfillment of the
requirements for the degree of Doctor of Philosophy in the
College of Engineering at the University of Kentucky

By

Alfred Jonathan Susilo
Lexington, Kentucky

Director: Dr. Michael E. Kalinski, Ph.D., P.E, Professor of Civil Engineering

Lexington, Kentucky

2016

ABSTRACT OF DISSERTATION

ENHANCING THE STRENGTH PROPERTIES OF FLY ASH BY ADDING WASTE PRODUCTS

For this study, the main material to be investigated is Class F fly ash that originates from the combustion of Appalachian coal. Alone, fly ash exhibits poor strength properties and is susceptible to liquefaction when subject to dynamic loading. This research is focused on investigating the effect of adding materials that would otherwise be considered as waste products to the fly ash. Materials to be considered include crumb rubber, shredded carpet and shredded paper. The benefits from this research are twofold. First, provide a method to stabilize fly ash. For large masses of fly ash such as those found at power plants and landfills, improved strength of the fly ash will make the mass safer and more reliable with respect to stability. Second, provide a use for waste materials that would otherwise be stockpiled or disposed of in landfills at a significant cost, which in turn will minimize the environmental impact. Using this approach, materials will be added to fly ash rather than using fly ash as an additive, which will increase the rate of fly ash usage and more directly address the issue the large volumes of fly ash that are being produced today.

To perform this research, representative samples of Class F fly ash were tested to characterize the physical properties of the materials. Later, this Class F fly ash was mixed with specific percentage of three waste materials to evaluate the behavior and performance of the fly ash admixture. Using these reconstituted specimens, a suite of laboratory tests to assess the static and cyclic strength properties of each specimen was performed, as well as the dynamic properties of the specimens. The expectations were to develop correlations between mixture ratios and the various measured properties, and to identify mixture ratios that will optimize the strength characteristics of the specimens.

In the end, crumb rubber was found to be the best additive to improve the properties of Class F fly ash compared to the other waste materials used. This conclusion can be used by power plant facilities to increase the safety factor against liquefaction at their impoundment facilities.

Alfred J. Susilo

July 12, 2016

ENHANCING THE STRENGTH PROPERTIES OF FLY ASH BY ADDING WASTE
PRODUCTS

By

Alfred Jonathan Susilo

<u>Dr. Michael E. Kalinski</u>

Director of Dissertation

<u>Dr. Yi-Tin Wang</u>

Director of Graduate Studies

July 21, 2016

To my parents

ACKNOWLEDGEMENTS

I would like to thank Dr. Michael E. Kalinski for his willingness of becoming my advisor, believing in me, orientating me to such an interesting research topic and also for his time, guidance, support, relentless effort and patience during my research. He is a very good advisor and I wish I could spend more time with him during my Ph.D. research.

I would like to express my gratitude for my committee members; L. Sebastian Bryson, Ph.D., P.E., Kyle A. Perry, Ph.D., Gabriel B. Dadi, Ph.D., P.E., LEED AP and John Silva-Castro, Ph.D. for their support, guidance, time, efforts and valuable information for this dissertation. I would also like to thank Braden Lusk, Ph.D. for agreeing to serve as external reviewer for my research.

I would like to extend my thanks to all the professors, staffs, and fellow graduate students in University of Kentucky for their support, assistance and mostly for their friendship. They help create a very welcoming and comfortable situation during my stay in Lexington, Kentucky.

I would like to express my appreciation to all personal in Geotechnical Consulting and Testing Systems LLC (GCTS) for their support, time and relentless effort during my research.

Finally, I want to thank my family especially my parents for their support, encouragement, and patience during my study which contributes to the completion of this dissertation.

TABLE OF CONTENTS

LIST OF TABLES

LIST OF FIGURES

Chapter 1

INTRODUCTION

1.1   Research Background

During the 2000s, the United States experienced a rapid increase in the amount of fly ash produced from coal power plants as well as the number of fly ash storage ponds and impoundment facilities. When coal is burned, roughly 10% of the coal remains as ash. Coal ash is comprised of several types of ash including fly ash, bottom ash, and boiler slag.

Bottom ash and fly ash are produced at rates of 12-20% by weight of the original coal (Chen et al., 1991) when coal is burned to produce steam for electricity generation. Bottom ash unlike fly ash, is the ash remaining in the bottom of a coal-fired boiler after combustion, while the flue gas carries fly ash as residue of the burnt coal, which is collected using electrostatic precipitators (ESP). This residue, called fly ash, is generally considered to be an industrial waste. Bottom ash is too heavy to rise so it settles at the bottom of the boiler as a relatively coarse, gritty material in contrast to fly ash which consists of very fine particles.

In 2008, the American Coal Ash Association (ACAA) estimated that 136 million tons of coal combustion products (CCP) were produced in the United States, with fly ash comprising 72 million tons. In contrast, only 64 million tons of fly ash were produced in 2004 (American Coal Ash Association, 2012).

Right et al. (1998) reported that only 20% of the ash by-products are recycled while 80% are landfilled at the power plant site. The total cost of managing coal combustion waste ranged from $2.20 to $34.14 per metric ton in 1988 (U.S. Environmental Protection Agency, 1988) and this cost will continue to rise in the future.

In the Commonwealth of Kentucky, which was the third highest coal producer in the United States during 2011 (Figure 1.1.), coal mining was by far the largest source of energy production which contributed to the economy, trade, and investments of Kentucky. In the same year, coal production in the United States increased to 1.09 billion tons and the state of Kentucky contributed to 10% of the production (Table 1.1). This increase was accompanied by an increase in the number of disposal facilities.

With the increase of ash production, the biggest challenge for disposal ponds is to provide sufficient capacity and maintain overall stability. To accommodate the problem, many options are available, including:

1. Construction of new facilities, which pose a significant cost;

2. Expansion of existing facilities, which require stabilization of larger masses of fly ash;

3. Construction of containment spill berms, which may pose a significant cost; and

4. Installation of treatment facilities and application of dry placement methods, which may be expensive but allow fly ash to be placed in larger embankments.

Although action was issued by the United States Mine Safety and Health Administration (MSHA) and the Kentucky Office of Mine Safety and Licensing (KOMSL) to provide safety and health standard regulation for coal mining wastes, these regulations do not explicitly provide guidance for treating, handling and storage of coal combustion byproducts such as fly ash.
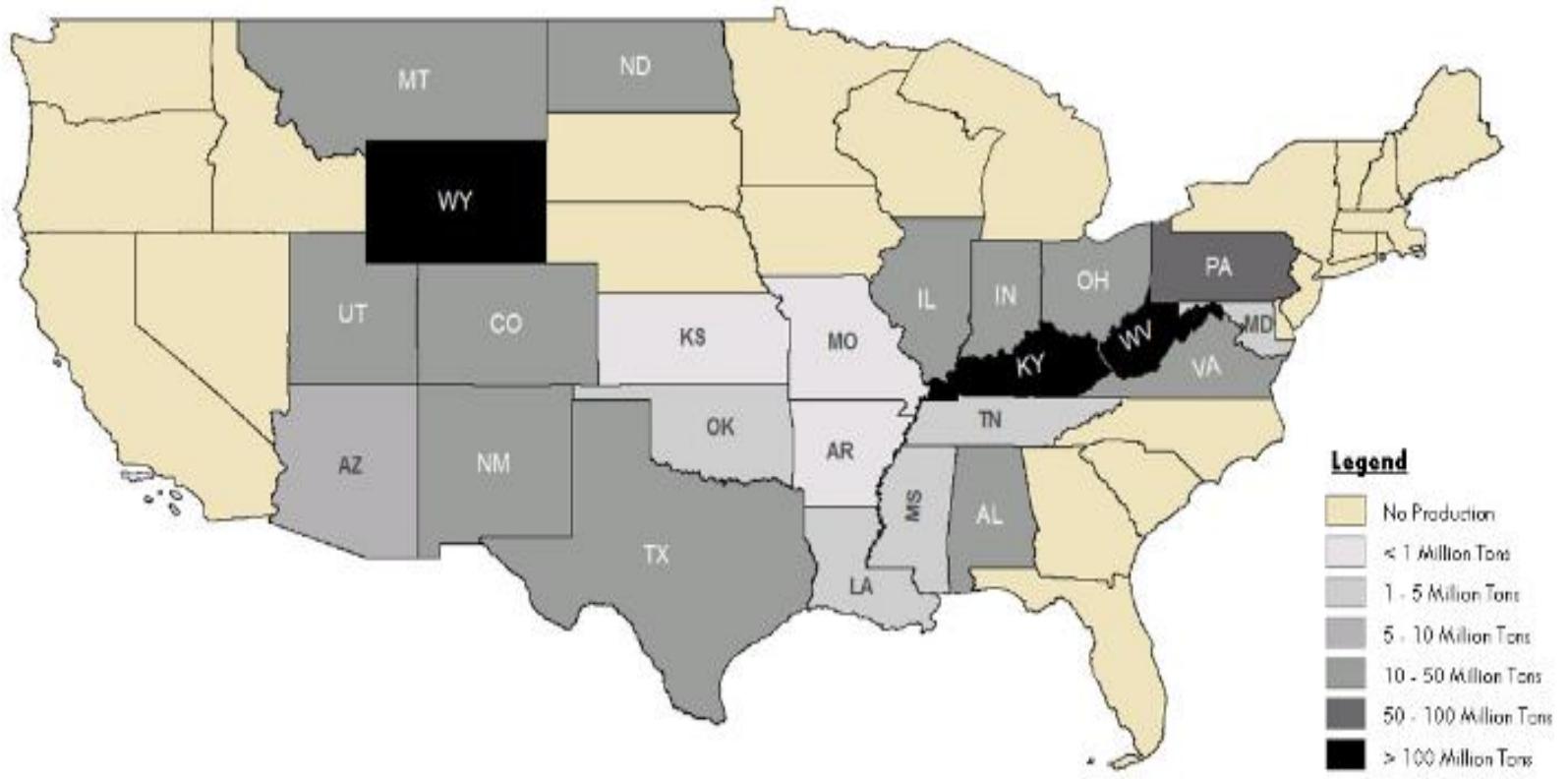
Figure 1.1: U.S. Coal Production, 2011 (Kentucky Energy and Environmental Cabinet, 2012)

Legend
- No Production
- < 1 Million Tons
- 1 - 5 Million Tons
- 5 - 10 Million Tons
- 10 - 50 Million Tons
- 50 - 100 Million Tons
- > 100 Million Tons

Table 1.1: U.S. Coal Production by state, 2011 (Kentucky Energy and Environmental Cabinet, 2012)

U.S. Coal Production by State, 2011			
State	Thousand Tons	Percentage	Region
Wyoming	438,205	41%	Western
West Virginia	138,030	13%	Appalachian
Kentucky	106,285	10%	Int. & App.
Pennsylvania	55,643	5%	Appalachian
Texas	45,904	4%	Interior
Montana	41,600	4%	Western
Indiana	38,193	4%	Interior
Illinois	37,608	4%	Interior
North Dakota	28,214	3%	Western
Ohio	28,118	3%	Appalachian
Colorado	26,890	2%	Western
Virginia	22,638	2%	Appalachian
New Mexico	21,922	2%	Western
Utah	19,648	2%	Western
Alabama	19,349	2%	Appalachian
Arizona	8,111	<1%	Western
Louisiana	3,865	<1%	Interior
Maryland	2,919	<1%	Appalachian
Mississippi	2,748	<1%	Interior
Alaska	2,149	<1%	Western
Tennessee	1,392	<1%	Appalachian
Oklahoma	1,145	<1%	Interior
Missouri	465	<1%	Interior
Arkansas	133	<1%	Interior
Kansas	37	<1%	Interior

Approximately 71.1 million tons of CCP were produced at coal power plants in the United States in 2005 (American Coal Ash Association, 2008). This number has steadily increased and 136 million tons were produced in 2008 by 460 power plants. Approximately 43% of fly ash produced was reused and the remaining fly ash was landfilled at a significant cost (American Coal Ash Association, 2008) as described in Chapter 5. Ash from coal combustion is the second largest stream of industrial waste in the United States at approximately 130 million tons produced per year (Southern Alliance for Clean Energy, 2013), but is less strictly controlled than municipal solid waste.

Fly ash disposal has historically been performed using one of two methods. In the first method, fly ash is hydraulically conveyed as slurry and deposited in ash ponds where it is allowed to settle (Figure 1.2). In the second method, fly ash is conditioned and then placed in a landfill (Figure 1.3). These methods are typically referred to as the wet disposal and dry disposal methods, respectively.

The most common method being used is wet disposal, which has advantages and disadvantages. The wet disposal method is cheaper, faster, and minimizes dust production, but the fly ash is not processed or screened and may be an environmental hazard due to leachate with dangerous chemical (arsenic, lead, mercury etc.). In the United States, there are at least 629 wet disposal storage ponds and 311 dry disposal landfills at power stations (Gottlieb et al., 2010). Storage ponds or impoundment

(Figure 1.4) volumes typically range from 10-8000 acre-ft., while ash landfills (Figure 1.5)

range from 20,000-100,000 acre-ft.

Figure 1.2: Wet disposal method

Figure 1.3: Dry disposal method

Figure 1.4: Wet disposal storage pond in Ohio Power Plant

Figure 1.5: Dry disposal storage in a coal ash landfill

The generation of soaring volumes of coal combustion products combined with rising environmental restrictions and increasing landfilling costs have become major concerns for utilities. Garlisch (2010) stated that fly ash is the ash that rises up and is trapped by the stack filters. About 74% of the ash generated is fly ash. Pollution from fly ash dumps significantly increases both cancer and noncancerous health risks and degrades water quality in groundwater supplies. The United States derives over half its electricity from coal fired power plants. There are up to 1,300 impoundments nationwide including wet ash ponds and dry landfill at power stations, offsite dry landfills and inactive dumps. Some states have recently started requiring liners for new impoundments scheduled to be built, while stack filtration devices such as scrubbers reduce fly ash emissions by around 95%, thus leaving about 5% of the fly ash produced to be released into the atmosphere.

With time, many existing dry disposal landfills will be closed. These closed landfills, if abandoned without any treatment, or if a fly ash fill is emplaced in low lying or swampy terrain, will generate leachate. The leachate may flow downward into the ground water and impact water quality if the leachate is not properly managed. Ghosh & Subbarao (1998) presented the concentrations of metals in leachate samples from fly ash landfills analyzed by an atomic absorption spectrophotometer for the metals, Cd, Cr, Cu, Fe, Mg, Ni, Pb, and Zn. The lowest of the permissible limits for primary drinking water quality standards for the World Health Organization (WHO, 1984) and U.S EPA

(1988) and for the guidelines for Canadian Drinking Water Quality (Health Canada, 1979), considered as the allowable limits, were often exceeded.

Furthermore, leachate generated by Class F fly ash (the type found in Kentucky) also can caused problems. Since Class F fly ash has a lower lime content compared to Class C fly ash, it also has a higher hydraulic conductivity compare to Class C, so leachate can flow more freely through Class F fly ash. The typical hydraulic conductivity for Class F fly ash is around 1.0×10^{-5} cm/s.

Leachate can be minimized by using covers, liners and leachate collection and removal systems. To illustrate how leachate can endanger wildlife, there was one catastrophic event that happened at Belews Lake in North Carolina, which killed 19 of the 22 species of fish in the lake and remains a problem over a decade later (Lemly, 2001).

Fly ash ponds are used to store ash generated from coal combustion at power plants. To dispose of the ash, a power plant usually constructs their own fly ash ponds. Each pond has a suitable capacity and site limitations. To monitor the condition of each pond, the Federal National Pollutant Discharge Elimination System (NPDES) regulates and permits guidelines that each facility should follow, and yearly inspection is used to assure the stability of fly ash ponds and minimize loss of property and casualties from pond failure.

After the Kingston Tennessee fly ash spill in 2008 (Environmental Protection Agency, 2009), the U.S. Environmental Protection Agency (EPA) was forced to release information regarding impoundments with high hazard ratings to avoid similar disasters. In 2009, the EPA published a list of 26 facilities with a total of 44 coal fired power plant waste sites that were identified with a high hazard rating. The rating applies at which a dam failure would most likely cause loss of human life, but does not include an assessment of the likelihood of such an event. A revised listing of High Hazard Potential Units based on the Assessment effort is presented in the Table 1.2 and Figure 1.6 . This information is current as of July 2014 (Environmental Protection Agency, 2009).

Figure 1.6: Location of 26 facilities with a total of 44-coal-fired power plant waste sites, or coal ash ponds, identified with a high-hazard rating by the EPA (U.S. Environmental Protection Agency, 2009)

Table 1.2: Location of 26 facilities with a total of 44-coal-fired power plant waste sites, or coal ash ponds, identified with a high-hazard rating by the EPA (U.S. Environmental Protection Agency, 2009).

List of High Hazard Potential Units

Company	Facility Name	Unit Name	Location/State Contact	Original Hazard Potential Rating (As Reported in Responses to EPA's Information Request)	Current Hazard Potential Rating (Based on EPA's CCR Dam Assessment Effort)	Assessment Round
Alabama Power Co	Ernest C. Gaston Electric Generating Plant	Ash Pond Dam	Wilsonville, AL	NONE	HIGH	5
Allegheny Energy	Pleasants Power Station	McElroy's Run Embankment	Willow Island, WV	HIGH	HIGH	3
American Electric Power	Big Sandy	Fly Ash	Louisa, KY	HIGH	HIGH	3
American Electric Power	Cardinal	Fly Ash Reservoir 2	Brilliant, OH	HIGH	HIGH	2
American Electric Power	General James M Gavin	Fly Ash Pond	Cheshire, OH	HIGH	HIGH	1
American Electric Power	General James M Gavin	Bottom Ash Pond	Cheshire, OH	HIGH	HIGH	1
American Electric Power	John E Amos	Fly Ash Pond	St. Albans, WV	HIGH	HIGH	2
American Electric Power	Mitchell	Fly Ash Pond	Moundsville, WV	HIGH	HIGH	2
American Electric Power	Muskingum River	Unit 5 Bottom Ash Pond (Lower Fly Ash Pond)	Waterford, OH	HIGH	HIGH	3
American Electric Power	Muskingum River	Upper Fly Ash Pond	Waterford, OH	HIGH	HIGH	3
American Electric Power	Muskingum River	Middle Fly Ash Pond	Waterford, OH	HIGH	HIGH	3
American Electric Power	Philip Sporn	Fly Ash Pond	New Haven, WV	HIGH	SIGNIFICANT	2
American Electric Power	Tanners Creek	Fly Ash Pond	Lawrenceburg, IN	HIGH	SIGNIFICANT	2
Arizona Electric Power Cooperative Inc	Apache Station Combustion Waste Disposal Facility	Ash Pond 4	Cochise, AZ	HIGH	HIGH	2
Arizona Electric Power Cooperative Inc	Apache Station Combustion Waste Disposal Facility	Ash Pond 1	Cochise, AZ	HIGH	HIGH	2
Arizona Electric Power Cooperative Inc	Apache Station Combustion Waste Disposal Facility	Ash Pond 3	Cochise, AZ	HIGH	HIGH	2
Arizona Electric Power Cooperative Inc	Apache Station Combustion Waste Disposal Facility	Scrubber Pond 2	Cochise, AZ	HIGH	HIGH	2
Arizona Electric Power Cooperative Inc	Apache Station Combustion Waste Disposal Facility	Scrubber Pond 1	Cochise, AZ	HIGH	HIGH	2
Arizona Electric Power Cooperative Inc	Apache Station Combustion Waste Disposal Facility	Evaporation 1	Cochise, AZ	HIGH	HIGH	2
Arizona Electric Power Cooperative Inc	Apache Station Combustion Waste Disposal Facility	Ash Pond 2	Cochise, AZ	HIGH	HIGH	2

Company	Facility Name	Unit Name	Location/State Contact	Original Hazard Potential Rating (As Reported in Responses to EPA's Information Request)	Current Hazard Potential Rating (Based on EPA's CCR Dam Assessment Effort)	Assessment Round
Arizona Public Service Company	Cholla	Bottom Ash Pond	Joseph City, AZ	HIGH	HIGH	2
Arizona Public Service Company	Cholla	Fly Ash Pond	Joseph City, AZ	HIGH	HIGH	2
City of Columbia	Columbia	Ash Settling Pond	Columbia, MO	N/A	HIGH	12
City of Sikeston	Sikeston Power Station	Bottom Ash Pond	Sikeston, MO	NONE	HIGH	4
Dayton Power & Light Co	Killen Station	Bottom Ash Pond	Manchester, OH	LOW, CLASS I	HIGH	10
Dayton Power & Light Co	Killen Station	Fly Ash Pond	Manchester, OH	LOW, CLASS I	HIGH	10
Duke Energy Corp	Allen Steam Plant	Active Ash Pond	Belmont, NC	HIGH	SIGNIFICANT	1
Duke Energy Corp	Belews Creek Steam Station	Active Ash Pond	Walnut Cove, NC	HIGH	HIGH	2
Duke Energy Corp	Buck	New Primary Pond	Spencer, NC	HIGH	SIGNIFICANT	1
Duke Energy Corp	Buck	Secondary Pond	Spencer, NC	HIGH	SIGNIFICANT	1
Duke Energy Corp	Buck	Primary Pond	Spencer, NC	HIGH	SIGNIFICANT	1
Duke Energy Corp	Dan River	Secondary Pond	Eden, NC	HIGH	SIGNIFICANT	1
Duke Energy Corp	Dan River	Primary Pond	Eden, NC	HIGH	SIGNIFICANT	1
Duke Energy Corp	Marshall Steam Station	Active Ash Pond	Terrell, NC	HIGH	SIGNIFICANT	1
Duke Energy Corp	Riverbend	Secondary Pond	Mount Holly, NC	HIGH	SIGNIFICANT	1
Duke Energy Corp	Riverbend	Primary Pond	Mount Holly, NC	HIGH	HIGH	1
Dynegy Midwest Generation Inc	Havana	East Ash Pond	Havana, IL	HIGH	HIGH	1
Dynegy Midwest Generation Inc	Wood River	East Ash Pond (2 cells)	Alton, IL	HIGH	HIGH	1
First Energy Generation Corp	Bruce Mansfield	Little Blue Run Dam	Shippingport, PA	HIGH	HIGH	1
Georgia Power	Plant Branch	E	Milledgeville, GA	HIGH	HIGH	3
Georgia Power	Plant McDonough	Ash Pond 4	Symra, GA	HIGH	HIGH	3
Indianapolis Power & Light Co	Eagle Valley Generating Station	D Pond	Martinsville, IN	NONE	HIGH	4
Indianapolis Power & Light Co	Harding Street Power Station	Pond 2	Indianapolis, IN	NONE	HIGH	4
Indianapolis Power & Light Co	Harding Street Power Station	Pond 4	Indianapolis, IN	NONE	HIGH	4
Kentucky Utilities Company	E W Brown	Auxiliary Pond	Harrodsburg, KY	HIGH	HIGH	4
Kentucky Utilities Company	E W Brown	Ash Pond	Harrodsburg, KY	HIGH	HIGH	3
Kentucky Utilities Company	Ghent	Gypsum Stacking Facility	Ghent, KY	HIGH	HIGH	3
Kentucky Utilities Company	Ghent	Ash Pond Basin 1	Ghent, KY	HIGH	HIGH	3
Kentucky Utilities Company	Ghent	Ash Pond Basin 2	Ghent, KY	HIGH	HIGH	3

Company	Facility Name	Unit Name	Location/State Contact	Original Hazard Potential Rating (As Reported in Responses to EPA's Information Request)	Current Hazard Potential Rating (Based on EPA's CCR Dam Assessment Effort)	Assessment Round
Louisville Gas & Electric Co	Cane Run	Ash Pond	Louisville, KY	HIGH	HIGH	3
Louisville Gas & Electric Co	Mill Creek	Ash Pond	Louisville, KY	SIGNIFICANT	HIGH	2
Northern Indiana Pub Serv Co	R.M. Schahfer Power Station	Final Settling Basin	Wheatfield, IN	NONE	HIGH	4
Northern Indiana Pub Serv Co	R.M. Schahfer Power Station	Intake Settling Basin	Wheatfield, IN	NONE	HIGH	4
Ohio Valley Electric Corp	Kyger Creek Station	Bottom Ash Pond	Gallipolis, OH	SIGNIFICANT	HIGH	3
Ohio Valley Electric Corp	Kyger Creek Station	South Fly Ash Pond	Gallipolis, OH	SIGNIFICANT	HIGH	3
PPL Generation	Martins Creek	Ash Basin 4	Bangor, PA	SIGNIFICANT	HIGH	2
PPL Montana LLC	Colstrip Steam Electric Station	Units 1 & 2 Stage Evaporation Ponds (STEP)	Colstrip, MT	HIGH	HIGH	1
Progress Energy Carolinas Inc	Asheville	1982 Pond	Arden, NC	HIGH	HIGH	1
Progress Energy Carolinas Inc	Asheville	1964 Pond	Arden, NC	HIGH	HIGH	1
Sunbury Generation LLC	WPS Energy Services Sunbury Generating Station	Residual Waste Ash Basin No. 1	Shamokin Dam, PA	NONE	HIGH	4

14

Due to sludge release incidents, the EPA formally requested that electric utilities that have surface impoundments or similar units provide information about the structural integrity of their units and give more attention regarding this concern. In this case, structural integrity of storages pond can be affected by any movement such as earthquakes, blasting, machinery vibrations, etc.

Furthermore, facilities with impoundments also need to obtain wastewater discharges permits and install ground water monitoring wells (Figure 1.7) to address the chemical constituents of effluent that discharge directly to surface and underground waters both upstream and downstream of the discharge area.

Figure 1.7: Groundwater monitoring well

One example that coal ash might threaten public health was from the 2008 Kingston coal ash disaster in Tennessee (Figure 1.8). Based on the report published by

the United States Environmental Protection Agency (EPA) in 2011 (Environmental Integrity Project, 2013), the groundwater around TVA's Johnsonville power plant impoundment (Figure 1.9) remains impacted, with toxic contaminants including arsenic, boron, cobalt, and manganese. The affected area traveled across Emory River and Clinch River covering up to 300 acres (1.2 km^2).

Figure 1.8: TVA's Johnsonville power plant impoundment (Southern Alliance for Clean Energy, 2013)

Figure 1.9: Kingston coal ash disaster (Associated Press; Samuel M. Simpkins/The Tennessean) December 22, 2008

In Kentucky, the potential for earthquake-induced strong ground motion has gained significant attention. Seismic zones that are active and produce strong ground motion in Kentucky include the New Madrid Seismic Zone, The Wabash Valley Seismic Zone and Southern Appalachian Seismic Zone (Figure 1.10). The Southern Appalachian Seismic Zone was the source of the biggest earthquake ever recorded in the state of Kentucky. It occurred near Sharpsburg in Bath County on July 27, 1980 with a magnitude of 5.2. The New Madrid Seismic Zone, located in Western Kentucky, produced earthquakes with magnitude of 8.0 in 1811 and 1812 with return periods on the order of 400-1,000 years (Nuttli, 1974), but were not recorded.

In Kentucky, coal mining is performed in areas that are susceptible to strong ground motion (Figure 1.11). As a result, fly ash ponds in these regions may also be exposed to strong ground motion.
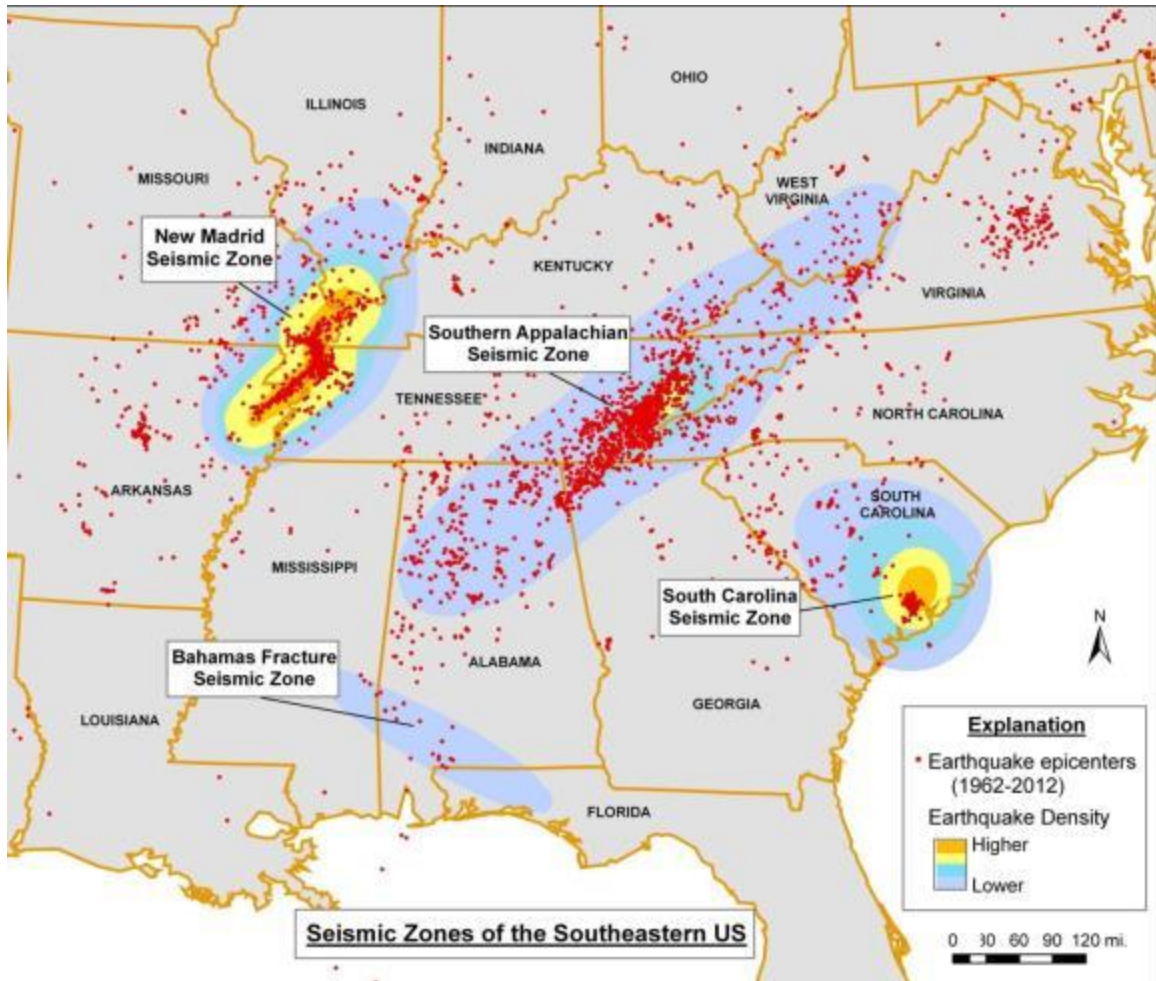
Figure 1.10: Topographic map showing earthquakes greater than magnitude 2.5 (circles) in Southeastern US from 1962 – 2012 (Alabama Earthquakes, 2016)
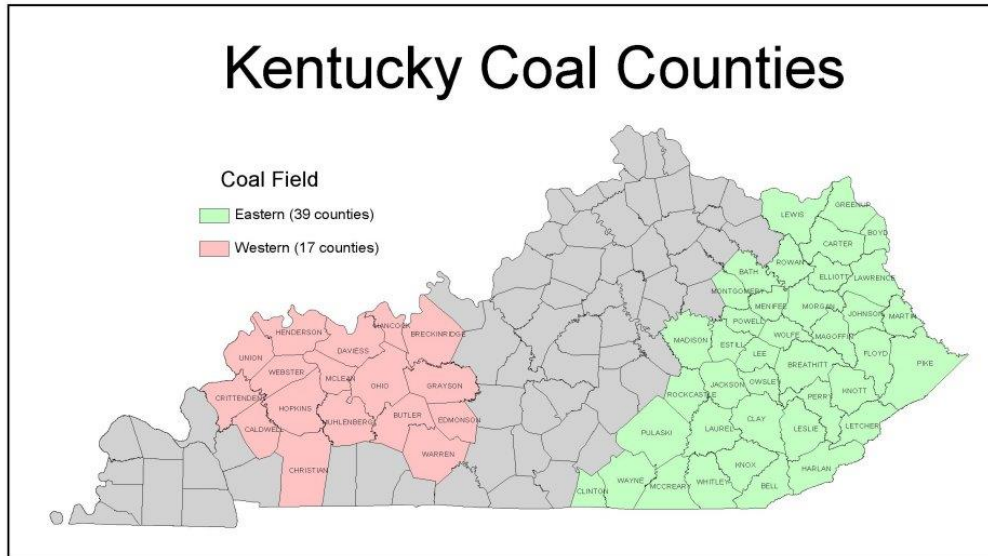
Figure 1.11**:** Coal producing counties in Kentucky, 2014 (Kentucky Transportation Cabinet, 2015)

The frequent need to upgrade the engineering properties of "marginal" soils, including fly ash, has made soil stabilization a common practice. However, increasing demand for coal in the U.S. has resulted in enormous amounts of fly ash being produced. This, coupled with the increasing cost and regulatory burden of coal ash disposal and the implementation of the Beneficial Use of Coal Ash Act by the Federal Highway Administration (FHWA) in 1987, has led to greater interest in identifying useful applications for fly ash.

1.2   History of Incidents at Fly Ash Impoundments

In the past, many fly ash impoundments were built with the assumption that fly ash is resistant to liquefaction. Recently, this assumption has come into question due to many accidents which have also resulted in some fatalities. One of the more significant factors leading to ground failure during earthquakes is the liquefaction of loose to medium-dense sands below the water table (Seed and Harder, 1990), but cohesionless fine-grained material like fly ash is also susceptible to liquefaction. During shaking, the ash tends to densify. The water in the pores cannot escape quickly enough, so excess pore pressure develops. In turn, effective stress decreases. Ash depends on the effective stress between the grains to mobilize shear strength. Therefore, the increasing pore water pressure leads to strength loss. The example illustrated in Figure 1.12-Figure 1.17 is from the Dayton Power and Light (DPL) power plant in Maysville, Ohio where a mass of hydraulically placed fly ash failed due to dynamic loading in (vibrations) from machinery, which induced liquefaction in the material and a flow failure that engaged several dozen acres of the impoundment and resulted in one fatality.

Figure 1.12: Fly ash impoundment at the DPL Power Plant after an accident

Figure 1.13: Slope failure occurred as a result of fly ash flow at the DPL Power Plant

Figure 1.14: Movement of fly ash at the DPL impoundment

Figure 1.15: Trackhoe engulfed in fly ash at the DPL impoundment after a fly ash failure caused by liquefaction

Figure 1.16: Side picture of Trackhoe covered with fly ash caused by fly ash failure at the DPL impoundment

Figure 1.17: Portion of a fly ash flow failure in an impoundment at the DPL power plant

Another noteworthy fly ash impoundment failure happened at a Tennessee Valley Authority (TVA) facility in Kingston, Tennessee on December 22, 2008. (Figure 1.18) The resulting release of fly ash destroyed three homes and severely impacted the Watts Bar Reservoir (Kennedy, 2008). During this failure, approximately 5.4 million cubic yard of ash released because of a wall failure. (Figure 1.19)

Figure 1.18: Kingston Plant coal ash retention pond two years before the December 2008 failure (EPA, 2009)

Figure 1.19: Ash sludge released from containment dikes in Kingston (EPA, 2009)

The TVA ash storage site is located in Roane County, Tennessee in close proximity to two faults, including an unnamed fault approximately 0.25 mile south of the failure area and the Kingston Fault. However, this failure was not attributed to seismicity in the area because there were no events of significant size on these faults in the time frame of the failure.

From the final report of the investigation, AECOM identified four factors that contributed to the failure of the Kingston fly ash impoundment, including fill geometry, increased fill rates, soft foundation soils and loose saturated ash (AECOM, 2009). However, for the research presented herein, the presence of loose saturated fly ash is being considered.

The Kingston incident raised concerns within the electric power industry and the general public regarding the geotechnical behavior of coal combustion products (CCP) and their engineering properties. Therefore, it has become of great interest amongst members of the geotechnical engineering community serving the utility industry to establish whether or not there is potential for CCR to liquefy at a site under certain credible loading conditions such as blasting and vibrations from machinery.

1.3   Other Research Related to Fly Ash

The following section contains a brief review of related research where the dynamic and cyclic behavior of fly ash was investigated. Although a large amount of literature exists on the cyclic resistance of sands, silts, and clays, less has been done to determine the liquefaction potential of fly ash. The test programs had varying objectives and correlation between tests is limited. However, common behavioral patterns and properties are identified. Much of the available literature on stabilizing fly ash embankments is based upon test results from university research projects, industry sources and private engineering firms.

There are many factors related to failure of fly ash embankments. Those factors include ash type, ash solubility, degree of compaction, overconsolidation ratio, moisture content, and position relative to the groundwater table. Some attempts have been made to predict the behavior of coal ash using the Cone Penetration Test (CPT) and Standard Penetration Test (SPT). However, correlations between cyclic resistance and CPT or SPT may not be reliable. Cunningham et al. (1977) suggested that in loose

26

conditions ash may liquefy during CPT and SPT testing, which may lead to misleading results. According to Leonards and Bailey (1982) the behavior of compacted ash cannot be inferred from SPT or CPT largely because these tests do not adequately sense the effect of pre-stressing due to compaction.

Zand et al. (2007) and Zand et al. (2008) investigated the liquefaction, post liquefaction and settlement behaviors of fly ash by performing cyclic triaxial tests on fly ash samples at different densities, confining stresses and cyclic stress ratios using the standard cyclic triaxial test method (ASTM D5311). Results from their investigation showed that the shear strength of fly ash is closely related to dry unit weight. The consolidation rate of fly ash was measured using conventional oedometer consolidation testing to investigate the long-term settlement behavior of Class F fly ash.

In addition, a considerable amount of research has been conducted to study different techniques such as vacuum dewatering, electro-osmosis consolidation, vibrocompaction, stone-sand columns, blasting compaction, lime stabilization and fiber mix stabilization to improve the density, stiffness and bearing capacity of fly ash. Kumar et al. (2006) investigated the effect of polypropylene fibers to stabilize fly ash embankments. According to this, randomly distributed discrete fibers can be used to improve shear strength, CBR value and modulus of subgrade reaction of fly ash embankments. The tests were performed on unreinforced soil-fly ash and reinforced soil-fly ash systems. The reinforcement was varied from 0% to 2% by weight of the soil and fly ash, with the aspect ratio of 90. Triaxial test results indicate that fiber aspect

ratio (l/d) or fiber length divided by its diameter significantly affects the magnitude of both the critical confining stress, and the strength of soil-fiber composite.

Many researchers have attempted to evaluate the behavior of adding fiber into fly ash as a means to reduce cost of construction and encourage sustainable development. Choudhary et al. (2011) analyzed the shear strength of fiber reinforced fly ash. The material of added fiber used is polyethylene (synthetic) with fiber contents of 0.25, 0.50 and 1.0 % by mass of dry fly ash. The results show that the stiffness of fly ash increases with increasing fiber content, with improvements in elastic modulus, shear strength, cohesion and friction angle.

Puppala et al. (2001) conducted tests on expansive soil stabilization using recycled waste materials. Both fly ash and polypropylene fiber, the typical fiber found in carpet, were mixed with expansive soils. The test result shows that both materials increased strength and decreased shrinkage strains of the soils. The waste materials reduce the volume change of expansive soil during saturated and dried conditions.

Mohan et. al. (2012) used natural fiber such as coconut fiber mixed with fly ash and concrete. Four different coconut fibers percentages of 0.15, 0.30, 0.45 and 0.60% were used. The results show that the addition of coconut fiber increased the strain at which the material failed. Fly ash is classified as low plasticity silt (ML). The improvement in unconfined compressive strength is believed to be due to skin friction between the fibers and fly ash. When the specimen is loaded axially, the fly ash are

believed to apply confining pressure on the fibers, and in this process they get stretched with mobilization of tensile force. The tensile force T varies with the orientation of the fibers within the specimen (Kumar and Singh, 2010).

Boominathan and Hari (2002) concluded that at low confining pressure, randomly distributed geosynthetic fiber/mesh reinforcement provides a higher rate of improvement in liquefaction resistance of fly ash. Addition of randomly distributed mesh and fiber elements increases significantly the liquefaction resistance of fly ash at low relative densities. Randomly distributed mesh elements (the ratio of longest to the shortest side) should be near 1.0 to better arrest liquefaction when compared with randomly distributed fiber elements because the mesh elements provide better interlocking of the fly ash and also provide faster dissipation of pore pressure along the sample length. The optimum percentage of fiber/mesh content is found to be 2% to resist liquefaction. The gain in liquefaction resistance of fly ash due to mesh/fiber reinforcements is more pronounced at lower confining pressures and hence reinforcing fly ash with mesh/fiber elements is a better choice among available ground improvement techniques to improve liquefaction resistance of fly ash.

In agreement, Kumar et al. (2006) presented the effect of inclusion of polypropylene fibres in fly ash. The percentage increase in CBR value is higher at lower percentages of fiber content, where 0.5% fibre content is seen to be the optimum.

Kulkarni (2003) investigated the effect of filler-fiber on the compressive strength of fly ash and short-fiber epoxy composited (reinforced epoxy layers). The results show that the decrease in density can be attributed to the tendency of fibers to bunch. The properties of such composites are greatly influenced by shape, size, and distribution of the reinforcing phase in addition to their chemical composition and volume fraction.

Viswanathan et al. (1997) used fly ash as an admixture to stabilize subgrade soils. The reactions involved in the stabilization of soils with fly ash admixtures are categorized as short term (immediate) and long term reactions. The short term reaction in clays is the exchange of cations on the surface of the clay particles which results in a decrease in its plasticity index (PI). However, in cohesionless coarse grained soils, the admixture serves as "micro aggregate" resulting in an increase in the maximum dry density. The long term reactions are pozzolonic and occur over a period of weeks or months. Pozzolonic reactions result in the formation of cementious products such as calcium silicate hydrate and calcium aluminate hydrate which increases the strength, stability and durability of soil.

1.4   Gaps in the Current State of Knowledge

From the previous section, the mechanics of liquefaction in fly ash are now well understood and the potential for occurrence can be estimated and avoided with a reasonable degree of confidence. Although a large amount of literature exists on the cyclic resistance of fly ash and fly ash admixtures especially with fibers (Kaniraj et al, 2003); none has been done to determine the liquefaction potential of fly ash admixtures

with waste products. To address this subject an experimental program along with an analytical study was conducted to evaluate the effect of adding waste products such as crumb rubber, shredded carpet and shredded paper; to enhance the strength properties of fly ash.

A secondary objective of this research is to identify an alternate method to recycle used tires and shredded carpet, materials that would otherwise be considered as waste products.

In order to address this concern, cyclic triaxial testing combined with analytical analyses were conducted to evaluate the liquefaction potential of reconstituted fly ash specimens to depict the material in the impoundment facilities and to evaluate the strength properties of the material. Based on this, we can investigate the effect of waste products on fly ash liquefaction.

Although a large amount of conducted research already provides methods to stabilize fly ash, none calculate the costs to implement the method in the actual field and shows comparison matrix costs between methods. This calculation is very substantial especially if impoundment facilities want to select the most appropriate method to solve the problem with fly ash stability.

1.5   Research Objectives

This study will focus on utilizing cyclic triaxial testing to collect information such as deviator stress, axial deformation and excess pore pressure from every specimen

tested. This recorded information will be used to make hysteresis loop and develop cyclic resistance ratio (CRR). Using this information the expectations of this research were as follows:

1) A method would be identified to stabilize fly ash in storage ponds with respect to static stability.

2) A method would be identified to re-task waste products such as crumb rubber, shredded carpet, and shredded paper to reduce waste stream.

3) Methods will be developed to analyze the liquefaction resistance of fly ash admixtures against dynamic loading from earthquakes and vibrations

4) A cost matrix would be developed to quantify the benefit of using waste products as addictives to provide justification for the method.

1.6   Research Limitations

Time limitations, number of waste products, cyclic stress ratio (CSR), the amount of specimens tested, laboratory testing equipment and specimen ratio or composition; mentioned are the limitations applied for this research.

Time limitation affected the number of specimen tested and how long one specimen gets tested. Pore pressure parameter B-value, according to ASTM D5311, sample is considered saturated if B-value is greater than 95%. To accommodate this requirement, minimum of 2 days to a maximum of 1 week were needed to establish saturation, resulted in limited number of specimens tested

Byproduct of tires, shredded carpet and paper, previously mentioned were the only waste products used for this research. The selected materials were in high consideration that will help to enhance the strength properties of fly ash.

Initially, the cyclic stress ratio (CSR) used ranged from 0.30 to 0.80, but changed to 0.15 - 0.50. The changed was made because specimens tested at cyclic stress ratio higher than 0.50, gave a small number of cycles to liquefaction (Less than 4). These results show that all specimens with different composition and waste materials showed same behavior at cyclic stress ratio higher than 0.50. After decreasing the CSR, the number of cycles to liquefaction ranged from 2 cycles to more than 100 cycles.

The testing equipment used on this research was cyclic strength testing instrument and it is adequate to see the effect and analyze the results for each specimens.

Finally, specimen composition contains Class F fly ash with waste material up to a maximum of 20% by dry weight. This limit of up to 20% waste material was used because the amount of waste products more than the maximum limit tends to occupy more volume than fly ash and also to maintain fly ash as the primary material and not secondary material or filler.

1.7   Dissertation Outline

In Chapter 2, the physical properties of fly ash and also other materials considered to be used in this research are explained. Physical properties to be explained

include specific gravity and grain size distribution. Also in this chapter, current uses and disposal method of fly ash, crumb rubber, shredded carpet and paper are explained briefly.

Chapter 3 is used to explain and describe triaxial testing, including basic information about the machine, how the instrument works, the assumptions used, input parameters, and expected output.

Chapter 4 results of the physical and chemical properties of selected material for this research. This chapter also will briefly explain how to run the laboratory testing such as specific gravity, grain size distribution and strain-controlled cyclic triaxial testing. Further, chemical composition of fly ash specimen from the X-Ray diffraction (XRD) test is discussed.

In chapter 5, the typical results from geotechnical and cyclic triaxial testing are presented. These results including specific gravity, grain size distribution curve and plots generate from cyclic triaxial testing.

Finally, chapter 6 provides the conclusions obtained from the research. Several recommendations for further research are also included in this chapter.

Chapter 2

WASTE MATERIALS USED IN THIS STUDY

2.1   Fly Ash

The American Society for Testing and Materials (ASTM) standard C618 identifies two classes of fly ash. Class C fly ash is derived from the combustion of younger lignite or sub bituminous coal. It generally contains more than 20% of quicklime (CaO) and is self-cementing when mixed with water. Class F fly ash is derived from the combustion of older anthracite or bituminous coal.   It contains less quicklime and is not self-cementing. Typical compositions of Class C and Class F fly ash are given in Table 2.1.

Table 2.1: Typical composition of fly ash (FHWA, 1999)

Compounds	Fly Ash Class	
	Class F	Class C
SiO_2	54.9	39.9
Al_2O_3	25.8	16.7
Fe_2O3	6.9	5.8
CaO(Lime)	8.7	24.3
MgO	1.8	4.6
SO_3	0.6	3.3

Overall, fly ash is a poorly-graded, fine-grained material (Figure 2.1). Fly ash particles are nearly spherical because they are formed by the solidification of molten minerals as they ascend the smokestack in a power plant (FHWA, 1999). Fly ash is collected in the smokestacks using water and the resulting slurry is hydraulically placed in stockpiles at landfills for subsequent land-filling. Generally, fly ash possesses a specific gravity of around 2.2 – 2.3, which is lower than the specific gravity of clay or sand due

to the amorphous, glass-like crystalline structure of the silica. Depending on the particle size, hydraulic conductivities of reconstituted specimens of fly ash are around 1.0 x 10^{-5} cm/s. As a frictional material, the friction angle of fly ash typically ranges from 15 – 32 degrees, while the cohesion of fly ash is generally very low (< 0.05 psi).
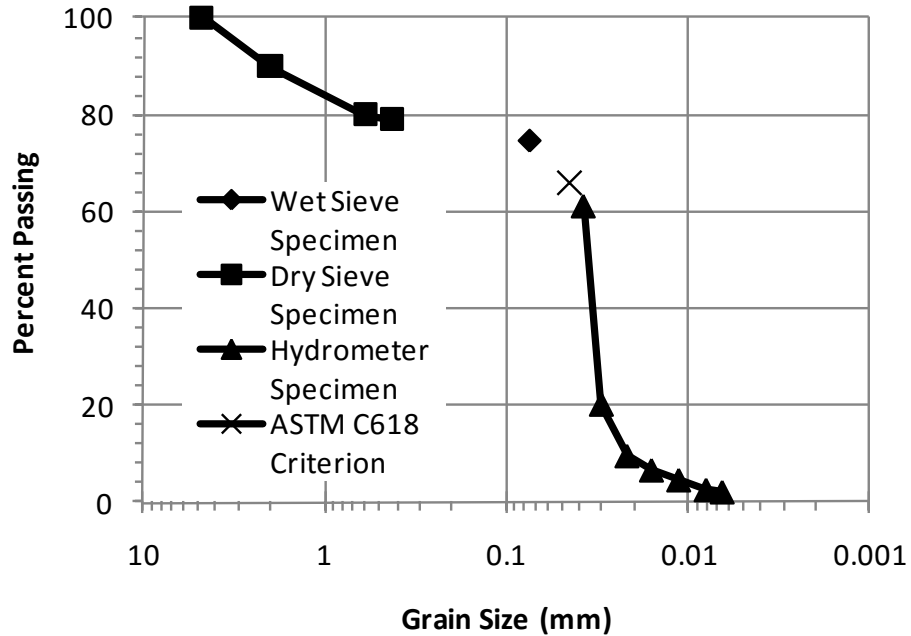
Figure 2.1: Typical gradation curve for fly ash (after Kalinski and Hippley, 2005)

Based on grain size distribution, Tsuchida (1970) provided a graph of limits in the gradation curves separating liquefiable and non-liquefiable soils, where gradation curve of fly ash is plotted inside the boundaries and identified as a potentially liquefiable material (Figure 2.2). The composite curves between gradation curve provided by Tsuchida and gradation curve from this study will be presented in Chapter 5.

The "Chinese Criteria" is one of the oldest procedures to confirm the liquefaction susceptibility of silts and clays and is established in the summary reports from the 1996

NCEER and 1998 NCEER/NSF workshops on the evaluation of liquefaction resistance of soils (Youd et al., 2001). According to Chinese Criteria, specimens in this study were classified using specifications of the sample as follows: liquid limit (LL), plasticity index (PI), and w_c/LL (where w_c = water content), and percentage of particles smaller than 5 µm as determined from the hydrometer test.
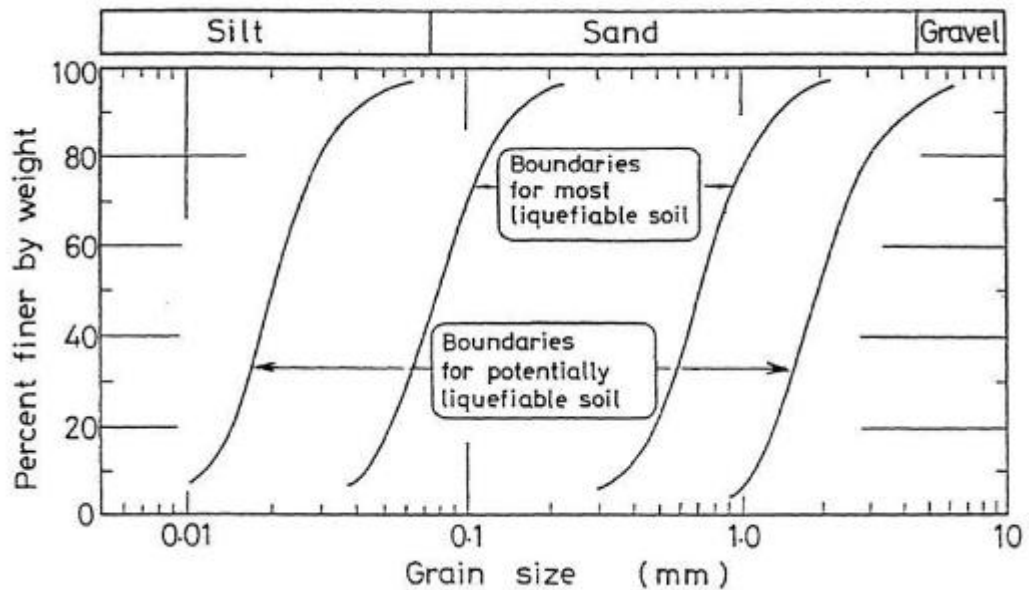
Figure 2.2: The gradation curves separating liquefiable and nonliquefiable soils (Tsuchida, 1970)

Liquefaction is also facilitated in fly ash storage ponds because the phreatic surface is typically near the top of the impoundment. Furthermore, it is placed hydraulically as slurry, which leads to very loose materials with high void ratios. Coupled with the location of fly ash ponds in close proximity to seismic zones in the eastern United States, earthquake-induced liquefaction of fly ash is a concern.

Class C fly ash contains greater than 20% quicklime and is self-cementing similar to portland cement. Products derived from Class C fly ash have been used as concrete admixtures, brick additives, and for soil stabilization (ACI 2010). Class F fly ash, on the other hand, is not used as a cementing agent, but is sometimes used as an additive to concrete to improve flowability. With the addition of a cementing agent such as quicklime or portland cement, fly ash is sometimes used as a fill material.

Nevertheless the reuse of fly ash is not widespread, and most fly ash produced at power plants is ultimately placed in landfills. However, there are some novel uses for fly ash being discovered. For instance, The Recycle Material Resource Center (RMRC) provides an option to use fly ash as a fill material to help reclaim coal strip mines (Recycle Material Resource Center, 2012). This method is a breakthrough to utilize unused fly ash. The ash used in this method should be dewatered to an optimum moisture content before use.

Disposal of large amounts of waste materials such as fly ash is a significant problem in the United States and worldwide from both an economic and an environmental perspective. Fly ash is designated as a special waste because of the large volumes, and because it is generally considered less hazardous than municipal solid waste (MSW). Special wastes often have separate, less restrictive requirements for landfills. In addition to the technical and site restrictions imposed by The Resource Conservation and Recovery Act (RCRA), other economic and political conditions also affect the landfilling of MSW and special wastes. Considerations such as cost of land,

proximity to waste stream sources, and proximity to existing infrastructure also play a role in decisions regarding how and where to place the waste.

2.2   Crumb Rubber

Tires in the form of crumb rubber were used in this study as an additive to fly ash. Crumb rubber particle size (Figure 2.3) typically range from gravel-sized to sand-sized. The size of crumb rubber used in this research was 0.20 – 0.25 in. in width and 0.100 - 0.125 in. in thickness with a specific gravity of approximately 1.1. This size was chosen because it is easy to find and many companies sell recycled tires in this size, meaning that companies have capability to cut tires into this size and also to accommodate the minimum size require for cyclic triaxial testing.

Crumb rubber is commonly used as an additive for rubberized asphalt concrete, is used in clothing, and is considered as safe ground cover for playgrounds and schoolyards. In Missouri, shredded waste tires have been used as fill material for road subgrades (Engstrom and Lamb, 2003).

Figure 2.3: Crumb Rubber

Like fly ash, disposal of a large volume of used tires is also a significant problem in the United States and worldwide from both an economic and an environmental perspective. Based on information from United States Environmental Protection Agency in 2003, the United States generated approximately 290 million scrap tires and much of this ended up in used tires landfills (Figure 2.4) to become a habitat for mosquitoes and rodents (Illinois EPA, 2015). Fires are also a common occurrence at the landfills, which create a negative environmental impact.

Figure 2.4: Landfill of used tires (Hudson, CO: World's Largest Tire Dump) (Leather, 2010)

Since 1990, there have been markets for both recycling and beneficial use of scrap tires. The Scrap Tire Cleanup Guidebook is a guidebook to help effectively clean up scrap tire piles (U.S. Environmental Protection Agency, 2006), but scrap tire landfills and stockpile volumes are still rising and creating more problems for the environment.

Traditionally, tires were simply buried in landfills. However, this method of disposal is now, for all practical purposes, no longer possible. Tires not only take up a lot of space, but over time, the tires tend to float to the top, working their way up through the waste and soil. Once they break through the surface, the landfill's cover is broken, exposing its contents to insects, rodents and birds and allowing landfill gases to escape

(South Central Iowa Solid Waste Agency, 2016). The oil and ash created during fires can also cause leaching problems. Therefore, for both practical and environmental reasons, most municipalities in the United States no longer permit the inclusion of tires in regular landfills. Landfills dedicated to shredded tires (monofills) are an effort to dispose of tires, rather than recycle them. While monofilling could potentially reduce some of the environmental problems of mixing tires with other landfill materials, it requires substantial expenditures for land, shredding and handling. It is also unlikely that monofilled tires will be reclaimed at a later date for fuel or any other worthwhile purpose. This is not a current practice, but rather one under consideration in a number of locations including Ohio and North Carolina. With tires being banned from landfills, undisposed waste volume has increased rapidly (Yang et al., 2002).

According to the EPA, most recycled tires are used as fuel (scrap tires and used oil are being converted to energy sources through the tire liquefaction process (Siuru, 1993) while the rest are used as ground rubber and other rubber-modified or rubber-based products such as rubberized asphalt. Although most tires are already recycled and used to create byproducts, there are still 265 millions of tires in stockpiles as summarized in Table 2.2.

Table 2.2: Statistics of tire recycling and disposal in the U.S (Rubber Manufacturers Association, 2004)

Number of scrap tires generated annually:	290 million
Percentage of total solid waste generated:	2.0 percent
Number of scrap tires going to a market:	233 million
Number of scrap tires used for fuel:	130 million
Number of scrap tires used in civil engineering projects:	56 million
Number of scrap tires used in ground rubber applications:	28 million
Number of scrap tires punched/stamped into new products:	7 million
Number of tires exported:	9 million
Number of tires in stockpiles:	265 million

2.3   Shredded Carpet

For shredded carpet fiber, material obtained from Republic Machine was used. Republic Machine is a Louisville, Kentucky-based company that produces carpet shredding equipment (Figure 2.5). Because of the high demand and relatively high price for shredded carpet fiber passing through multiple shredding processes, Republic Machine could only provide shredded carpet with larger dimensions as shown in Figure 2.6 with dimensions of 1.0 - 1.5 inches width and 0.250 to 0.275 inches thick.

Due to the size the company provided and the requirement to assemble acceptable cyclic triaxial test specimens, the shredded carpet provided was stripped manually by hand before being used as a mixture (Figure 2.7). The size of the stripped carpet was smaller than 1/6 the specimen diameter, thus meeting the requirement for acceptable cyclic triaxial test specimen preparation.

Shredded carpet is most commonly used to manufacture new carpet and flooring, and as a general recycled plastic (Lave et al., 1998).

Figure 2.5: Carpet Shredder machinery

Figure 2.6: Shredded carpet

Figure 2.7: Shredded carpet after hand shredding

Figure 2.8: Used carpet Landfills

Used carpet is typically disposed of in municipal solid waste (MSW) landfills (Figure 2.8), which are governed by federal and state regulations, including the Resource Conservation and Recovery Act (RCRA) as promulgated under Title 40 of the United States Code of the Federal Register (40 CFR).

Used carpet is a significant portion of the overall municipal solid waste (MSW) stream in the United States. Approximately 3 to 4 billion pounds of carpet are disposed in landfills annually, which correspond to 1% of all MSW by weight and 2% by volume (U.S. Environmental Protection Agency, 2010).

The State of California has also documented issues with respect to used carpet disposal. According to statistics from the U.S. Environmental Protection Agency, over 24 million pounds of waste carpet were buried in the King County's Cedar Hills Landfill in Maple Valley in 2002, while less than 4 percent of the waste carpet was recycled (Watson, 2006). The 920-acre Cedar Hills Regional Landfill is located in Maple Valley, about 20 miles southeast of Seattle, WA and owned by King County.

2.4   Shredded Paper

The shredded paper used in this study had a dimension of 0.7 x 1.3 x 0.003 inches for width, length and thickness, respectively (Figure 2.9). Paper is not waste material but in this study the use of shredded paper is due to its shape and weight, with the expectation that shredded paper will replicate the workability of fiber in concrete fiber composite material.

Figure 2.9: Shredded Paper

Chapter 3

DESCRIPTION OF LABORATORY TEST METHOD

3.1 Laboratory Testing of Mechanical Properties

3.1.1 Index Properties

The properties obtained from the experiments included index properties and strength properties. All experiments were performed according to American Society of Testing Materials (ASTM) standards. All samples were tested immediately after preparation and therefore time effects were not considered in the entire study. Test methods used include specific gravity, grain size distribution and modulus and damping properties using the cyclic triaxial apparatus. Because Class F fly ash is non-plastic, Atterberg limits were not determined.

First, specific gravity of soil solids, G_s, is the mass density of the mineral solids in soil normalized relative to the mass density of water (Kalinski, 2011). Alternatively, it can be viewed as the mass of a given volume of soil solids normalized relative to the mass of an equivalent volume of water at a temperature of 20 degrees Celsius.

To prepare the samples, ASTM D854 (Standard Test Method for Specific Gravity of Soils) was used. To get the appropriate result, the entire sample de-aired for at least 24 hours although according to ASTM D854, oven-dried specimens only need 2 to 4 hours of applied vacuum for adequate de-airing. Extra vacuumed time was used because according to the ASTM standard the minimum vacuum source should be 12.8 psi. The vacuum source available in our laboratory was less than 12.8 psi so alonger

vacuum time was used, in this study a 24 hours vacuum time was used. The water used is distilled water and the oven temperature is at 110 degree Celsius per the ASTM standard.

In this study, there were four (4) different compositions (Class F fly ash, Class F fly ash with shredded carpet, Class F fly ash with crumb rubber and Class F fly ash with shredded paper) with a total of ten (10) samples tested. To prepare the specimen, fly ash and waste materials were combined in a given ratio (Table 4.3) and mixed using a mixer until they were completely blended together. The samples were then oven dried at a temperature of 110 ^{0}C. The apparatus used for this test included a flask bottle, squeeze bottle, plastic funnel, scale, spoon and tin container. The testing procedure to determine the specific gravity was in accordance with the ASTM D854 standard.

Fly ash specimens for this research were Class F specimen from the combustion of Appalachian coal in Kentucky specifically from Dayton Power Light (DPL) power plant in Maysville, Ohio. From earlier investigations, test results had shown that this type of fly ash has a specific gravity of around 2.20.

3.1.2   Grain Size Distribution

Grain size distribution testing (dry sieving) was performed in accordance with ASTM standard D422. The sieves used were #4, #10, #20, #40, #60, #140, and #200. Grain size refers to the size of an opening in a square mesh through which a grain will

pass. Because fly ash consists of fines particle typically smaller than 0.075 mm, the hydrometer test was also performed to complete the gradation curve.

In this study, the liquefaction susceptibility of fly ash material was investigated by using the available liquefaction criteria such as Chinese criteria, Tsuchida (1970), Seed et al. (2003) and Bray & Sancio (2004), results were used to confirm whether fly ash is susceptible to liquefaction according to mechanical properties and gradation curve. The test results are presented in Chapter 5.

3.1.3 Shear Modulus and Damping Ratio (Strain-Controlled Cyclic Loading)

The dynamic and cyclic properties were tested (shear modulus and material damping) using the cyclic triaxial apparatus per the ASTM D3999 standard. To find these properties, fly ash specimens were tested using strain-controlled cyclic loading. The relative importance of parameters affecting shear modulus and damping has been documented by, Hardin & Drnevich (1972) and others.

For soil and rock, the outcome from this test is to quantify the response of specimens to strong ground motion. The outcome properties of tested specimens from this test are shear modulus (G), material damping (D), and shear strain (γ). Typically, as strain increases, damping ratio increases while shear modulus decreases. The plots of modulus reduction curves for Class F fly ash used in this study are shown in Chapter 4.

In this test, specimens of Class F fly ash were reconstituted. The basic properties of specimen used for this test are shown in Chapter 4. Specimen preparation and input

data for this test is identical to the cyclic triaxial method (ASTM D5311) but the amplitude of cyclic load much smaller than used in liquefaction assessment. By applying small cyclic deviator stress which maintains axial strain from passing elastic limit but enough to trigger measureable response from the specimen, the recording information from this test transmitted through pore pressure transducer and deformation gauge during shearing phase.

The test starts with 2 psi cyclic loading and proceeds by gradually increasing the deviator stress until 5 psi cyclic load. The test stopped at 0.01% shear strain as stated in the standard. The ASTM D3999 standard states the test result is valid if no disturbance such as noise induced by the equipment occurs during testing. Figure 3.1 shows the acceptable and non-acceptable deviator stress for this test according to the standard and Figure 3.2 shown the typical deviator stress applied to the specimen during this test and its acceptable range.
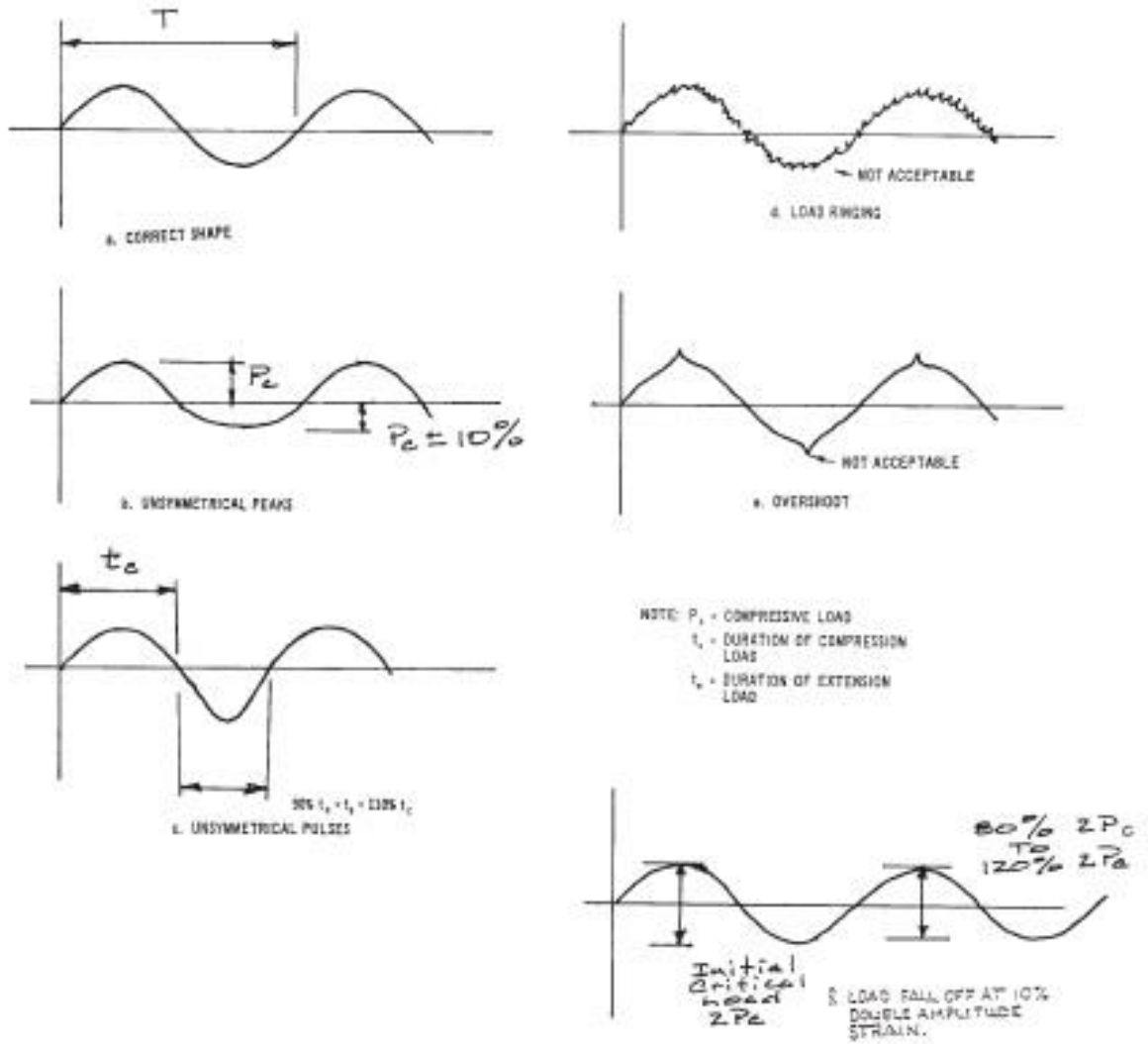
Figure 3.1: Examples of Acceptable and Unacceptable Sinusoidal Loading Wave Forms For Cyclic Triaxial Load Control Tests (ASTM D3999).
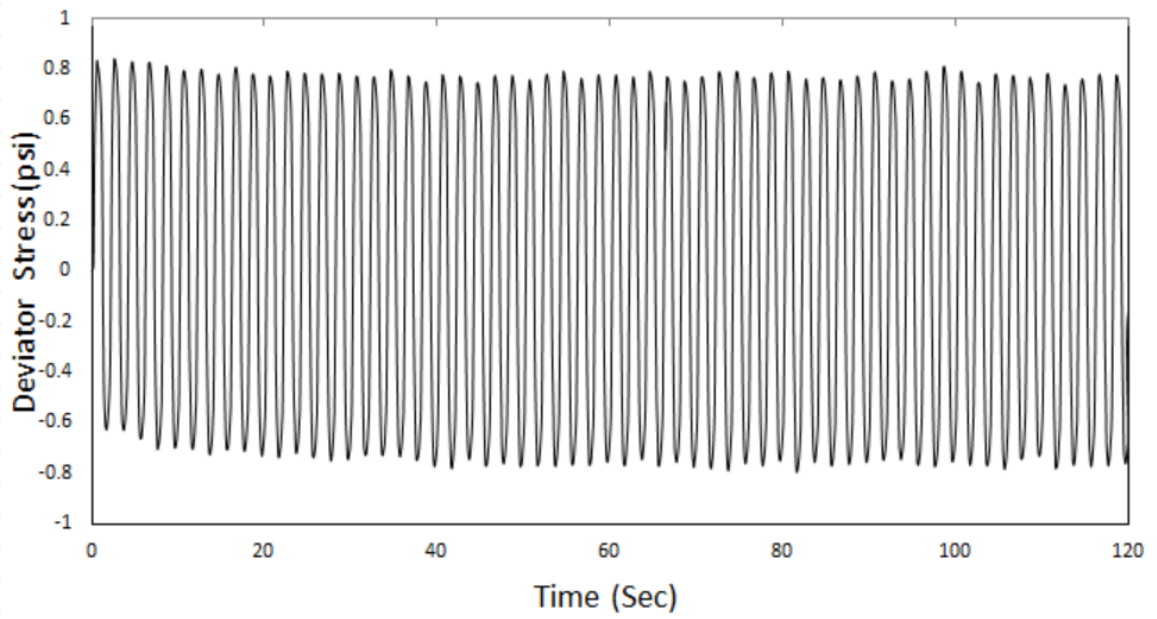
Figure 3.2: Deviator stress versus time at 2 psi
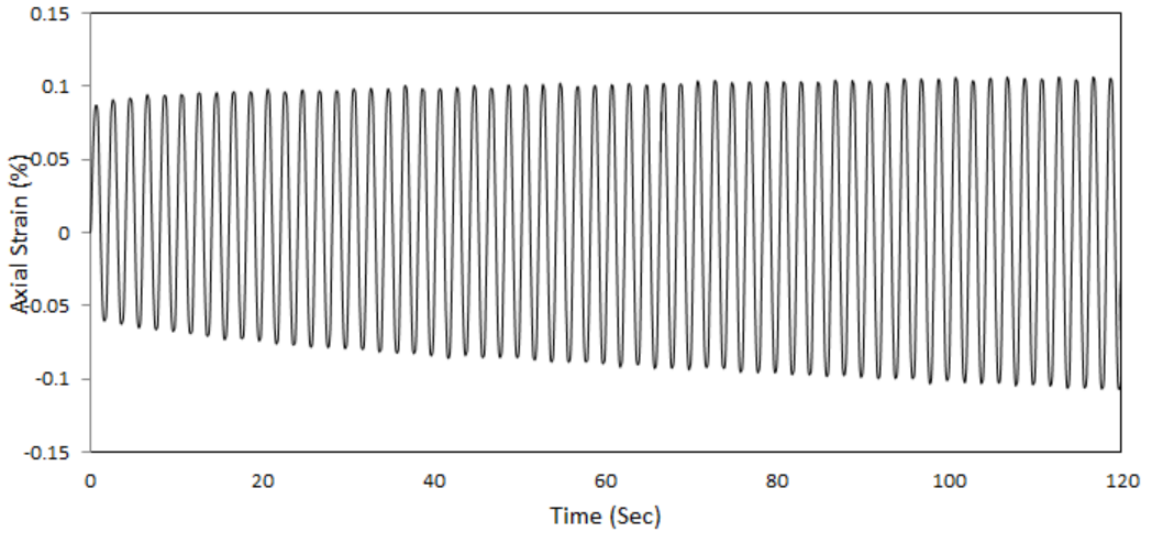
Figure 3.3: Axial strain versus time at 5 psi

Figure 3.3 shows the deformation of a specimen tested at 5 psi indicating that the specimen experienced deformation in the elastic region or recoverable range, so no permanent deformation occurred and it is acceptable according to the standard.

3.2 CHEMICAL PROPERTIES OF THE MATERIALS

Most of the coal used in Appalachian power plants is bituminous coal mined from local deposits, although significant anthracite deposits exist. According to ASTM C618, the SiO_2 +AL_2O_3+FE_2O_3 content must be greater than 70% and the SO_3 content must be greater than 5% for the fly ash to be considered Class F (Table 3.1). Class F fly ash is also characterized by a low CaO content (less than 20%) and is not considered self-cementing like Class C fly ash.

Table 3.1: Chemical Requirements for Fly Ash Classification (ASTM C 618)

Properties	Fly Ash Class	
	Class F	Class C
Silicon dioxide (SiO2) plus aluminum oxide (Al_2O_3) plus iron oxide (Fe_2O_3), min, %	70.0	50.0
Sulfur trioxide (SO_3), max, %	5.0	5.0
Moisture Content, max, %	3.0	3.0
Loss on ignition, max, %	6.0	6.0
CaO Content, %	< 20.0	> 20.0

Fly ash used on this research was Class F (Figure 3.4). Class F fly ash contains less than 20% lime (CaO) while Class C fly ash generally contains more than 20% lime (CaO). With that characteristic Class C fly ash hardens when exposed to water.

For this research, the chemical composition of the fly ash was determined using X-Ray diffraction (XRD). The diffractograms results are presented in Chapter 4.

Figure 3.4: Class F Fly ash used in this research

3.3   Cyclic Triaxial Testing

For this research, samples with various ratios of fly ash to waste additive (carpet, rubber or paper) were reconstituted. The specimens were tested using the cyclic triaxial method (ASTM D5311) to identify the optimum additive ratio with respect to cyclic behavior.

To reconstitute the samples, the pouring method was used to simulate the hydraulic placement method of fly ash storage ponds. This method was used to successfully create samples with void ratios ranging from 0.8 to 1.1.

Cyclic triaxial tests (ASTM D5311) were conducted under undrained conditions to simulate undrained field conditions during earthquake or other cyclic loading on impoundment facilities such as vibrations from machinery. Cyclic triaxial strength tests are destructive. Failure may be defined on the basis of the number of stress cycles required to reach a limiting strain or a pore pressure ratio of unity.

Cyclic strength depends upon many factors, including density, confining pressure, applied cyclic shear stress, stress history, grain structure, age of soil deposit, specimen preparation procedure, frequency, uniformity, and shape of the cyclic wave form. Thus, close attention must be given to testing details and equipment.

Cyclic triaxial testing was performed using a SBEL triaxial testing system in the University of Kentucky (UK) laboratory, which was modified in 2009 by GCTS Testing Systems Company to perform cyclic triaxial testing. Cyclic triaxial testing was performed on reconstituted specimens based on the ASTM Standard Test Method for Load Controlled Cyclic Triaxial Strength of Soil (D 5311). Table 3.2 shows the specimen preparation checklist based on the ASTM D5311 test standard. This list should be satisfied to validate the result from the test.

Table 3.2: Specimen preparation check list for cyclic triaxial testing (ASTM D5311)

Specimen Preparation	Status
1. Cylindrical and have a minimum diameter of 51 mm (2.0 in.)	
2. Height-to-diameter ratio between 2.0 and 2.5	
3. The largest particle size shall be smaller than 1/6 the specimen diameter	
4. Reconstituting Specimens method: • Pouring Method • Dry or moist vibration Method • Tamping Method	
5. Place the cap in place and seal the specimen with O-rings or rubber bands	
6. Apply partial vacuum of ≤ 35 kPa (5 psi) to the specimen before removing the jacket	
7. Measured specimen volume before and after vacuum application	
8. Diameter measurements using a circumferential measuring tape to the nearest 0.025 mm (0.001 in.)	
9. Height measurements using calipers or similar measurement equipment, to the nearest 0.025 mm (0.001 in.) at four locations	
10. Measure Masses to the nearest 0.01 g for specimens 63.5 mm (2.5 in.) or less in diameter and 0.1 g for specimens having diameters greater than 63.5 mm	

In addition, the cyclic triaxial machine is able to measure small-strain shear modulus and secant shear modulus per the ASTM D3999 standard. In doing so, liquefaction resistance can be measured and modulus reduction curves (stiffness and damping versus strain) can be developed.

Cyclic triaxial strength test results are used to evaluate the ability of a soil to resist shear stresses induced by earthquake or other cyclic loading. Testing is performed at strains that exceeded the cyclic threshold strain where volume changes and pore pressure changes began to occur under static stresses that are representative of typical in situ stresses encountered in the field. Variation of pore pressure ratio, r_u (equal to pore pressure divided by initial effective stress; at initial liquefaction, r_u = 1.0) versus variations in cyclic ratio, N/N_L (equal to the number of loading cycles divided by the number of cycles required for liquefaction) are measured (Figure 3.5) to quantify the development of excess pore pressure during cyclic loading.
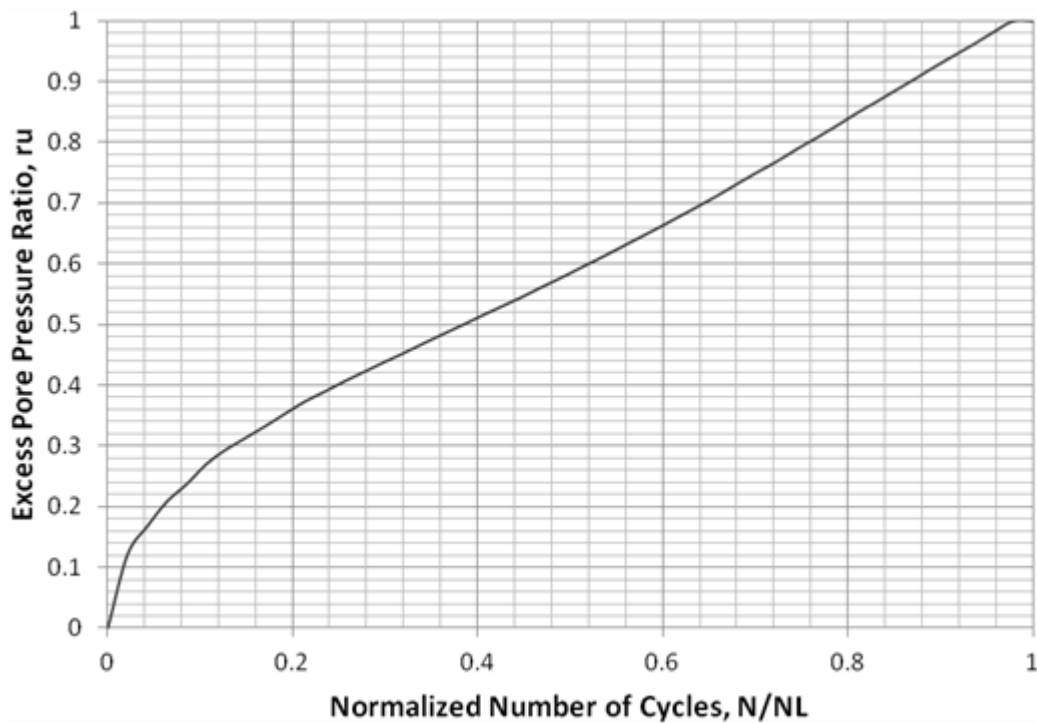

Figure 3.5: Schematic Illustration of pore pressure data derived from cyclic triaxial testing

Liquefaction is defined as the transformation of a granular material from a solid to a liquefied state as a consequence of increased pore-water pressure and reduced effective stress (Marcuson, 1978). Increased pore-water pressure is induced by the tendency of granular materials to compact when subjected to cyclic shear deformations. The change of state occurs most readily in loose to moderately dense granular soils with poor drainage, such as silty sands or sands and gravels capped by or containing seams of impermeable sediment.

In loose materials, the softening is also accompanied by a loss of shear strength that may lead to large shear deformations or even flow failure under moderate to high shear stresses, such as beneath a foundation or sloping ground. Loose soils also compact during liquefaction and reconsolidation, leading to ground settlement.

Sand boils may also erupt as excess pore water pressures dissipates. Calculation, or estimation, of two variables is required for evaluation of liquefaction resistance of soils: (1) the seismic loading on a soil layer, expressed in terms of cyclic stress ratio (CSR); and (2) the capacity of the soil to resist liquefaction, expressed in terms of cyclic resistance ratio (CRR).

Liquefaction is identified as the point where the pore pressure ratio reaches unity and a dramatic increase in the axial deformation occurs, as seen in Figure 3.6. Note for the plots, compression corresponds to positive stresses and strains, while extension corresponds to negative stresses and strains.
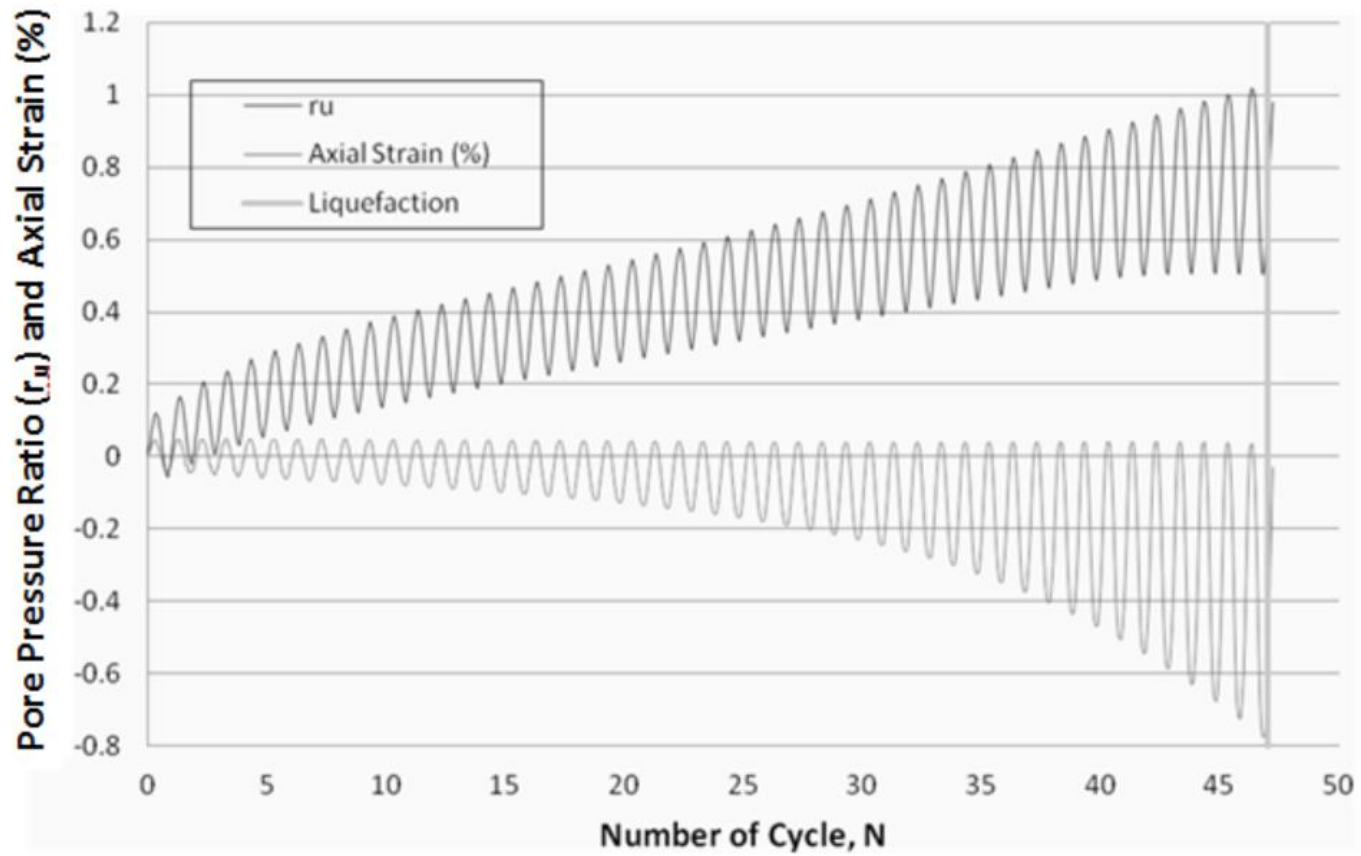
Figure 3.6: Schematic Illustration of Identification of liquefaction from cyclic triaxial test

To help analyze the performance of fly ash material under dynamic loading, the method presented by Youd et al. (2001) regarding liquefaction resistance in soil deposits is adapted. This is considered an acceptable approach based on the similarity between fly ash and soil. By utilizing this approach, the cyclic resistance ratio (CRR) can be estimated based on laboratory methods such as cyclic triaxial or cyclic simple shear. Cyclic resistance ratio (CRR) is a measure of liquefaction resistance, and is defined as:

$$CRR = \frac{\tau_{cyc}}{\sigma'_{vo}}$$

(3.1)

Where τ_{cyc} is the cyclic shear stress at liquefaction (when effective stress in the material reaches zero), and σ'_{vo} is the initial vertical effective stress prior to cyclic loading.

There are also three (3) common field methods used to evaluate liquefaction resistance, in terms of CRR: standard penetration test (SPT); cone penetration test (CPT), and shear wave velocity.

To calculate the factor of safety against liquefaction for horizontally layered sites, the CRR is divided by the cyclic stress ratio (CSR), which is dependent on anticipated peak ground surface acceleration, a_{max}, due to earthquake loading (Seed and Idriss, 1971):

$$CSR = 0.65 \frac{a_{max} \, \sigma_{v0} r_d}{g \sigma'_{vo}}$$

$$\text{(3.2)}$$

Where σ_{vo} is the total vertical stress, r_d is a stress reduction coefficient to account for soil deformability, and g is the gravitational acceleration constant.

To equate transient field shaking to cyclic laboratory shaking, a factor of 0.65 is introduced. Since the method used to calculate the factor of safety is based on an earthquake magnitude of 7.5, the equation is adjusted using a magnitude scaling factor. To account for variations in shaking duration caused by earthquakes of different magnitudes. Additionally, Seed and Idriss introduced the relation between percent fines in soil and liquefaction-resistance (Figure 3.7).

The same approach was applied to this research with the expectation that the percentage addition of waste products will effectively increase fly ash resistance against earthquake loading.
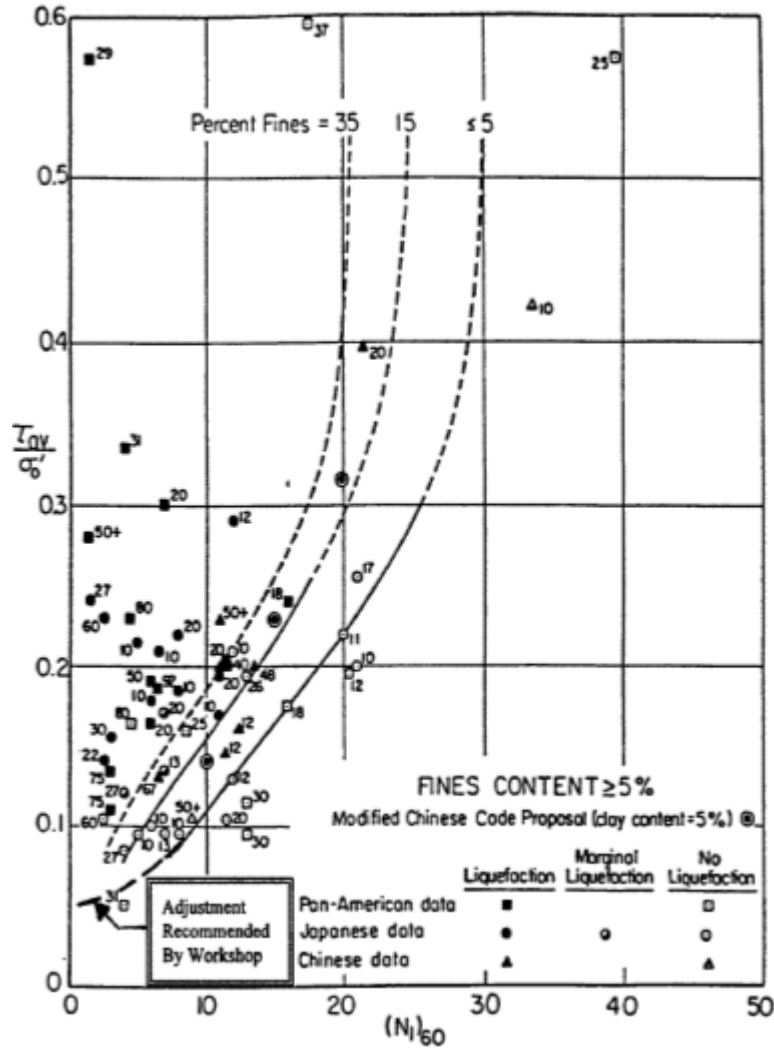
Figure 3.7: Correlation between equivalent uniform cyclic stress ratio and SPT ($N_{1)60}$ – Value for events of magnitude M ≈7.5 for varying fines contents, (Youd, et al, 2001).

Based on Youd, et al., (2001), correlation between equivalent uniform cyclic stress ratio (CSR) and Standard Penetration Test (SPT) for Magnitude (M) = 7.5 for varying fines contents, with adjustments at low cyclic stress ratio as recommended by the National Center for Earthquake Engineering Research (NCEER) working group.

In this study, using CSR values of 0.15, 0.30 and 0.50 already cover low to high CSR and using 0.50 CSR as a maximum limit for this research is appropriate because CSR greater than 0.50 would normally result in the liquefaction of the specimens with very low number of cycles and it will be very difficult to compare.

Chapter 4

TYPICAL RESULTS FROM LABORATORY TESTING

4.1   Introduction

In this chapter, selected representative results from this study are presented. The results will be separated in two sections. In the beginning, the mechanical and chemical properties of Class F fly ash and waste materials are summarized. Next, shows the dynamic properties of Class F fly ash from cyclic shear strain and used to find the relationship between the shear modulus and the damping ratio versus cyclic shear strain.

4.2   Static Tests

This section shows the results of specific gravity, grain size distribution, and XRD-testing. First, specific gravity is presented. These properties are important because they are used as input data to run cyclic triaxial testing.

The waste materials used in this study have lower specific gravity than Class F fly ash and when used as additives decreased specific gravity of the fly ash sample. The average of specific gravity results were used as an input data for cyclic triaxial testing with the assumption that specimen combination tested govern and also used to determine the confining pressure during testing.

There are ten (10) samples in this study, three (3) for specimens of Class F fly ash, two (2) for 10% rubber, three (3) for 5% carpet fiber and two (2) for 10% paper. As shown in Table 4.1, the results for specific gravity testing range from 2.02 to 2.19. The result shows agreement that fly ash particles are cenosphere or hollow particles made largely of silica and alumina. The prior characteristics (i.e. hollow, spherical particles and uniform gradation) in turn explain the lower compacted densities of fly ash relative to conventional earth fill compacted to the same effort.

Next static tests, including grain size distribution, were run to get the results of representative samples prepared and tested using mechanical sieve and hydrometer. Figure 4.1 shows the combined results of Class F fly ash from mechanical sieve and hydrometer. The gradation curve will be used to determine liquefiable potential of Class F fly ash using Tsuchida (1971), "Chinese Criteria", Seed et al. (2003), and Bray & Sancio (2004). The discussion will be explained in Chapter 5.

.

Table 4.1: Specific gravity of selected samples used in this study

Specimen	F100			F90R10	
Mass of flask filled with water (grams)	678.9	678.35	673.56	668.78	678.52
Mass of flask filled with soil and water (Grams)	713.27	712.75	706.69	699.23	709.15
Mass of dry soil (Grams)	63.56	63.19	61.09	60.43	60.35
Specific gravity of soil solids (Gs)	2.17	2.19	2.18	2.02	2.03
Water Temperature (Celcius)	20.5	20.5	20.5	20.5	20.5
Correction factor (K)	0.9999	0.9999	0.9999	0.9999	0.9999
Specific gravity of soil solids at 20 degree celsius	2.17	2.19	2.18	2.02	2.03
Average	2.18			2.02	

Specimen	F95C5			F90P10	
Mass of flask filled with water (grams)	678.28	671.3	678.82	675.32	678.98
Mass of flask filled with soil and water (Grams)	711.18	703.59	711.86	708.17	713.29
Mass of dry soil (Grams)	60.39	60.58	63.04	60.94	64.62
Specific gravity of soil solids (Gs)	2.20	2.14	2.1	2.17	2.13
Water Temperature (Celcius)	20.5	20.5	20.5	20.5	20.5
Correction factor (K)	0.9999	0.9999	0.9999	0.9999	0.9999
Specific gravity of soil solids at 20 degree celsius	2.20	2.14	2.10	2.17	2.13
Average	2.15			2.15	

Definitions:

F = Class F Fly Ash   R = Crumb Rubber

C = Carpet Fiber   P = Shredded Paper

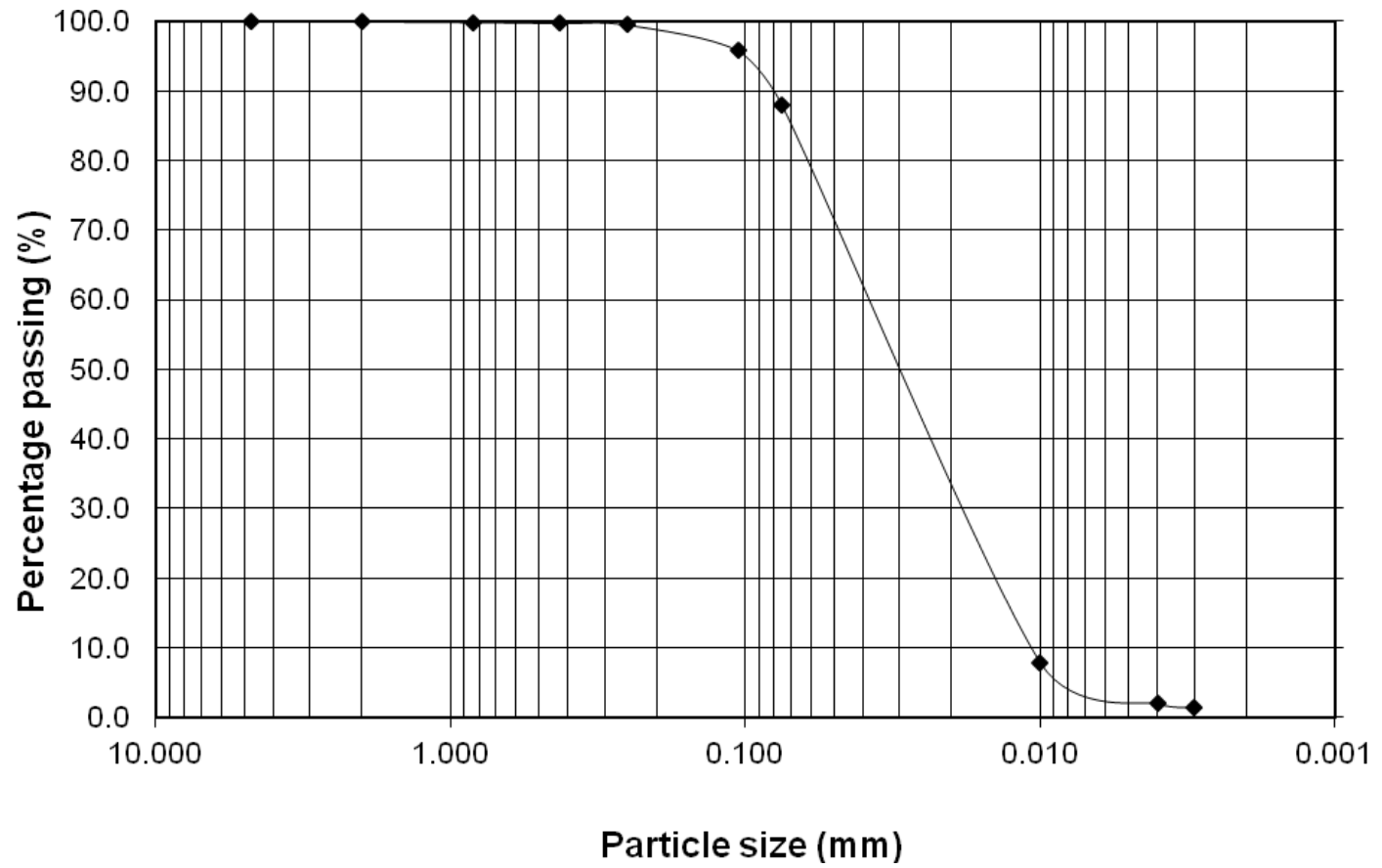100, 95, 90, 10, and 5 = Percentage of Waste Material by Dry Weight

Figure 4.1: Grain size distribution of Class F fly ash used in this study

For this research, to establish the chemical composition of the fly ash specimens, the X-Ray diffraction (XRD) method was used (Figure 4.2). The XRD uses x-ray radiation. For preparation, a powder sample of Class F fly ash specimen is pressed into a sample holder with a smooth surface (Figure 4.3) and the sample is placed at an angle of 45 degrees. After mounted, the sample is exposed to X-rays while rotate in the path at an angle, which scatters the X-rays into a pattern or reflections. Figure 4.4 shows the diffractograms result, with the X-axis in degrees (2-theta) and the Y-axis is the counts per second.

Figure 4.2: The X-Ray diffraction (XRD) machine used in this study

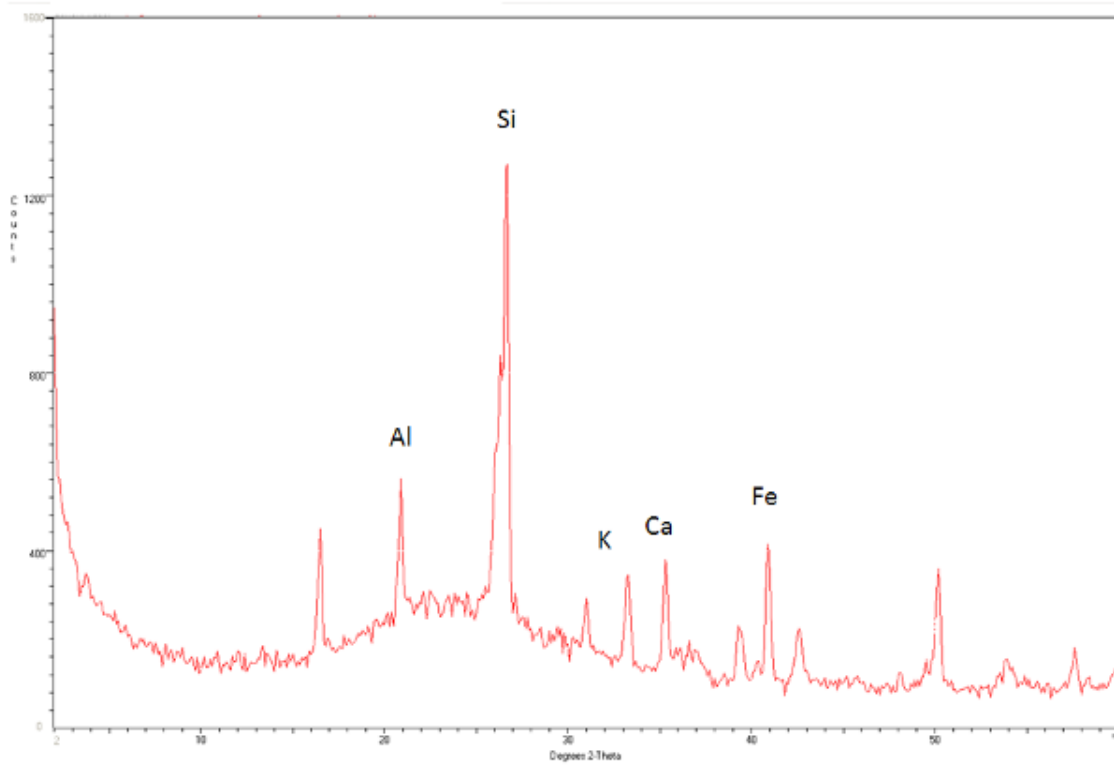Figure 4.3: Sample holder for the X-Ray diffraction (XRD) test

Figure 4.4: Chemical composition of typical Class F fly ash used in this study

Based on mineralogy from XRD test above, the fly ash used in this study (Figure 4.4) contains more than 70% of quartz (major constituent of most soils and glassy constituents) and lower calcium (CaO or lime) content which is in agreement with typical Class F fly ash.

4.3   Dynamic Tests

4.3.1   Development of Modulus Reduction Curves

In determination of site response analysis in geotechnical engineering, shear modulus and damping ratio of the material are used (ASTM D3999). For clay and sand, these properties can easily be estimated using existing references but for fly ash can be measured by performing cyclic triaxial tests in the elastic deformation range per the ASTM D3999 standard. The reconstituted specimens were tested using relatively small cyclic deviator stress (1 psi) so that the deformation was very small (in the elastic range) and the increase in the pore pressure was minimal. The intent was to measure the shear modulus and the damping ratio of the sample in the inelastic shear strain. Figure 4.5 shown a schematic hysteresis loop produced during a cyclic triaxial test.
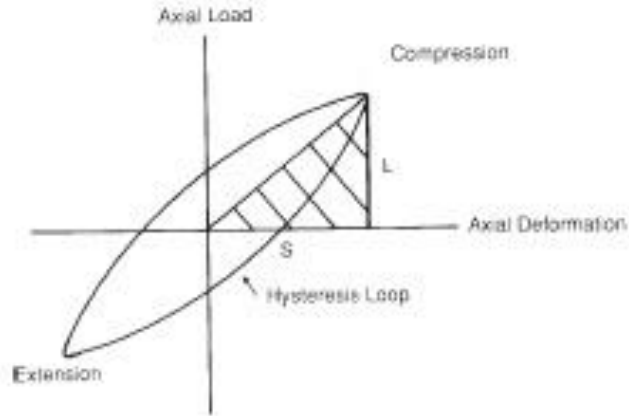
Figure 4.5: Schematic illustration of a hysteresis loop from cyclic triaxial testing (ASTM D3999).

The damping ratio of the material at a given shear strain imposed by harmonic cyclic loading is calculated as:

$$D = \frac{A_L}{4\pi A_T} \tag{4.1}$$

where, A_L is the area of the loop and A_T is the area of the hatched triangle.

The shear modulus of the sample at this strain level is calculated by $G = E/2(1+v)$, in which E is the Young's modulus of the specimen and v is the Poisson's ratio. The shear modulus values are normalized to the maximum shear modulus value, G_{max}, obtained at less than 0.001% of shear strain. Since the samples are saturated before applying the load, the Poisson's ratio is assumed to be 0.5 and Young's modulus is calculated as:

$$E = \frac{L_{DA}}{S_{DA}} \times \frac{L_S}{A_S} \qquad\qquad (4.2)$$

where L_{DA} is the double amplitude load, S_{DA} is the double amplitude deformation, L_S is the height of the specimen after consolidation and A_S is the area of the specimen after consolidation.

The imposed shear strain in this loop is calculated by using:

$$\gamma_{SA} = \varepsilon_{SA}.(1+v) \qquad\qquad (4.3)$$

where ε_{SA}, single amplitude axial strain, is found by using $\varepsilon_{SA} = \varepsilon_{DA}/2$, where ε_{DA} is the double amplitude axial strain and is calculated by $\varepsilon_{DA} = S_{DA}/L_S$. Additional validation is performed by checking if the specimen experienced shear strains that exceeded the recommended value of 0.01% per the ASTM D3999 standard.

It should be noted that the results for shear modulus and damping ratio versus cyclic strain ratio of Class F fly ash used in this study are best fit lines as shown in Figure 4.6 and Figure 4.7. However, it is emphasized that the number of tests in this study were limited and the measurement of small strains were not highly accurate. Table 4.2 shows the properties of Class F fly ash specimens used to generate the modulus reduction curves developed in this study.

Table 4.2: Properties of fly ash specimens used to develop modulus reduction curves

Composition	γSat (Pcf)	e	Asked SD P-P (Psi)	Confining Pressure (Psi)	CSR
F100	93.710	0.95	2	7.13	0.035
			3	7.13	0.052
			4	7.13	0.069
			5	7.13	0.087

Definitions:

F = Class F Fly Ash

100 = Percentage of Waste Material by Dry Weight
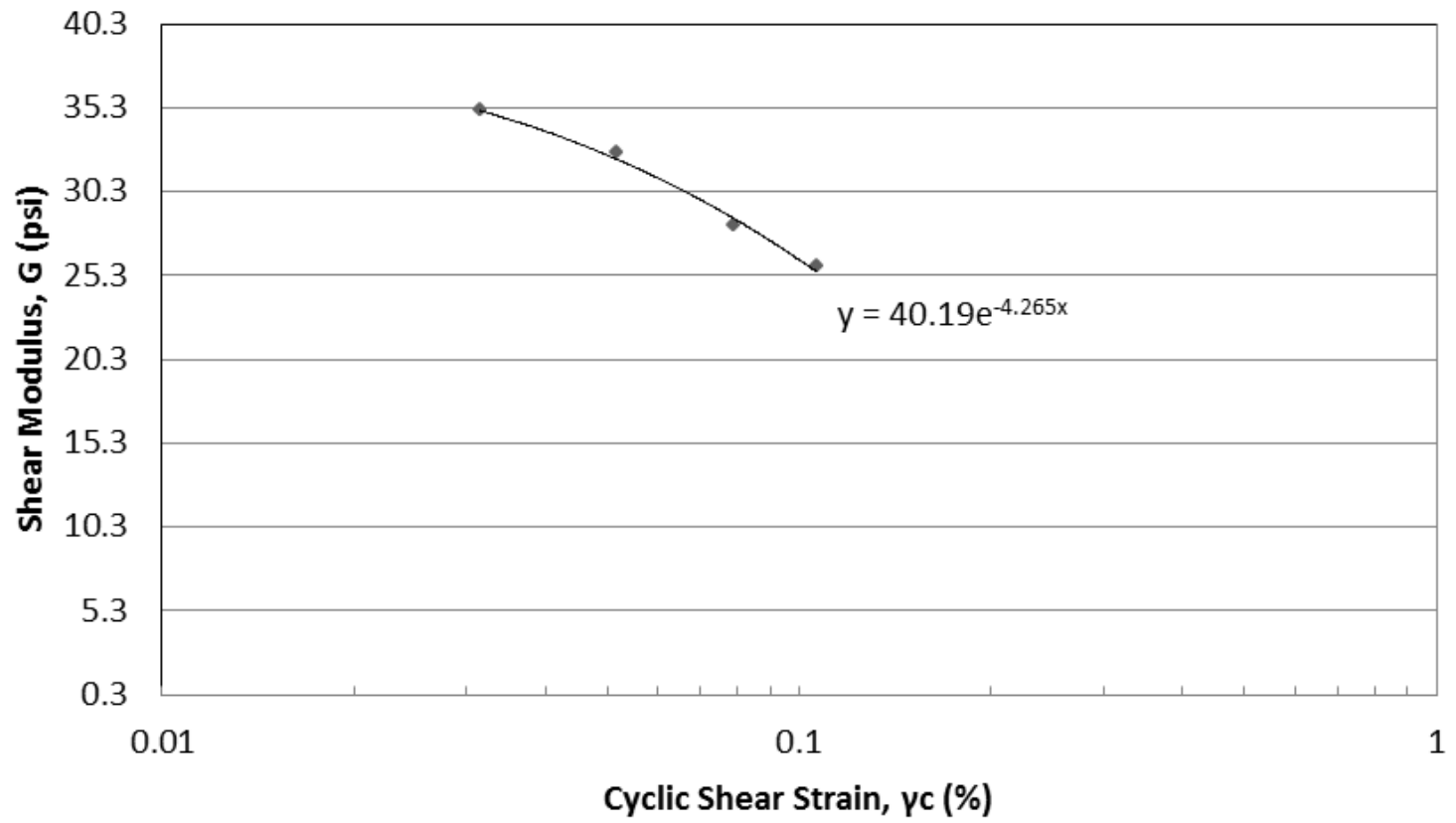
SD P-P = Standard deviator peak-to-peak

$$y = 40.19e^{-4.265x}$$

Figure 4.6: Shear modulus versus cyclic shear strain graph
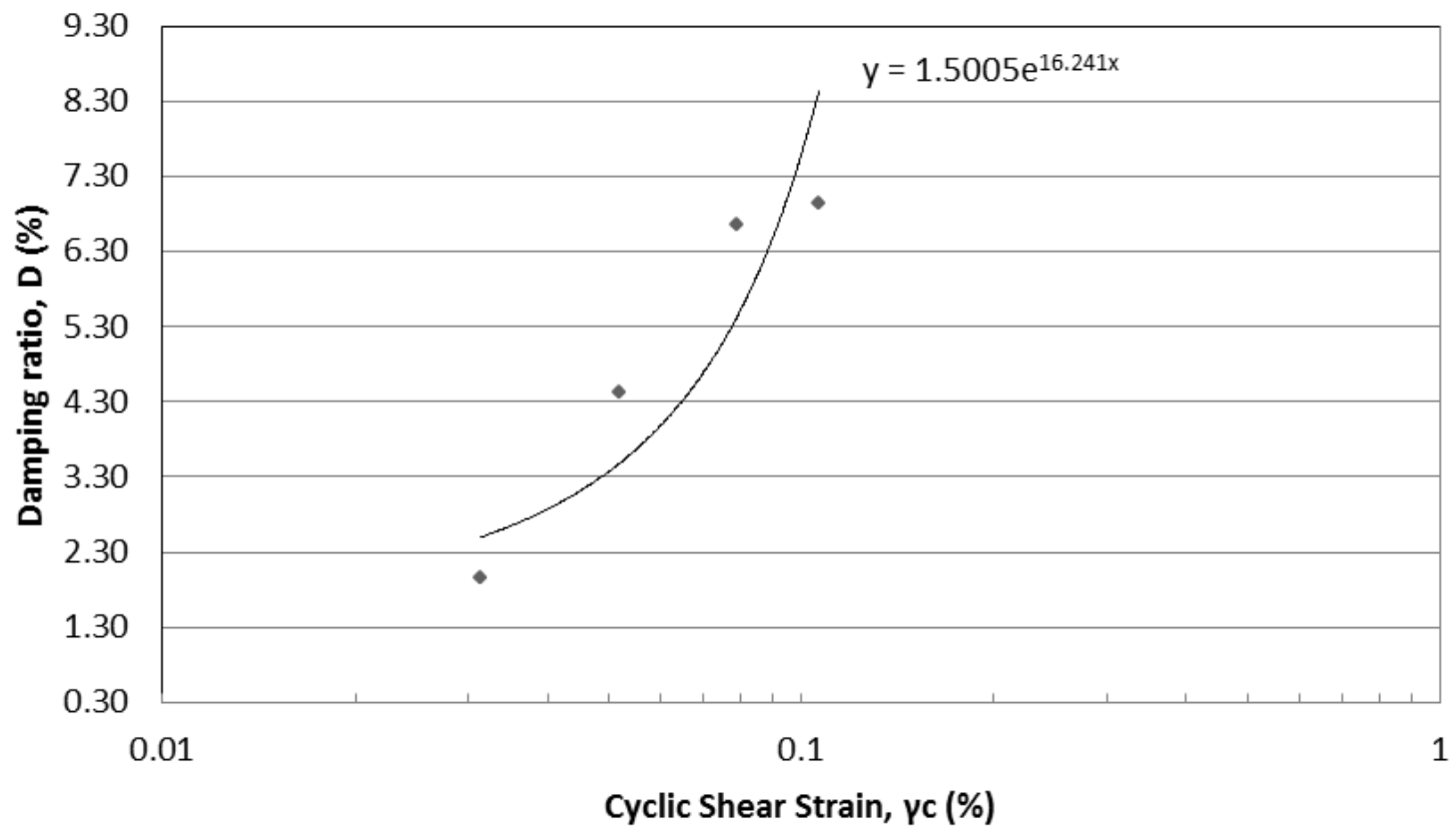
Figure 4.7: Damping ratio versus cyclic shear strain graph

4.3.2 Cyclic Triaxial Testing (ASTM D5311)

This test is commonly used to measure the variation of pore pressure and strain potential of saturated soils. For this test, there are 11 different combinations with the compositions of waste materials range from 1.5 – 20.0% as shown in Table 4.3.

To refer to each individual sample based on percentage of dry weight of waste material, a code system was used using alphabetical characters and number. For example, a specimen with a combination of Class F fly ash and crumb rubber with a composition of 90% fly ash and 10% crumb rubber was named F90R10 (F = Class F fly ash, R = Crumb rubber and 90 and 10 is the amount of dry weight used). The same code also applied to carpet fiber and shredded paper using code of C and P, respectively.

The specimen compositions reported in this research are based on dry weight. The maximum amount of 20% ratio was used as a maximum value to maintain fly ash as the primary material. The decision was based on specimen dimensions, especially for carpet and paper, where a ratio higher than 20% tended to occupy more space and make the primary material (fly ash) behave more like a filler. Figure 4.8 shows how 20% shredded paper combination makes fly ash behave as filler to the paper.

Table 4.3: Various ratios of fly ash specimens and results data from different tests

Percentage Specimen	Class F Fly Ash	Crumb Rubber	Shredded Paper	Shredded Carpet
F100	100	-	-	-
F98.5C1.5	98.5	-	-	1.5
F98C2	98	-	-	2
F95C5	95	-	-	5
F80C20	80	-	-	20
F95R5	95	5	-	-
F90R10	90	10	-	-
F80R20	80	20	-	-
F98P2	98	-	2	-
F90P10	90	-	10	-
F80P20	80	-	20	-

Definitions:

F = Class F Fly Ash   R = Crumb Rubber

C = Carpet Fiber   P = Shredded Paper

100, 98.5, 98, 95, 90, 80, 20, 10, 5, 2 and 1.5 = Percentage of Waste Material by Dry Weight

Figure 4.8: 80% Fly ash Class F and 20 % shredded paper

The deviator stress applied in this study is in cyclic form and is determined based on a CSR value. There were three (3) CSR values used; 0.15, 0.30 and 0.50. The cyclic deviator stress was applied at a frequency of 0.5 Hz.

For this test stresses are selected based on an assumed depth of the specimen a 10.0 m (32.8 ft). The reason of using this depth was based on failure history of storage pond treatment in The Ohio Power Plant (Figure 4.9 and Figure 4.10,). Depth of the specimen is used to select the confining pressure applied to the sample during testing.

Figure 4.9: Storage pond failure at a power plant in Ohio

Figure 4.10: Height of impoundment facilities failure at a power plant in Ohio

To interpret the results from testing, parameters including axial strain, deviator stress, time, number of cycles, pore pressure, and cell pressure were evaluated.
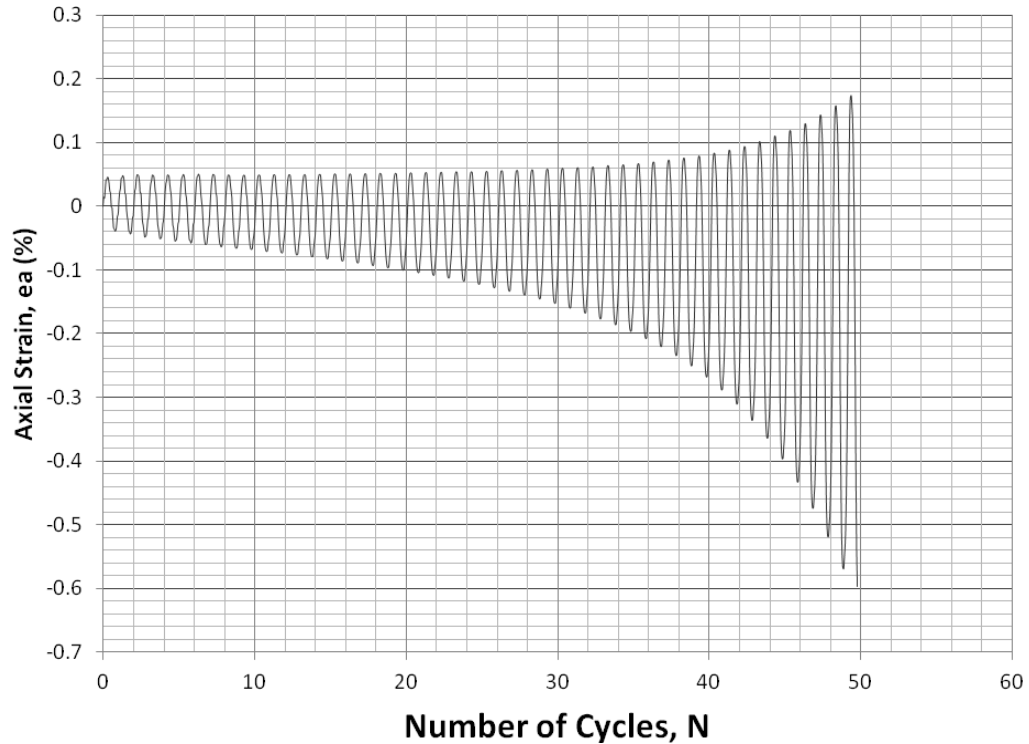
Figure 4.11: Schematic Illustration of axial Strain versus number of cycle graph

Figure 4.11 depicts axial strain versus number of cycles for a typical test.   From the graph when the axial strain shows negative value this means the specimen is in extension and positive value means the specimen is in compression. As a common strength property of soil materials, the tensile resistance is much less than the compressional resistance. However, axial strains remain relatively low (less than 2%) throughout the test.

In this study specimens were tested under load controlled and strain-controlled test. Load controlled test means stress applied to the specimen is constant during testing. In this study the deviator stress is applied based on depth, density, volume and weight of the specimen. For the cyclic triaxial tests deviator test is related with cyclic stress ratio (CSR), the *CSR* is denoted by CSR_{TX}, and is defined as the ratio of the half the applied peak deviator stress to the initial isotropic effective stress $(CSR_{TX} = \sigma_d/2\sigma_c')$. Under undrained conditions (i.e. a Mohr-Coulomb failure envelope with a friction angle of zero), the term $\sigma_d/2$ is equal to the cyclic shear stress, τ_{cyc}.

Although deviator stress during testing should be constant, after time, deviator stress decreases and as axial strain increase slightly before the effective stress reaches zero. This occurs because during testing the deviator stress decrease means the specimen cannot withstand the stress given and has been softened by cyclic loading.

The expectation from deviator stress versus number of cycles graph is to record the stress a specimen can handle at pre and post-liquefaction as shown in Figure 4.12.
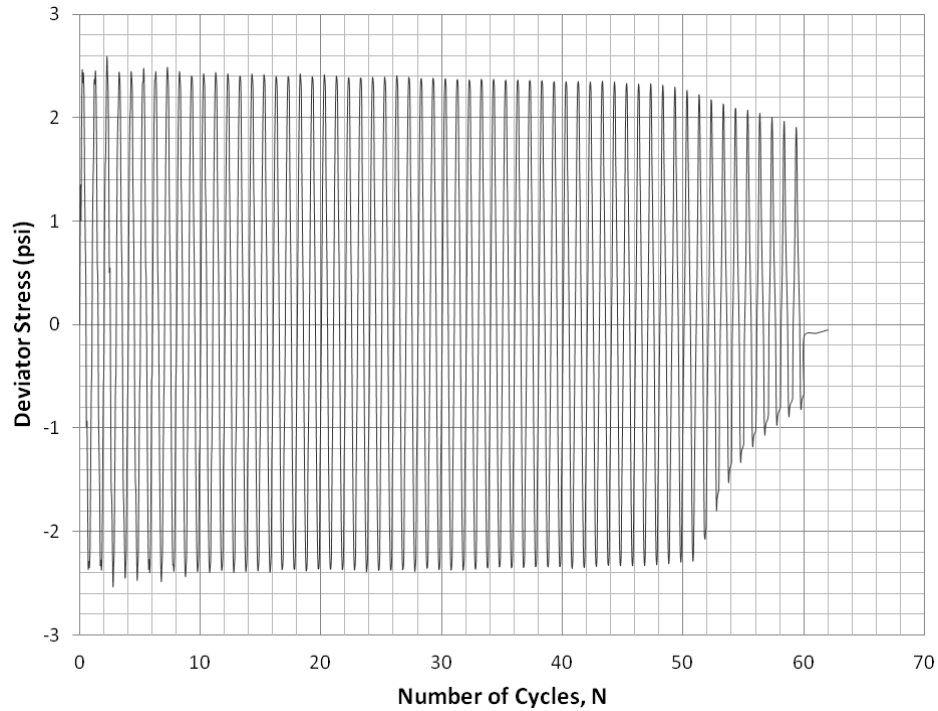
Figure 4.12: Schematic Illustration deviator stress versus number of cycle graph

Next, examples of excess pore pressure versus number of cycles graph (Figure 4.13) and excess pore pressure ratio versus normalized number of cycles graph (Figure 4.14) are presented. The importance of these graphs is to show how many cycles are necessary for the sample to liquefy. The number of cycles is normalized by dividing the number of cycle by the total number of cycles required to reach a pore pressure ratio of 1.0. Specimens with a 0.08 cyclic stress ratio (CSR) need more cycle to liquefy compare to specimen with a higher CSR. In the cyclic triaxial testing performed in this study, pore water pressure was measured using a pressure transducer connected to the bottom of the specimen. The reliability of the pore water pressure values recorded by the transducer depends on the hydraulic conductivity of the specimen and the rate at which the pore pressure variations distribute throughout the specimen.

85
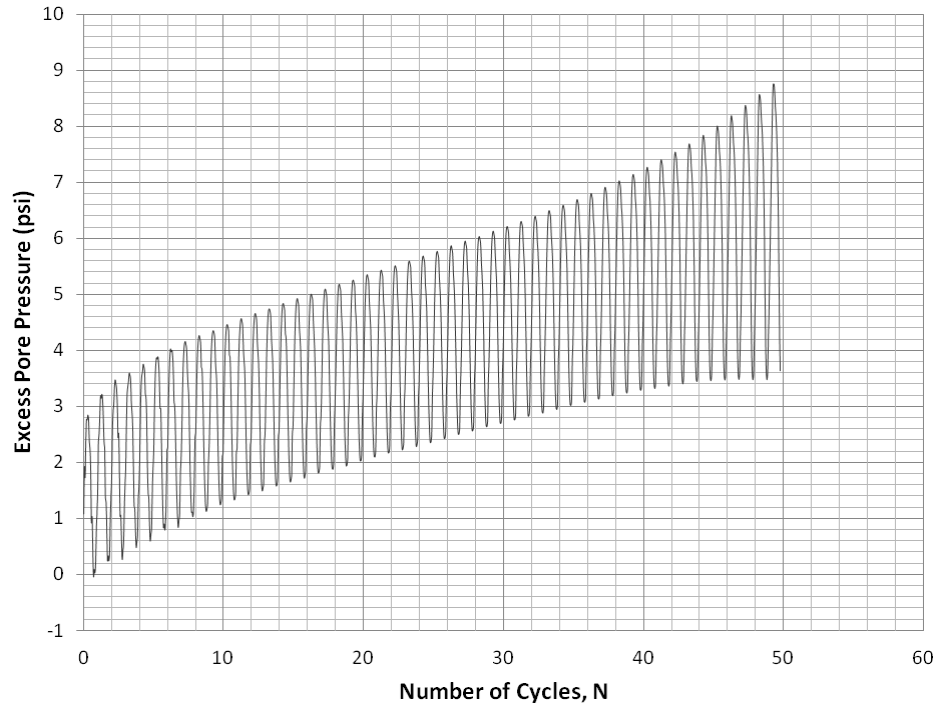
Figure 4.13: Schematic Illustration of excess pore pressure versus number of cycles graph
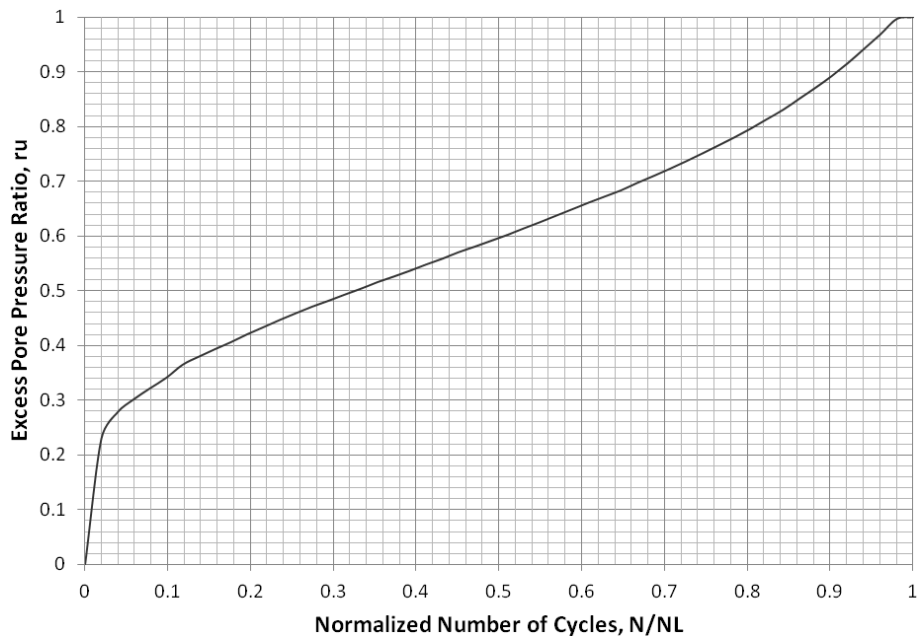
Figure 4.14: Schematic Illustration of excess pore pressure ratio versus normalized number of cycles graph

The graph of excess pore pressure versus number of cycles is also used to investigate how waste material will affect the number of cycles. Comparison tables and graphs are presented in Chapter 5.

Finally, peak-to-peak deviator stress versus axial strain is evaluated (Figure 4.15). The hysteresis loops shown in the beginning specimen still have higher stiffness and the loops are relatively steep. As the test progresses, the loops flatten as the specimen softens. The hysteresis loops also shows the change in length during testing. Initially, the samples shorten and lengthen at equal amounts. However, this condition only stands while the specimens have higher stiffness before excess pore pressure developed. Afterward, shortening exceeds extension. The loop also becomes broader as the specimen experience higher strain levels.

Before the test end, the loops begin to exhibit a banana-like shape which is indicative of strain hardening. At this stage, the sample begins to dilate. This strengthening effect enhances the ability of fly ash to hold higher stresses at the post-liquefaction condition.
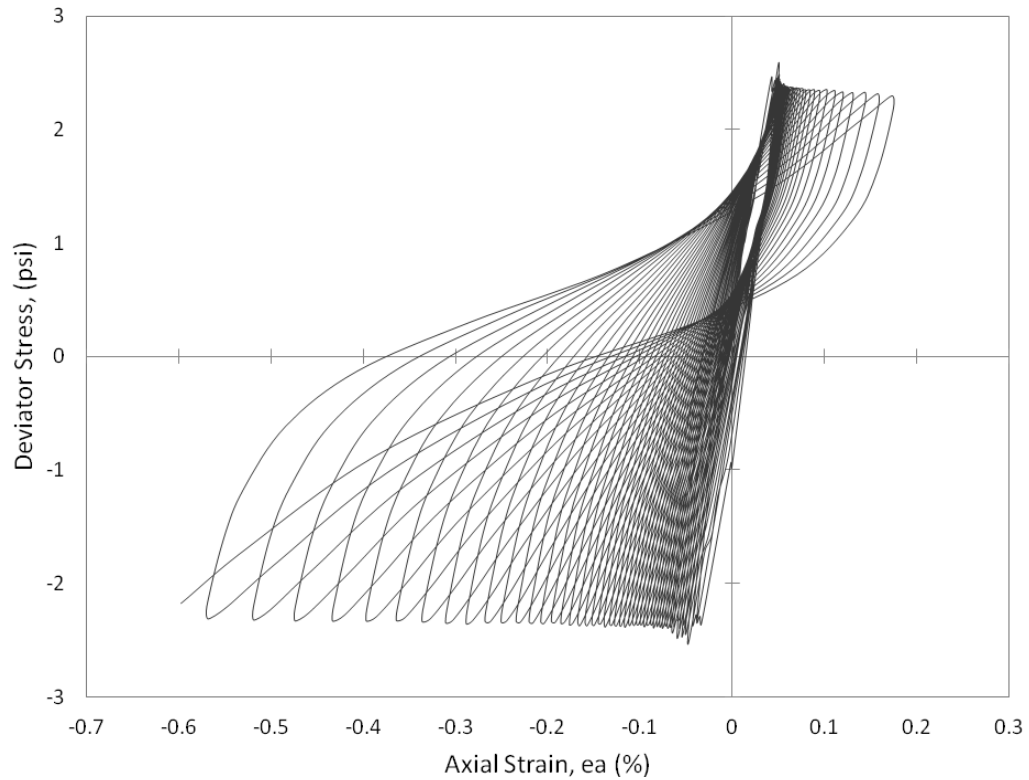
Figure 4.15: Schematic Illustration of deviator stress versus axial strain graph

After the graphs are evaluated, the next step is to determine the liquefaction limit. In this study liquefaction is defined in two ways. First, the excess pore pressure ratio (r_u) which is the ratio of excess pore pressure to confining pressure, is equal to 1 at liquefaction, and at this point the specimen experiences larger strain levels. Second, a 5% axial strain typically means the sample has liquefied.
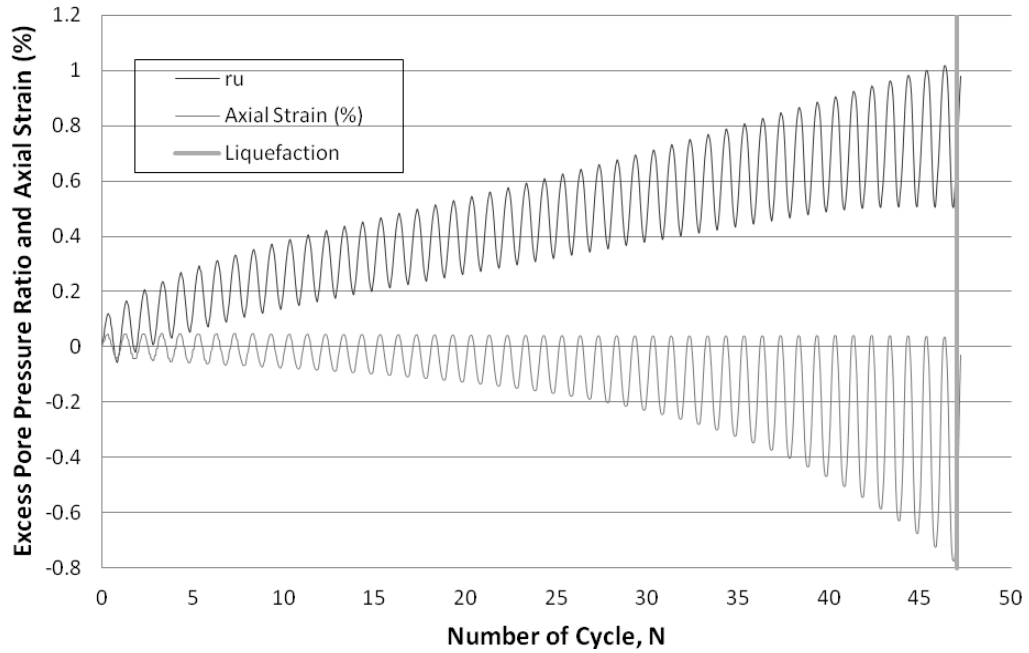
Figure 4.16: Schematic Illustration of excess pore pressure ratio and axial strain versus number of cycles graph

Figure 4.16 is an example of how to determine the number of cycles to liquefaction based on two definitions. As seen from the graph, r_u reached a ratio of 1 at an axial strain only 0.8% which in this case excess pore pressure (r_u) is define liquefaction Here, strain is limited due to cyclic mobility.

Chapter 5

INTERPRETATION OF TEST RESULTS

5.1   Overview

In this chapter, the analysis of mechanical properties and cyclic triaxial test results performed on fly ash and waste materials is addressed. The correlation between measured parameters with results from other research is explained. Samples were reconstituted following the ASTM D5311 procedure using the pouring method. The reconstituted specimens were created to represent specimens created using the field method of wet dumping. The fly ash samples are usually normally consolidated due to the dumping method. They have been constantly loaded and the overburdened stress has never been removed. In the lab, the samples were tested in the cyclic triaxial chamber as normally consolidated samples.

5.2   Specific Gravity

As shown in Table 5.1, specific gravity ranged from 2.02 to 2.19. One explanation for this lower average specific gravity is the fact that a high proportion of fly ash particles are cenospheres (hollow particles) made largely of silica and alumina which, partially explains the lower compacted densities of fly ash relative to conventional earth fill compacted to the same effort.

For cyclic triaxial input data, the value of specific gravity used was based on the average of the specific composition. The assumption used for specific gravity was the combination of fly ash with one additional material that used the same value although

the distribution of secondary material varies; in this case, 10% rubber, 5% carpet fiber

and 10% paper govern.

Table 5.1: Specific gravity results for specimens tested

Specimen	Specific Gravity
F 100	2.18
F98P2	
F90P10	2.15
F80P20	
F98.5C1.5	
F98C2	
F95C5	2.15
F80C20	
F95R5	
F90R10	2.02
F80R20	

Definitions:

F = Class F Fly Ash   R = Crumb Rubber

C = Carpet Fiber   P = Shredded Paper

100, 98.5, 98, 95, 90, 80, 20, 10, 5, 2 and 1.5 = Percentage of Waste Material by Dry Weight

5.3   Grain Size Distribution

Table 5.2 is the grain size distribution of fly ash used in this study, which is similar to the typical fly ash gradation curve presented in Chapter 2. Many of the commonly used procedures for evaluating liquefaction are largely based on field and laboratory testing of clean sands or sands with a limited amount of fines. Wang (1979) was one of the first to establish liquefaction criteria based on the observations from many earthquakes. His criteria stated that soils are susceptible to liquefaction if they meet the following criteria: Percent of particles less than 5 μm < 15% to 20%, and w_c/LL > 0.9.

Based on the observations of Wang (1979), Seed and Idriss (1982) developed the "Chinese Criteria" which stated that clayey soils can be susceptible to liquefaction only if all three of the following conditions are met: Percent of particles less than 5 μm or 0.005 mm < 15%, LL < 35, and w_c/LL > 0.9. As shown in Table 5.2, fly ash used in this study contains a percent of particles less than 5 μm or 0.005 mm of 2.0 %, which is less than 15%. Because fly ash is non-plastic material, the plasticity index (PI) is equal to 0, which makes liquid limit (LL) also equal to 0, so all three criteria mention previously are satisfied and fly ash can be categorized as liquefiable material. As shown in Figure 5.1, the fly ash used in this study (symbolized with A star) falls in the susceptible area.
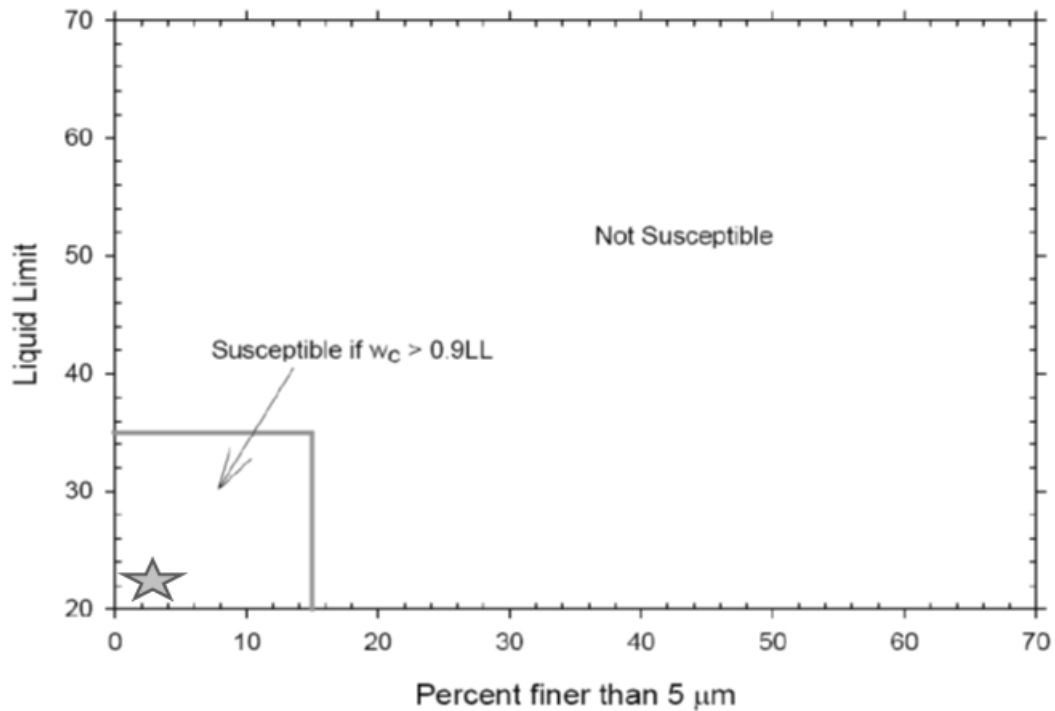
Figure 5.1: Liquefaction susceptibility based on Chinese criteria

Tsuchida (1970) provides 2 boundaries in the graph (Figure 5.2); potentially liquefiable and most liquefiable. The range for most liquefiable is narrower than the range for potentially liquefiable. Most liquefiable encompasses sandy type soils while potentially ranges from clay to gravelly type of soil.

Figure 5.2 is a composite of the Tsuchida curves with the fly ash grain size distribution from this research. The grain size distribution curve for fly ash is inside the range of susceptible liquefaction soil proposed by Tsuchida (1970). In agreement, Dey et al. (2008) concluded that pond ash is potentially liquefiable.

Table 5.2: Grain size distribution of Class F fly ash used in this study

SIEVE NUMBER	Diameter (mm)	Mass of Empty Seive (g)	Mass of Sieve + Soil Retained (g)	Soil Retained (g)	Cumulative % Retained	Cumulative % Passing
4	4.75	530.3	530.3	0	0.0	100.0
10	2	439.8	439.9	0.1	0.0	100.0
20	0.84	428.1	428.3	0.2	0.1	99.9
40	0.425	355.2	355.5	0.3	0.3	99.7
60	0.25	375.6	376.1	0.5	0.5	99.5
140	0.106	462.9	470.5	7.6	4.2	95.8
200	0.075	385.9	402.3	16.4	12.1	87.9
Pan	0.01	299.6	482.6	183	100	7.9
Hydrometer	0.004					2.0
	0.003					1.5
	0.0025					1.0
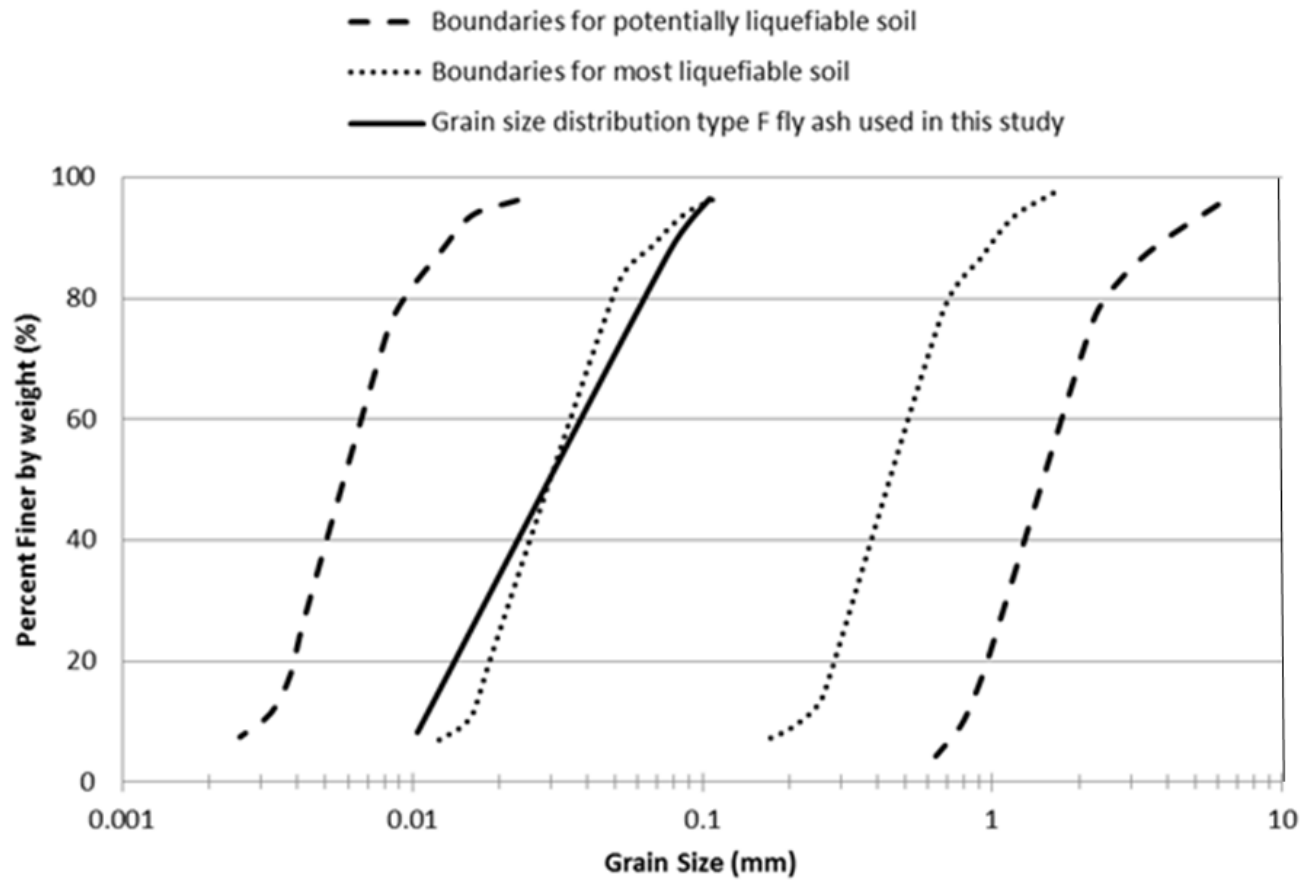
Figure 5.2: Tsuchida (1970) Vs. Grain size distribution of Class F fly ash used in this study

To investigate liquefaction susceptibility using Seed et al. (2003), Figure 5.3 has been prepared. This criterion relies on Plasticity Index (PI), w_c (water content) and Liquid limit (LL) and, is recommended for soil with fines content greater than 20% if the plasticity index is greater than 12% and soil with fines content greater than 35% if the plasticity index is smaller than 12%. Fly ash used in this study is non-plastic and fully saturated with a fines content of 87.9%, so it falls in Zone A (Symbolized with A star), meaning that the sample is potentially susceptible to liquefaction.
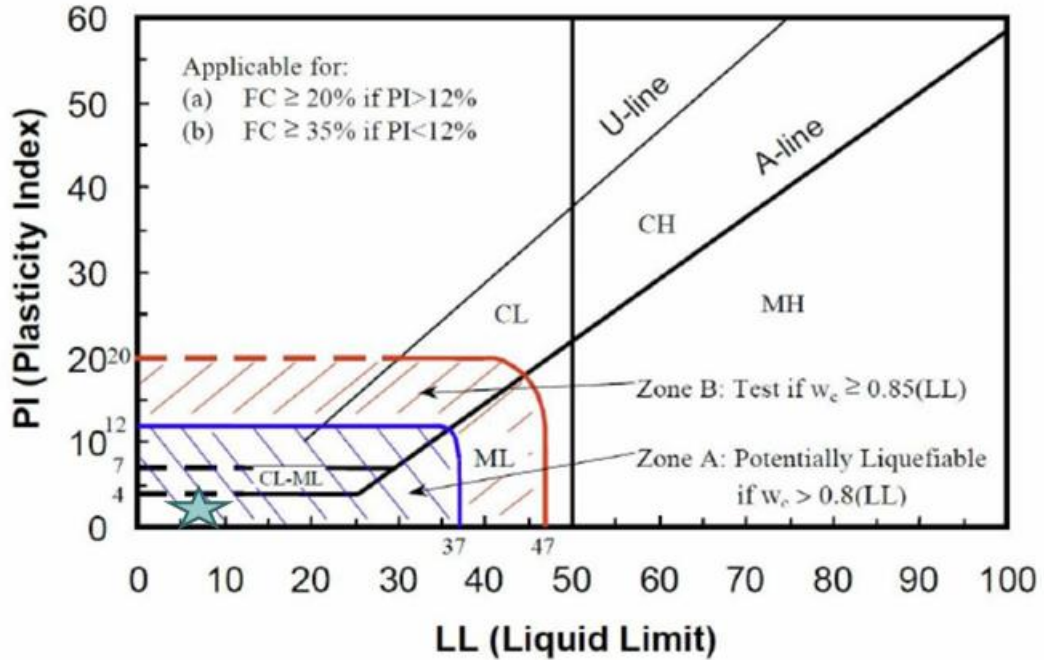
Figure 5.3: Liquefaction susceptibility based on Seed et al. (2003)

For Bray & Sancio (2004), there are three zones: susceptible, moderately susceptible and not susceptible. This criterion focuses on the type of soil minerals present in the structure of the soil and not the influence of fines content. The parameters used in this method are plasticity index (PI) and water content (w_c) over

liquid limit (LL) or w_c / LL. Fly ash samples used in this study had a characteristic: non-plastic and fully saturated, resulted in falling in the susceptible area (Symbolized with A star), which means the sample is potentially susceptible to liquefaction.
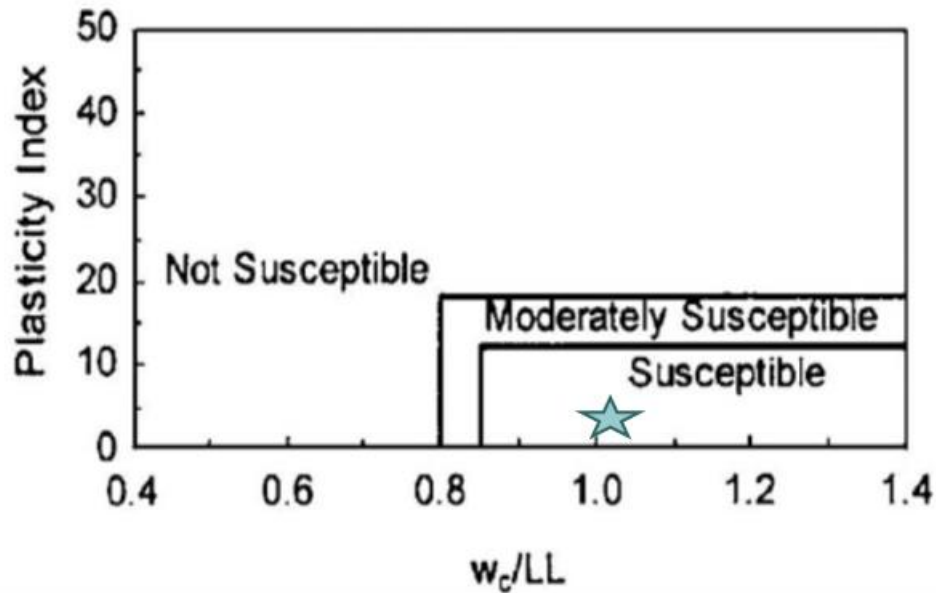
Figure 5.4: Liquefaction susceptibility based on Bray & Sancio (2004)

5.4   Plotting of Data to Identify Optimum Blends

There were four (4) specimens with different ratios tested for each type of waste materials. The objective here was to identify the percentage of each composition that shows the optimum performance with respect to cyclic loading. The test results are summarized in Table 5.4 and each waste material composition was plotted to identify the optimum blend (Figs. 5.5 – 5.7). The percentage of additive used ranged from 1.5% to 20.0% of dry mass. The cyclic test ratio (CSR) used to compare the results was 0.30.

For carpet fiber, a ratio above 5% of dry weight generates a specimen whose behavior is dominated by the additional material (carpet fiber) instead of the fly ash. The reason is the weight of carpet fiber. The mold used in this study has maximum diameter of 2.8 in and according to the ASTM D5311, a height-to-diameter ratio for the sample tested is 2.0 – 2.5 is desired. For this study the target ratio was 2.0 which made the height and diameter of all specimens tested relatively the same. Specimens of fly ash and carpet fiber had the lowest weight compared to others at the same percentage of dry weight as shown in Table 5.3. Because the fly ash and carpet fiber specimens had the lowest weight means shredded carpet used more space inside the mold. Nevertheless, 20% carpet fiber test was conducted to maintain fairness in comparison at the same maximum percentage for all waste materials. Due to the difficulties during mixing and to maintain fly ash as primary material, no specimens were tested above 20 percent content.

Table 5.3: Weight of specimens

Specimen	Net. Solid weight (lb)
F100	1.3519
	1.3879
	1.3997
F98P2	1.2547
F90P10	1.2312
	1.2765
	1.2794
F80P20	1.0973
F98.5C1.5	1.2642
F98C2	1.1155
F95C5	1.1155
	1.1447
	1.194
F80C20	0.922
F95R5	1.2536
F90R10	1.1986
	1.1968
	1.22
F80R20	1.2919

Definitions:

F = Class F Fly Ash   R = Crumb Rubber

C = Carpet Fiber   P = Shredded Paper

100, 98.5, 98, 95, 90, 80, 20, 10, 5, 2 and 1.5 = Percentage of Waste Material by Dry Weight

Afterward the blends where tested using CSR of 0.15 and 0.50 and the results were compared with Class F fly ash specimen tested using the same CSR. The expectation is one or more of the blend shows better results than Class F fly ash specimen.

Table 5.4: Specimen test results to find optimum combination

Specimen	Compositon	CSR	Void Ratio e	N cycles
Class F Fly Ash & Shredded carpet	F100C0	0.30	0.96	26
	F98.5C1.5	0.28	1.19	5
	F95C5	0.30	1.37	8
	F80C20	0.28	1.5	7
Class F Fly Ash & Crumb Rubber	F100C0	0.30	0.96	26
	F95R5	0.30	0.98	4
	F90R10	0.30	1.09	11
	F80R20	0.30	0.89	7
Class F Fly Ash & Shredded paper	F100C0	0.30	0.96	26
	F98P2	0.30	1.04	4
	F90P10	0.30	1.06	7
	F80P20	0.30	1.26	7

Definitions:

F = Class F Fly Ash   R = Crumb Rubber

C = Carpet Fiber   P = Shredded Paper

100, 98.5, 98, 95, 90, 80, 20, 10, 5, 2 and 1.5 = Percentage of Waste Material by Dry Weight
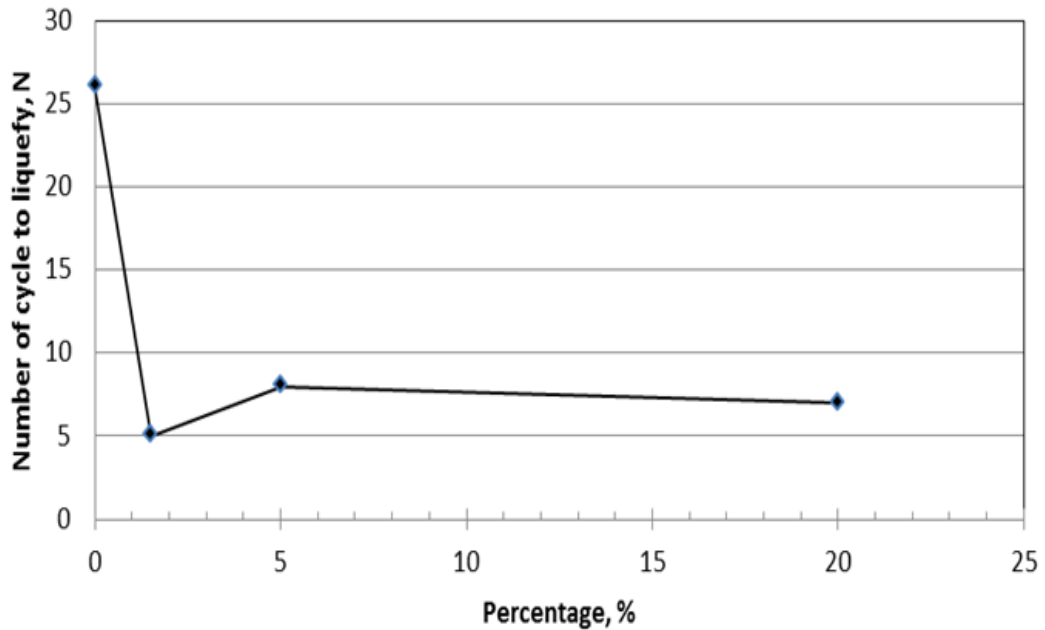
Figure 5.5: Number of cycles to liquefy versus percentage graph by dry weight (Fly ash Class F and Shredded carpet) at CSR = 0.30
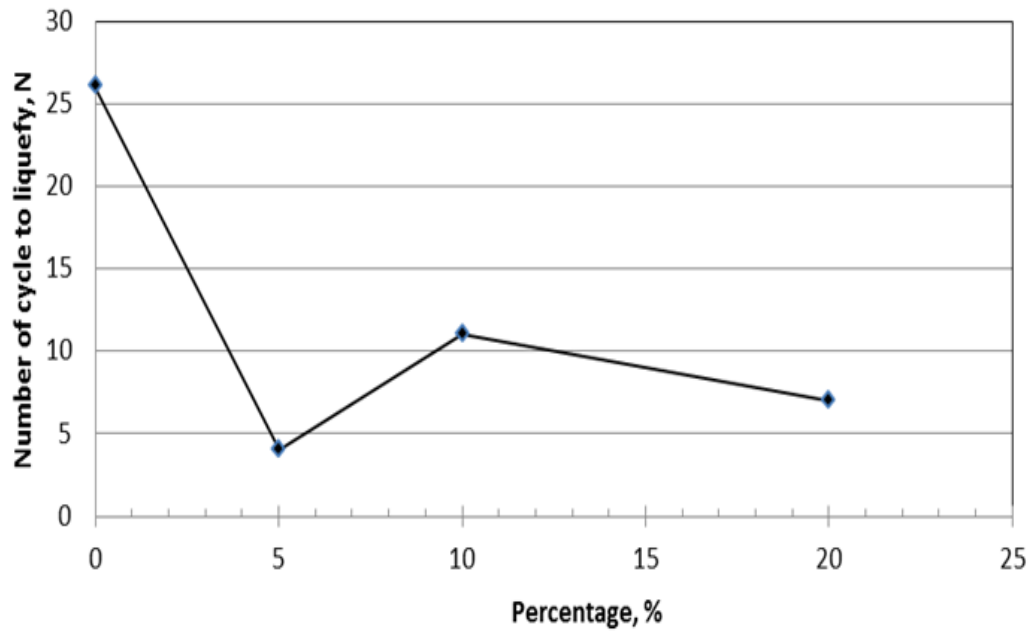
Figure 5.6: Number of cycles to liquefy versus percentage graph by dry weight (Fly ash Class F and Crumb rubber) at CSR = 0.30
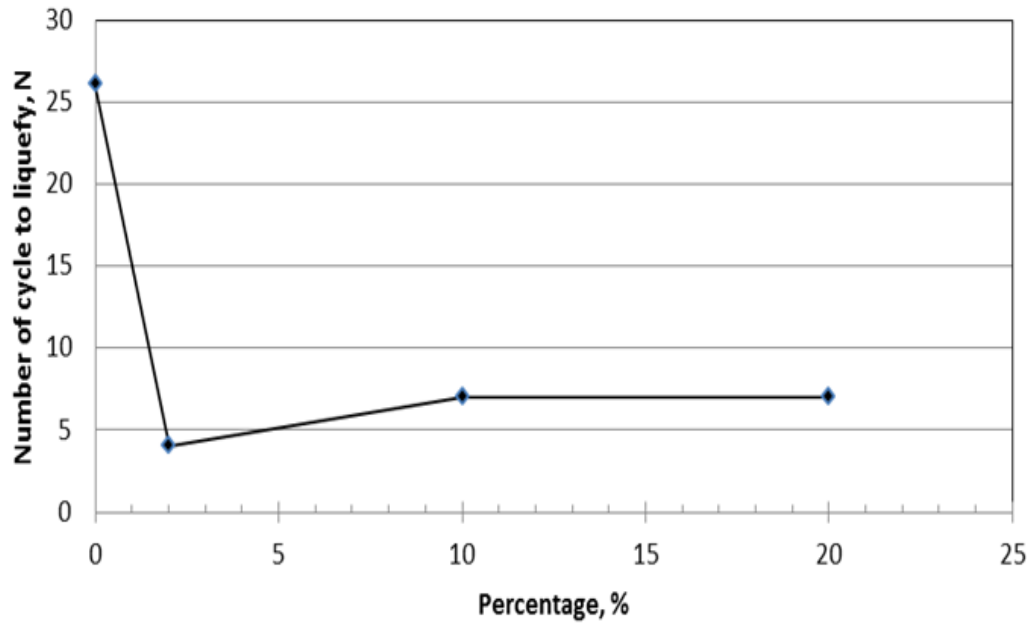
Figure 5.7: Number of cycles to liquefy versus percentage graph by dry weight (Fly ash Class F and Shredded paper) at CSR = 0.30

Shown in Figs. 5.5 – 5.7, there was an anomaly for 0% waste materials. The parameters that affected this condition are low void ratio, high confining pressure and high saturated density compare to others.

It should be noted that according to tests performed on reconstituted Sacramento River sand by Lee and Seed (1967) and Castro and Poulos (1977), the peak deviator stress required to cause peak cyclic pore pressure ratio of 100% increased linearly with an increase of the initial effective confining stress Also, it should be considered that these samples are reconstituted samples with variable void ratio. Therefore, the influence of void ratio, initial confining pressure and disturbance in applied deviator stress was not studied in depth. However, the preparation of reconstituted specimens was controlled for repetition and actual peak-to-peak deviator stress was observed to be relatively similar with target stress.

Without accounted 0% percentage, crumb rubber and shredded paper are optimum at around 10% composition. While for carpet fiber, the graph shows that sample with ratio of around 95% of fly ash plus 5% carpet is the best combination. The slight decrease in N at higher percentage was ascribed to the tendency of filler waste material to bunch. The properties of such composites are greatly influenced by shape, size, and distribution of the reinforcing phase apart from its chemical composition and volume fraction.

Therefore, percentage of around 10% may be taken as the optimum for shredded paper and crumb rubber. While for carpet fiber, a 5% composition was optimum.

Table 5.5 shows the summarized results of specimen comparison at optimum blend by dry weight. As shown, void ratio are varies from 0.96 to 1.46; in comparison, field in-situ void ratio for 12 meter ash deposit is 0.54-1.10 (Gandhi et al., 1997). Void ratio is a key indicator of the tendency of a soil to undergo volume change during drained shear and this volume change can be either contractive or dilative. As confining pressure increased, however, the behavior of the fly ash specimen started to exhibit contractive characteristics.

This study is load-controlled, so deviator stress during testing should be constant. Input data for deviator stresses were calculated from CSR values of 0.15, 0.30 and 0.50, but the machine might not be able to apply the input stresses as instructed. Based on the standard deviator or stresses executed by the machine, back calculation is needed to find the actual CSR values. Actual CSR can be calculated by adding maximum value of deviator stress and absolute value of minimum deviator stress for each tested specimen divided by 4.

Summarized results from Table 5.5 were also plotted in Figure 5.8. To illustrate the observed trend, linear trend lines were fitted to each dataset to extend the curves.

It shows at CSR higher than 0.4, the number of cycle for mixed specimens is 4. It means at this CSR number of cycle to liquefy and the strength properties do not increase.

Next, at a CSR around 0.30 the effect of waste materials has still not improved the fly ash properties. Finally, an effect of waste material is found at around 0.15 CSR with a combination of 90% fly ash with 10% rubber where the number of cycles to liquefy is higher than 100% Class F fly ash.

Table 5.5: Specimen information and test result of Class F Fly ash and selected composition

Specimen	γSat (Pcf)	e	Deviator Stress (Psi)	Confining Pressure (Psi)	Actual CSR	N cycles
F100	98.44	1.04	7.5	7.5	0.44	3
	99.91	0.96	4.7	7.8	0.30	26
	99.46	0.99	2.5	7.7	0.17	51
F95C5	91.61	1.46	6.2	6.2	0.44	4
	92.69	1.37	3.9	6.4	0.29	8
	92.5	1.38	2.2	6.7	0.16	29
F90R10	93.08	1.07	6.9	6.9	0.48	4
	92.86	1.09	4.1	6.8	0.30	11
	93.37	1.05	2.1	6.5	0.17	86
F90P10	96.85	1.08	7.8	7.8	0.47	4
	97.22	1.06	4.4	7.4	0.29	7
	96.09	1.13	2.5	7.6	0.17	47

Definitions:

F = Class F Fly As R = Crumb Rubber

C = Carpet Fiber P = Shredded Paper

100, 95, 90, 10, and 5 = Percentage of Waste Material by Dry Weight
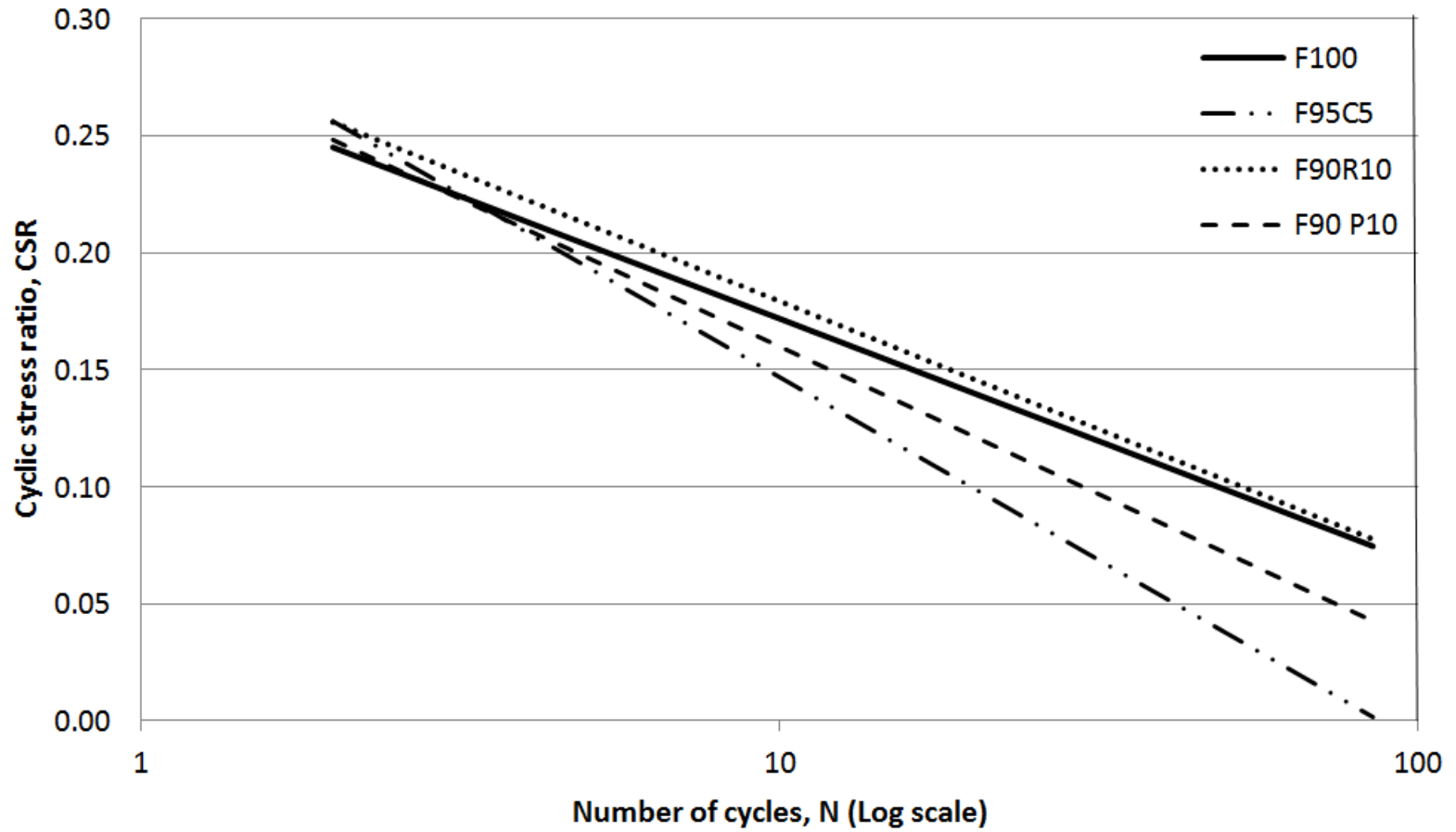
Figure 5.8: Test result of Class F Fly ash and selected composition

The improvement in fly ash admixtures, from earlier research as mentioned in Chapter 1, is due to skin friction between fly ash and other waste materials. When the specimen is loaded, skin friction and/or adhesion between fly ash and other waste material is functioning; the material apply pressure on fly ash, and the specimen get stretched with mobilization of tensile force but for this study the orientation of the fibers within the specimen was not accounted.

At 0.15 CSR, skin friction and/or adhesion between fly ash and other waste material was functioning before experiencing cyclic loading and liquefy. That is why the number of cycles to liquefaction of mixed specimen was higher compare to Class F fly ash. But at higher CSR (0.30 and 0.50 CSR) the same condition could not be found. Because at high CSR value, there were not enough time for the mixed materials to bonded together but suddenly experiencing cyclic loading, getting worse because the specimen has high void ratio.

Number of liquefaction can be increased by giving proper compaction to the specimen to reduce the void ratio, the same procedure will also press each particle inside the specimen to assure that skin friction and/or adhesion between fly ash and other waste material is functioning before undergoing cyclic loading.
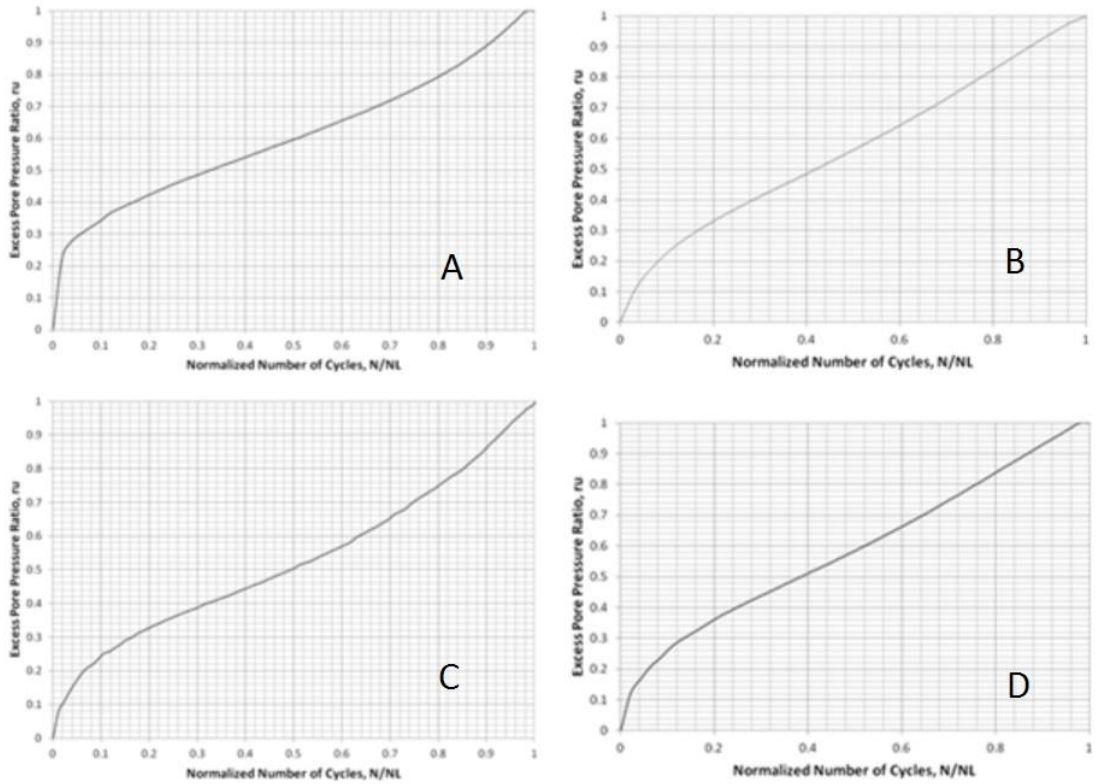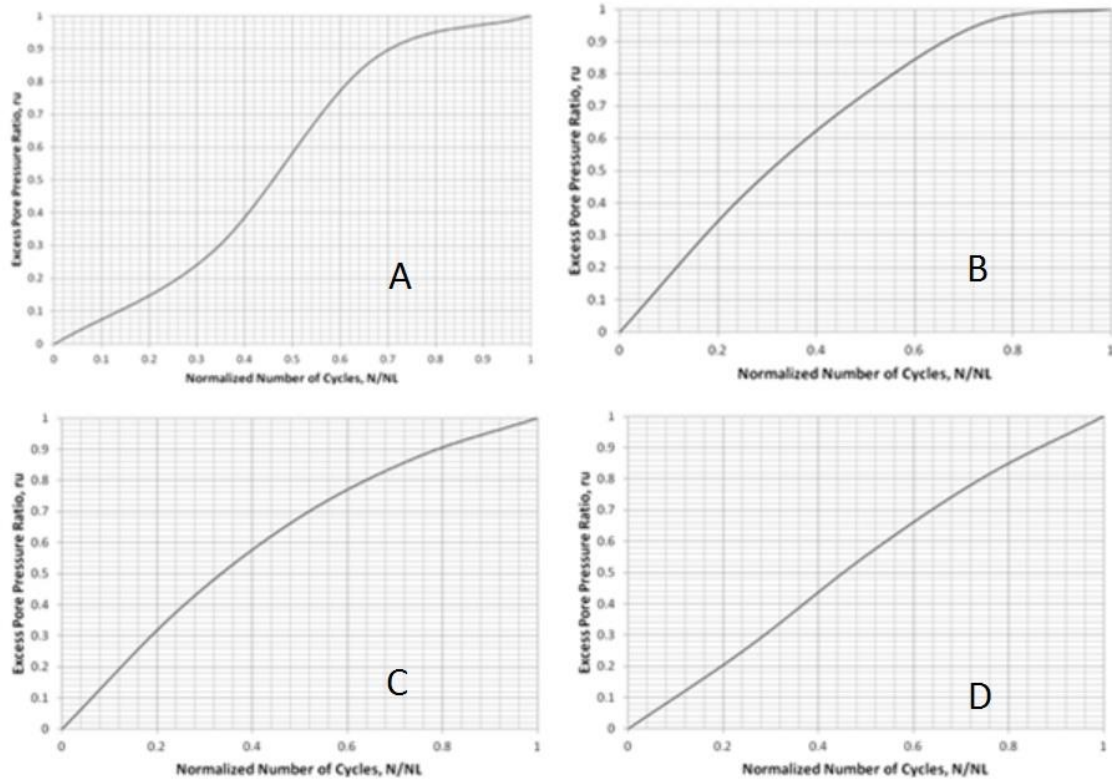
Figure 5.9: r_u versus N/N_L graph of 100% Class F fly ash (A), 5% carpet fiber (B), 10% crumb rubber (C) and 10% shredded paper (D) at 0.15 CSR

At lowest deviator stress used in this study or 0.15 CSR, as shown in Figure 5.9, all specimens reached liquefaction in same behavior. In the beginning of the test, when the specimen starts experiencing the pressure, the graph suddenly rises. This behavior happened because deviator stress not gradually increase up to target CSR but the input CSR value started from beginning. In this phase, the particle inside specimen starts to filling the void and getting denser. Next, after the specimen got compressed the graphs make a steady increase until reach liquefaction. At 0.15 CSR, there were no dissimilar behavior between Class F fly ash and mixed specimen because at low CSR, reaction between fly ash and waste material able to functioning at the beginning of the phase.
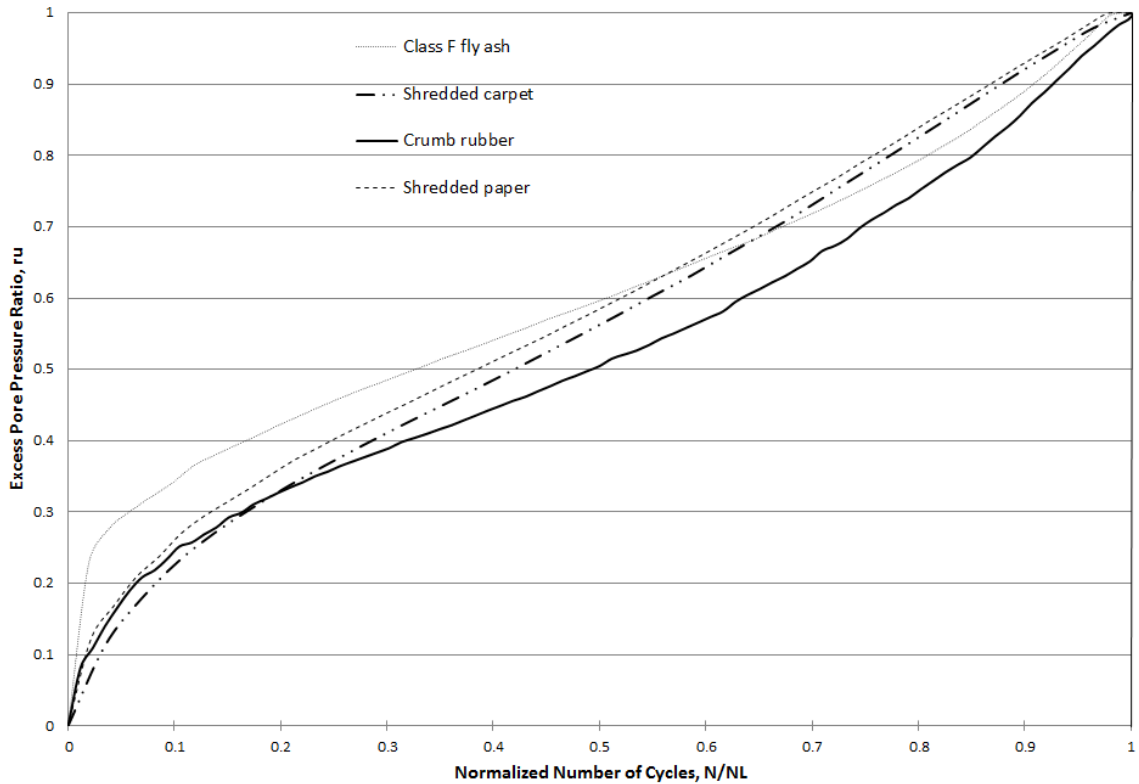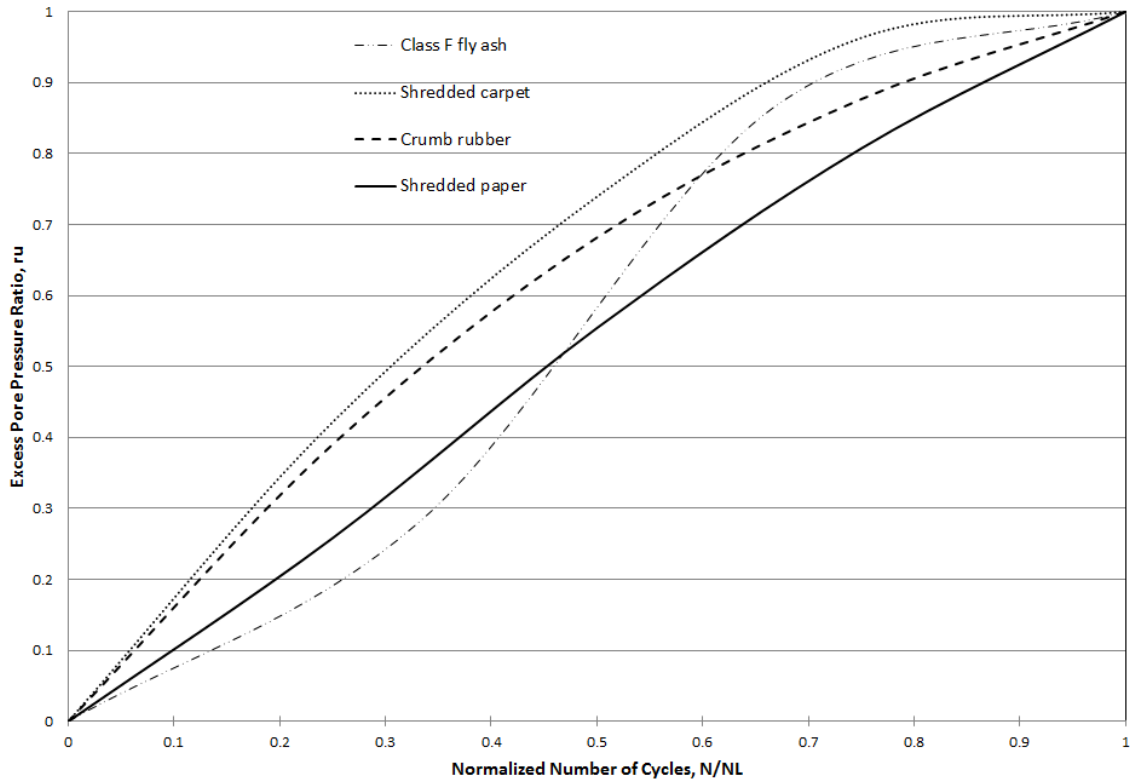
Figure 5.10: r_u versus N/N_L graph of 100% Class F fly ash, 5% carpet fiber, 10% crumb rubber and 10% shredded paper at 0.15 CSR

In the composed graph (Figure 5.10), the addition of crumb rubber help slowed the buildup of excess pore pressure during loading. The other information is the addition of any waste materials avoids a jump in excess pore pressure at the beginning of loading. This behavior happened because waste material helped specimen to fill the void faster.
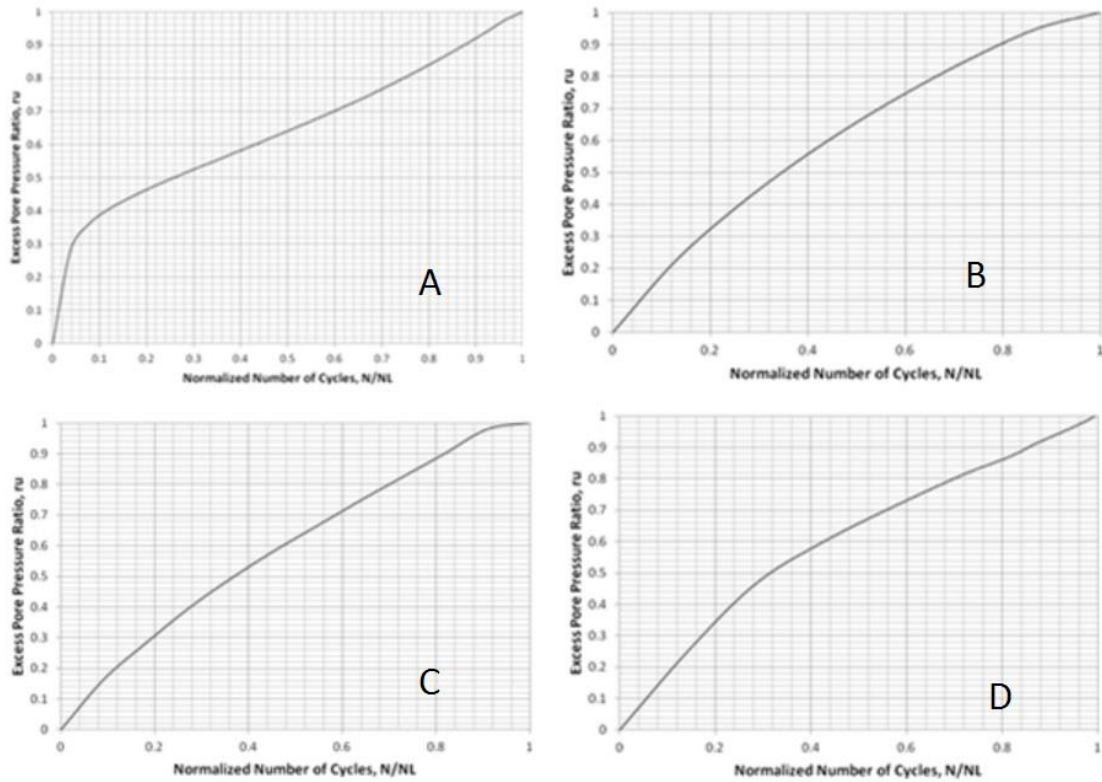
Figure 5.11: r_u versus N/N_L graph of 100% Class F fly ash (A), 5% carpet fiber (B), 10% crumb rubber (C) and 10% shredded paper (D) at 0.30 CSR

Different condition happened at 0.30 CSR, Figure 5.11 shown that for mixed specimens there seems no indication for skin friction and/or adhesion functioning between fly ash and other waste material before experiencing cyclic loading resulted in rapid buildup of excess pore pressure. Sudden raise of excess pore pressure also happened in fly ash specimen but this condition only in early phase and followed by constant build up.
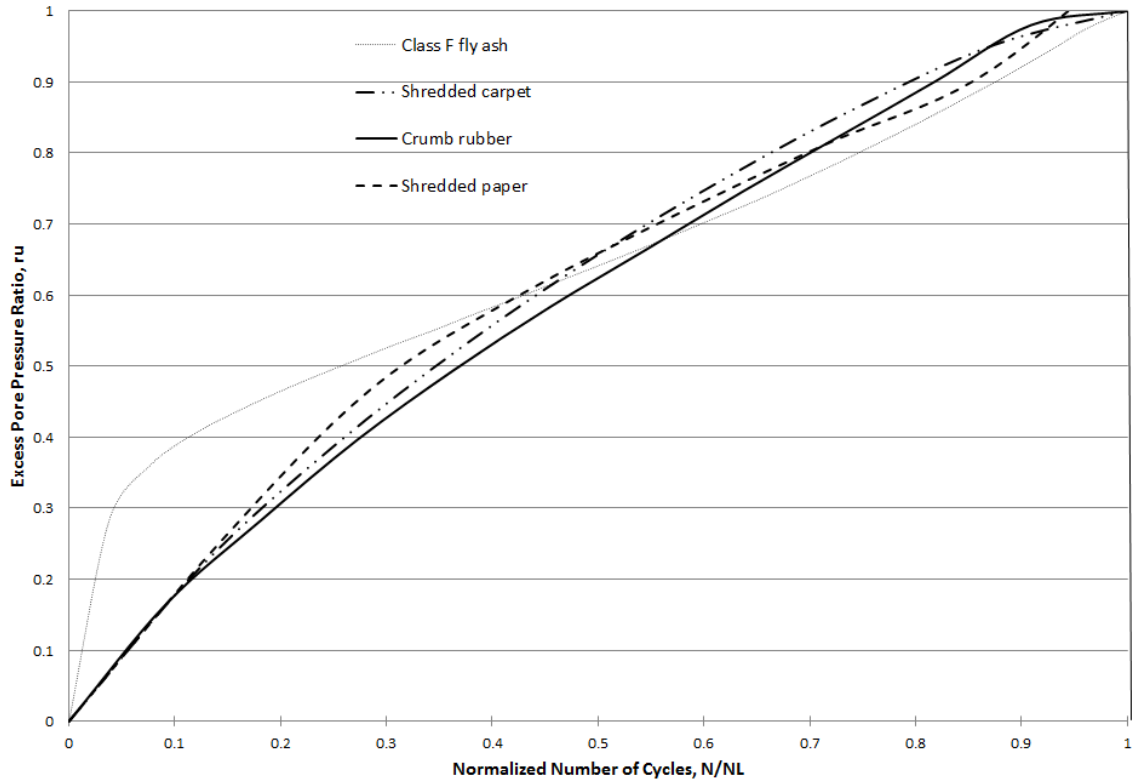
Figure 5.12: r_u versus N/N_L graph of 100% Class F fly ash, 5% carpet fiber, 10% crumb rubber and 10% shredded paper at 0.30 CSR

Figure 5.12 shown all specimens reached liquefaction in similar behavior. Although for fly ash specimen, in the beginning phase, there is a jump in excess pore pressure. At 0.30 CSR seems that the addition of waste material is not really effective in long term loading and only works at short term loading by not creating a jump in excess pore pressure.

Figure 5.13: r_u versus N/N_L graph of 100% Class F fly ash (A), 5% carpet fiber (B), 10% crumb rubber (C) and 10% shredded paper (D) at 0.50 CSR

Faster build up can be seen at 0.50 CSR (Figure 5.13). At this CSR, all specimen shown steeper graph slope, means liquefaction will happened suddenly after specimens experiencing applied deviator stress. Although, for mixed specimens the behavior of pore pressure buildup is mostly because of high void ratio and not enough time for the fly ash and waste material to interact.

Figure 5.14: r_u versus N/N_L graph of 100% Class F fly ash, 5% carpet fiber, 10% crumb rubber and 10% shredded paper at 0.50 CSR

In Figure 5.14, mixed specimens shown similar behavior with shredded paper performing better compared to other, while the fly ash specimen shows a slow increase in excess pore pressure at early stages but faster increase after the half loading period. In the early phase, fly specimen works better because skin friction and/or adhesion is functioning faster, but later the waste material works as a reinforcement, resulting in better skin friction and/or adhesion for crumb rubber and shredded paper specimens.

Based on excess pore pressure graphs comparisons, it can be concluded that if the specimen is experiencing cyclic loading equivalent to 0.15 CSR, all mixed specimens are able to develop skin friction and/or adhesion between fly ash and other waste

material during testing, especially crumb rubber specimen resulting in higher number of liquefaction compare to other combination. Meanwhile, at higher cyclic loading (0.30 and 0.50 CSR), skin friction and/or adhesion between fly ash and other waste material were not able to perform properly, resulting in lower number of cycles to liquefaction for mixed specimens compare to fly ash specimen.

Besides investigating each specimen according to dry weight, evaluating specimens based on volume is also necessary to find the effect of the number of cycles to liquefaction.

The information from Figure 5.15 is shredded paper starts to affect mixed specimens at 3% until it reached optimum at 15%, so it is useless to add more shredded carpet in specimen above 15% because number of cycles for liquefaction will not increase. Meanwhile for crumb rubber, the optimum of this waste material is at 21%. Similar performance is also shown by shredded carpet, which reached optimum at 38%. For crumb rubber and shredded carpet adding waste material more than the optimum percentage will decrease the number of cycles to liquefaction.

Lastly, based on volume comparison, shredded carpet, crumb rubber and shredded paper optimum at 38%, 21% and 15%, respectively.
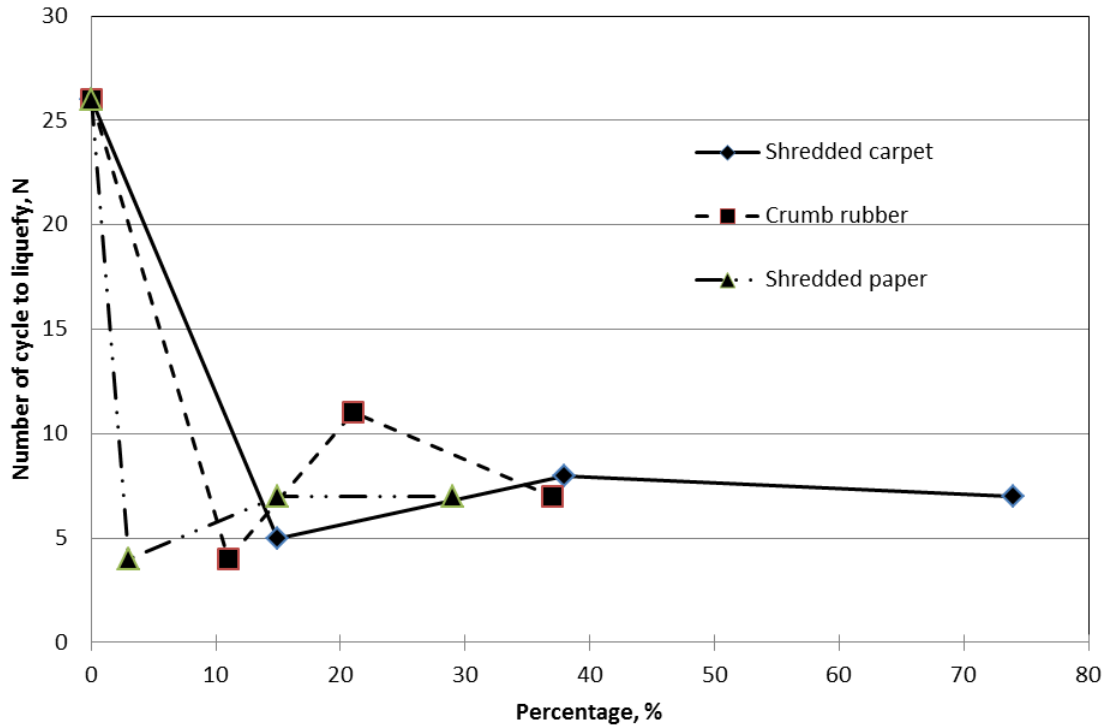
Figure 5.15: Number of cycles to liquefaction versus percentage of waste material by volume at optimum blend using 0.30 CSR

5.5 Identify Optimum Blends of Fly Ash and Other Waste Materials

To compare and analyze the performance of all specimens, three (3) graphs were plotted: Axial strain versus number of cycle graph (Figure 5.16 - Figure 5.17), standard deviator versus axial strain (Hysteresis Loops) graph (Figure 5.18 - Figure 5.19) and pore pressure versus normalized number of cycle graph (Figure 5.20 - Figure 5.21). In general, it is implied that the loading began by applying compression to the sample and the specimen experienced contraction, as a result the pore pressure increased and the lateral effective stress decreased. As the loading progressed, the specimen also starts

experiencing dilation and reached extension strain while the repeated cycle is in progress.

First, the axial strain versus number of cycles graph (Figure 5.16 - Figure 5.17) is used to compare the axial strain behavior of specimen before and after liquefaction. The graph shows axial strain is in compression and tension at the same time although the magnitude of the axial strain in extension is greater than compressive during testing while the next graph shows specimen axial strain always in extension state. It means that the specimen is already dense and not getting denser during loading.
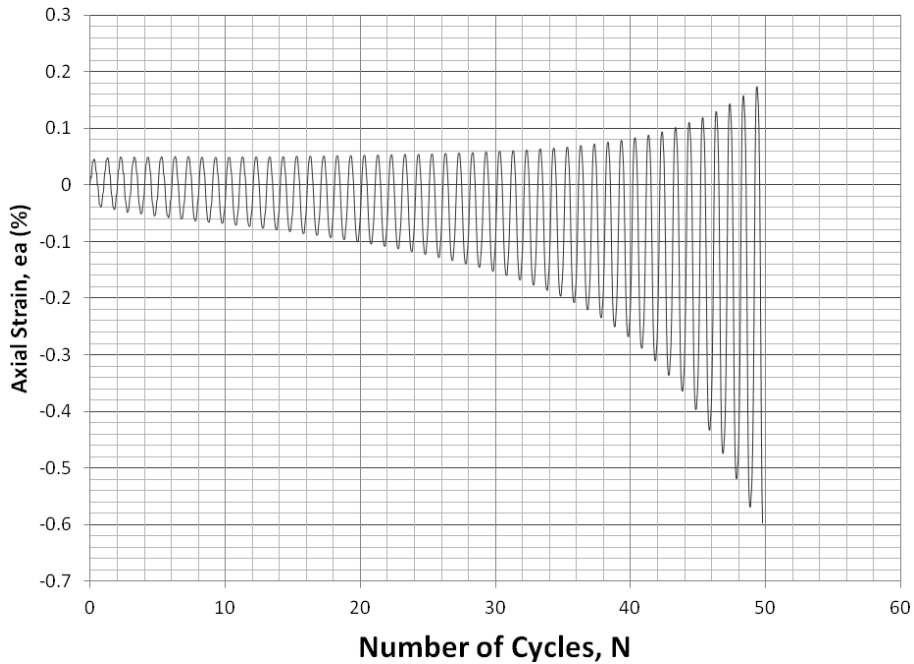
Figure 5.16: Schematic Illustration of axial strain graph shows specimen in extension and compression at the same time during testing
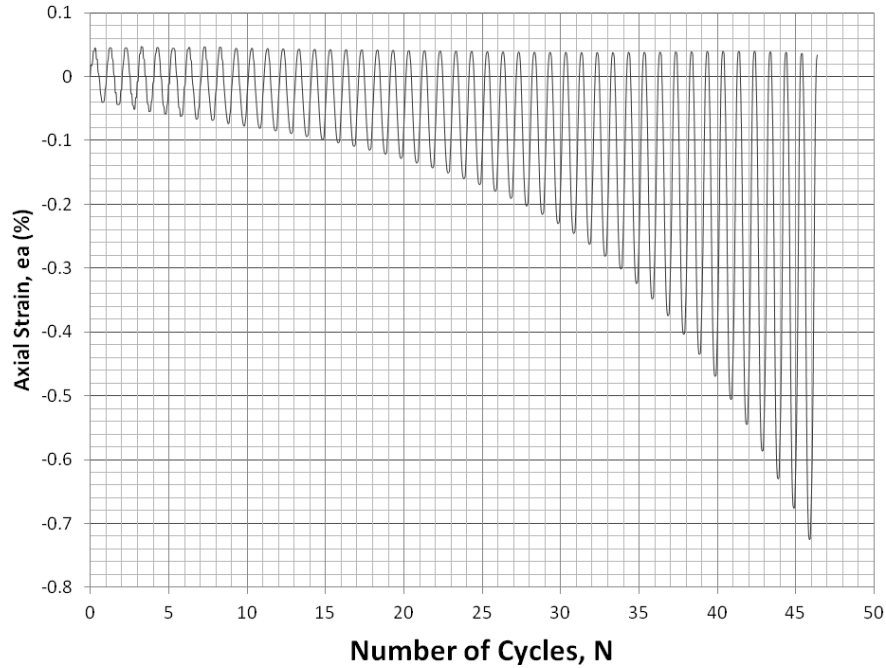
Figure 5.17: Schematic Illustration of axial strain graph shows specimen was in extension compare to compression

Deviator stress versus axial strain (Figure 5.18 - Figure 5.19) is used to show how axial strain changes. Most of the specimen maintains their height at the pre-liquefaction phase while at the post liquefaction phase there are two behaviors identified. First, the sample will experience shortening (Figure 5.18) and second, the specimen will not shorten (Figure 5.19).

As shown in Figure 5.18, the axial strain reached 0.2% during cyclic loading while Figure 5.19 shows that the same behavior was not happening with the sustained axial strain of only 0.7%.
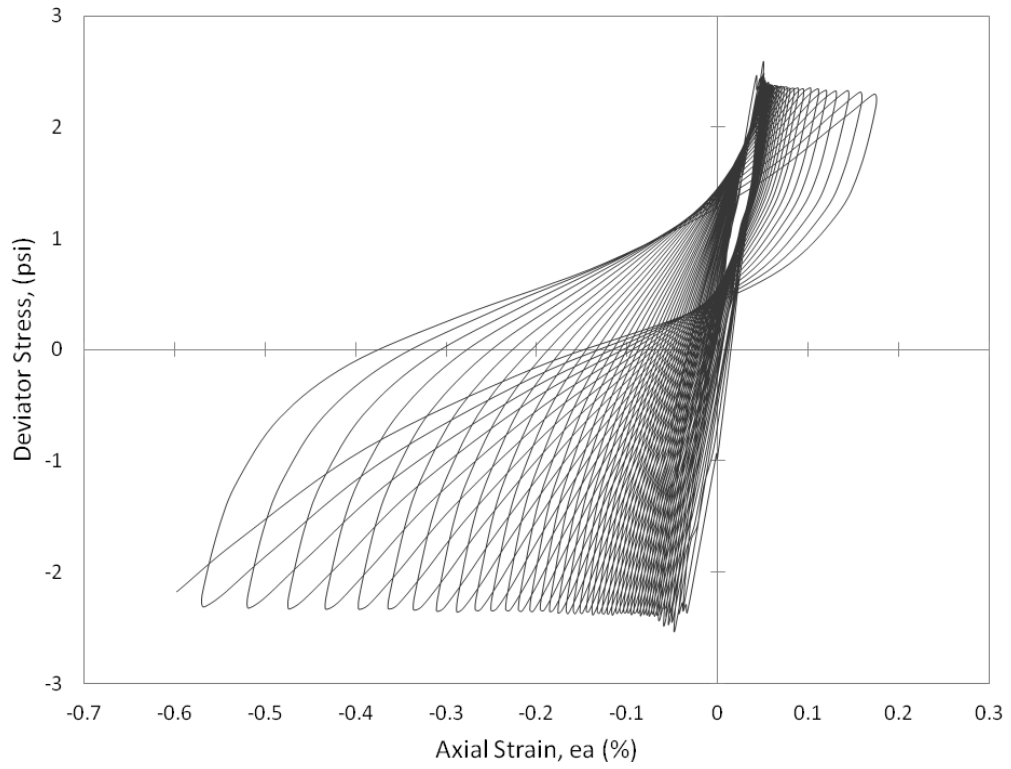
Figure 5.18: Schematic Illustration of deviator stress versus axial strain graph shows specimen contraction and extension at the same time
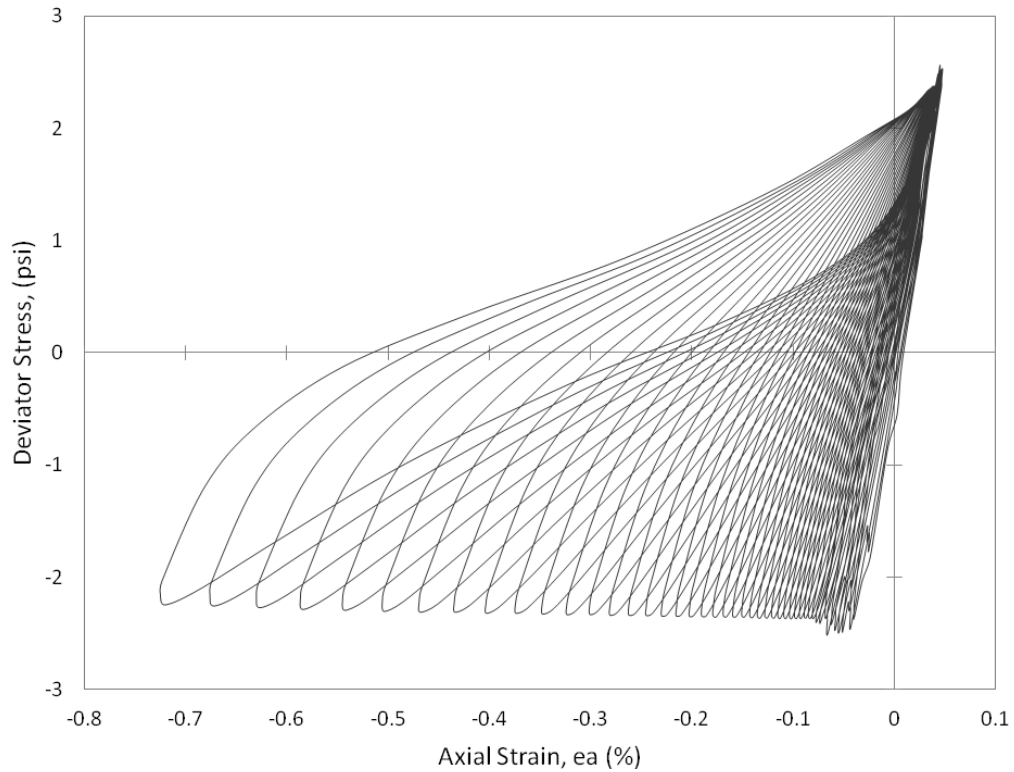
Figure 5.19: Schematic Illustration of deviator stress versus axial strain graph shows specimen in extension

Pore pressure versus normalized number of cycles graphs (Figure 5.20 - Figure 5.21) are used to show the specimen behavior from the start of loading until liquefaction (r_u = 1). There are two conditions for the outcome. First, at early stages of loading, r_u has a high rate of increase and later the rate decreases until liquefaction occurs. Another outcome shows specimen with a constant increment of pore pressure.

119
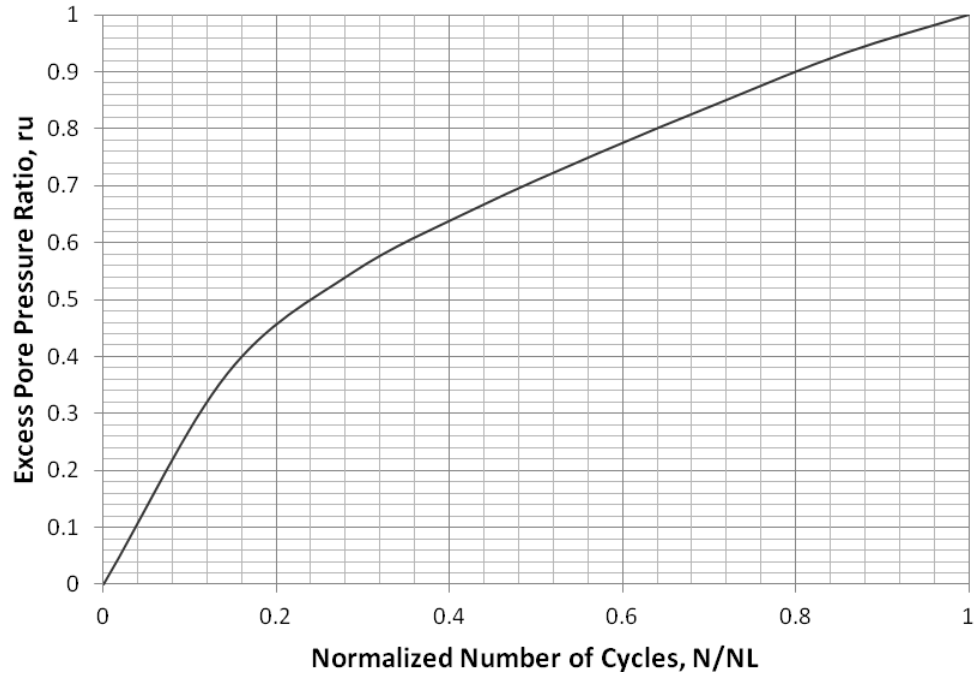
Figure 5.20: Schematic Illustration of r_u versus N/N_L graph showing rapid early increase in pore pressure
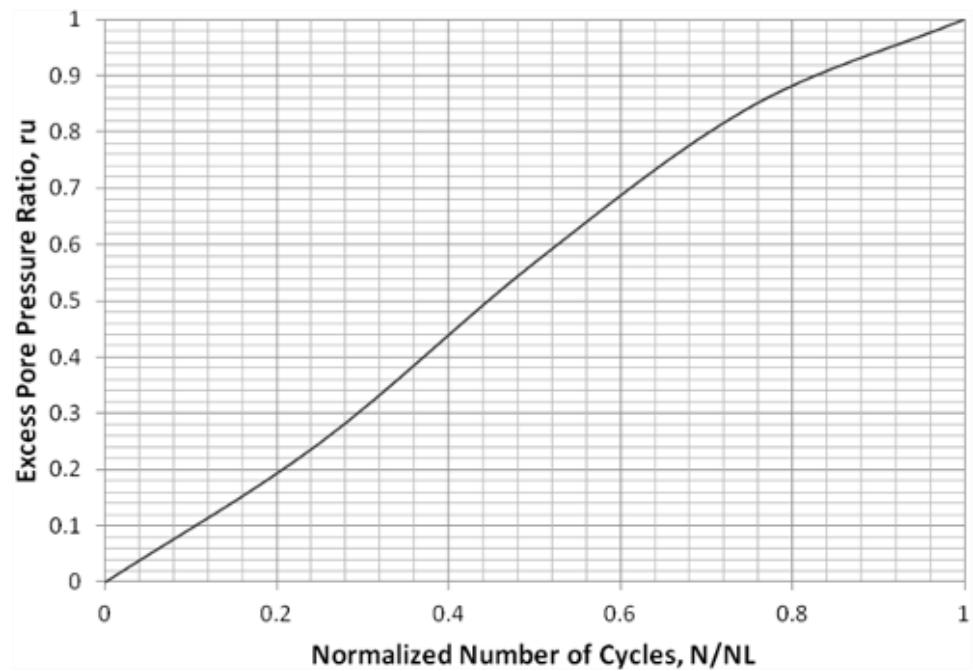
Figure 5.21: Schematic Illustration of r_u versus N/N_L graph showing a steady rate of pore pressure increase

For fly ash specimen, it is apparent that at the beginning and near the end of cycles, pore pressure accumulates faster but this condition is non-existent for specimen with waste material; pore pressure increase seems more evenly.

There is sudden buildup of pore pressure fly ash and this behavior is opposite to the behavior of sand. This behavior is due to the uniform particle size of fly ash, which permits rapid propagation of pore water pressure through the specimen.

The results from each specimen are summarized and plotted in Table 5.6 and Figure 5.22. To illustrate the observed trend, a power function trend line is fitted to each dataset. The distribution of the data is roughly following the power function trend line; although a scatter is observed as it appears from Figure 5.22. As shown from Table 5.6, the number of cycle from each specimen was influenced by density, void ratio, confining pressure and cyclic stress ratio.

In general, the results of Class F fly ash with crumb rubber works better by showing more number of cycles compare to 100% Fly ash at 0.15 CSR.

Table 5.6: Specimen information and results of all specimens tested

Composition	γSat (Pcf)	e	Confining Pressure (Psi)	Actual CSR	N cycles
F100	98.44	1.04	7.5	0.44	3
F100	99.91	0.96	7.8	0.30	26
F100	99.46	0.99	7.7	0.17	51
F98.5C1.5	95.18	1.19	6.9	0.27	5
F98C2	92.83	1.36	6.4	0.46	4
F98C2	93.78	1.29	6.6	0.30	6
F95C5	91.61	1.46	6.2	0.44	4
F95C5	92.69	1.37	6.4	0.29	8
F95C5	92.5	1.38	6.7	0.16	29
F95R5	93.17	1.07	6.9	0.37	2
F95R5	94.48	0.98	7.2	0.29	4
F90R10	93.08	1.07	6.9	0.48	4
F90R10	92.86	1.09	6.8	0.30	11
F90R10	93.37	1.05	6.5	0.17	86
F80R20	95.99	0.89	7.5	0.29	7
F98P2	97.5	1.04	7.4	0.28	4
F90P10	96.85	1.08	7.8	0.47	4
F90P10	97.22	1.06	7.4	0.29	7
F90P10	96.09	1.13	7.6	0.17	47
F80P20	94.17	1.26	6.7	0.29	7

Definitions:

F = Class F Fly Ash   R = Crumb Rubber

C = Carpet Fiber   P = Shredded Paper

100, 98.5, 98, 95, 90, 80, 20, 10, 5, 2 and 1.5 = Percentage of Waste Material by Dry Weight
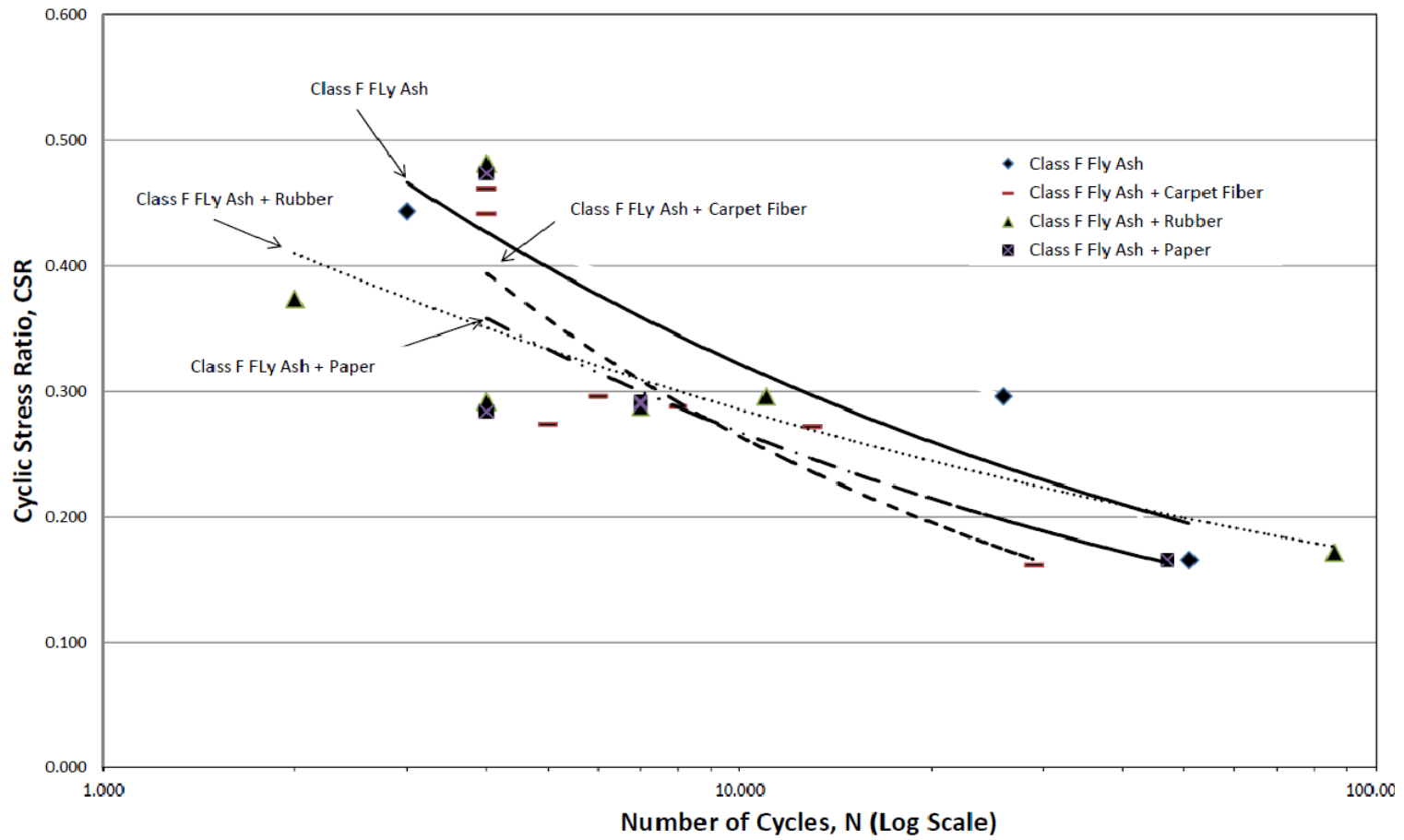
Figure 5.22: Cyclic stress ratio (CSR) Versus Number of cycles (N) of all specimen tested graph

Chapter 6

CONCLUSION AND RECOMMENDATIONS

6.1   Findings of the Study

In this section, the analysis of laboratory tests results performed on Class F fly ash and other waste material is addressed. Also the correlation between the laboratory measured parameters is discussed.

Using the cyclic shear test as described in ASTM D3999, the test results show that the maximum shear modulus of the specimens is 38.99 psi. Using the same information, normalized shear modulus reduction curves and damping ratio curves were generated and compared with other research (Figure 6.1 and Figure 6.7). Based on research conducted by Guoxi et al. (1985), it is found that the dynamic shear moduli increase as confining pressure increases and decrease as void ratio increases. In agreement, the material used in this study have high void ratio, which results in low shear modulus. Therefore, it may be concluded that fly ash is one kind of material which possess high void ratio and low shear modulus. Void ratio varies from 1.08 – 1.61.

The samples from this study responded with the lowest values of shear modulus and demonstrated the softest response. However, as the trend suggests, at lower shear strains higher values of shear modulus could be expected. The softer response of the specimen is related to the lower in-situ confining stress. Due to the lower confinement and looser structure, the Young's modulus of the sample was lower which resulted in

smaller value of shear modulus. One of the influencing parameters that is not quantified in these tests may be the age of the specimens.

The shear modulus values for specimens were normalized to the maximum shear modulus value, G_{max}, obtained from the best fit curve at 0.001% of shear strain. These values can be used in seismic site response analysis. In Figure 6.1, the proposed normalized shear modulus reduction curves are compared with the curves presented by Vucetic and Dobry (1991) for fine grained soils (Figure 6.2), Ishibashi & Zhang (1993) (Figure 6.3) and Darendeli (2001) (Figure 6.4), all with plasticity index (PI) equal to 0 to develop corresponding comparison because fly ash is a non-plastic material. It appears that the measured shear modulus curves are not following the same trend as the other curves. In other words, at higher shear strains, the shear modulus values decrease at a higher rate for fly ash samples compared to fine grained soils, sand and rock materials.

For damping ratio, the shape curves for the samples has a similar trend to that of fine grained soils; however the values of damping ratios for fly ash are lower compared to the fine grained soils with zero (0) plasticity index values. However, it is emphasized that the number of tests in this study were limited and the measurement of small strains were not highly accurate.

The modulus reduction curves of fly ash used in this study more fitted with higher plasticity clay proposed by Vucetic-Dobry and the values decrease at a faster rate at higher strains compared to fine grained soils. The shape of the damping ratio curves also follows the trend of highly plastic soils. On Figure 6.5 and Figure 6.6 the results

from Class F fly ash used in this study are superimposed with curves proposed by Vucetic-Dobry for clay with plasticity index (PI) equal to 0 and 200.
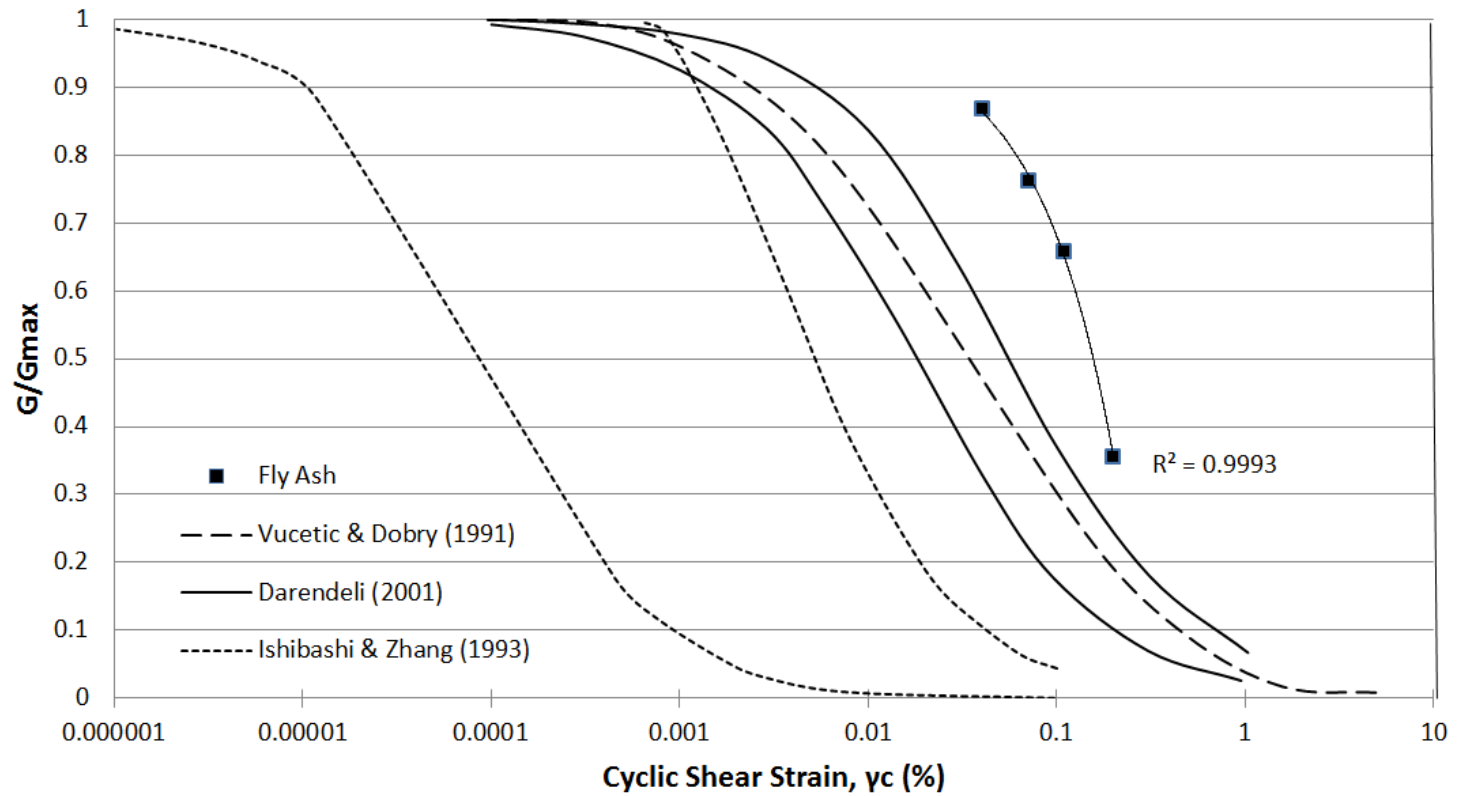
Figure 6.1: Comparison between the normalized shear modulus (G/G_{max}) of fly ash samples used in this study and the relationships suggested by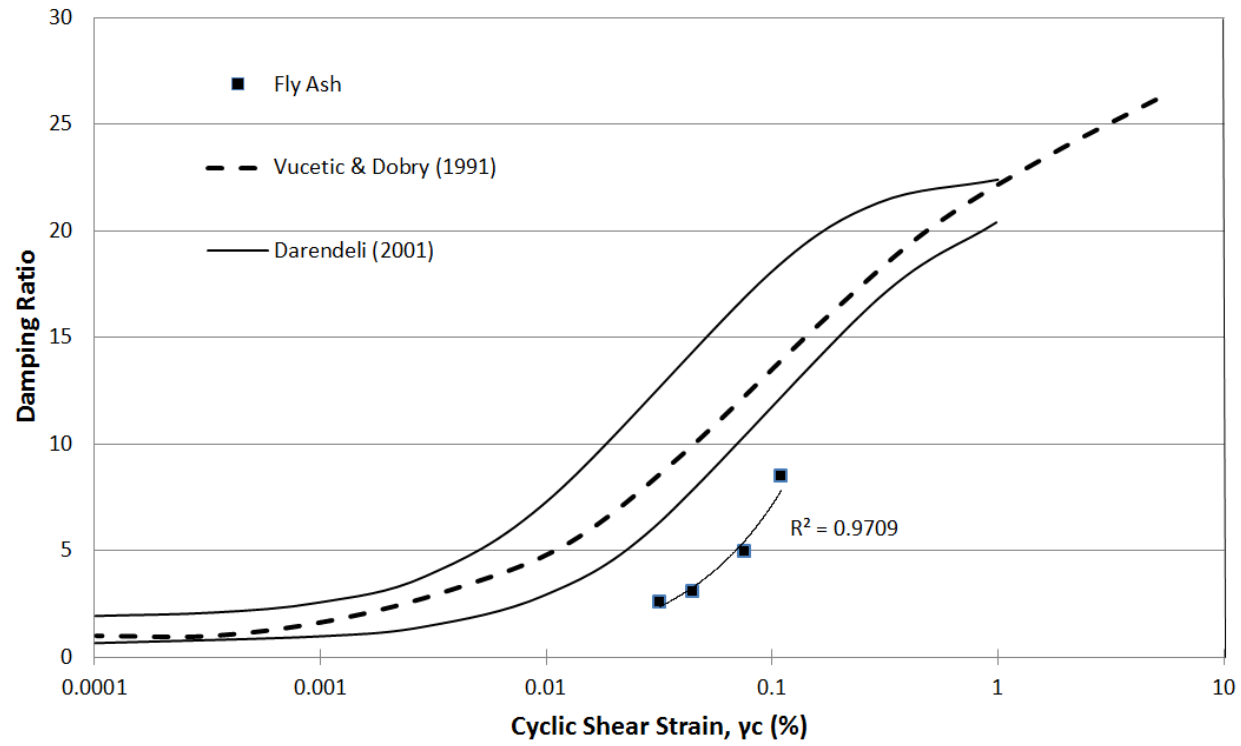 Vucetic and Dobry (1991) for clay with PI=0, Darendeli (2001) PI=0 and Ishibashi and Zhang (1993) for non-plastic soils.
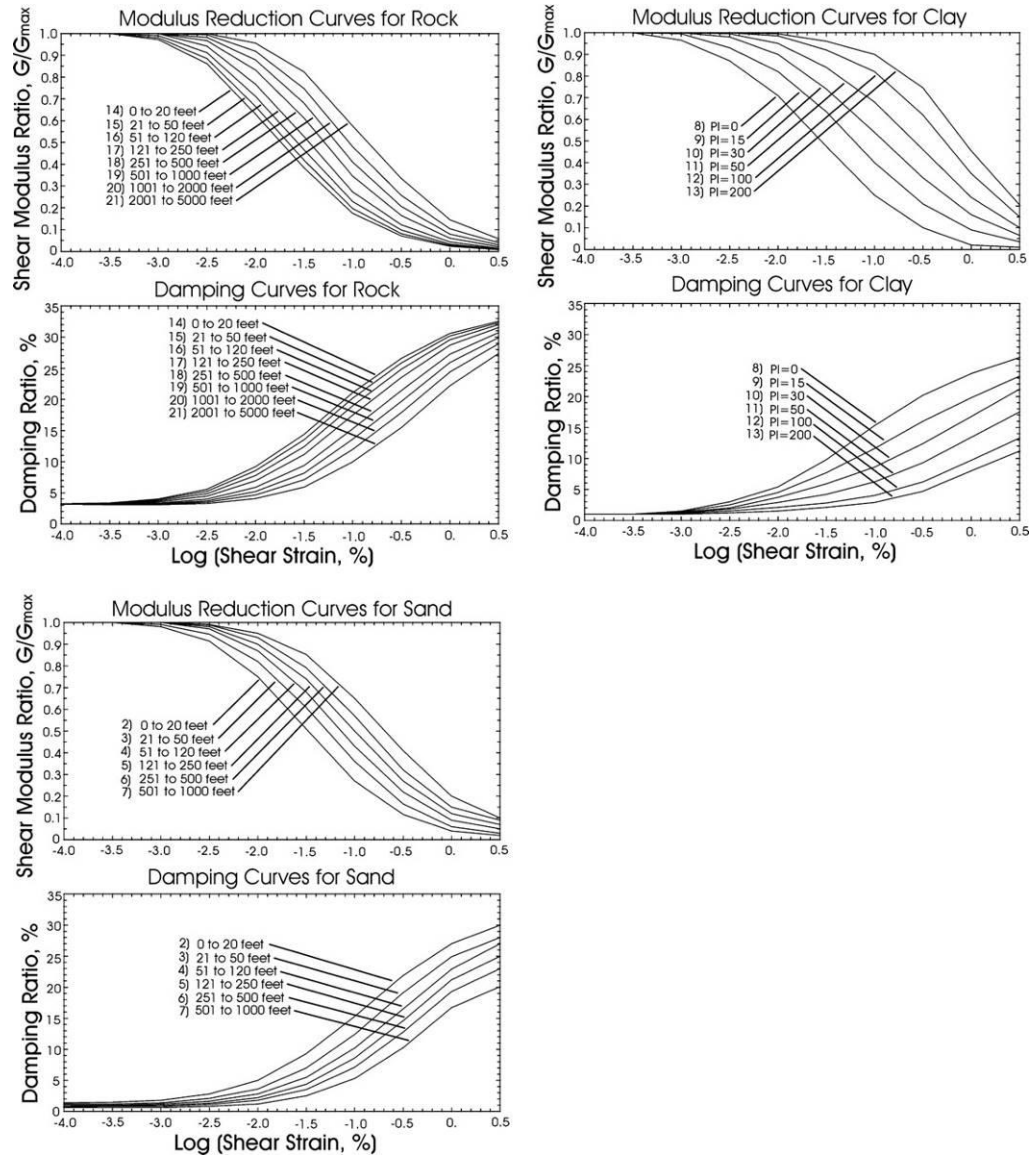
Figure 6.2: Three families of shear modulus reduction and damping ratio curves, developed by Vucetic & Dobry (1991)
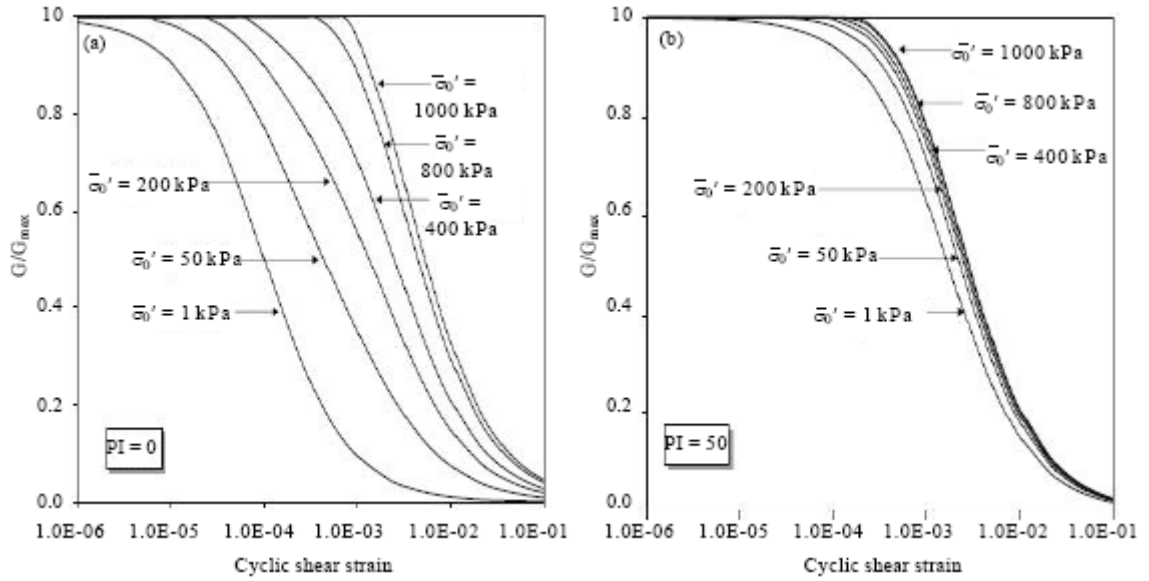
Figure 6.3: Influence of effective confining pressure on modulus reduction curves: (a) Non-plastic soil and (b) Plastic soil (Ishibashi and Zhang, 1993)
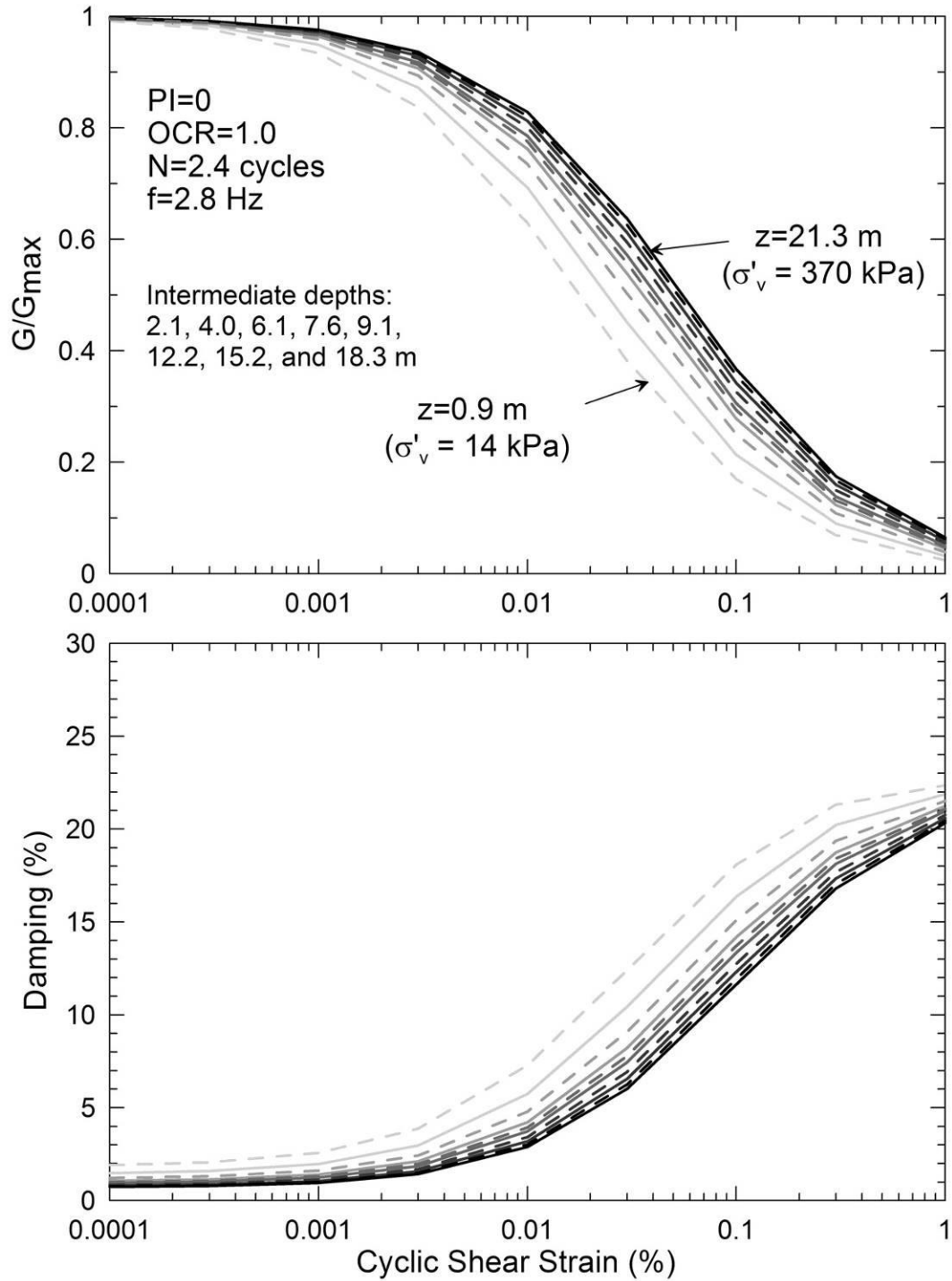
Figure 6.4: Prediction curves of increasing normalised shear modulus and decreasing damping ratio with increasing confining pressure (Darendeli,2001).
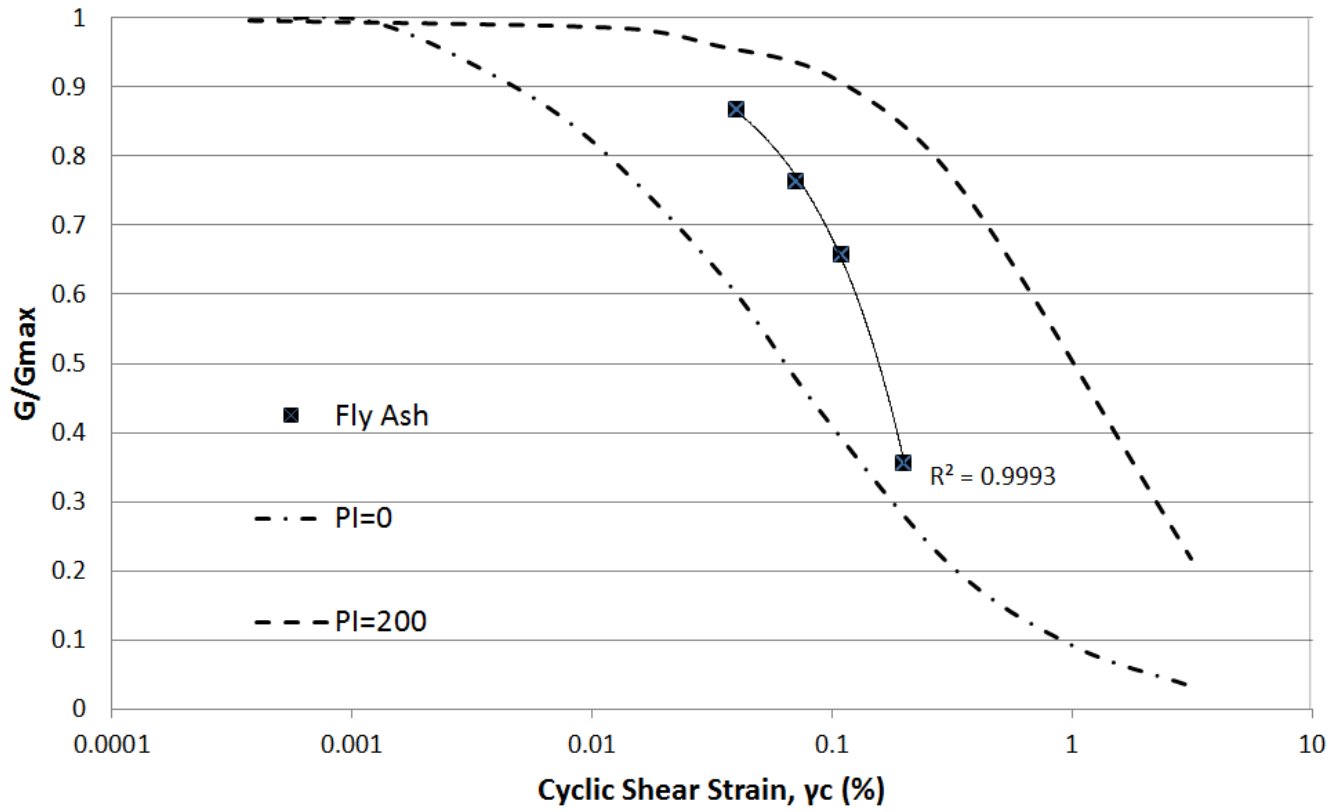
Figure 6.5: Comparison between the normalized shear modulus (G/G$_{max}$) of fly ash samples used in this study and the relationships suggested by Vucetic and Dobry (1991) for clay with PI=0 and PI=200.
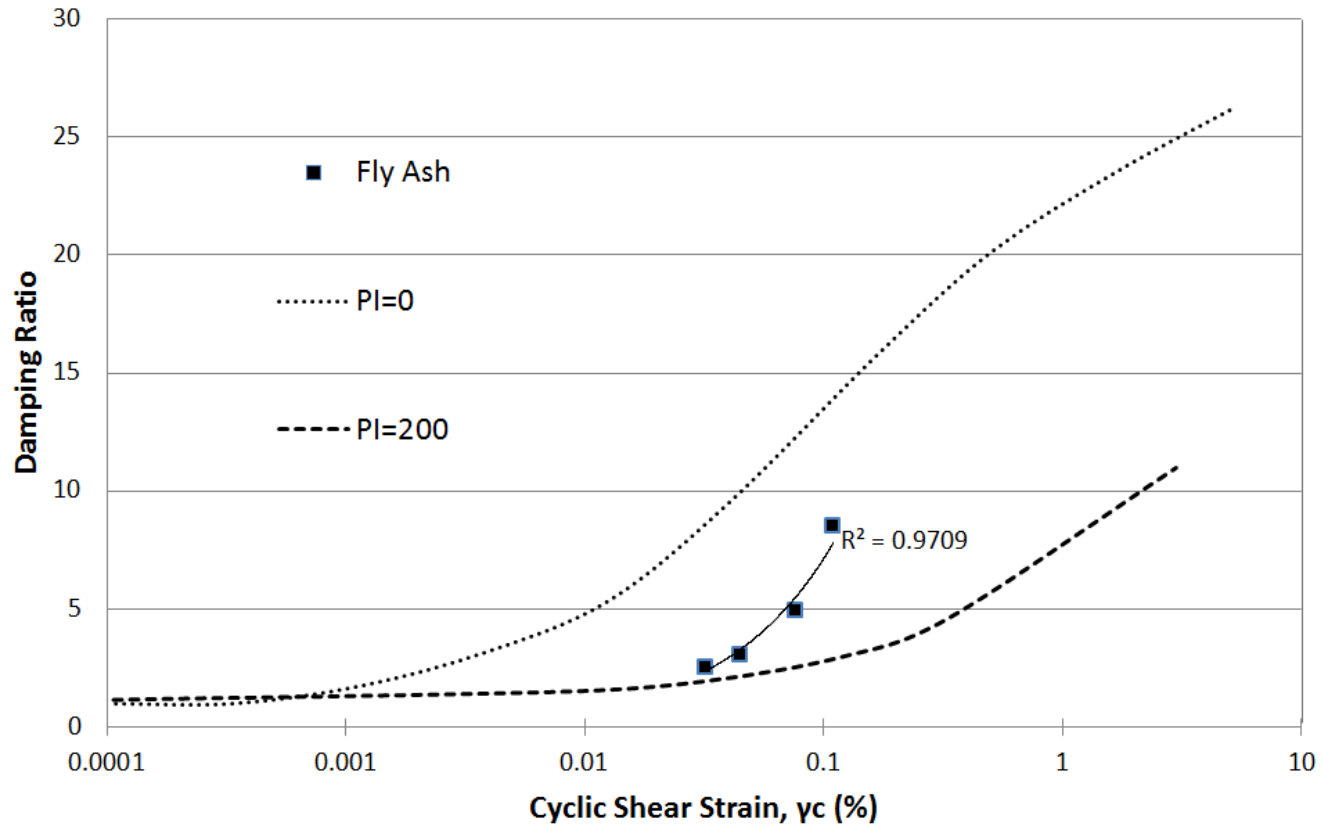
Figure 6.6: Comparison between the damping ratio of fly ash samples used in this study and the relationships suggested by Vucetic and Dobry (1991) for clay with PI=0 and PI=200.

Figure 6.7: Comparison between the damping ratio of fly ash samples used in this study and the relationships suggested by Vucetic and Dobry (1991) for clay with PI=0 and Darendeli (2001) PI=0.

The shear modulus of fly ashes varies with the degree of saturation. The size, gradation and shape of the grains will also influence the shear moduli. By comparison, Zhen (1985) stated that the dynamic shear moduli of fly ashes are about 30 to 60% the shear modulus of sand at same relative density which most likely makes fly ash the most effective isolation materials for vibrations in soil. However, when the aging effect on shear modulus is taken into account for fly ash its effectiveness as an isolation material is doubtful.

Next objective of this research is to predict liquefaction potential based on factor of safety. The factor of safety against liquefaction is as CRR divided with CSR. Based on factor of safety (FS) against liquefaction as shown in Table 6.1, the specimen that is less susceptible against liquefaction is the specimen with 10% crumb rubber at 0.30 CSR. Overall, the addition of any waste material will increase the factor of safety against liquefaction. Hence, densification is anticipated to improve the factor of safety against dynamic liquefaction in the critical zone of interest close to the ground surface.

Actual CSR in Table 6.1 were from adding maximum value of deviator stress and absolute value of minimum deviator stress for each individual testing specimen divided by 4. While CRR came from cyclic shear stress at effective stress reaches zero divided with initial vertical effective stress prior to cyclic loading. Next, divide found CRR with CSR gave factor of safety against liquefaction in Table 6.1

Table 6.1: Cyclic Resistance Ratio (CRR) and Factor of safety (FS) for typical scenarios

Specimen	Actual CSR	CRR	FS Liquefaction
F100	0.44	0.04	0.18
	0.30	0.20	1.33
	0.17	0.09	1.04
F98.5C1.5	0.27	0.24	1.79
F98C2	0.46	0.22	0.96
F95C5	0.44	0.27	1.20
	0.29	0.28	1.96
	0.16	0.14	1.74
F80C20	0.27	0.22	1.60
F95R5	0.29	0.06	0.44
F90R10	0.48	0.43	1.76
	0.30	0.29	1.99
	0.17	0.10	1.18
F80R20	0.29	0.10	0.69
F98P2	0.28	0.27	1.90
F90P10	0.47	0.46	1.96
	0.29	0.19	1.28
	0.17	0.14	1.66
F80P20	0.29	0.22	1.52

Definitions:

F = Class F Fly Ash   R = Crumb Rubber

C = Carpet Fiber   P = Shredded Paper

100, 98.5, 98, 95, 90, 80, 20, 10, 5, 2 and 1.5 = Percentage of Waste Material by Dry Weight

The parameters that low factors of safety were void ratio, confining pressure, saturated density, overconsolidation ratio, and age of the specimens. These parameters were not accounted to adjust the factor of safety. In general, the addition of the waste materials enhanced fly ash performance against cyclic loading and increases the factor of safety against liquefaction.

Better understanding of how waste materials enhanced fly ash performance against cyclic loading can be seen by comparing hysteresis loop. Material combinations used were optimum percentage by dry weight at 0.15, 0.30 and 0.50 CSR.
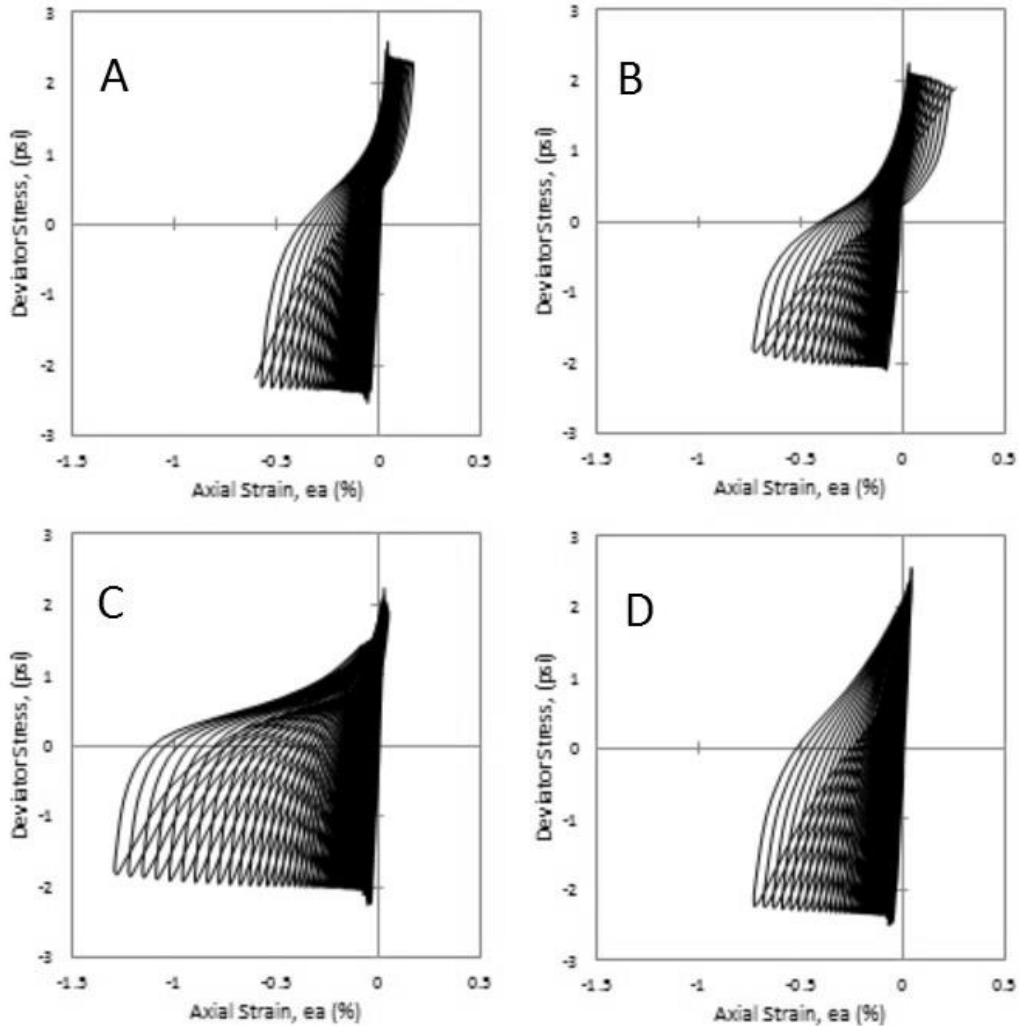
Figure 6.8: Hysteresis loop of 100% Class F fly ash (A), 5% carpet fiber (B), 10% crumb rubber (C) and 10% shredded paper (D) at 0.15 CSR

Hysteresis loop at 0.15 CSR (Figure 6.8) show that crumb rubber and shredded paper specimens did not shorten/compressed. Specimens composed of crumb rubber and shredded paper in a loose condition need higher than 0.15 CSR to get denser. An impoundment pond experiencing 0.15 CSR with crumb rubber or shredded paper will not consolidate.
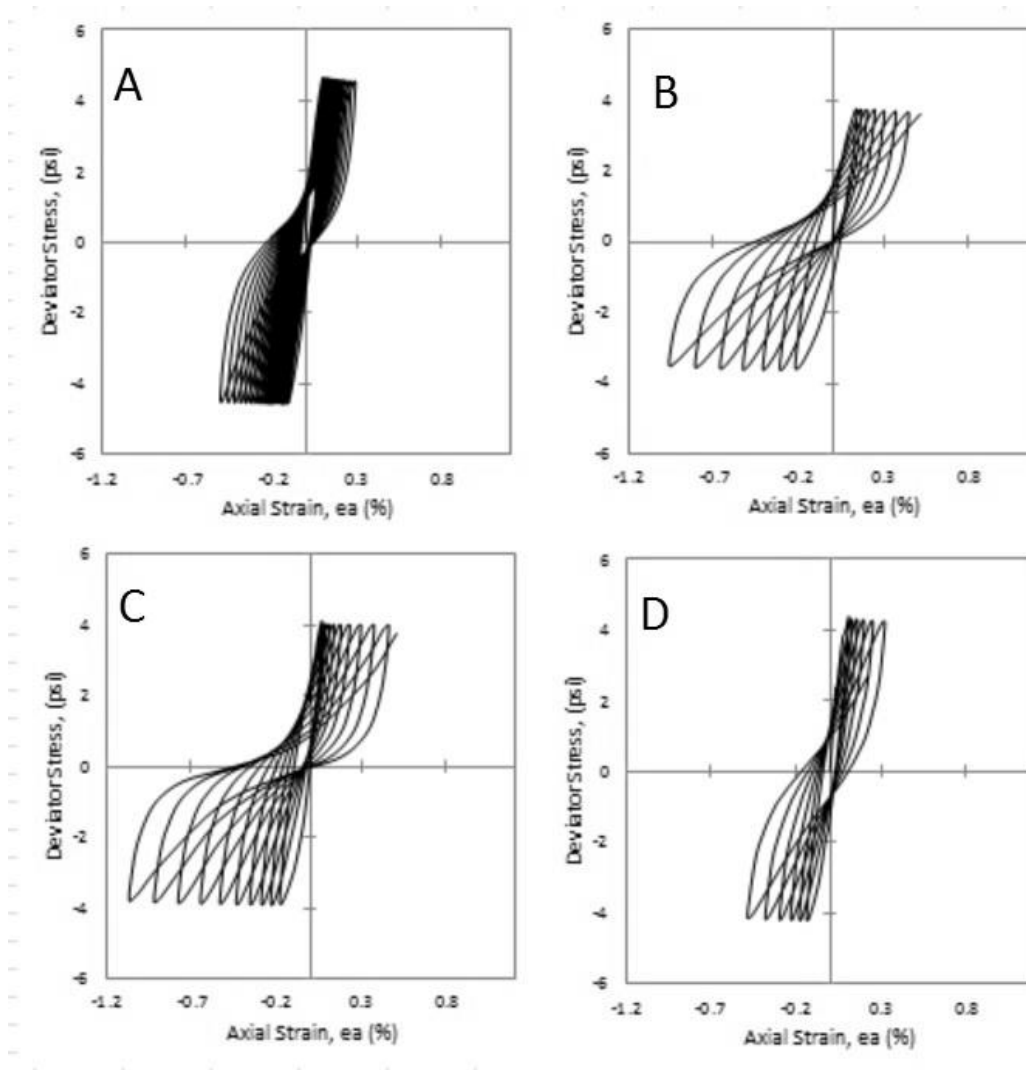
Figure 6.9: Hysteresis loop of 100% Class F fly ash (A), 5% carpet fiber (B), 10% crumb rubber (C) and 10% shredded paper (D) at 0.30 CSR

Figure 6.9 shown strain levels for Class F fly ash and fly ash with shredded paper as relatively the same, while, carpet fiber shows similarity with crumb rubber. Banana loops related with strain hardening showing a temporary increase in the shear stiffness eventually happened to all the specimens but are more pronounced in the Class F fly ash and crumb rubber.

137
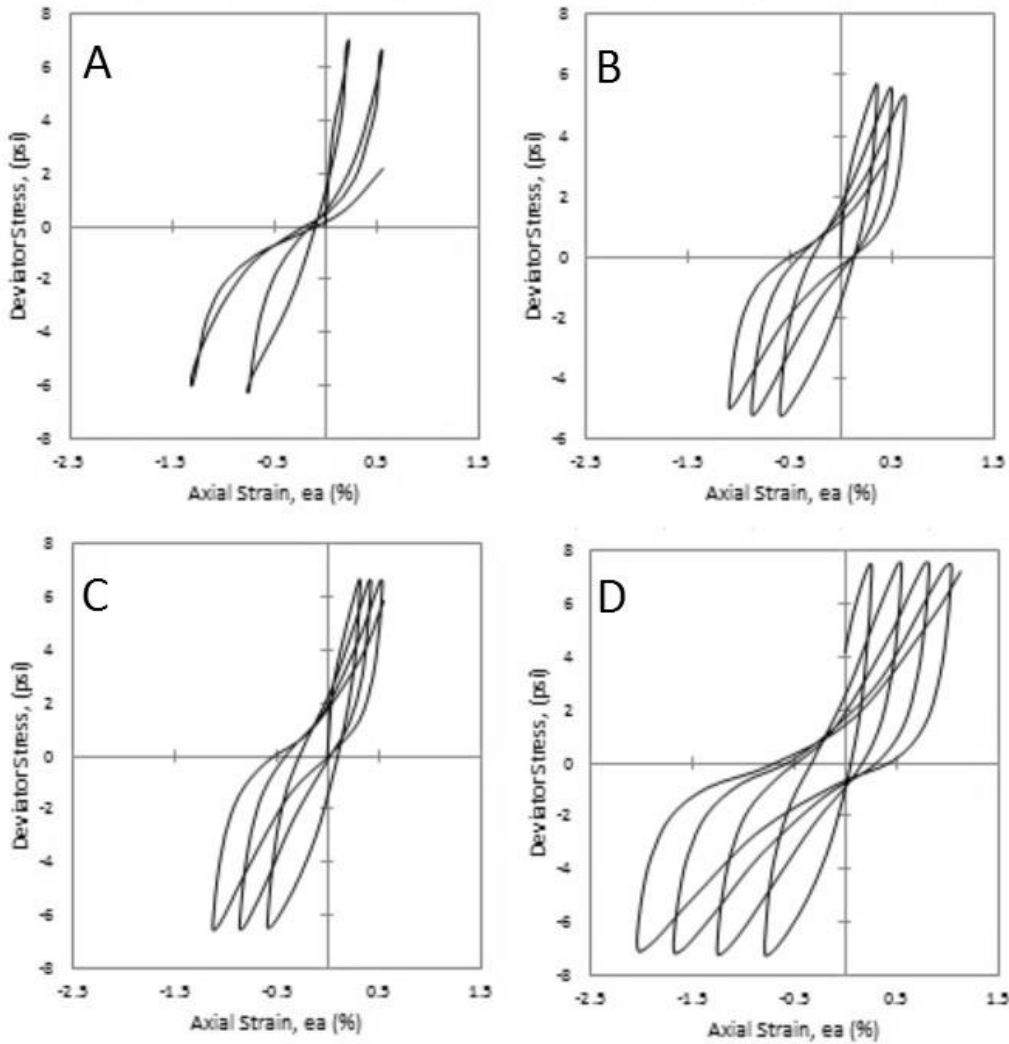
Figure 6.10: Hysteresis loop of 100% Class F fly ash (A), 5% carpet fiber (B), 10% crumb rubber (C) and 10% shredded paper (D) at 0.50 CSR

From the previous two hysteresis loops comparisons, the shape of hysteresis loops at 0.50 CSR (Figure 6.10) is similar with 0.30 CSR with higher axial strain, meaning at higher deviator stress the numbers of cycles to liquefaction changes but the axial strain shape remains the same.

In conclusion, at optimum percentage by dry weight based on hysteresis loop comparison, Class F fly ash with crumb rubber shows better performance; at low

deviator stress crumb rubber helps fly ash to control deformation while at high deviator stress crumb rubber increase the number of cycles to liquefaction.
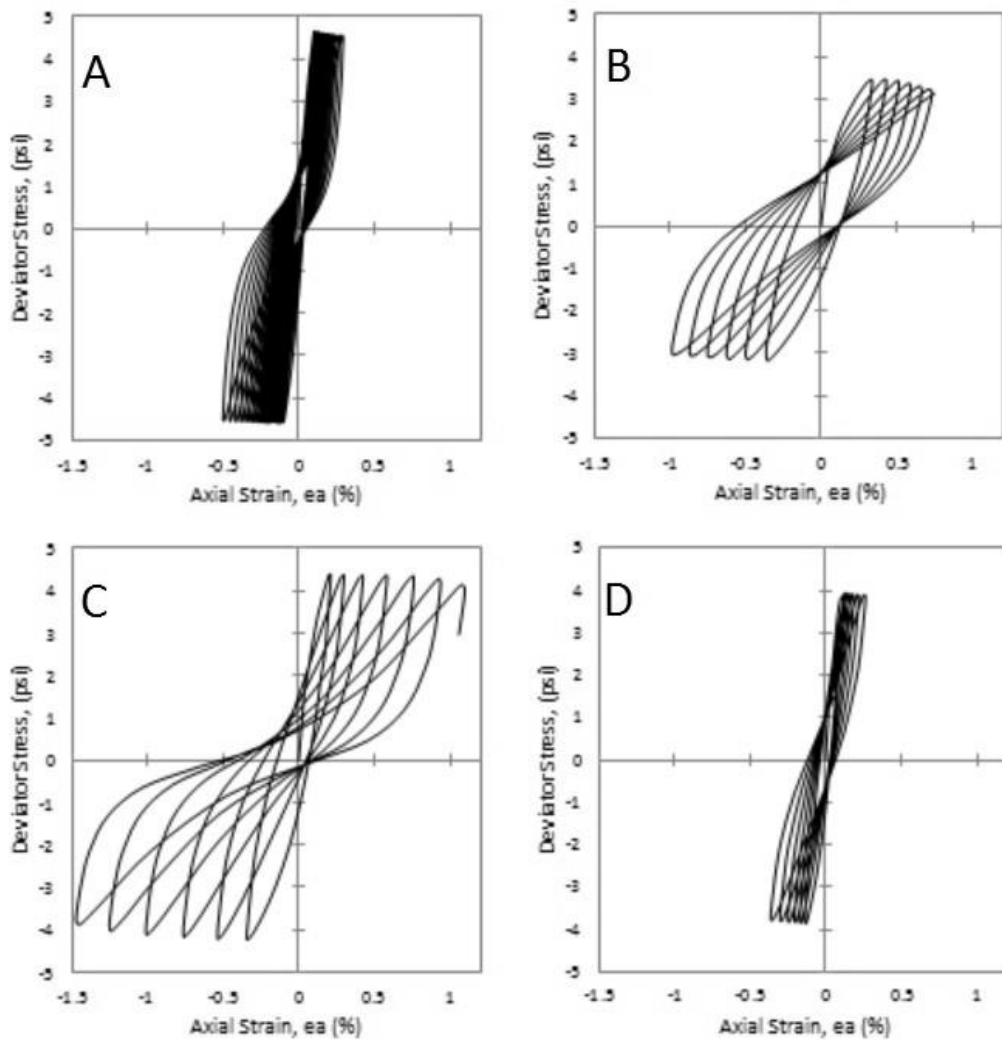
Figure 6.11: Hysteresis loop of 100% Class F fly ash (A), 20% carpet fiber (B), 20% crumb rubber (C) and 20% shredded paper (D) at 0.30 CSR

Hysteresis loop for 20% waste material at 0.30 CSR are also compared (Figure 6.11) and show that the hysteresis loop for Class F fly ash plus carpet fiber are comparable to with clay-like material instead of sand-like material. Therefore the hysteresis loop dissipates considerably more energy contrary to the observed narrow

loops typical to the sand-like materials. By increasing carpet fiber content, the loops become broader and thus it can be considered a clay-like behavior with cyclic mobility.

Summarizing the results, compositions of Class F fly ash with waste materials such as shredded carpet, shredded paper and crumb rubber that give optimum enhancement ranges from 5 to 10% by dry weight and 15 to 38% by volume.

6.2   Recommendations for Practitioners

Gray and Lin (1972) stated that fly ash has advantages when used in mass-fills. Properly compacted and stabilized fly ash is as durable as conventional compacted earth fill. Compacted fly ashes have been reported to exhibit age hardening behavior, i.e., a time-dependent increase in strength after compaction. Age hardening behavior or pozzolonic properties has been correlated with the presence of free lime in the fly ash. Fly ash which have been lagooned prior to compaction does not exhibit as much age hardening.

In addition, Gray and Lin (1972) describe the effect of degree of saturation on the compressibility of compacted fly ash; the partially saturated fly ash was considerably less compressible, in the case of fully saturated samples, a large proportion of total volume decrease occurs during the primary consolidation phase. Primary consolidation occurs very rapidly and in the usual field situation would not be as important as secondary compression in explaining or accounting for long term settlement.

Due to scarcity of land around power plants, one option for increasing the capacity of an ash pond is by raising its height. In this study, the expectation is to increase the useful capacity of storage pond by increasing the fly ash embankment.

In many places the total height of the deposit is higher than 30 m. The ash deposit placed in slurry form has a very low density and leads to problems such as liquefaction during earthquakes, poor bearing capacity, large settlement, etc. Considerable research has been conducted to improve the density of ash by different techniques such as vacuum dewatering, electro osmosis, vibro-compaction, stone columns, blasting, etc. (Gandhi, et al, 1999).

This study provides an option to increase the capacity of fly ash ponds by increasing the earthen dikes of an existing pond. When a fly ash material is stable then it can be placed in higher dikes. As shown on Table 6.1, any composition of waste material increases the factor of safety and Class F fly ash with 10% crumb rubber shows the highest safety factor of 1.99 which is adequate enough to withstand stress that is applied.

To help practitioners predict factors of safety against liquefaction, this study provide equations to approximate cyclic resistance ratio (CRR) using cyclic stress ratio (CSR). There are equations for each waste material (Class F fly ash, shredded carpet, crumb rubber and shredded paper) that are recommended to be used if the addition of

waste material not more than 20% percentage of dry weight and CSR ranging from 0.15

to 0.50.

Class F fly ash - $CRR = (0.4536\,CSR^{-2.763})^{1.69}$ (6.1)

Shredded carpet - $CRR = (0.8937\,CSR^{-1.855})^{1.627}$ (6.2)

Crumb rubber - $CRR = (0.2836\,CSR^{-3.306})^{2.024}$ (6.3)

Shredded paper - $CRR = (0.6740\,CSR^{-2.379})^{1.784}$ (6.4)

For these equations, first, CRR equation from cyclic resistance ratio (CRR) Vs.

Number of cycles (N) for all specimens tested (Figure 6.12) and CSR equations from

cyclic stress ratio (CSR) Vs. Number of cycles (N) for all specimens tested (Figure 5.22)

are identified using trend line equations. Second, because number of cycles (N) is the

same component, using N as substitute component resulted in equation with CRR and

CSR as unknown components. For practitioners, CSR can be easily calculated; in

contrary, CRR needs time because based on testing. So, using CRR equations developed

in this study, practitioners can approximate CRR and use it to predict factor of safety

against liquefaction. Should be noted that CRR equations developed in this study is

based on observation during testing, calculated CRR only estimation while waiting for

laboratory test result and CRR is not dependent to loading or CSR.

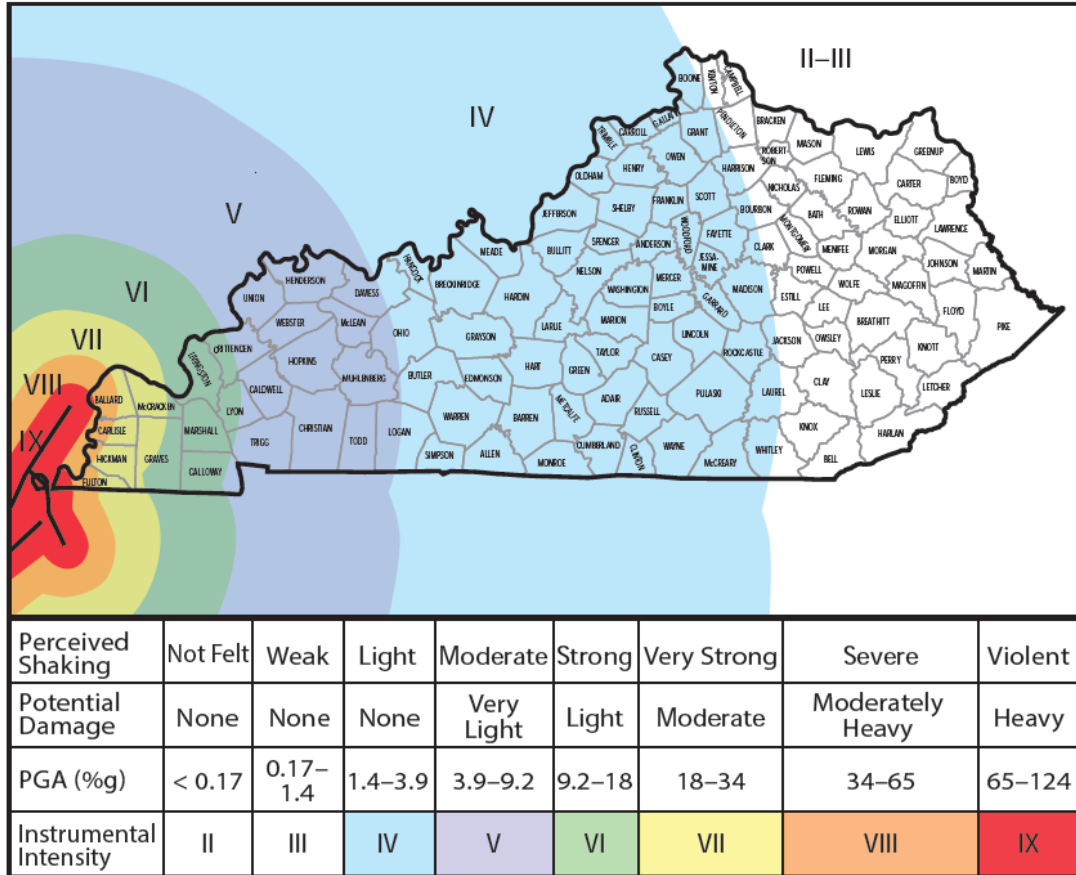To show how the equations works, below is an example to find factor of safety

using all zones in predicted peak ground acceleration (PGA), on hard rock from a

magnitude 7.5 earthquake in the New Madrid Seismic Zone (Figure 6.14) and predict the factor of safety using CRR from equations. The procedure for this example is shown in Figure 6.13. To find CSR in this example, α_{max} value is based from Figure 6.14 and γ_{sat} value is the average from tested specimen. The calculated CSR value will be used as an input for equation to get CRR and find factor of safety against liquefaction. The result for all zones is shown in Table 6.2.
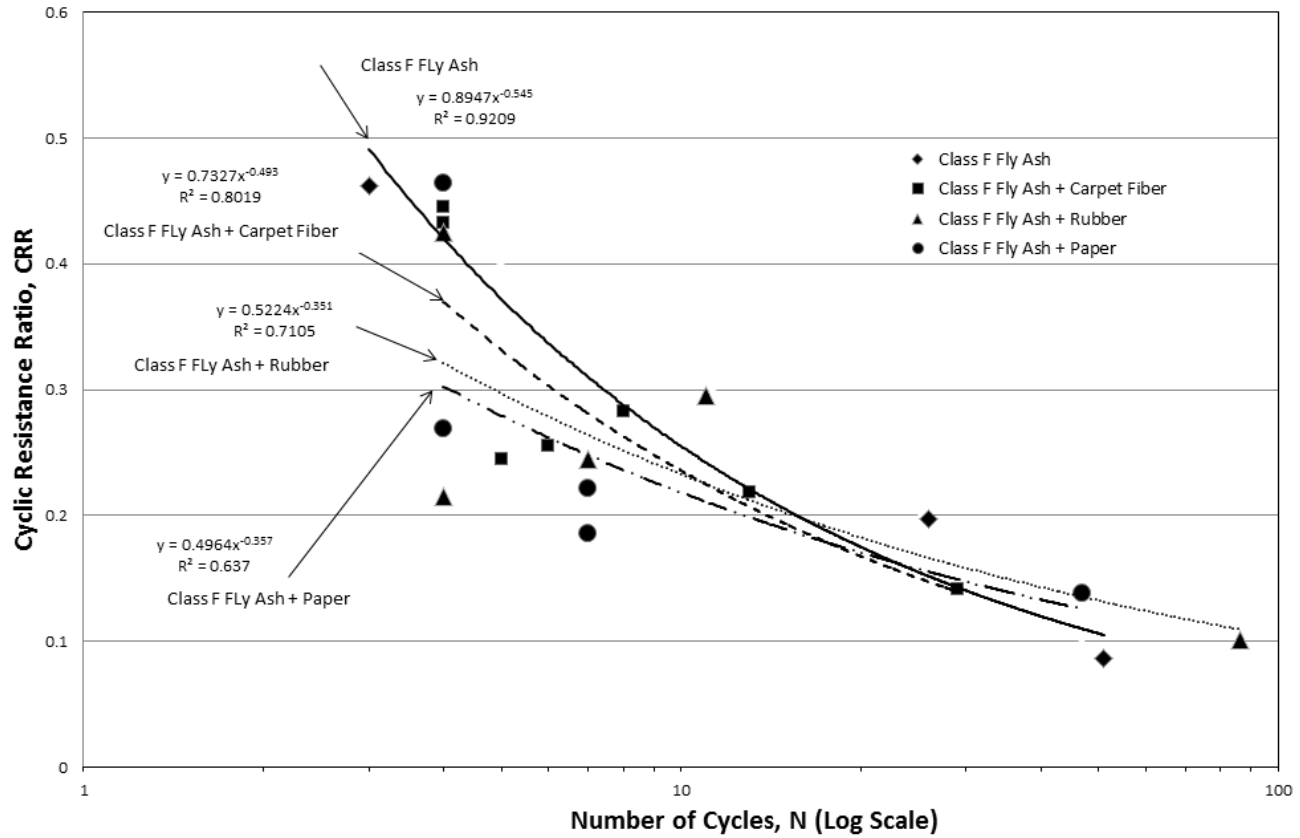
Figure 6.12: Cyclic resistance ratio (CRR) Vs. Number of cycles (N) for all specimens tested

Seismic Source: New Madrid Seismic Zone

Landfill Location :   Zone II - IX

Earthquake Magnitude: 7.5

$$CRR = \frac{\tau_{cyc}}{\sigma_{vo}}$$

$CRR =$	Cyclic Resistance Ratio	
τ_{cyc}	The cyclic shear stress at liquefaction	$= 0.65 \dfrac{a_{max}\ \sigma_v\ r_d}{g}$
	(Seed&Idriss, 1971) - "Simplified Approach"	
σ_{v}	Total Stress	
σ_{vo}	The initial vertical effective stress	

$$CSR = 0.65 \frac{a_{max}\sigma_{v0}r_d}{g\sigma_{vo}}$$

CSR =	Cyclic Stress Ratio
a_{max}	Peak Ground Surface Acceleration
σ_{vo}	The total vertical effective stress
r_d	A stress reduction coefficient to account for soil deformability
g	The gravitational acceleration constant
σ_{vo}	The initial vertical effective stress

FS =	Factor of Safety $= \dfrac{CRR}{CSR}$ MSF		(MSF=1)

Depth =   10 m

                 32.8 ft

Assumption of ground level elevation   ±0.00   ft

Input Data

a_{max}	PGA (%g)
	Use = g
r_d	1.174 - 0.0267 z for 9.15 m < x ≤ 23 m
	1.174 - 0.0267 * 10 m
	0.907
g (ft/s2)	32.174
γ_{water} (pcf)	62.43

Figure 6.13: Information to calculate factor of safety (SF) for all zone in predicted peak ground acceleration (PGA), on hard rock from a magnitude-7.5 earthquake in the New Madrid Seismic Zone

Table 6.2: Factor of Safety for all zones in predicted peak ground acceleration (PGA), on hard rock from a magnitude-7.5 earthquake in the New Madrid Seismic Zone

Material = Class F fly ash

Perceived shaking	αmax (g)	γ_{sat} (pcf)	σ_v (psf)	$\sigma_{vo}^{'}$ (psf)	τ_{cyc} (psf)	CSR	CRR	FS
Violent	1.24				1352.50	1.12	0.97	0.87
Severe	0.65				708.97	0.59	2.38	4.05
Very strong	0.34				370.85	0.31	5.82	18.96
strong	0.18	99.27	3256.06	1208.35	196.33	0.16	14.01	86.24
Moderate	0.092				100.35	0.08	35.42	426.46
Light	0.039				42.54	0.04	115.91	3292.48
Weak	0.014				15.27	0.01	477.30	37769.41
Not felt	0.0017				1.85	0.00	8786.23	5725718.00

Material = Class F fly ash + Shredded Carpet

Perceived shaking	αmax (g)	γ_{sat} (pcf)	σ_v (psf)	$\sigma_{vo}^{'}$ (psf)	τ_{cyc} (psf)	CSR	CRR	FS
Violent	1.24				1352.50	1.12	1.39	1.24
Severe	0.65				708.97	0.59	2.52	4.30
Very strong	0.34				370.85	0.31	4.60	14.99
strong	0.18	92.66	3039.25	991.54	196.33	0.16	8.30	51.07
Moderate	0.092				100.35	0.08	15.46	186.21
Light	0.039				42.54	0.04	34.28	973.72
Weak	0.014				15.27	0.01	88.65	7015.36
Not felt	0.0017				1.85	0.00	626.61	408339.72

Material = Class F fly ash + Crumb rubber

Perceived shaking	αmax (g)	γ_{sat} (pcf)	σ_v (psf)	$\sigma_{vo}^{'}$ (psf)	τ_{cyc} (psf)	CSR	CRR	FS
Violent	1.24				1352.50	1.12	0.89	0.80
Severe	0.65				708.97	0.59	2.60	4.44
Very strong	0.34				370.85	0.31	7.60	24.75
strong	0.18	93.96	3081.89	1034.18	196.33	0.16	21.73	133.76
Moderate	0.092				100.35	0.08	65.91	793.65
Light	0.039				42.54	0.04	272.30	7735.09
Weak	0.014				15.27	0.01	1480.93	117187.73
Not felt	0.0017				1.85	0.00	48322.71	31490448.19

Material = Class F fly ash + Shredded paper

Perceived shaking	αmax (g)	γ_{sat} (pcf)	σ_v (psf)	$\sigma_{vo}^{'}$ (psf)	τ_{cyc} (psf)	CSR	CRR	FS
Violent	1.24				1352.50	1.12	1.28	1.14
Severe	0.65				708.97	0.59	2.76	4.71
Very strong	0.34				370.85	0.31	5.97	19.45
strong	0.18	96.37	3160.94	1113.23	196.33	0.16	12.72	78.29
Moderate	0.092				100.35	0.08	28.26	340.32
Light	0.039				42.54	0.04	78.44	2228.28
Weak	0.014				15.27	0.01	265.34	20997.08
Not felt	0.0017				1.85	0.00	3258.45	2123431.36

The Peak Ground Acceleration (PGA) on the example used data from the Kentucky Geological Survey and the Kentucky Division of Emergency Management Publication that is published in 2014.

Perceived Shaking	Not Felt	Weak	Light	Moderate	Strong	Very Strong	Severe	Violent
Potential Damage	None	None	None	Very Light	Light	Moderate	Moderately Heavy	Heavy
PGA (%g)	< 0.17	0.17–1.4	1.4–3.9	3.9–9.2	9.2–18	18–34	34–65	65–124
Instrumental Intensity	II	III	IV	V	VI	VII	VIII	IX

Figure 6.14: Predicted peak ground acceleration (PGA), on hard rock from a magnitude-7.5 earthquake in the New Madrid Seismic Zone

Factor of Safety (FS) has a scaling factor to the CRR with respect with earthquake magnitude (Magnitude Scale Factor, MSF).

$$FS = \quad \text{Factor of Safety} \quad = \frac{CRR}{CSR} \ MSF$$

As for example the magnitude used is 7.5 and based on Figure 6.15 using data from Seed et al. (2001); the CRR use on the example should be multiply with a factor of 1.
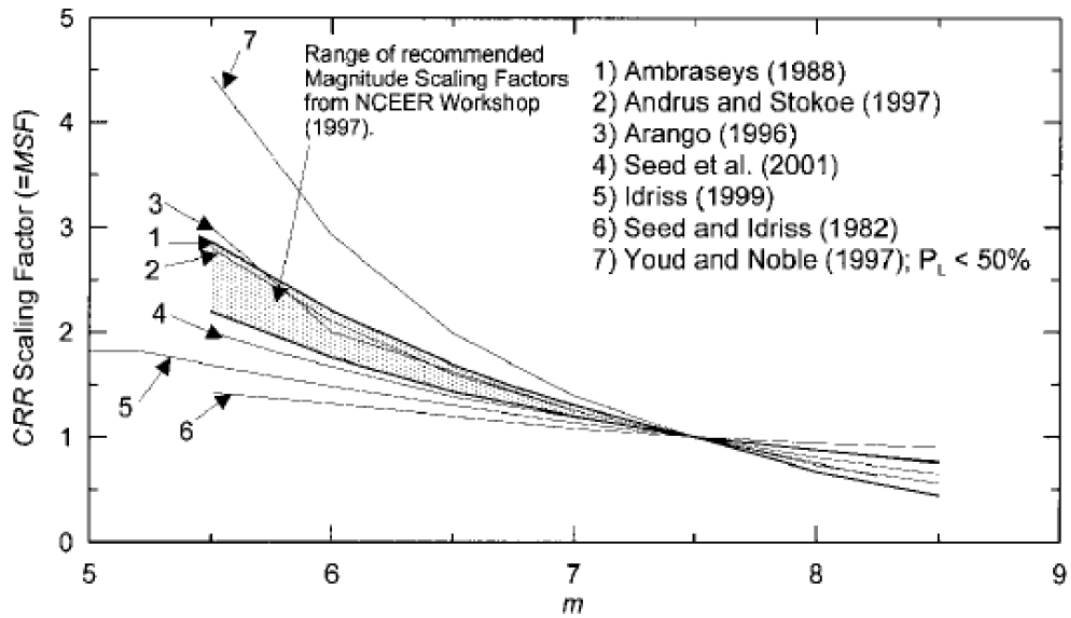
Figure 6.15: Comparison of Published CRR Weighting Factors

From the example above, it shows that all impoundment facilities at location Zone VIII is not at risk for liquefaction from New Madrid Seismic Zone. On the other hand, for impoundment facilities located in Zone IX with PGA of 34-65 %g, two specimens have lower factor of safety than 1, as can be seen in Table 6.2.

Using the information above, it is apparent that the effect of waste materials affecting factor of safety against liquefaction. As shown, without any addition of waste material, fly ash composition at zone IX has safety factor less than 1.

The result above also implies that specimen with waste material might withstand vibration from machinery used on impoundment facilities. Today, many storage ponds use back hoes to compact and denser fly ash layer, this mechanism can be replaced by vibrating the pond to get better and more stable conditions with the help of adding waste material to the existing fly ash layer. At the same time, the same materials also increase the safety of storage ponds while machinery is at work in order to make sure that a vibration generated by the machinery will not disrupt the stability of storage pond.

From an economical perspective, the compacted dry density of fly ash is typically in the range of 70 pcf to 80 pcf (Gray and Lin, 1972) which is well below most conventional fill materials such as clay (Around 110 pcf) and sand (Around 100 pcf) which gives an economical advantage. For example, 1 ton of compacted fly ash represents a greater volume than 1 ton of conventional earth fill. This is an advantage if

the fill or embankment must be placed on ground of low bearing capacity or where long term settlement is possible.

The cost of siting and preparing new areas for landfills rises every year, these existing impoundment locations are being considered for construction landfills. Before the impoundments can be used for this purpose, the stability of the impounded material must be determined.

Business and cost-effectiveness prospects can be appreciated in the long-term. In the beginning, money allocation to purchase shredder machinery in the facilities might be expensive but as time lapses the facilities will benefit from companies who utilize their impoundment facilities to dump used tires, carpet and paper. This usage will generate income for the company. In conclusion, these facilities will have 2 benefits; improved the stability of impoundment facilities and earned income.

To illustrate, a cost matrix comparison between adding crumb rubber, shredded carpet and paper is presented in Table 6.3. The condition for this comparison used a typical impoundment facilities dimensions with 10% additional waste materials by volume, material in impoundment facilities is in loose condition, but the price to buy shredder for waste material and fees to open and maintain ash impoundment facilities as stated in USEPA regulations are not in consideration.

Table 6.3: Matrix comparison from each waste material

	Fly ash	Waste materials		
		Tires	Carpet	Paper
Vol. 100% fly ash (sq. ft.)	14,287,680	-	-	-
90% of 100% fly ash (sq. ft.)	12,858,912	-	-	-
10% of 100% fly ash (sq. ft.)	-	1,428,768	1,428,768	1,428,768
10% of Waste materials (lb)	-	42,863,040	8,572,608	61,437,024
Money ($)	-	1,071,576	428,630	307,185

Where:

- The impoundment dimensions are 10 acre-ft. with 32.8 ft. depth and a total volume of 14,287,680 sq. ft.

- The density of tire shreds = 30 lb/ft3 (Office of Research, Development, and Technology, Office of Safety, RDT, 2012)

- The density of carpet = 6 lb/ft3 (Assistant Secretary for Housing Federal Housing Commissioner, 1993)

- The density of paper = 43 lb/ft3

- The price for dumping a passenger car tire = $0.50 per tire with average weight of passenger tires as scrap are 20 pounds (Department of Ecology state of Washington, 2010)

- The price for dumping carpet = 5 cents per pound

- The price for dumping paper = 0.5 cents per 50 pound

- Typical shredder machine price = $175,000 - $475,000

- Not under consideration: loss of fly ash volume in impoundment, legal fees, permit fees and other regulations (including tribal issues) such as wastewater collection, storage or treatment system permit and an NPDES permit (U.S. EPA, 2016)

As mentioned in Chapter 1, the total cost of managing coal combustion waste ranged from $2.20 to $34.14 per metric ton in 1988 (USEPA, 1988) and depends on the distance from power plant to the impoundment. With the money that power plants receive from opening their impoundment facilities to waste material the overhead cost might be reduced. From Table 6.3, 90% of fly ash is 12,858,912 sq. ft. and if converted to weight using a density of 70 pcf will give 450,062 ton. This amount of fly ash will cost power plants ranging from $990,136 to $15,365,114 to impound it and with the addition of waste material on their impoundment facilities this cost will decrease.

In conclusion, a number of factors affect disposal costs. The lowest cost occurs when a disposal site is located near the power plant and the material being disposed can be easily handled. If the material can be piped, rather than trucked, costs are usually lower. In these types of situations, cost may be as low as $3.00 to $5.00 per ton. In other areas, when distance is far away and the material must be handled several times due to its moisture content or volume, costs could range from $20.00 to $40.00 a ton. In some areas, the costs are even higher. If new sites are required and extensive permitting processes take place, the total cost of the facility may be increased, resulting in higher disposal costs over time.

Confidently with the results shown on this research, it can be implemented as an alternative to stabilize fly ash inside any treatment ponds, use fly ash admixtures as material for impoundments dikes and enhance liquefaction resistance against dynamic loading from earthquake while also reducing waste stream volumes

Finally, although fly ash is a liquefiable material nevertheless, it possesses some hidden potential such as durability, sustainability enhancements, safety enhancements reduction in pollutants and cost effectiveness/economic benefits.

6.3   Future Research

Many aspects can be modified, changed and improved to make this research better. One way to improve this research is to increase the size of sample specimen; this might generate a more precise result to represent in-situ condition.

Low permeability decreases the probability of extensive ground water percolation and the consequent in danger of soluble material being leached out of the fill. Low permeability, on the other hand, also means a high degree runoff or higher dikes; therefore precautions to prevent erosion of side slopes should be taken. The next step is to have a series of slope stability testing of compacted Class F fly ash and fly ash mixtures to find the factor of safety so it can be implemented on the field.

For future research, the variation in dimensions, specification and compositions of waste materials might be in considered for testing. Adding waste materials beside

crumb rubber, shredded carpet and shredded paper, with other waste material might proof to also enhance the strength properties of fly ash.

Materials that originate from construction and demolition (C & D) waste might also be in consideration. Construction and demolition materials can be collected from construction, renovation and demolition of any structures. This material consists of concrete, wood, metal, brick, glass, etc. Similar to other waste materials, C & D materials also get placed in landfills and experience the same problematic situation with the other waste materials. One of the options to reduce the waste is by reusing and recycling.

APPENDIX A

CYCLIC TRIAXIAL TEST RESULTS

In this section, a summary of the cyclic triaxial test results for each specimen are

presented (Table A.1 – A.4 and Figure A.1 – A.95).

Table A.1: Specimen Information for 100% Class F Fly Ash

Sample Information:			
Specimen	F100		
Target CSR	0.50	0.30	0.15
Depth (Meter)	9.1	9.1	9.1
Depth (ft)	30.0	30.0	29.9
Preparation phase:			
Net. Solid weight (lb)	1.3519	1.3879	1.3997
Diameter (inch)	2.7861	2.7797	2.7907
Height (inch)	5.7552	5.7025	5.7748
Ratio of height/diameter	2.07	2.05	2.07
Gs	2.18	2.18	2.18
Void ratio	1.04	0.96	0.99
γdry (pcf)	66.58	69.3	68.47
γsat (pcf)	98.44	99.91	99.46
Saturation phase:			
B-value (%)	98	96	98
Shear phase:			
Frequency (Hz):	0.5		
Period (Sec):	2		
Asked Deviator Stress (psi)	15.0	9.4	4.9
Confining Pressure (psi)	7.5	7.8	7.7
Actual CSR	0.444	0.296	0.166
Ncycle to liquefy	3	26	51

Definitions:

F = Class F Fly Ash

100 = Percentage of Waste Material by Dry Weight
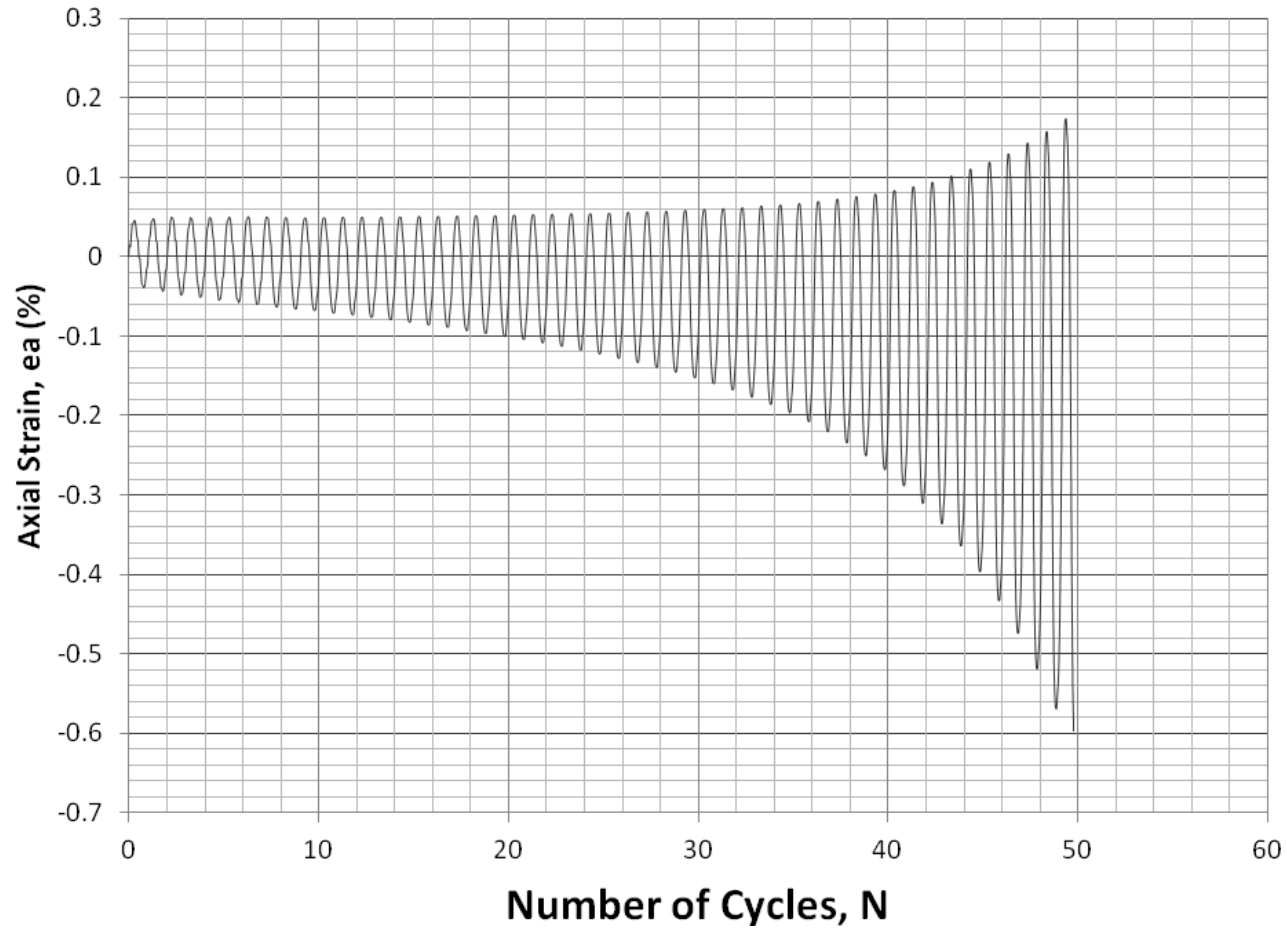
Figure A.1: Specimen F100 CSR 0.15 Axial Strain Versus Number of Cycles Graph
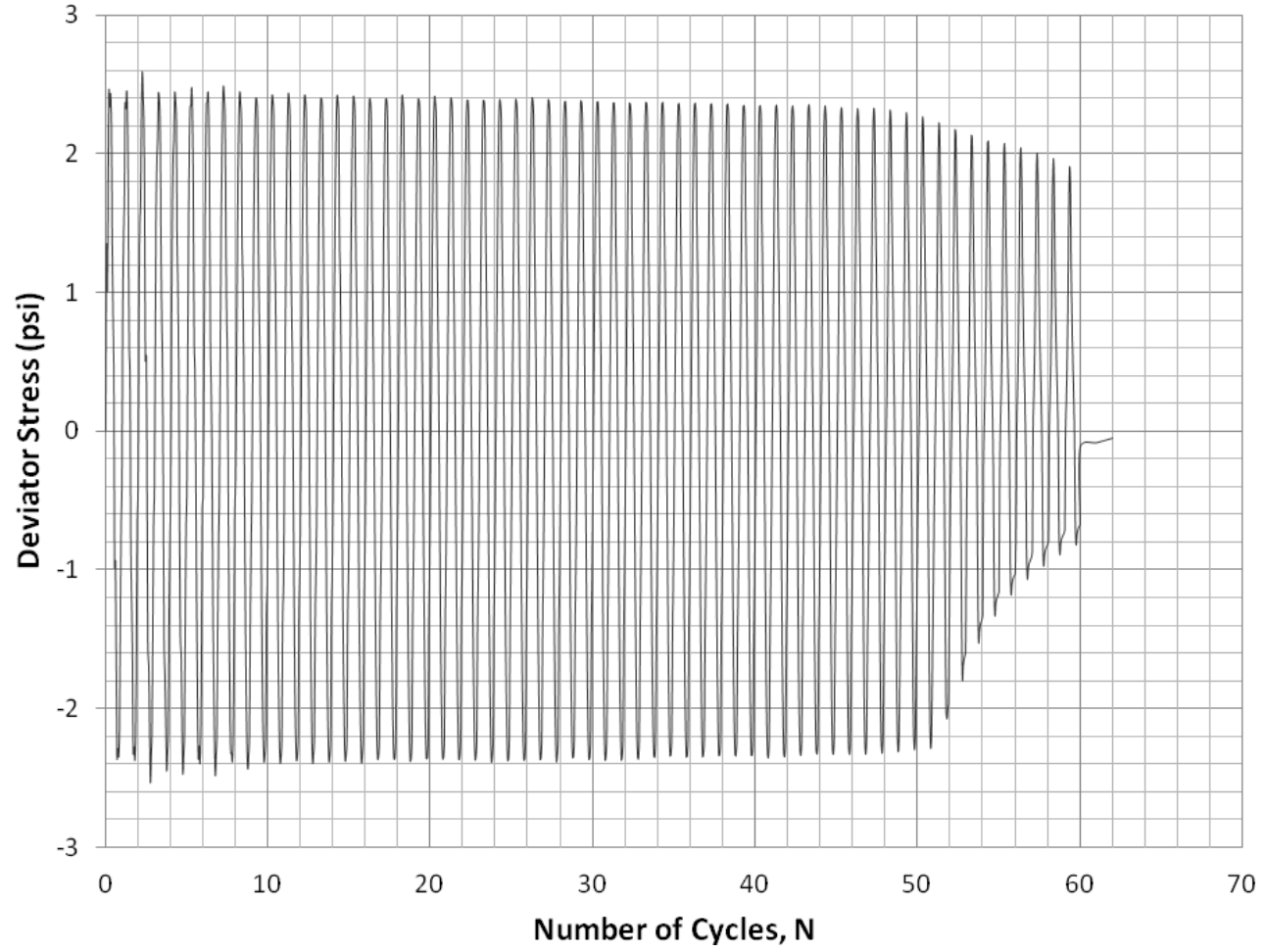
Figure A.2: Specimen F100 CSR 0.15 Deviator Stress Versus Number of Cycles Graph
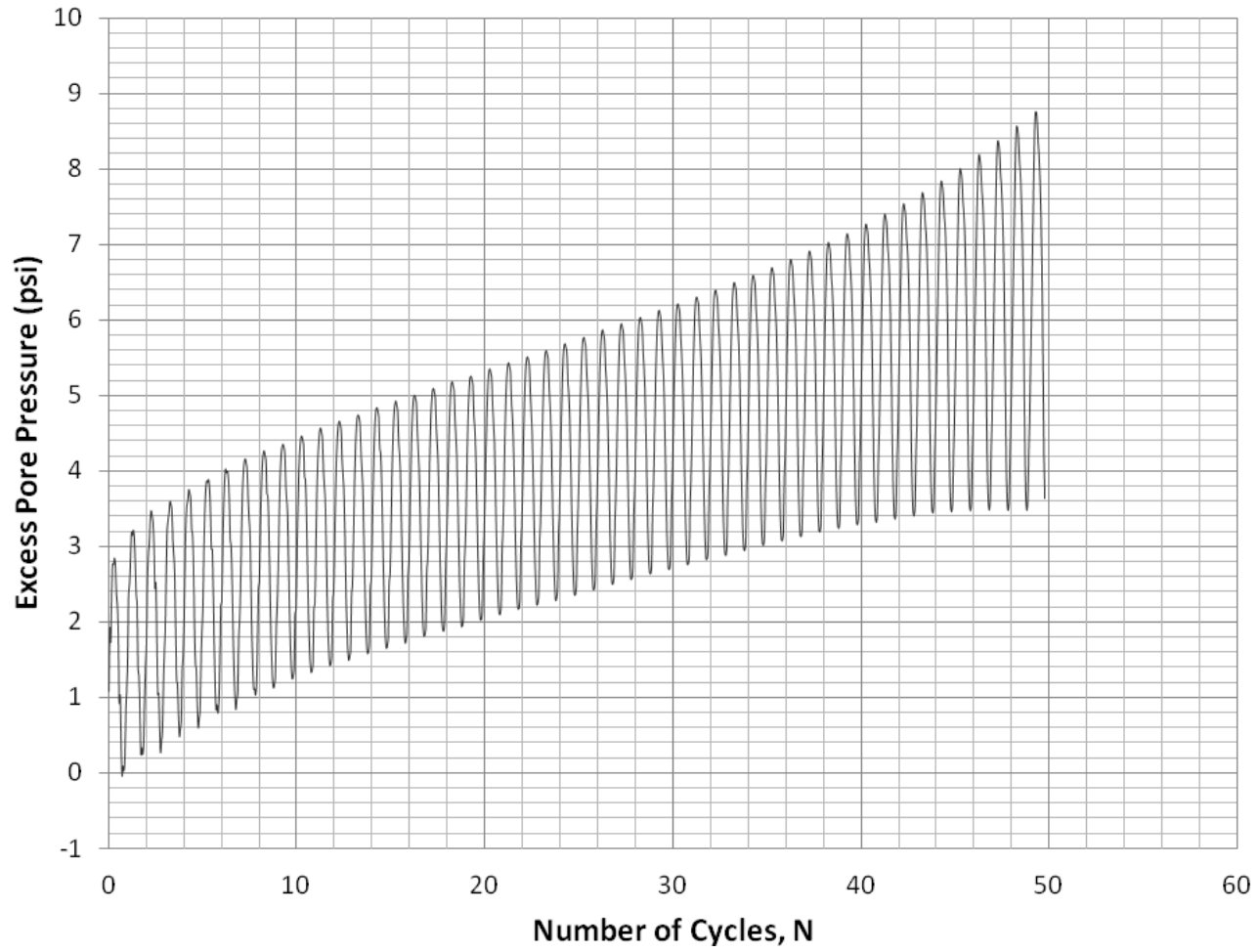
Figure A.3: Specimen F100 CSR 0.15 Excess Pore Pressure Versus Number of Cycles Graph
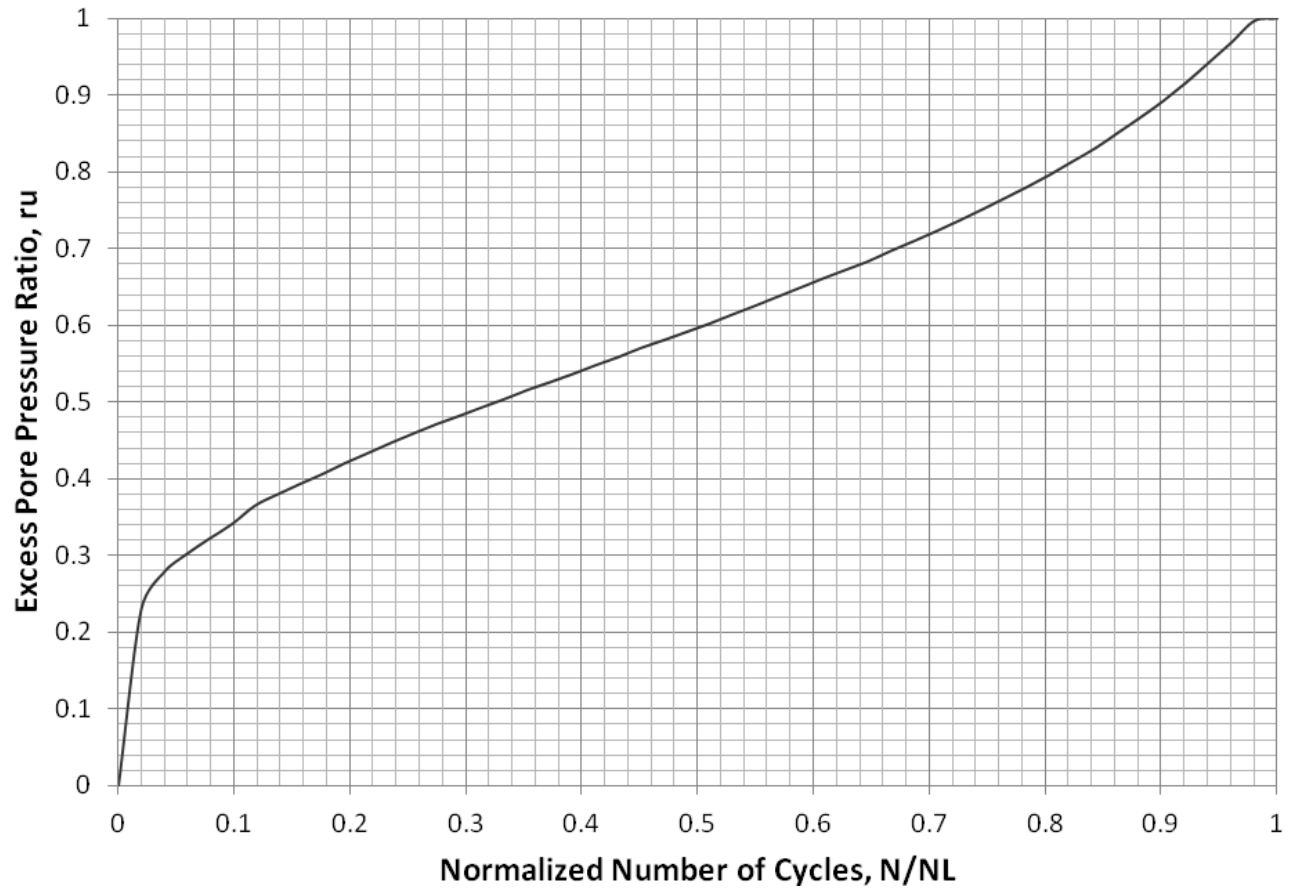
Figure A.4: Specimen F100 CSR 0.15 Excess Pore Pressure Ratio Versus Normalized Number of Cycles Graph
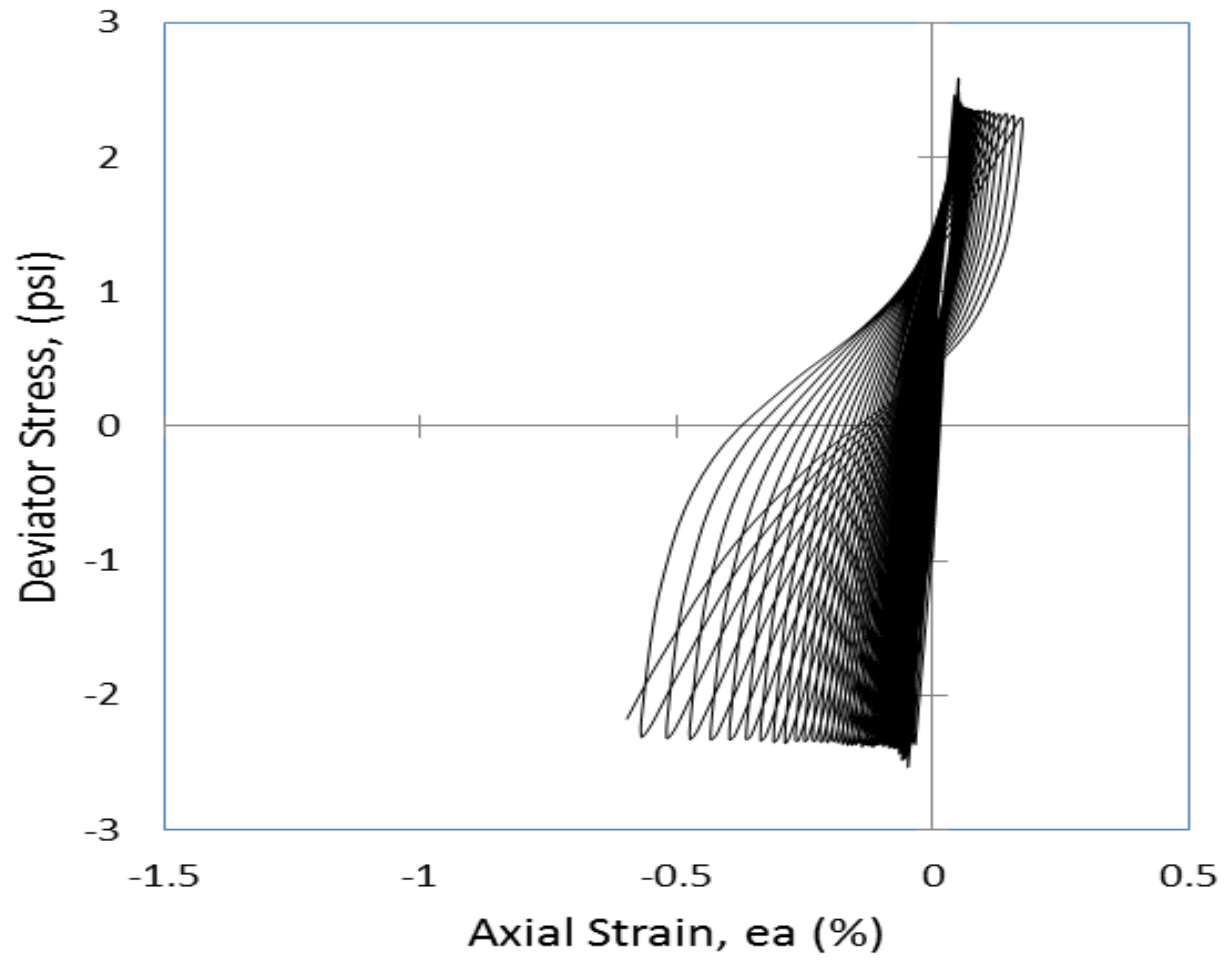
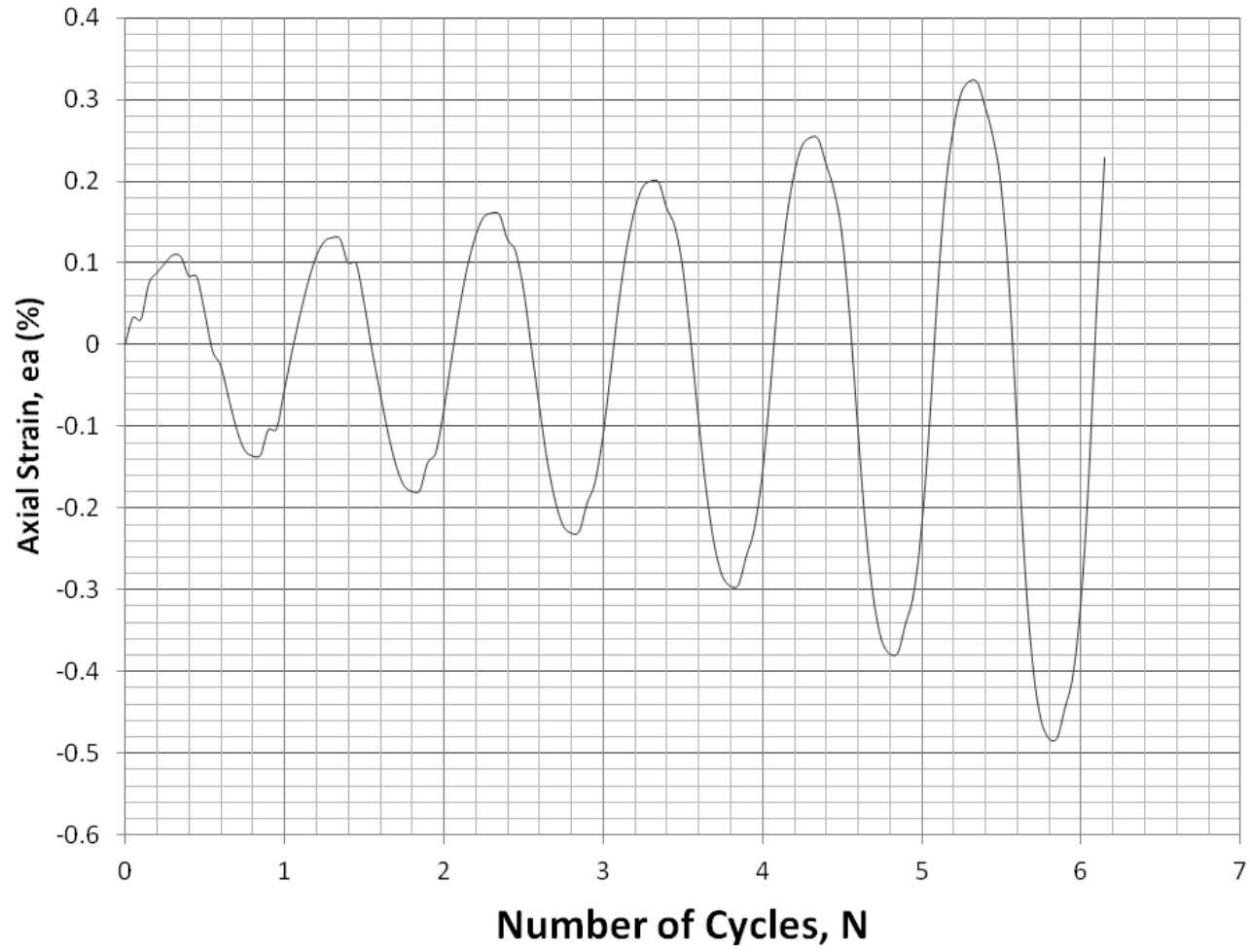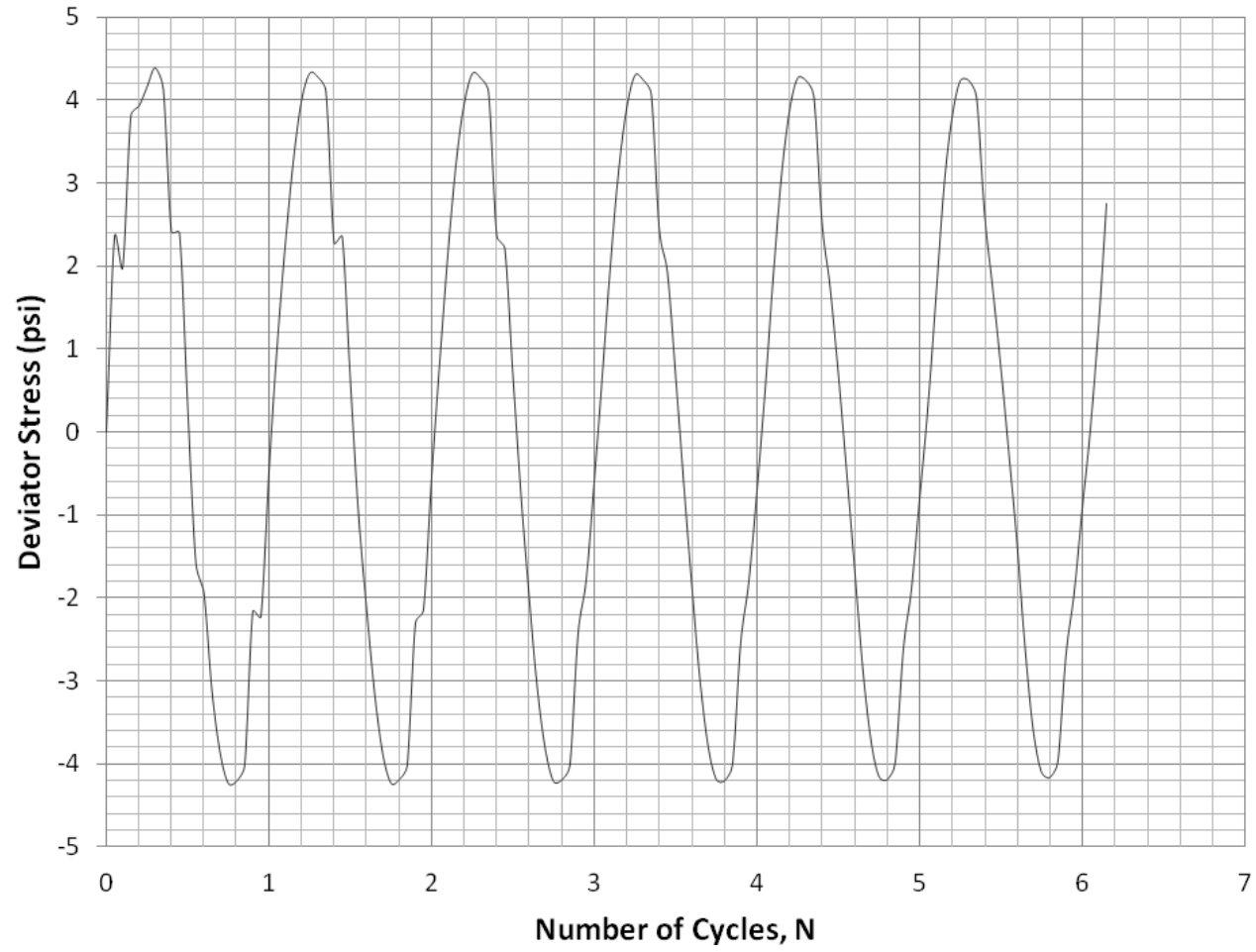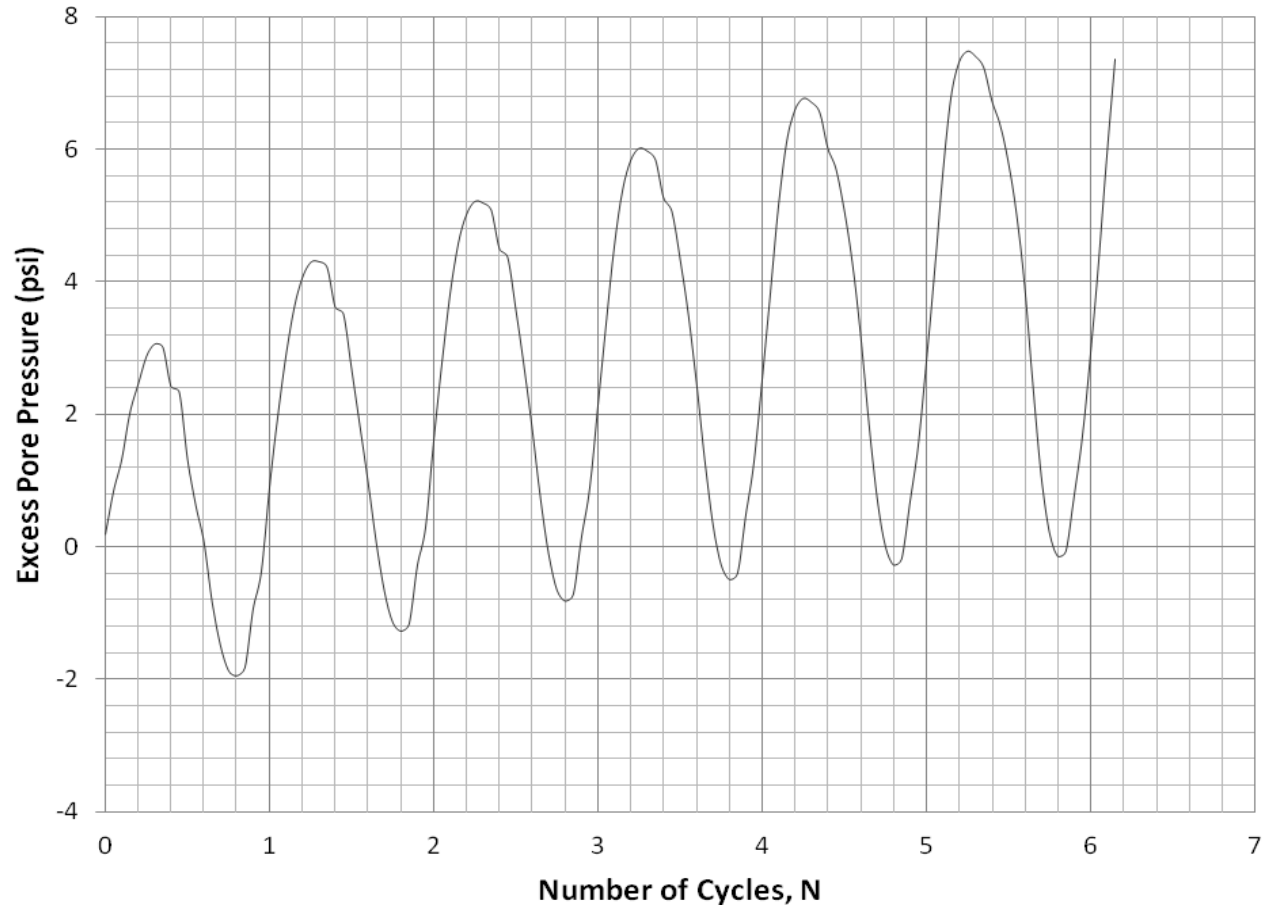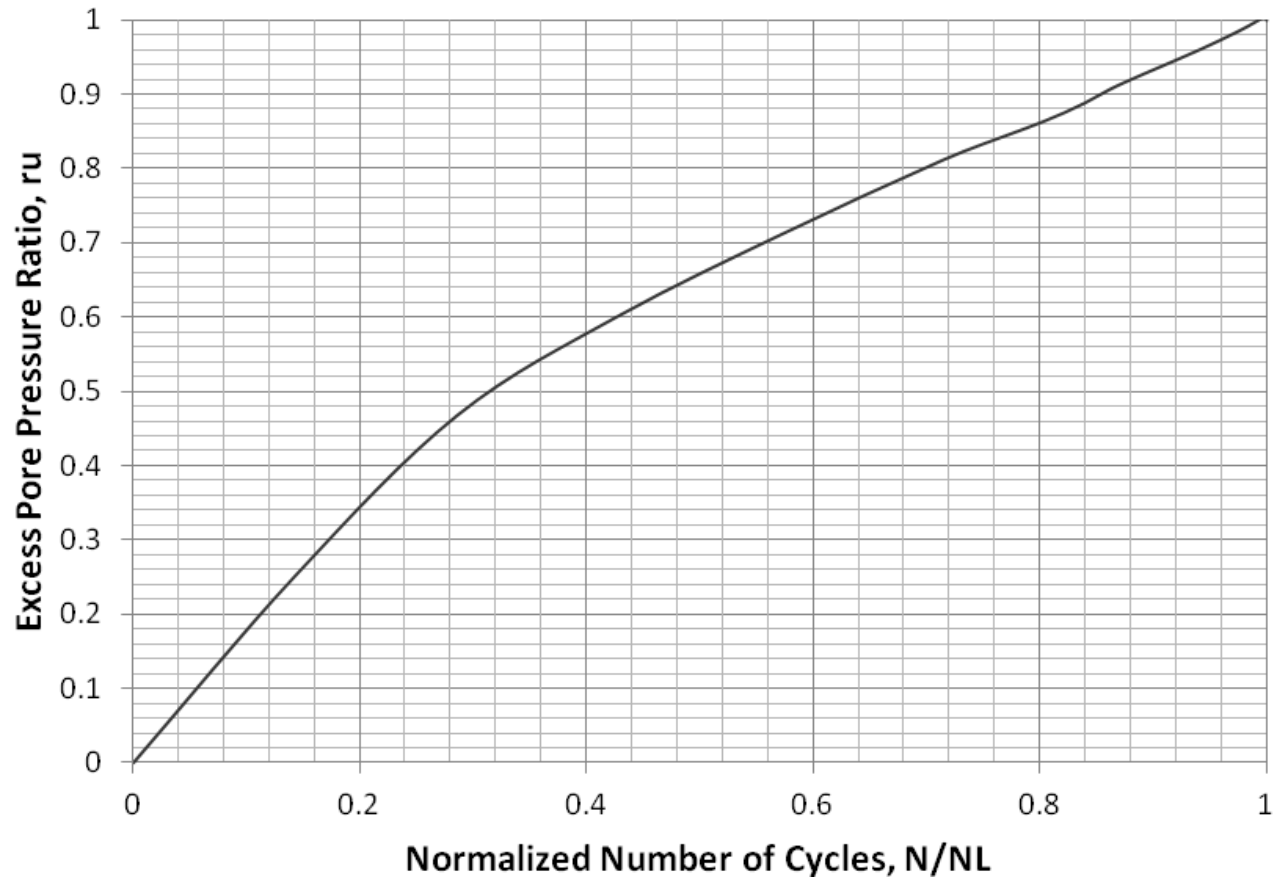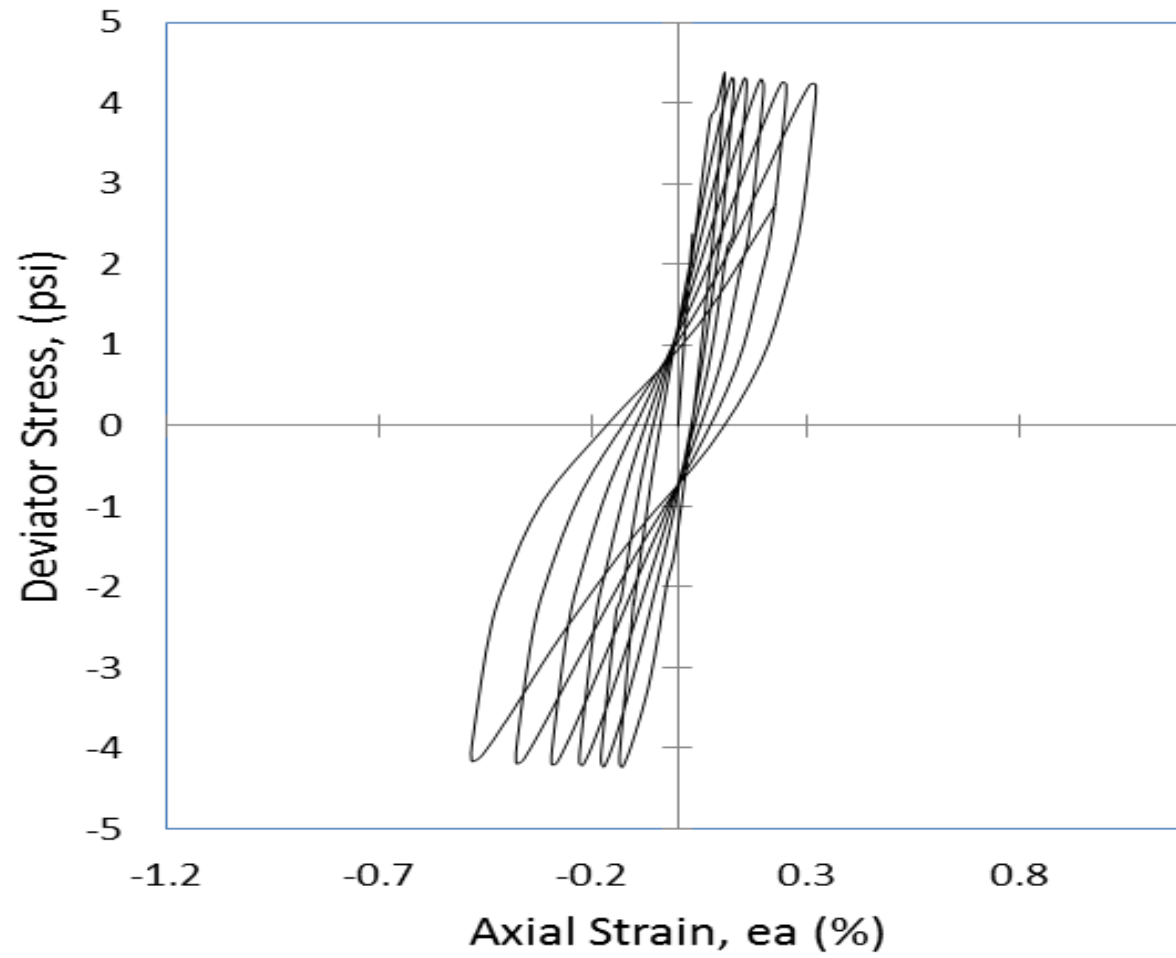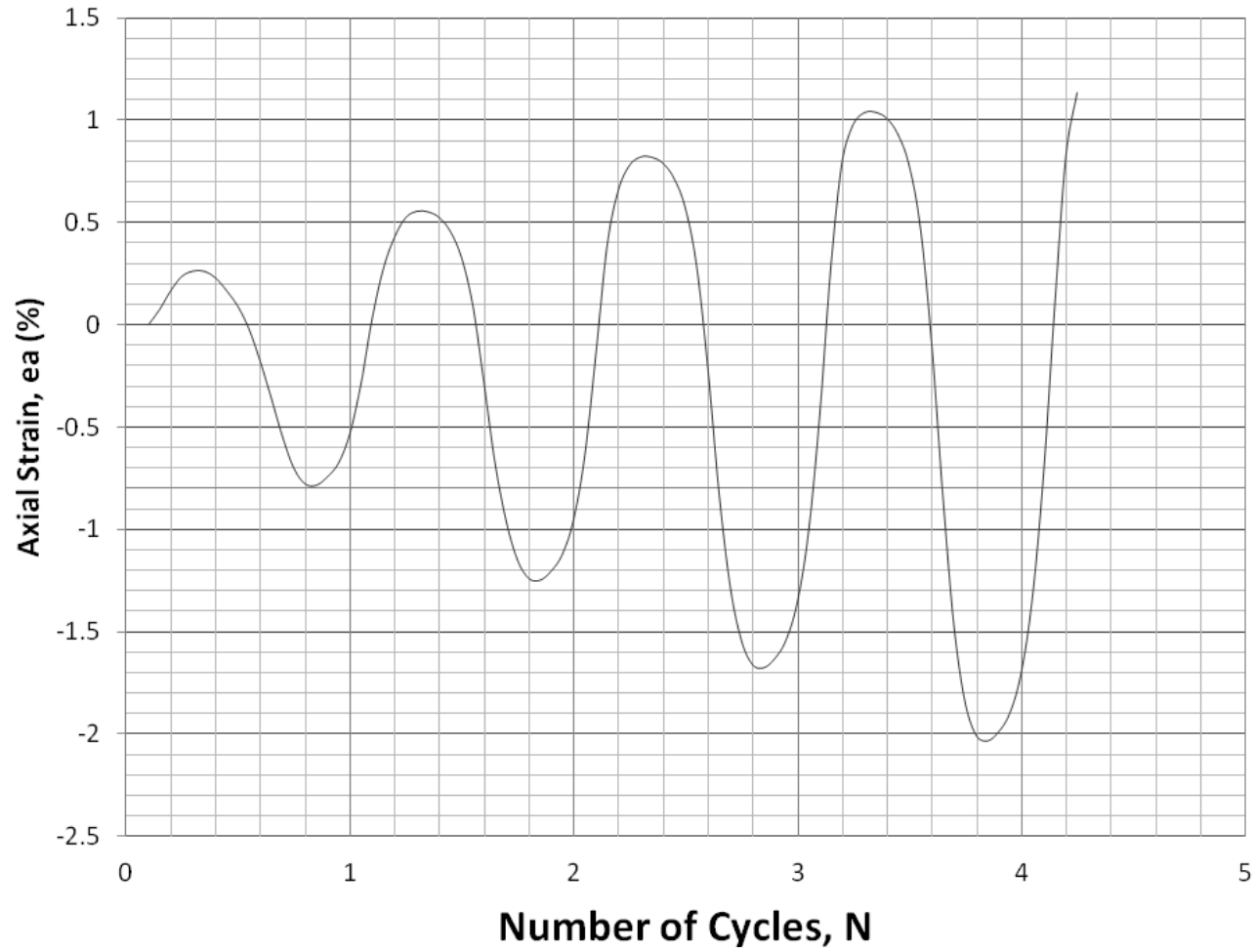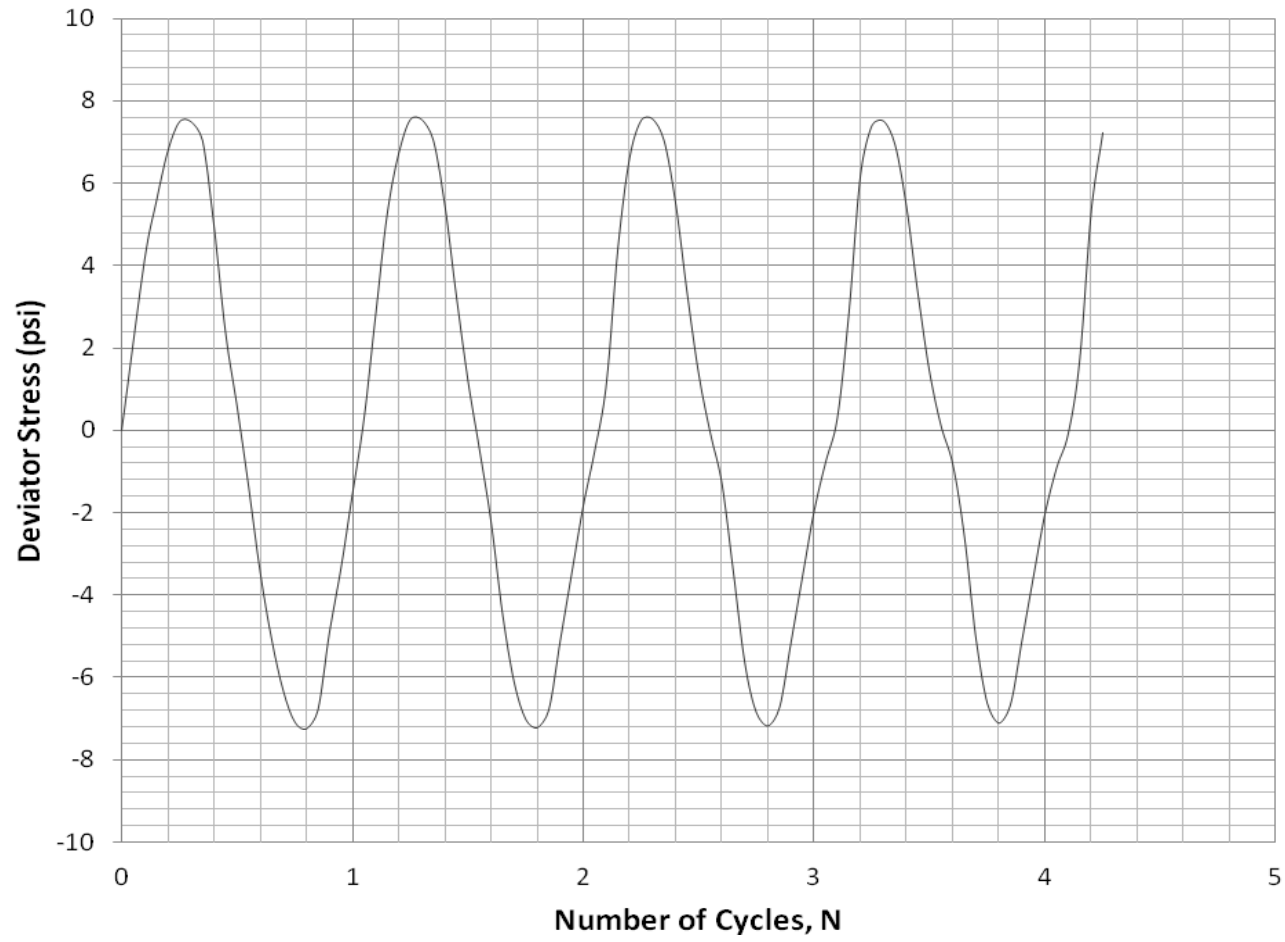Figure A.5: Specimen F100 CSR 0.15 Deviator Stress Versus Axial Strain Graph
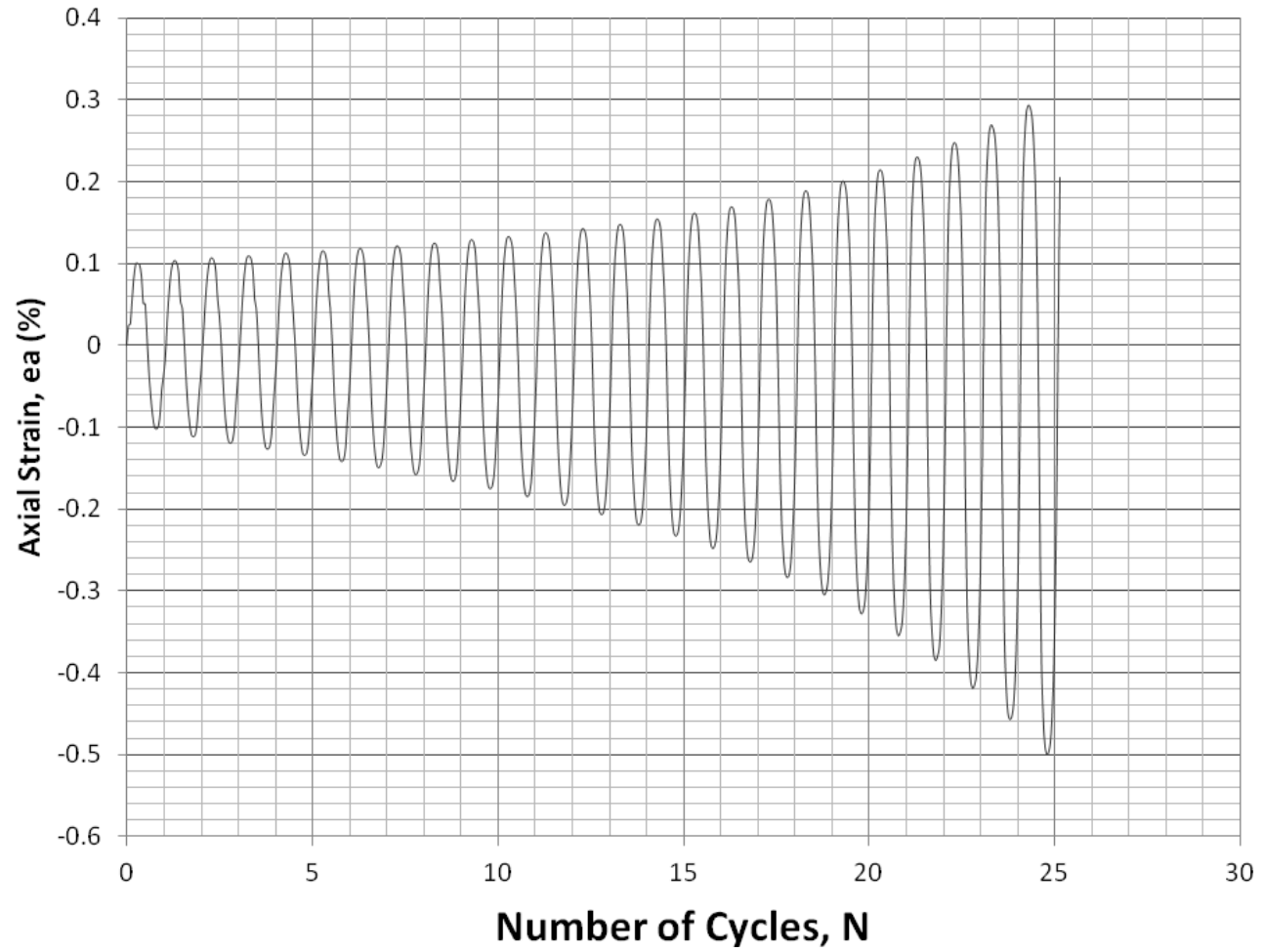
Figure A.6: Specimen F100 CSR 0.30 Axial Strain Versus Number of Cycles Graph
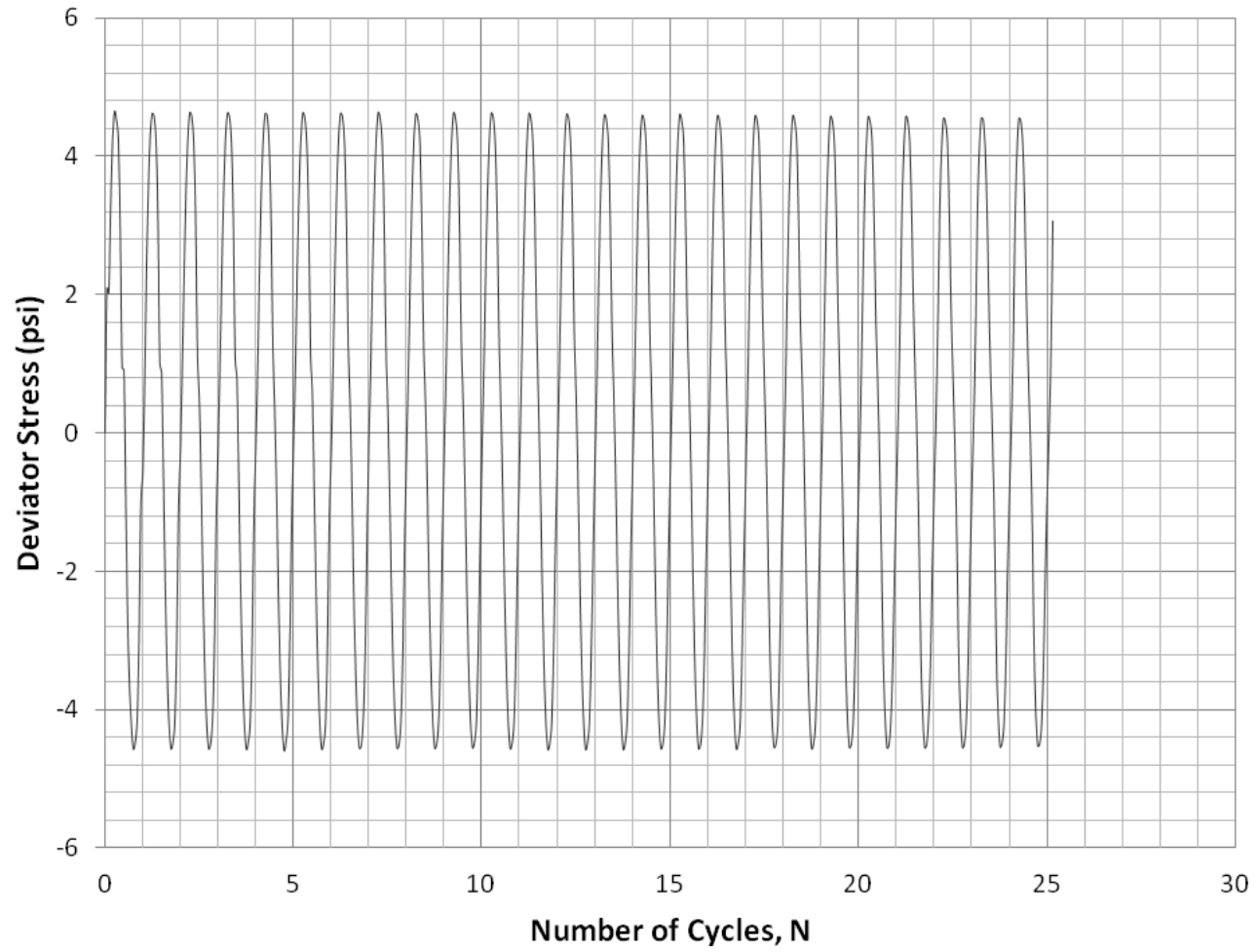
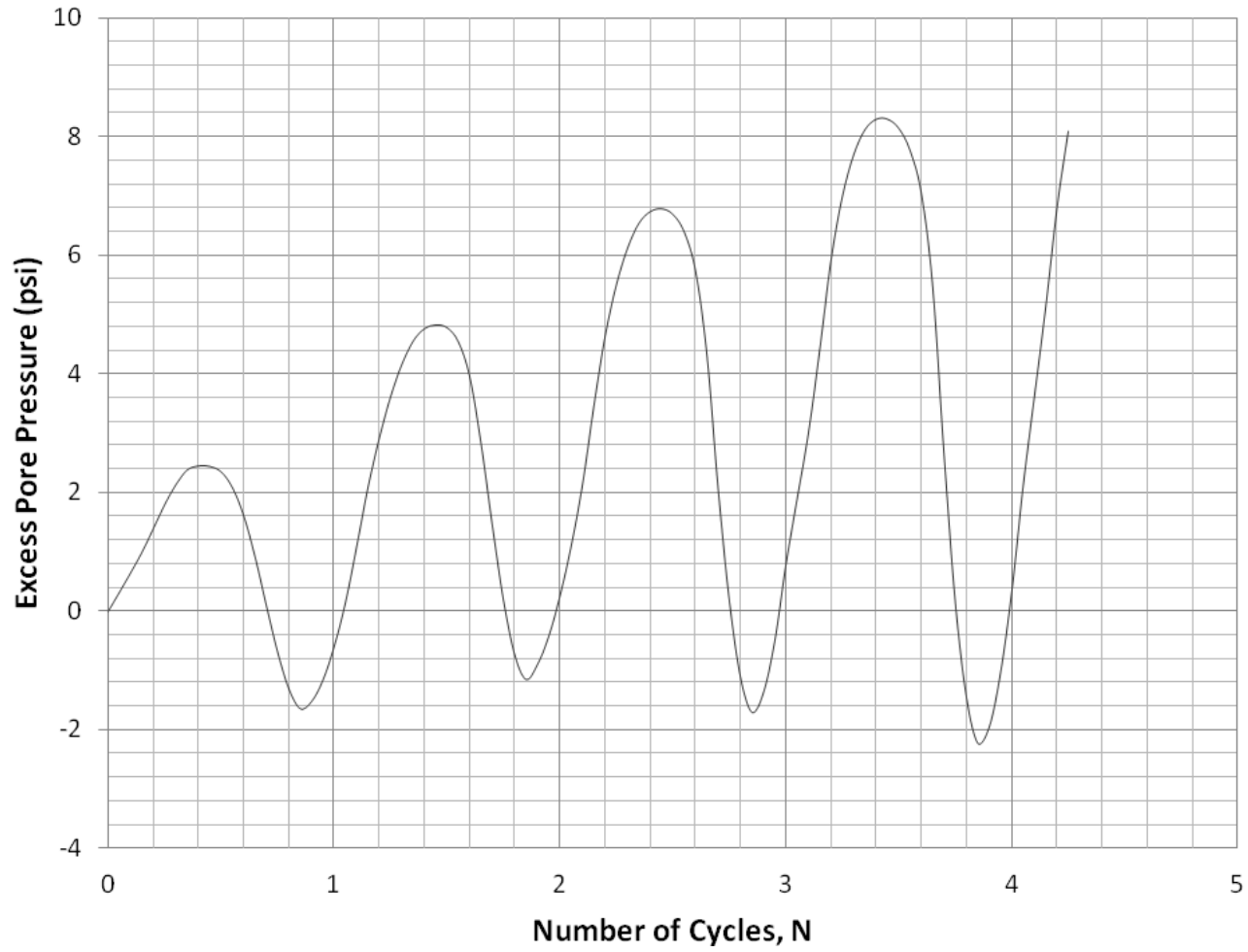Figure A.7: Specimen F100 CSR 0. 30 Deviator Stress Versus Number of Cycles Graph
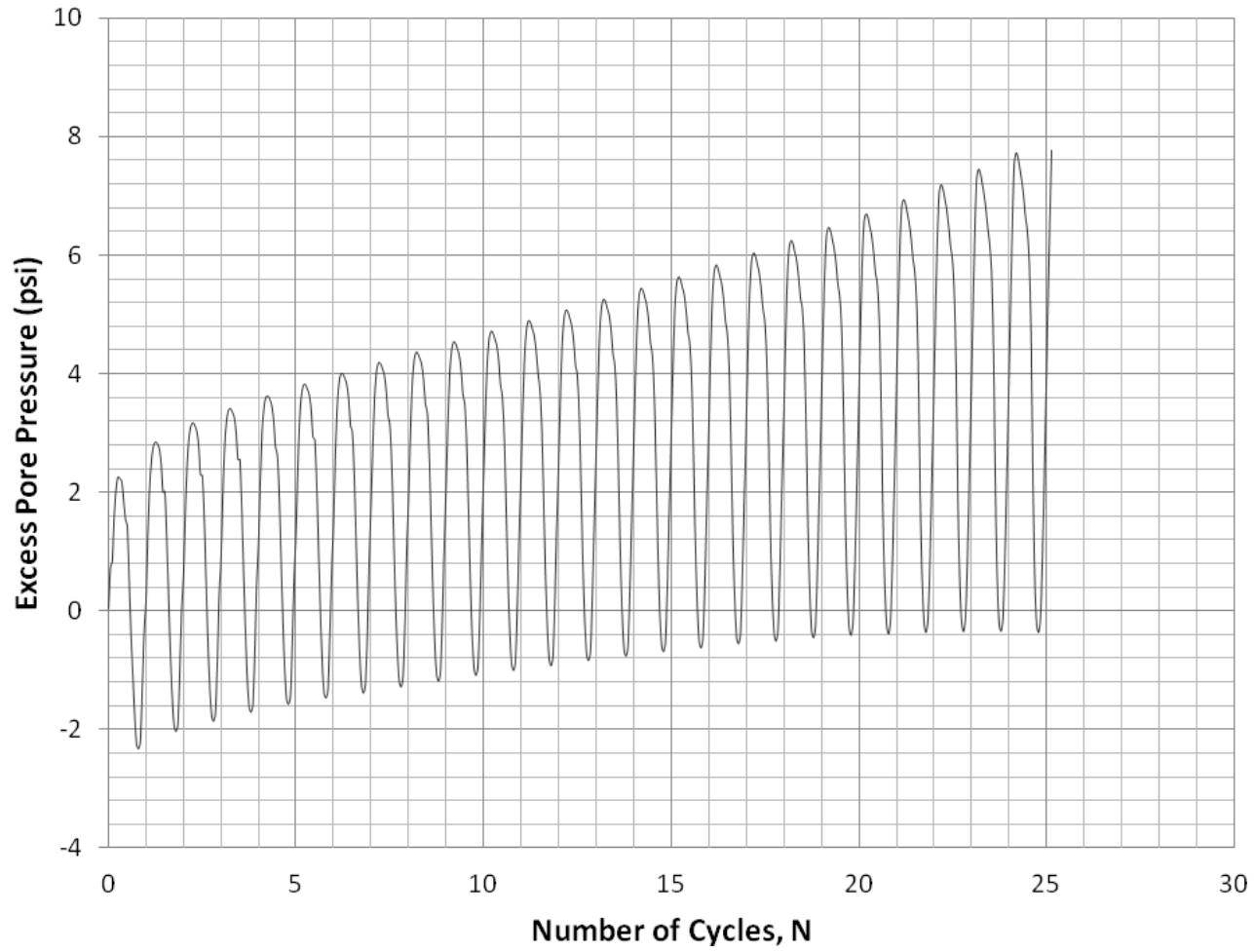
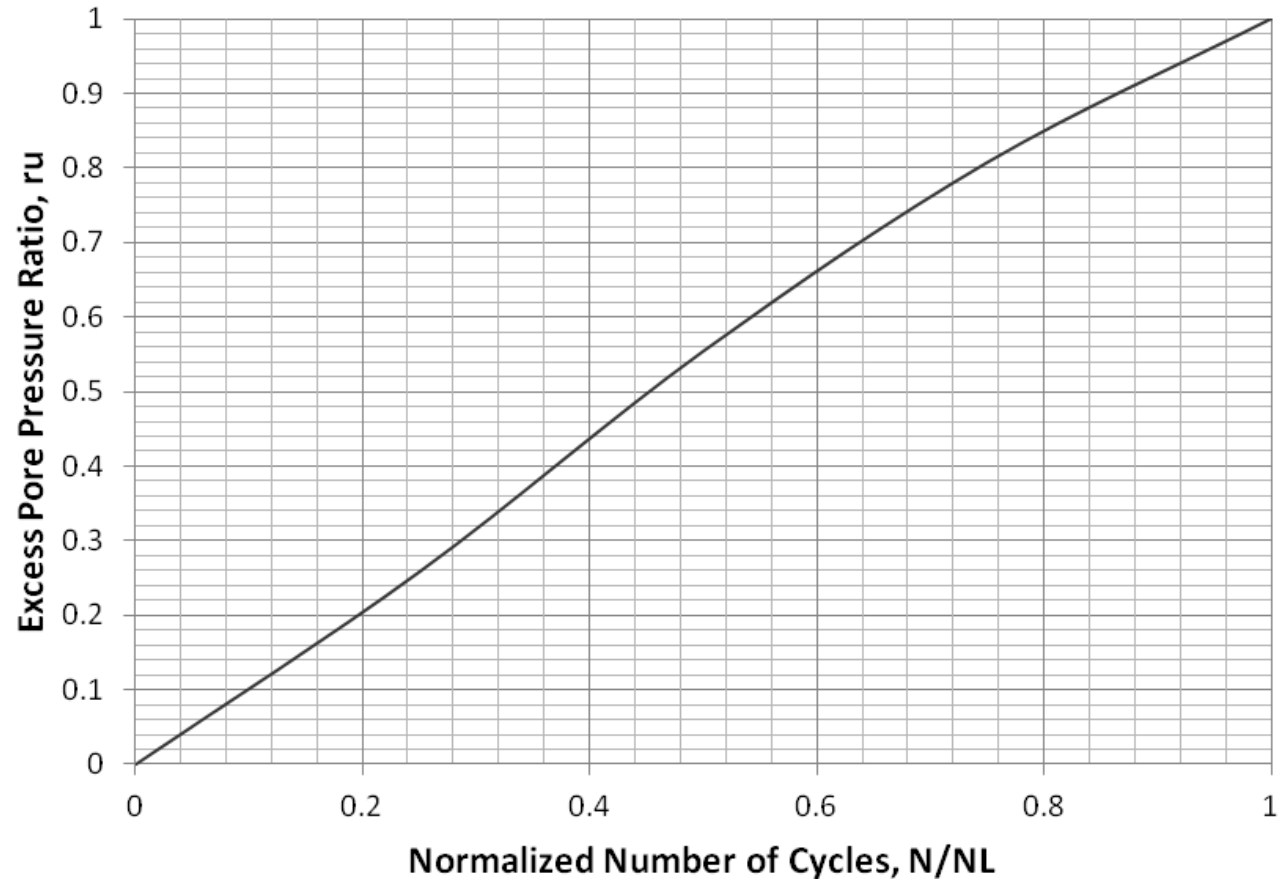Figure A.8: Specimen F100 CSR 0.30 Excess Pore Pressure Versus Number of Cycles Graph
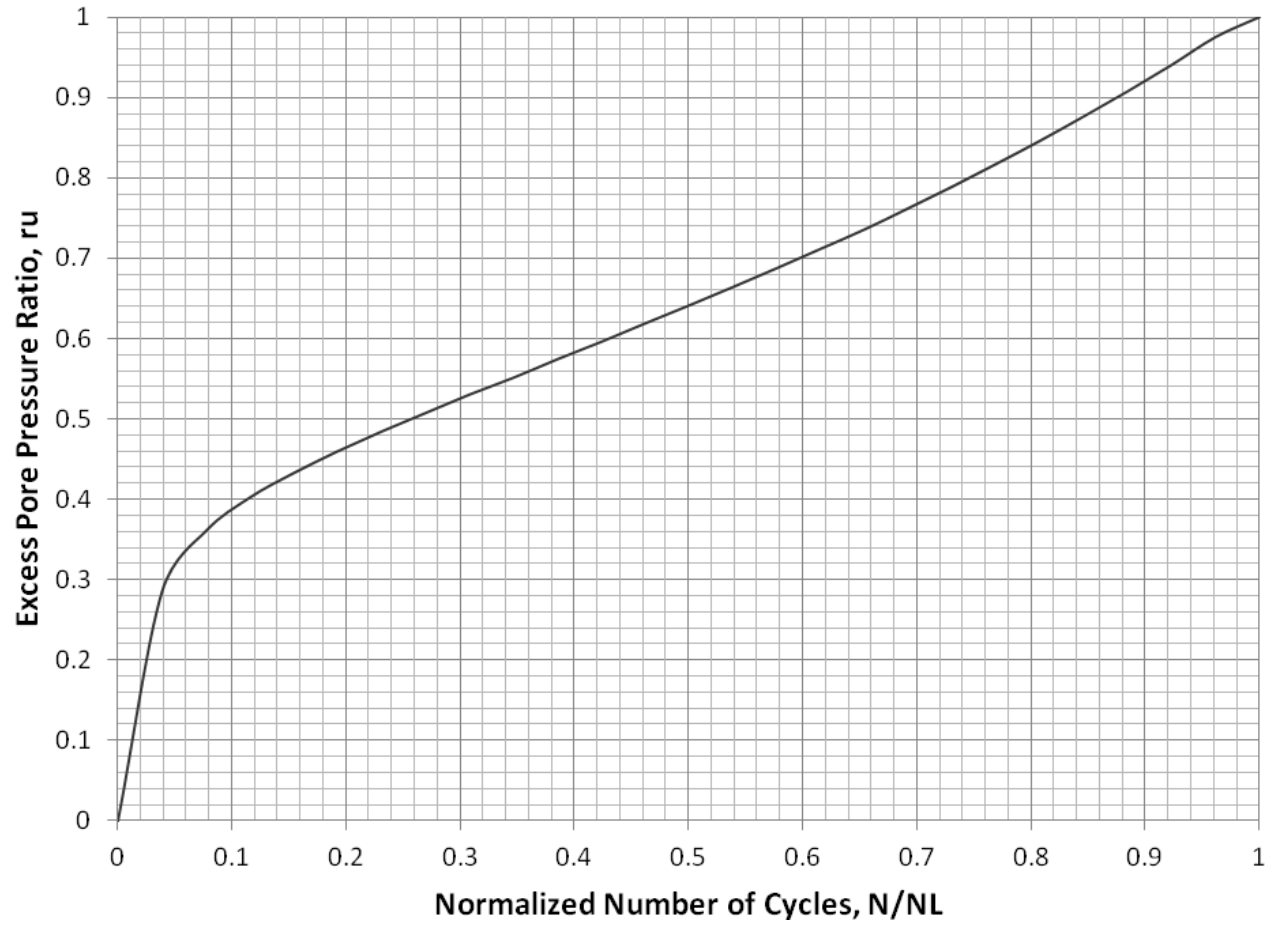
Figure A.9: Specimen F100 CSR 0.30 Excess Pore Pressure Ratio Versus Normalized Number of Cycles Graph
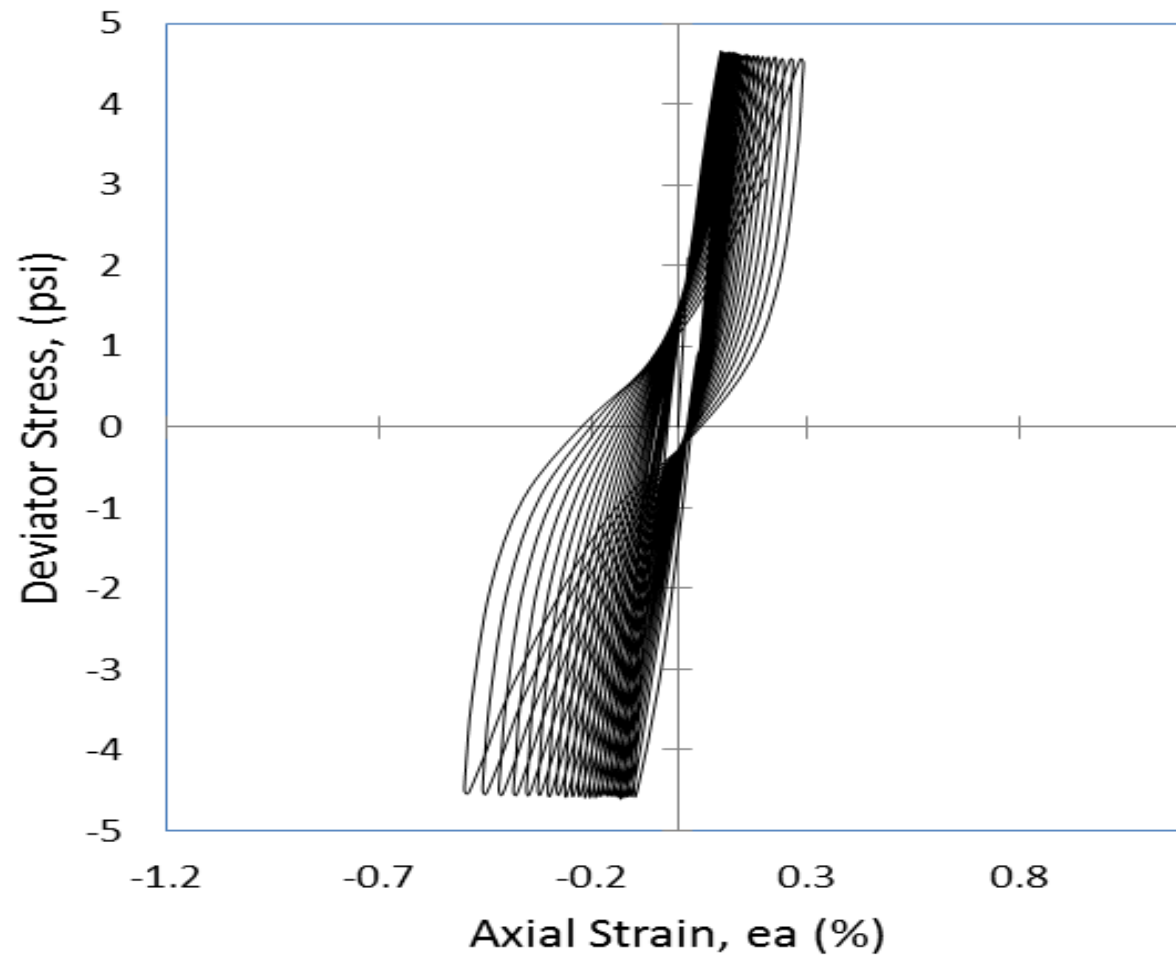
Figure A.10: Specimen F100 CSR 0.30 Deviator Stress Versus Axial Strain Graph
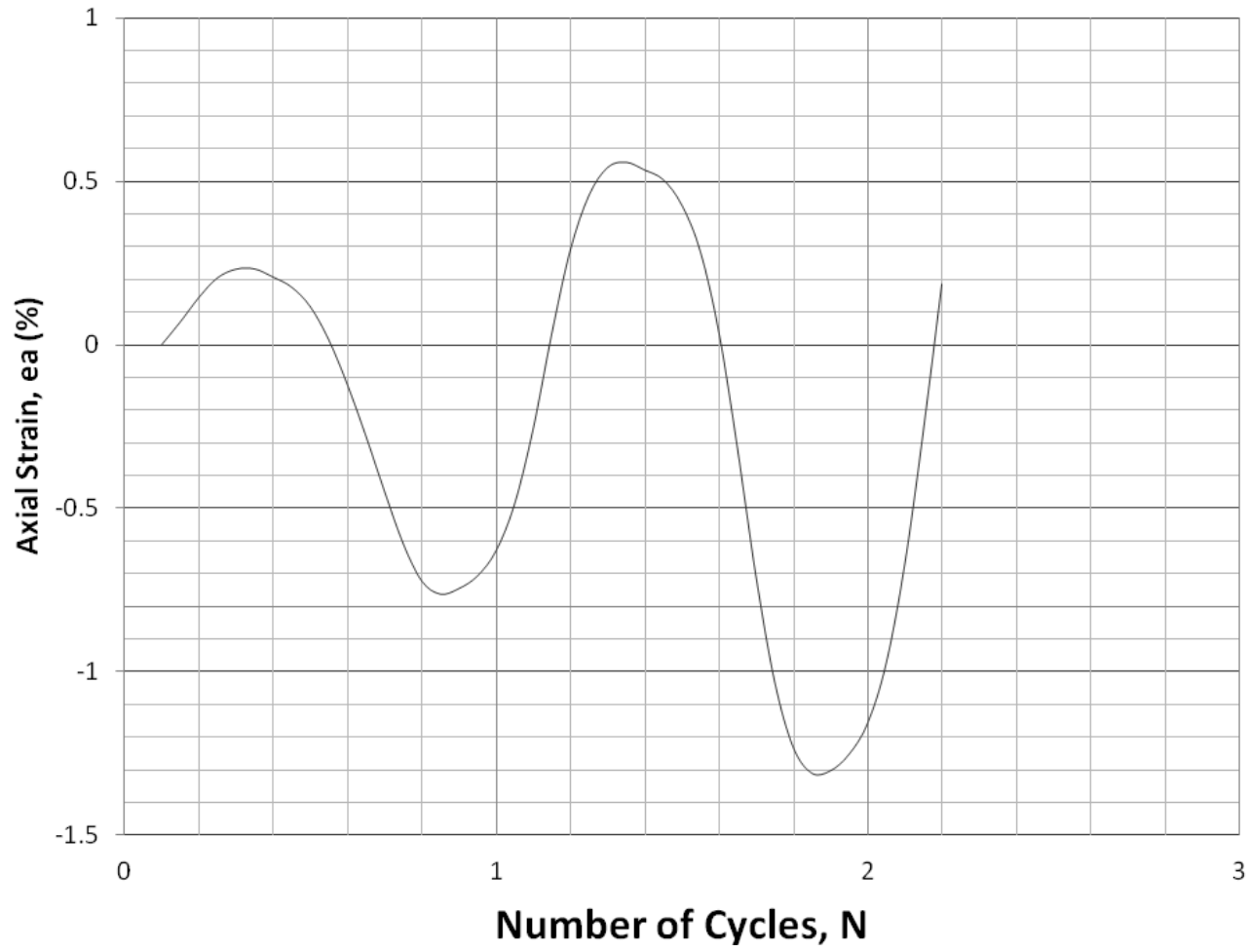
Figure A.11: Specimen F100 CSR 0.50 Axial Strain Versus Number of Cycles Graph
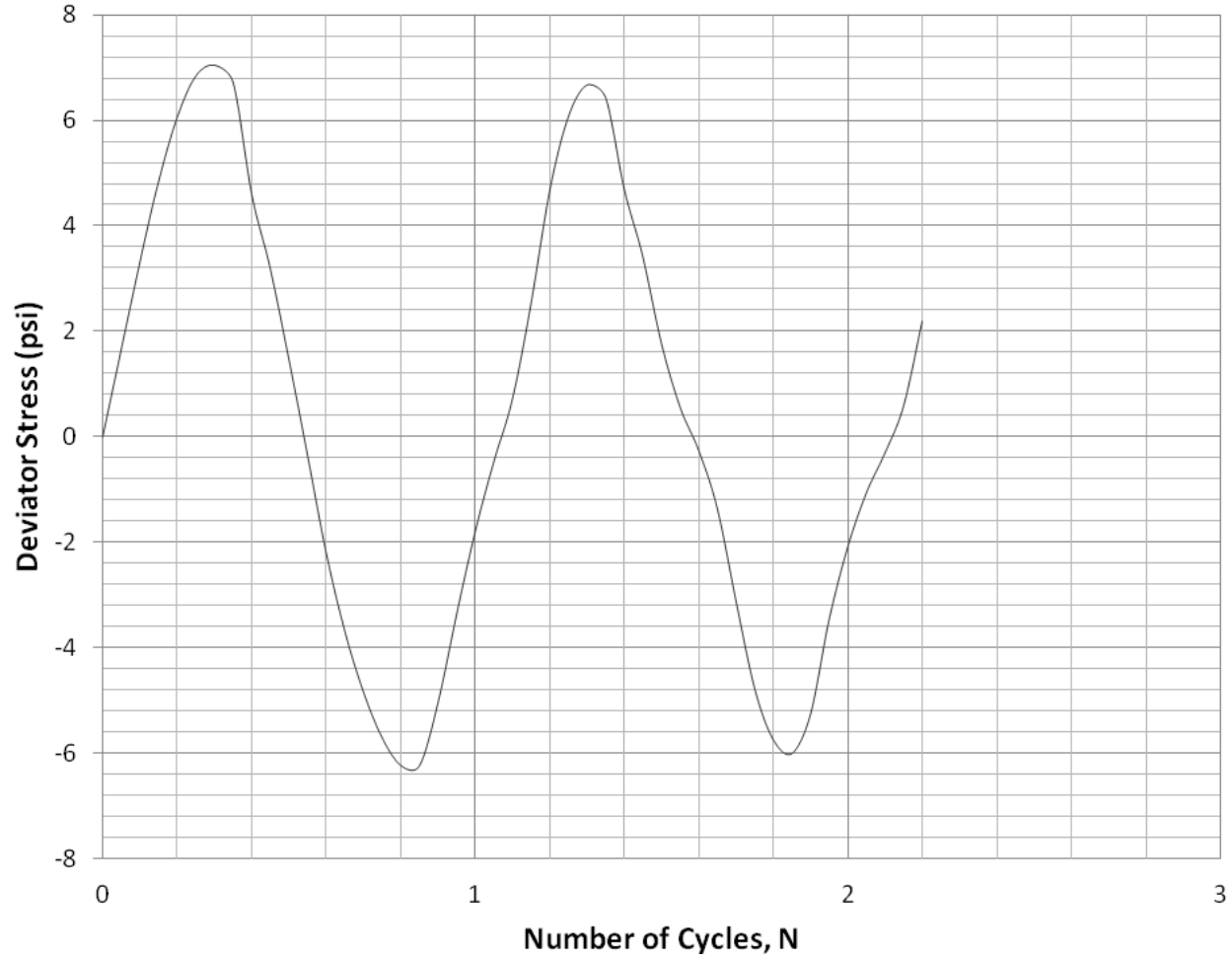
Figure A.12: Specimen F100 CSR 0.50 Deviator Stress Versus Number of Cycles Graph
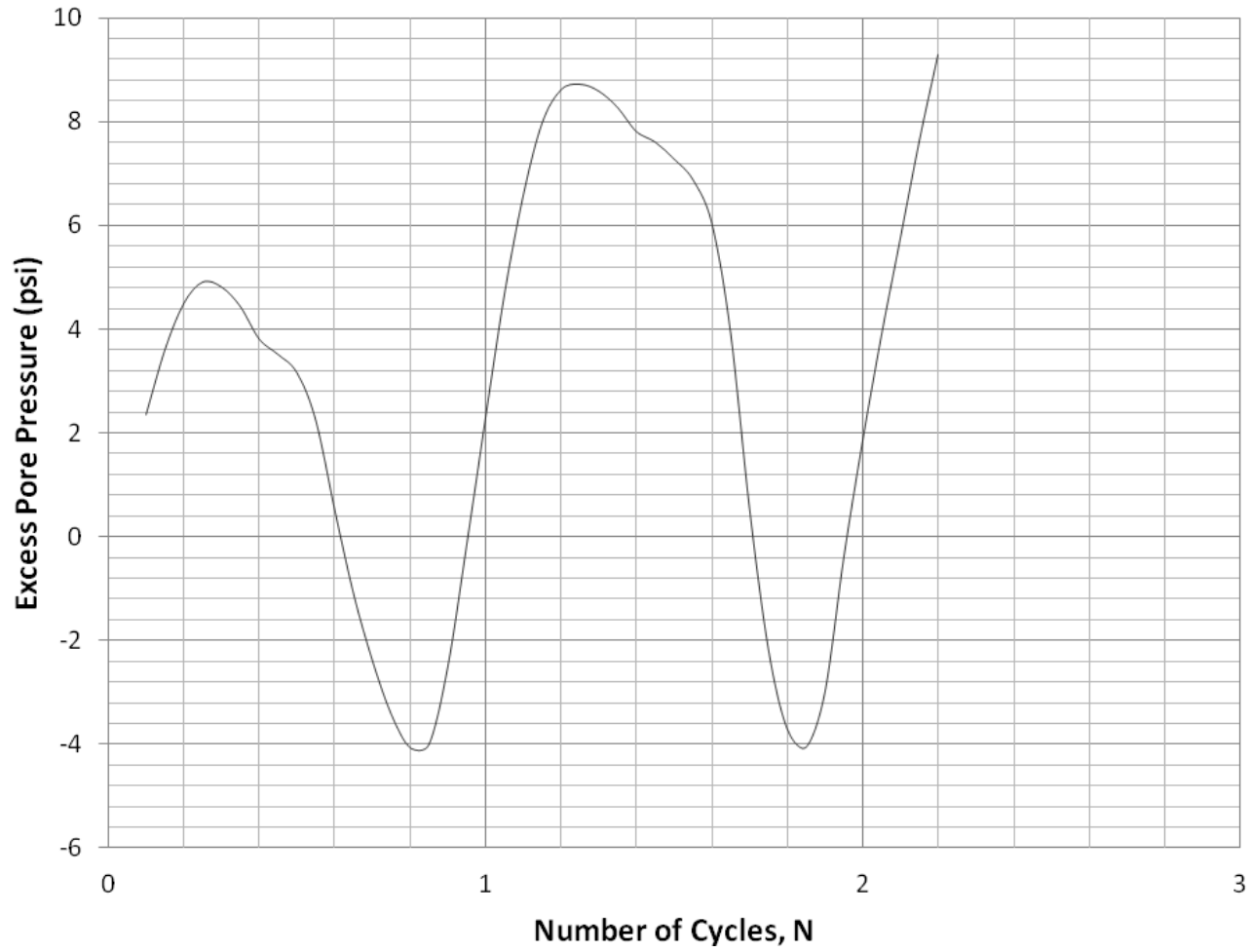
Figure A.13: Specimen F100 CSR 0.50 Excess Pore Pressure Versus Number of Cycles Graph
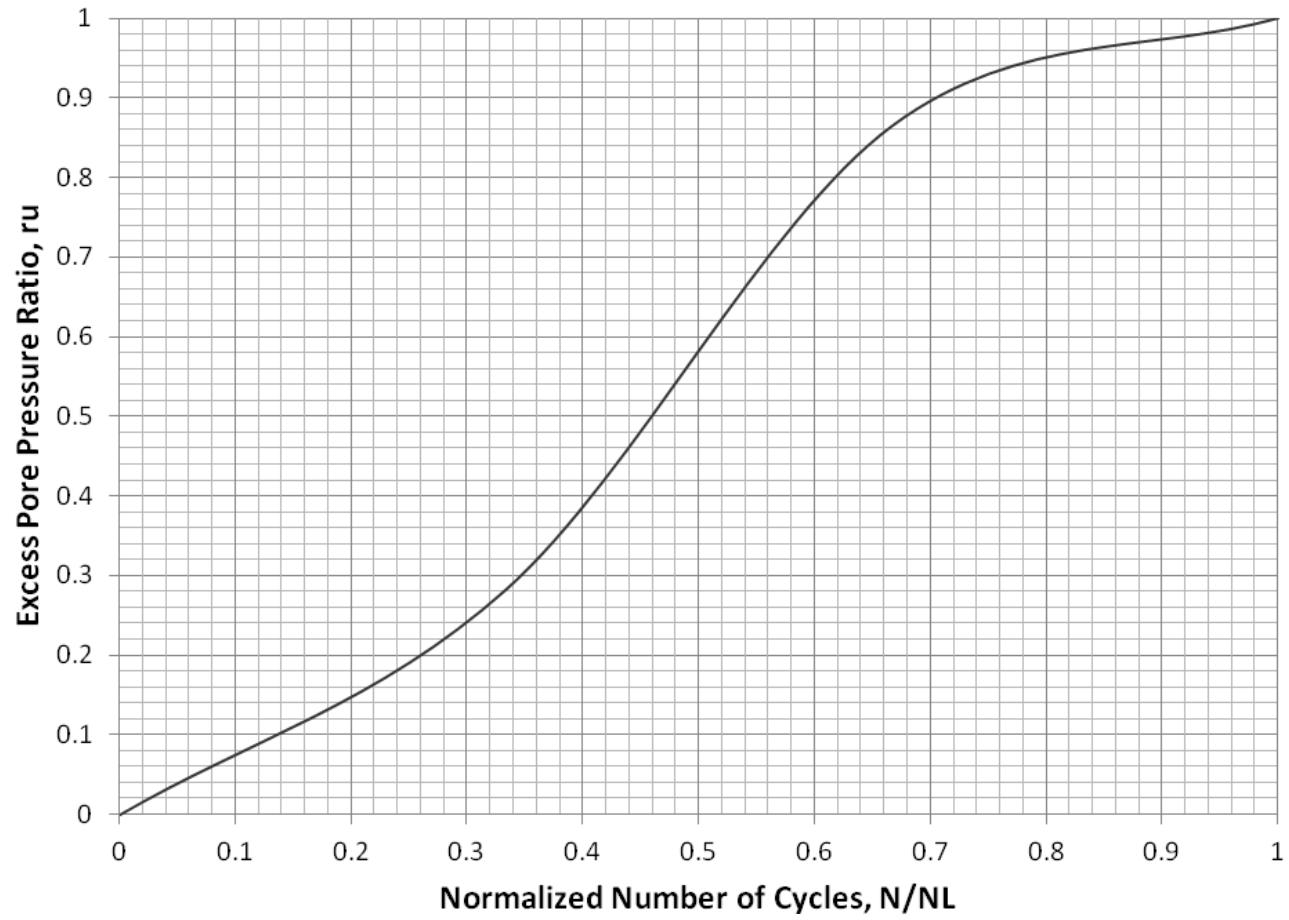
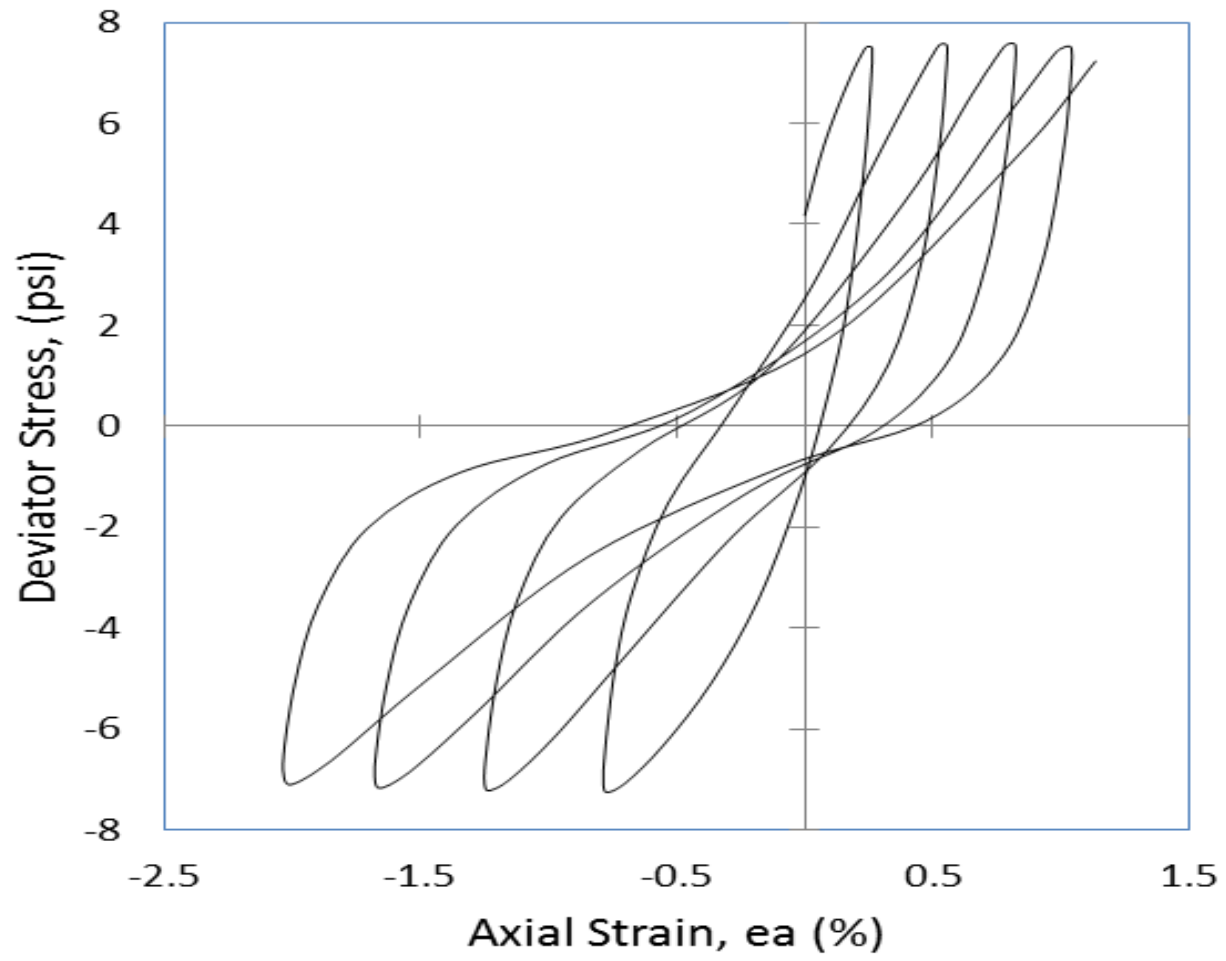Figure A.14: Specimen F100 CSR 0.50 Excess Pore Pressure Ratio Versus Normalized Number of Cycles Graph
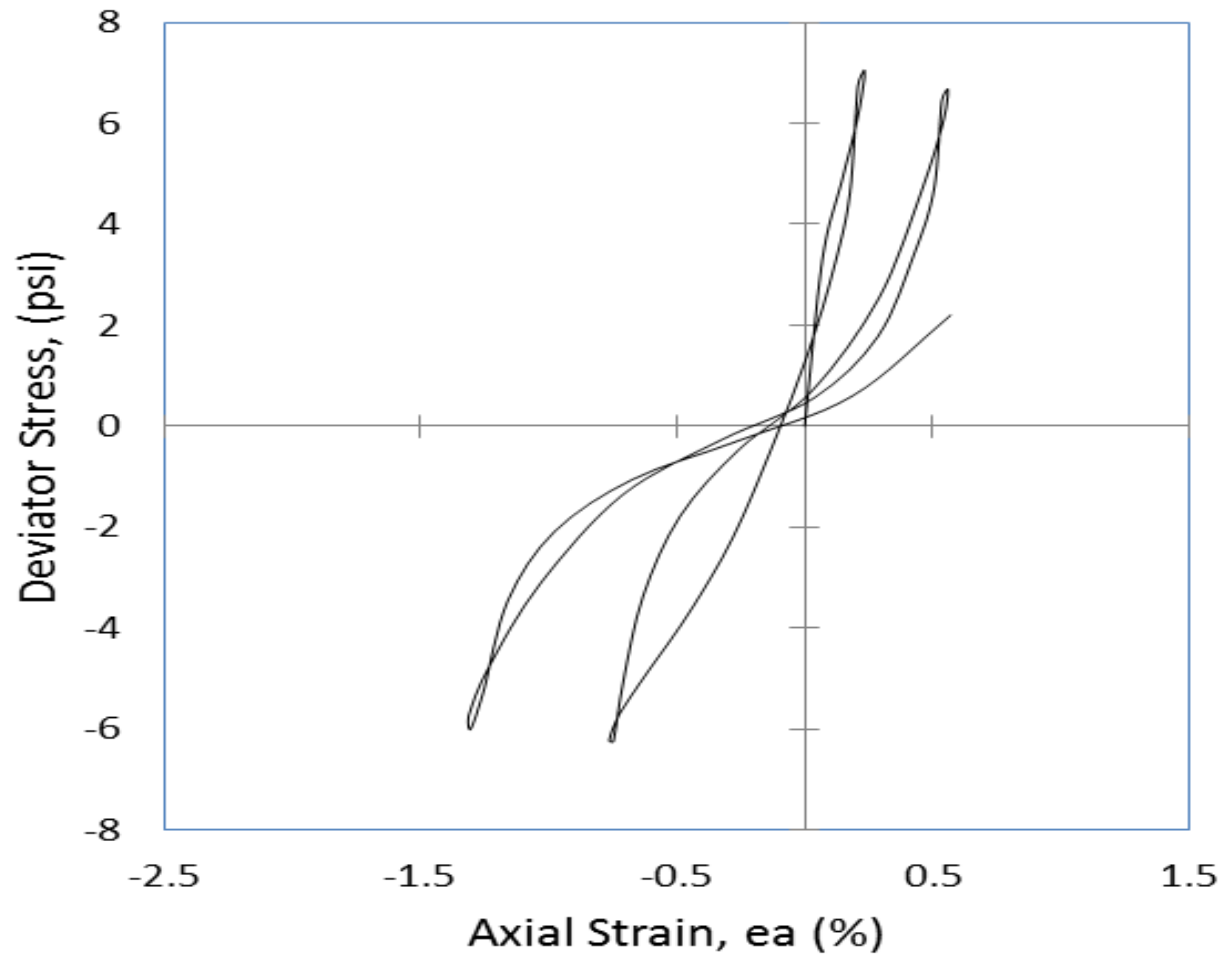
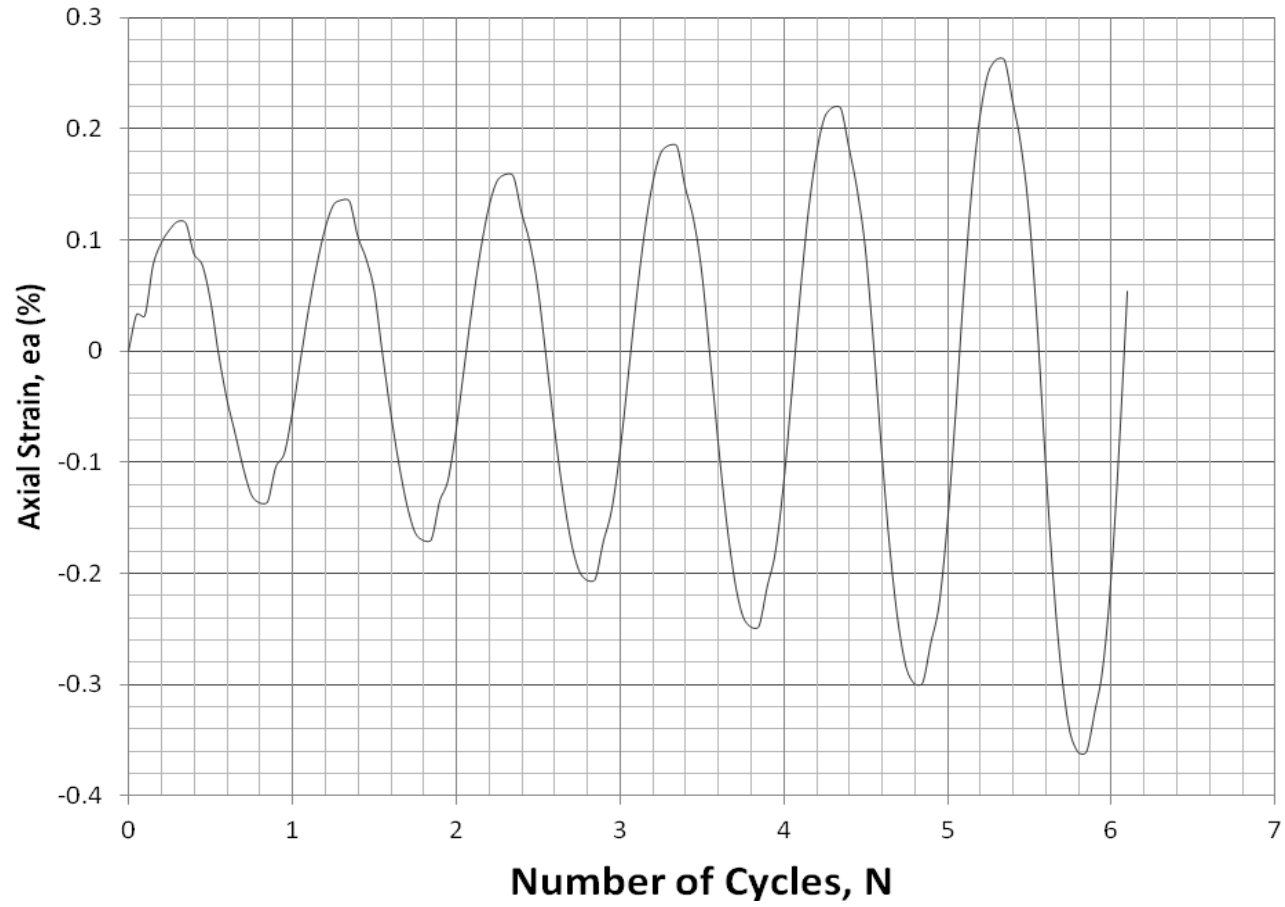Figure A.15: Specimen F100 CSR 0.50 Deviator Stress Versus Axial Strain Graph

Table A.2: Specimen Information for Class F Fly Ash + Shredded Paper

Sample Information:					
Specimen	F98P2	F90P10			F80P20
Target CSR	0.30	0.50	0.30	0.15	0.30
Depth (Meter)	9.3	9.9	9.3	9.9	9.3
Depth (ft)	30.4	32.5	30.4	32.5	30.4
Preparation phase:					
Net. Solid weight (lb)	1.2547	1.2312	1.2765	1.2794	1.0973
Diameter (inch)	2.7593	2.7258	2.776	2.7858	2.708
Height (inch)	5.5243	5.6613	5.5978	5.7587	5.5425
Ratio of height/diameter	2	2.08	2.02	2.07	2.05
Gs	2.15	2.15	2.15	2.15	2.15
Void ratio	1.04	1.08	1.06	1.13	1.26
γdry (pcf)	65.63	64.4	65.09	62.99	59.4
γsat (pcf)	97.5	96.85	97.22	96.09	94.17
Saturation phase:					
B-value (%)	92.08	95	97	96.04	97.98
Shear phase:					
Frequency (Hz):		0.5			
Period (Sec):		2			
Asked Deviator Stress (psi)	8.9	15.6	8.8	4.9	8.0
Confining Pressure (psi)	7.4	7.8	7.4	7.6	6.7
Actual CSR	0.284	0.474	0.290	0.166	0.292
Ncycle to liquefy	4	4	7	47	7

Definitions:

F = Class F Fly Ash

P = Shredded Paper

98, 90, 80, 20, 10, and 2 = Percentage of Waste Material by Dry Weight
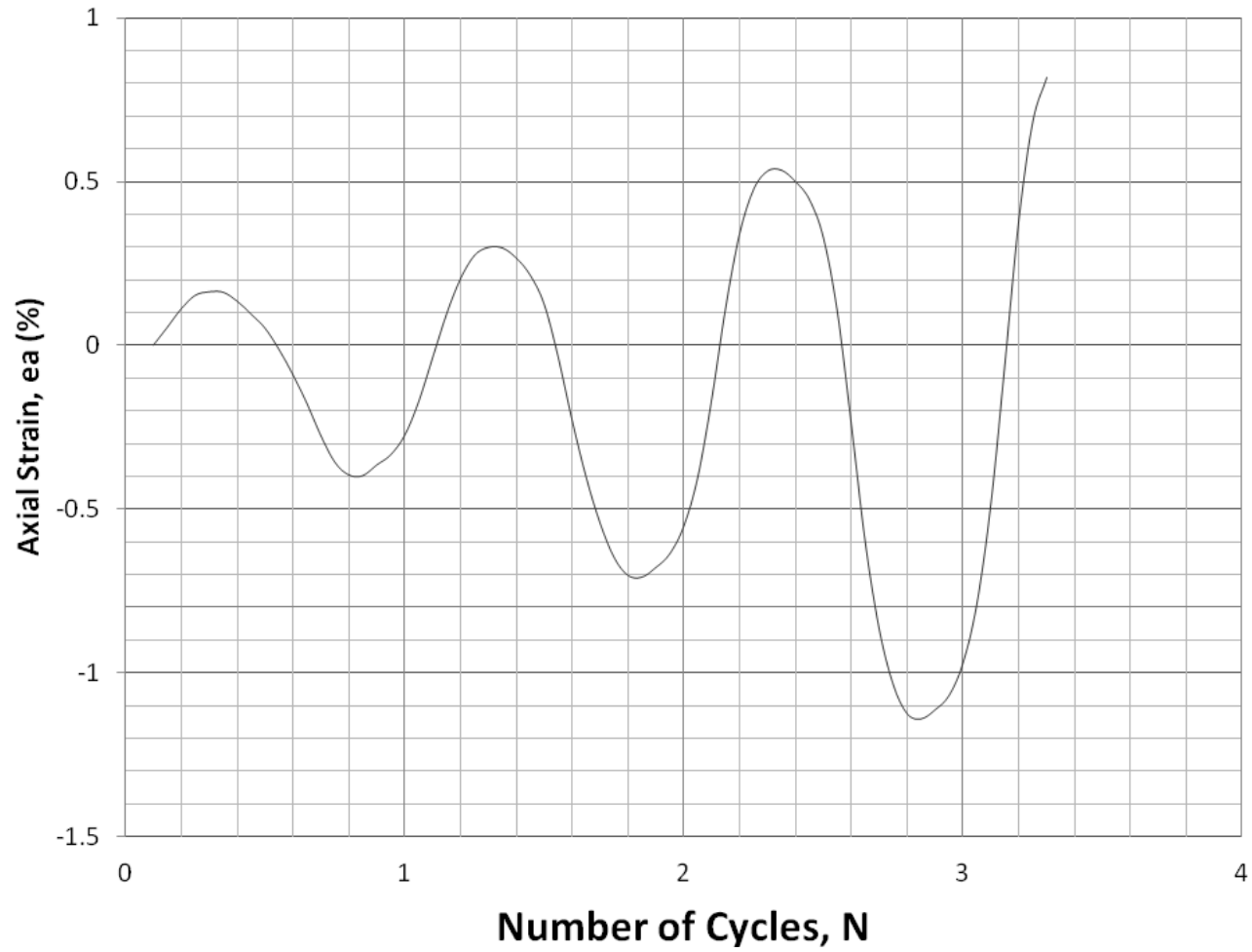
Figure A.16: Specimen F98P2 CSR 0.30 Axial Strain Versus Number of Cycles Graph
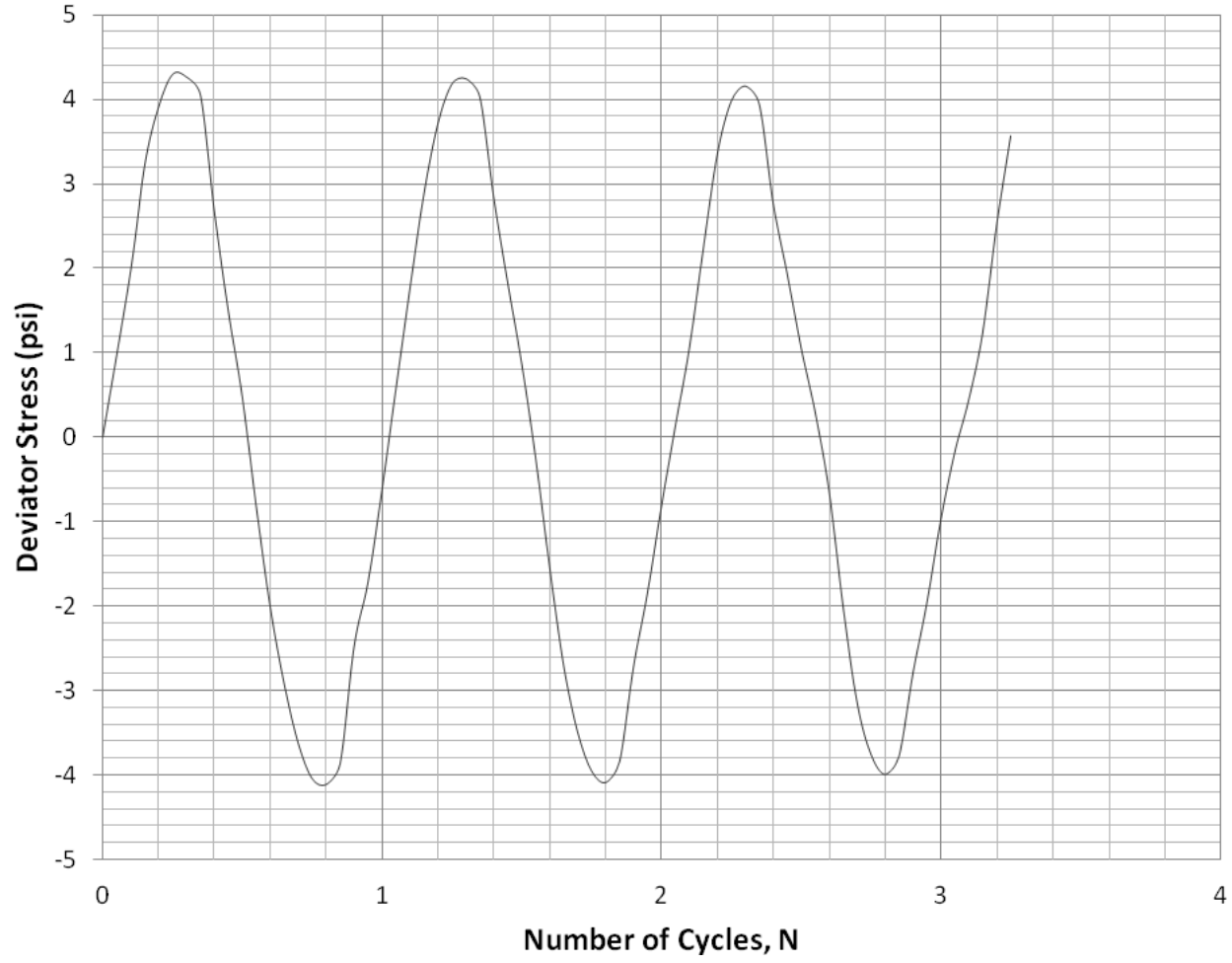
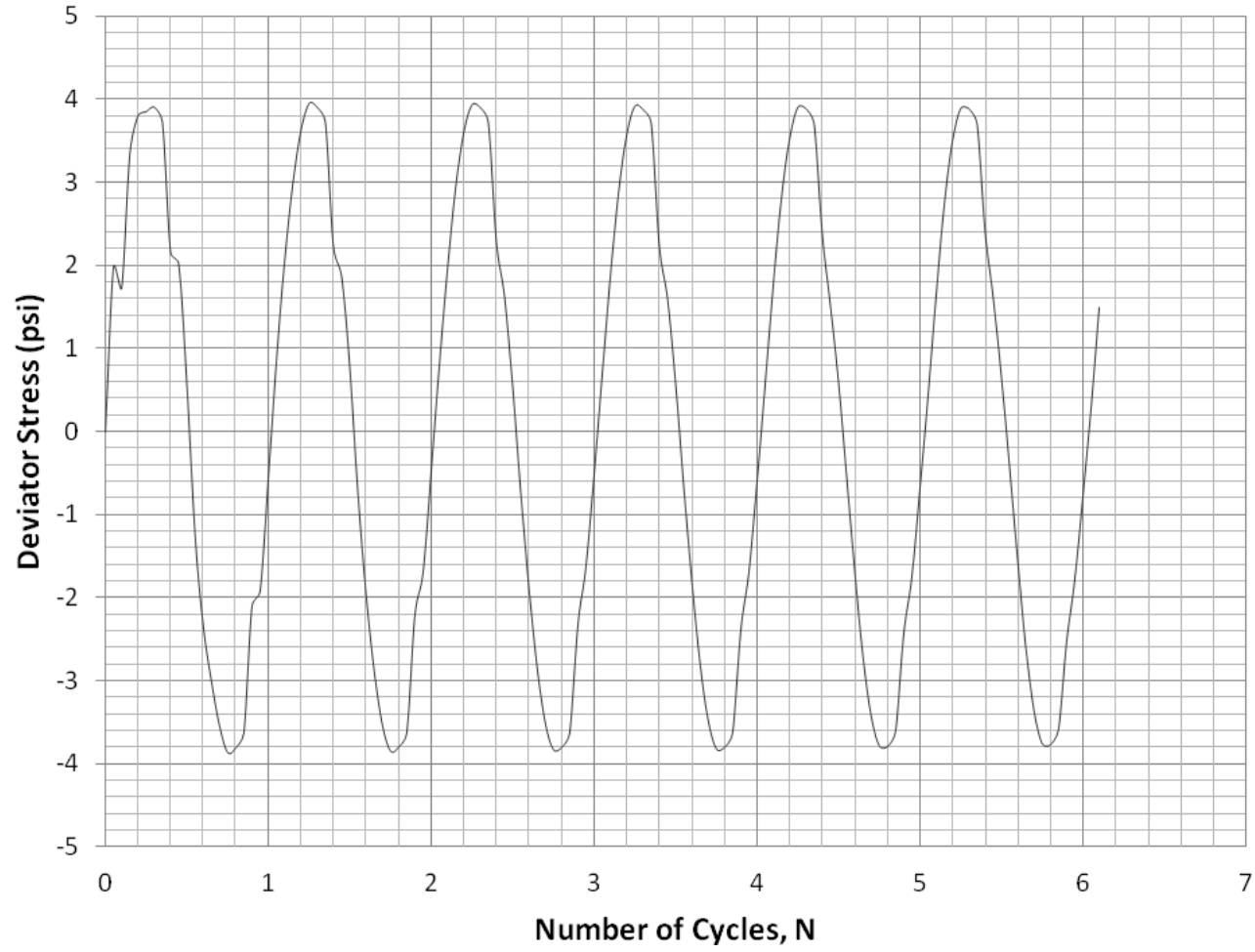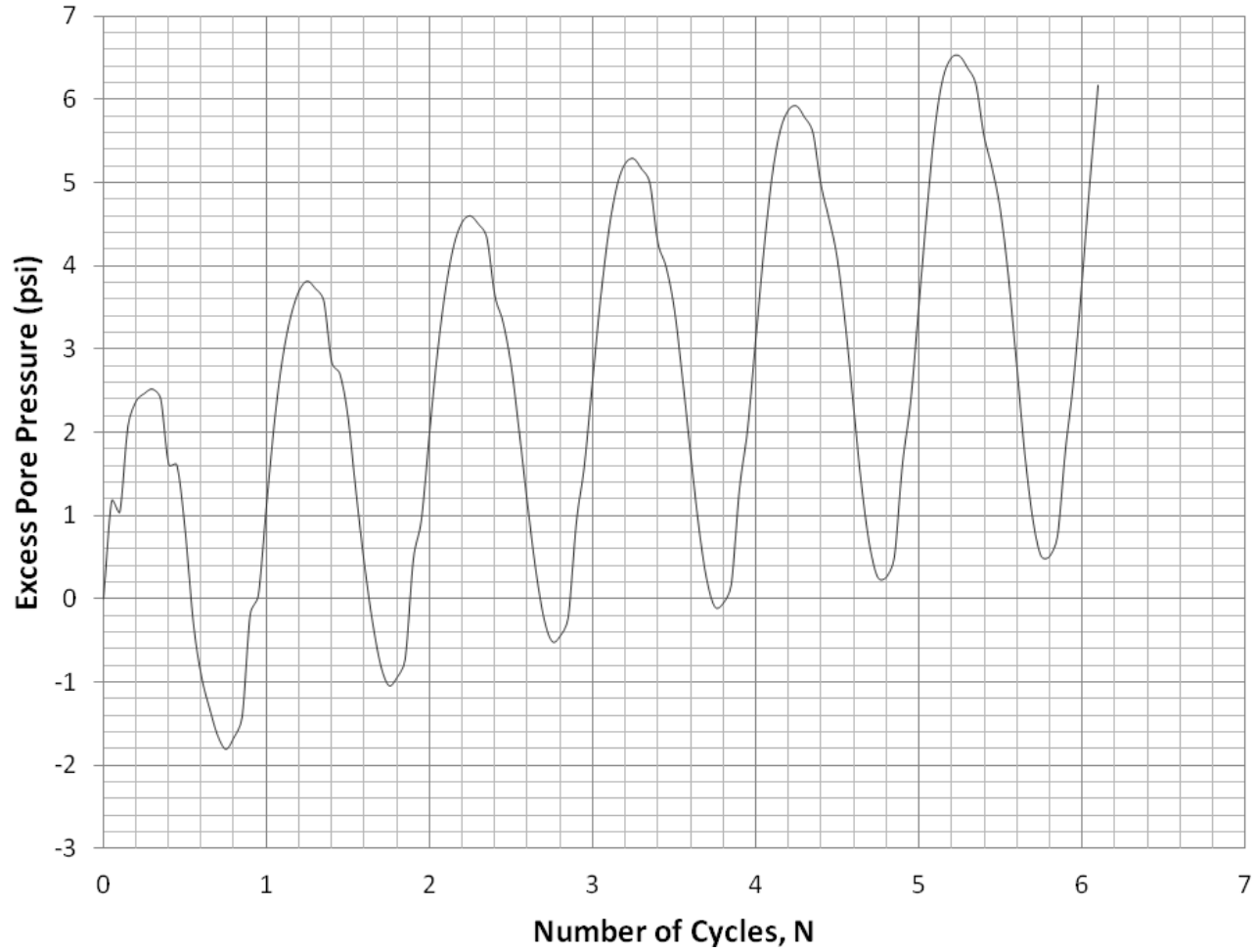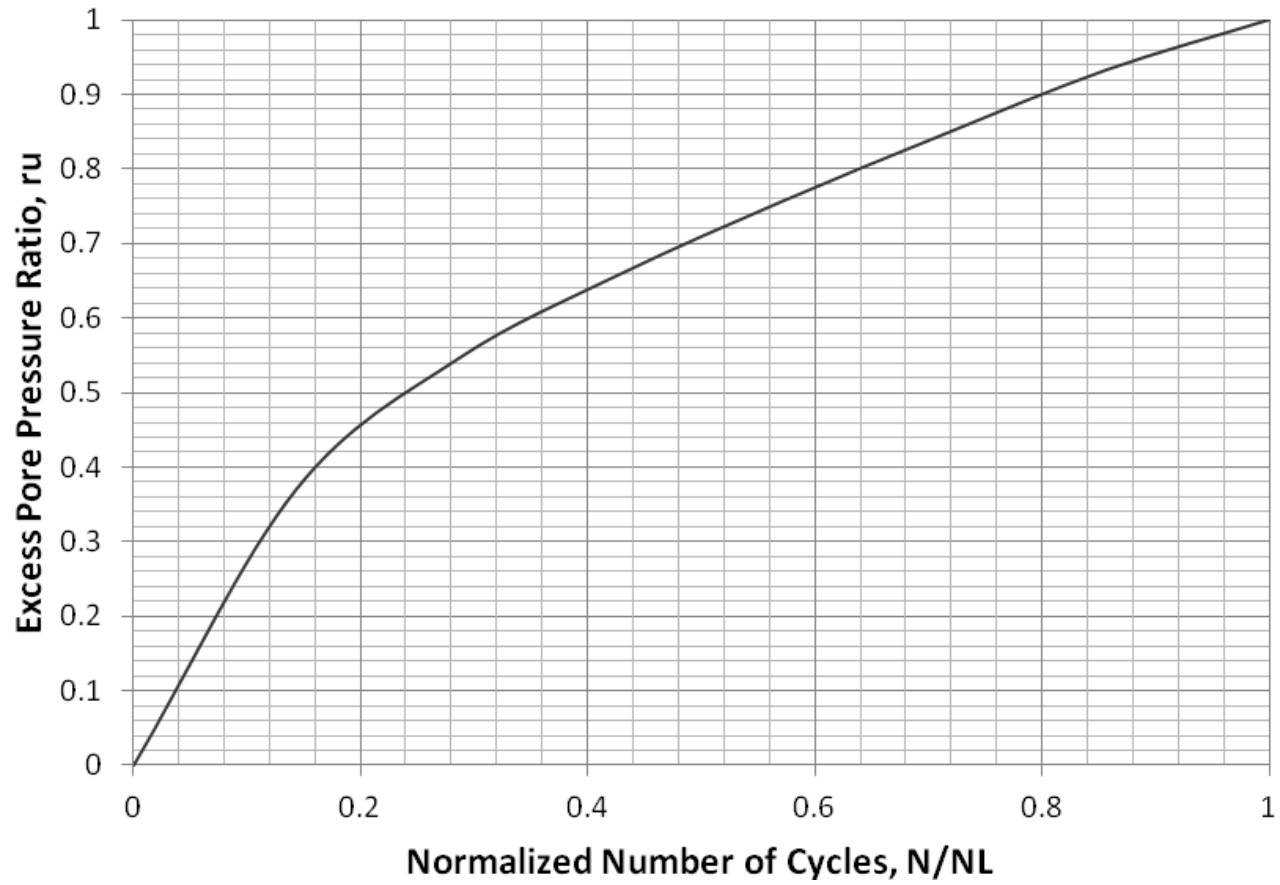Figure A.17: Specimen F98P2 CSR 0.30 Deviator Stress Versus Number of Cycles Graph
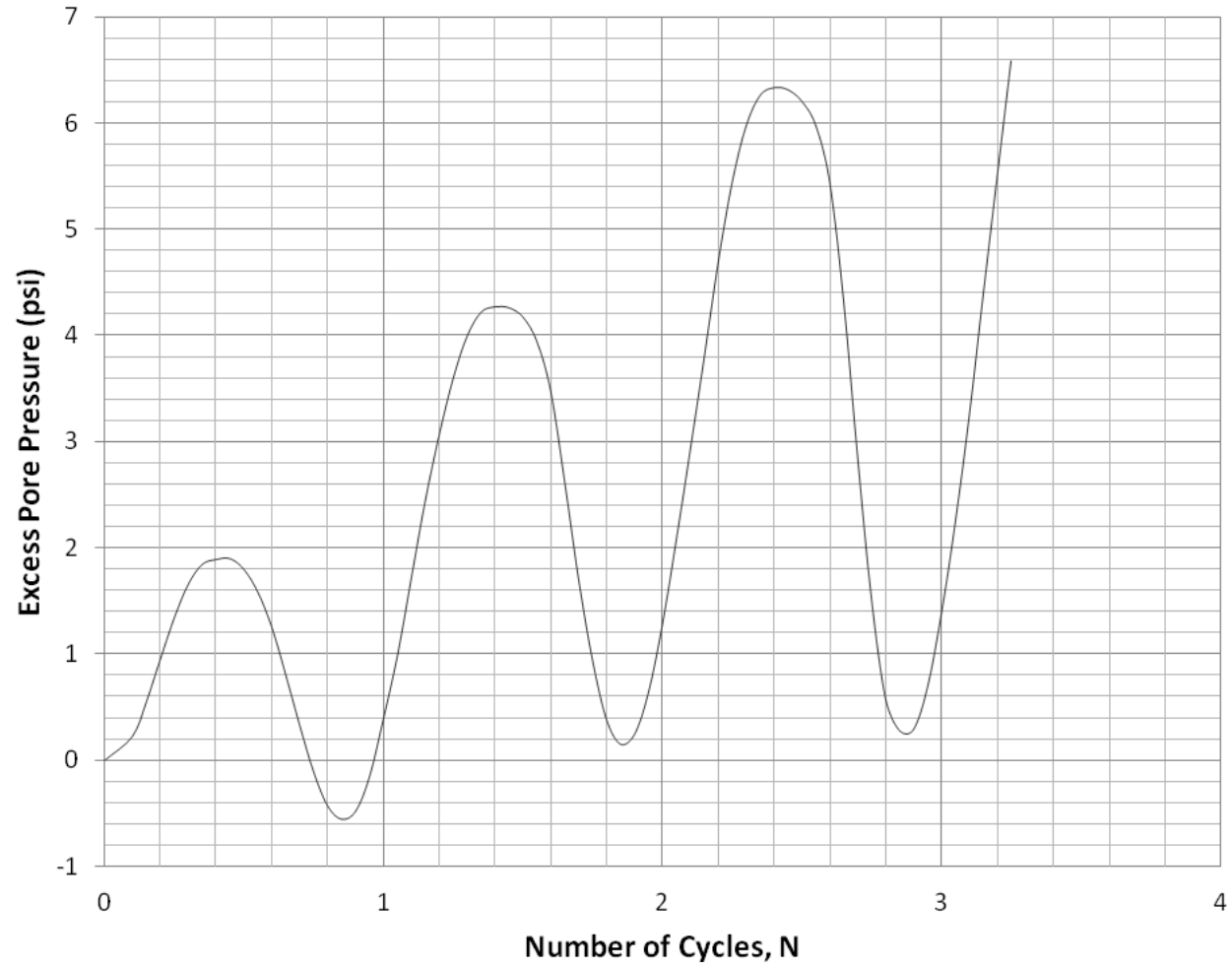
Figure A.18: Specimen F98P2 CSR 0.30 Excess Pore Pressure Versus Number of Cycles Graph
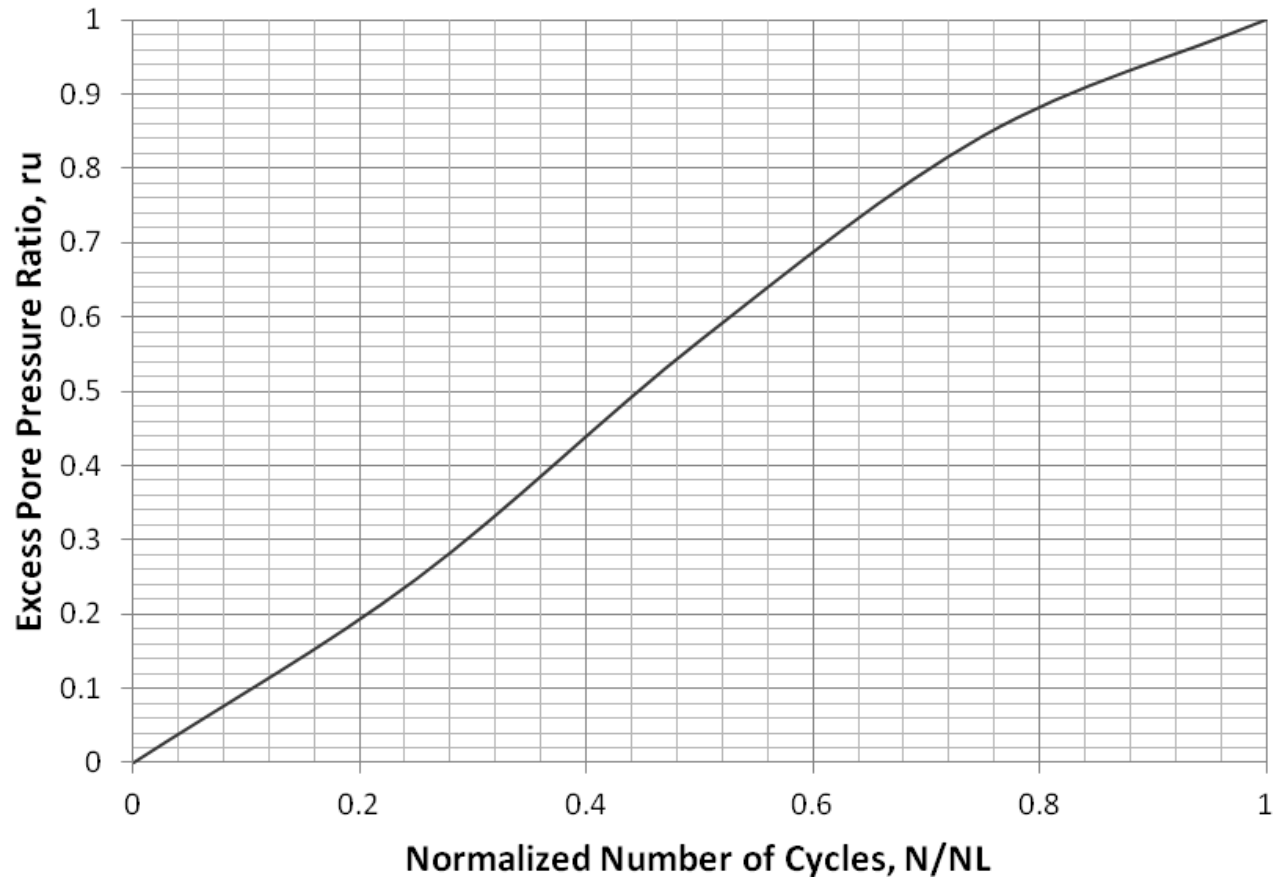
Figure A.19: Specimen F98P2 CSR 0.30 Excess Pore Pressure Ratio Versus Normalized Number of Cycles Graph
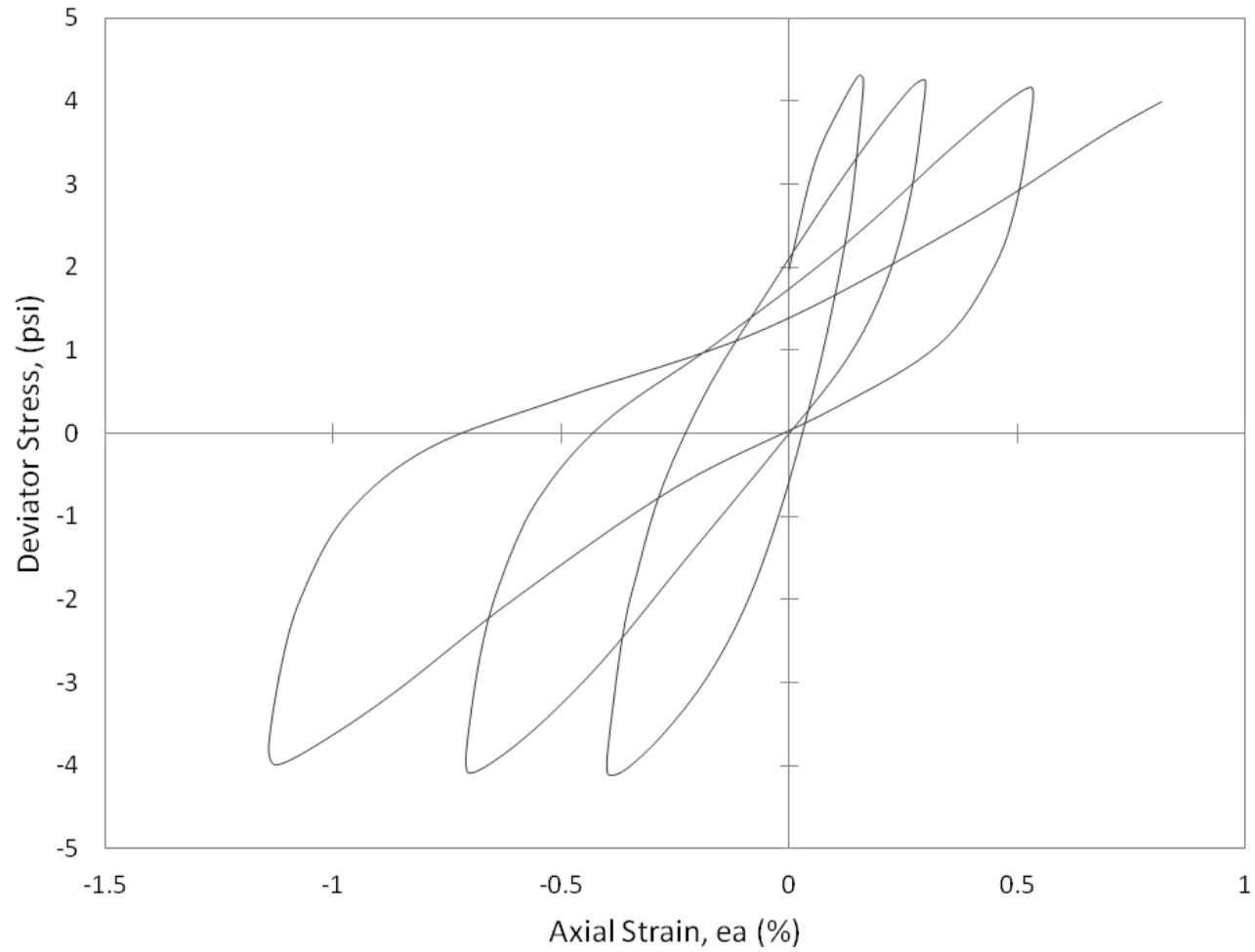
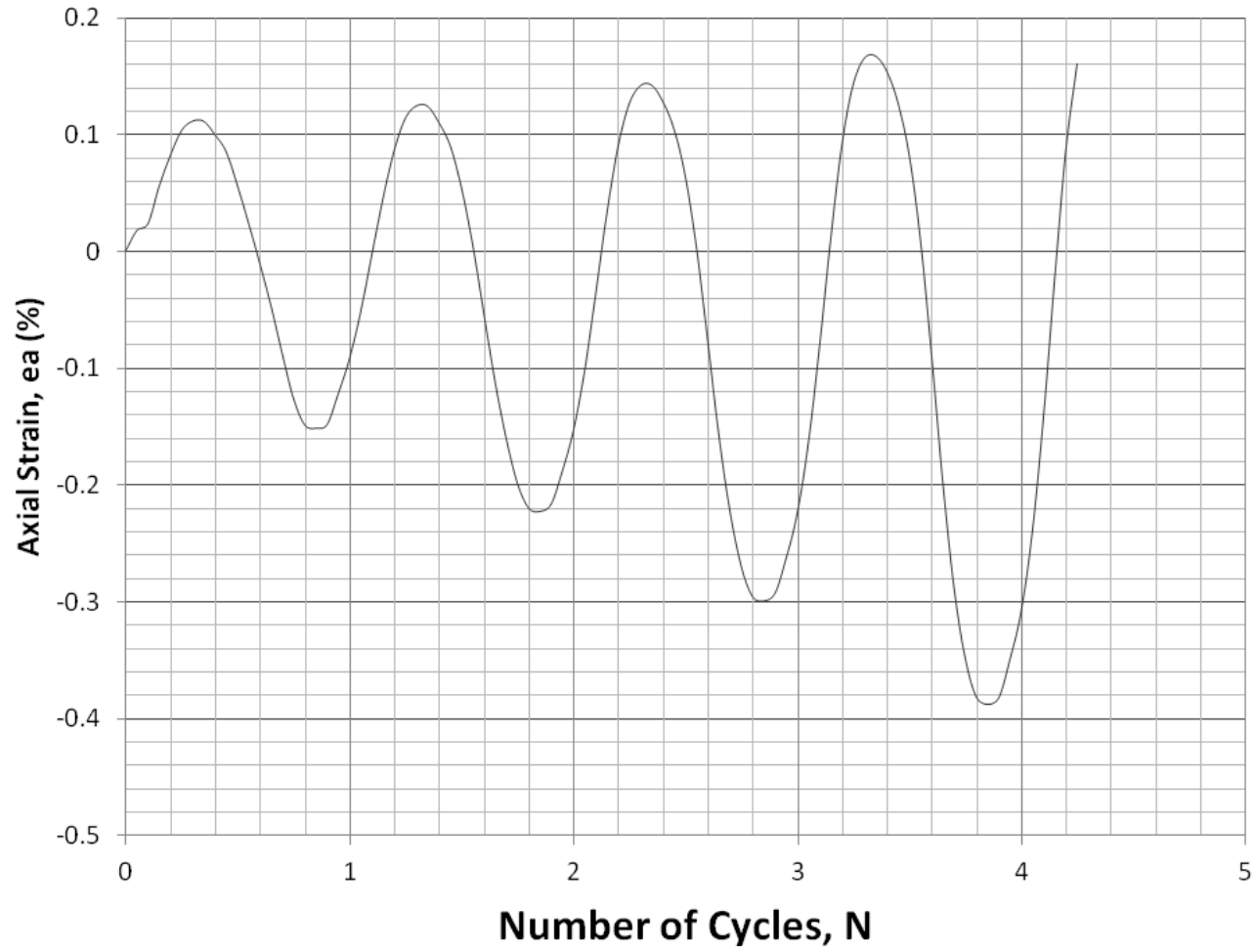Figure A.20: Specimen F98P2 CSR 0.30 Deviator Stress Versus Axial Strain Graph
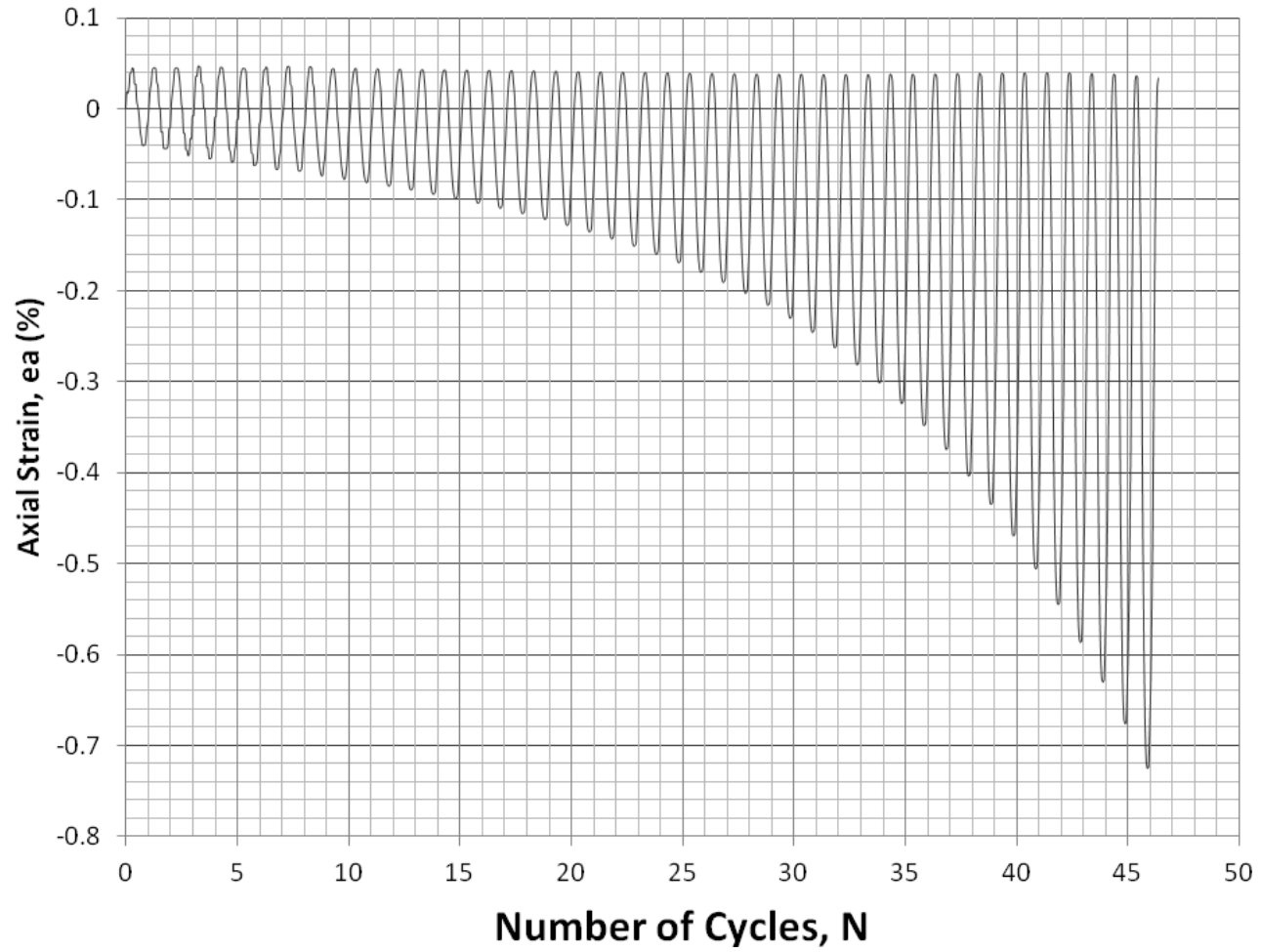
Figure A.21: Specimen F90P10 CSR 0.15 Axial Strain Versus Number of Cycles Graph
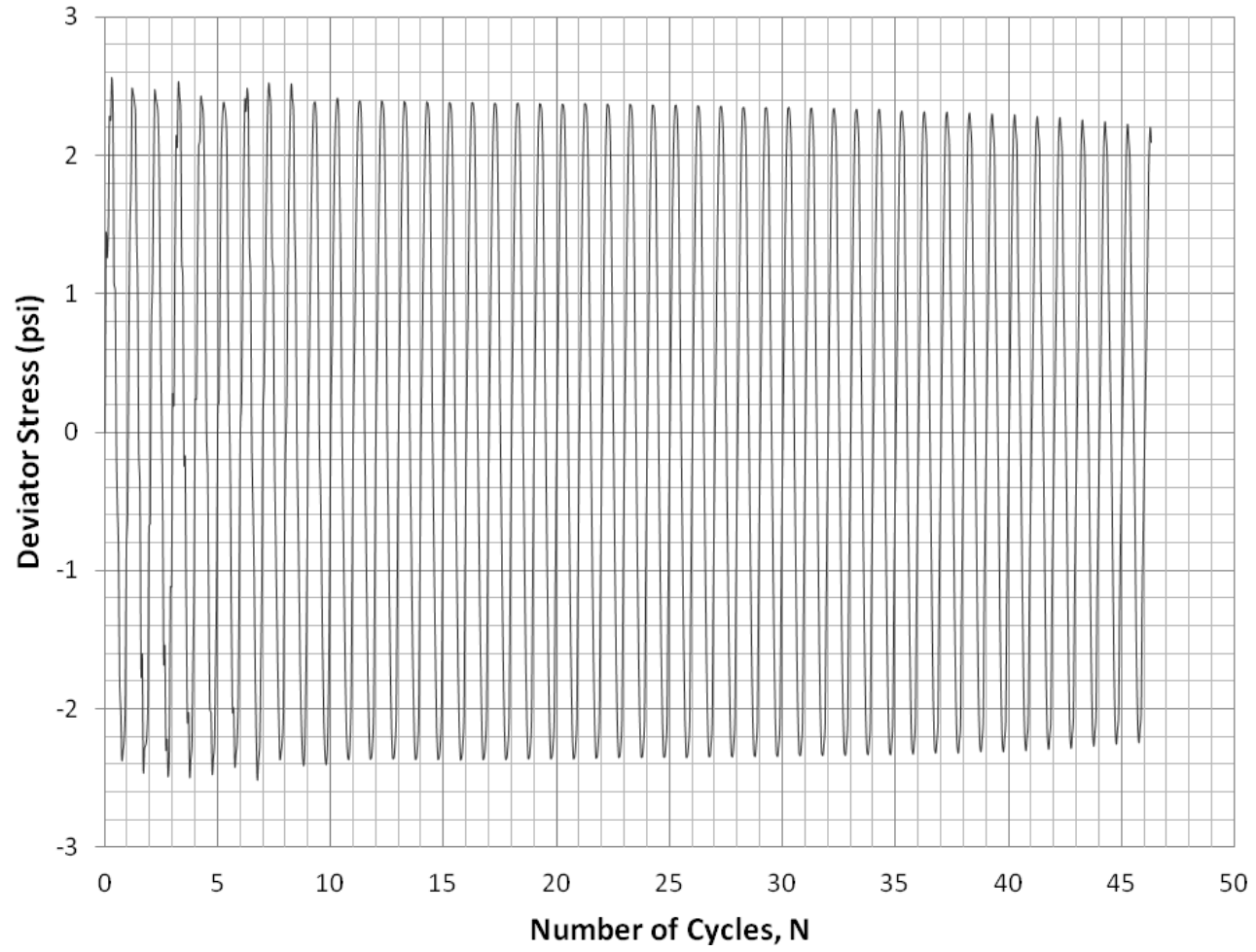
Figure A.22: Specimen F90P10 CSR 0.15 Deviator Stress Versus Number of Cycles Graph
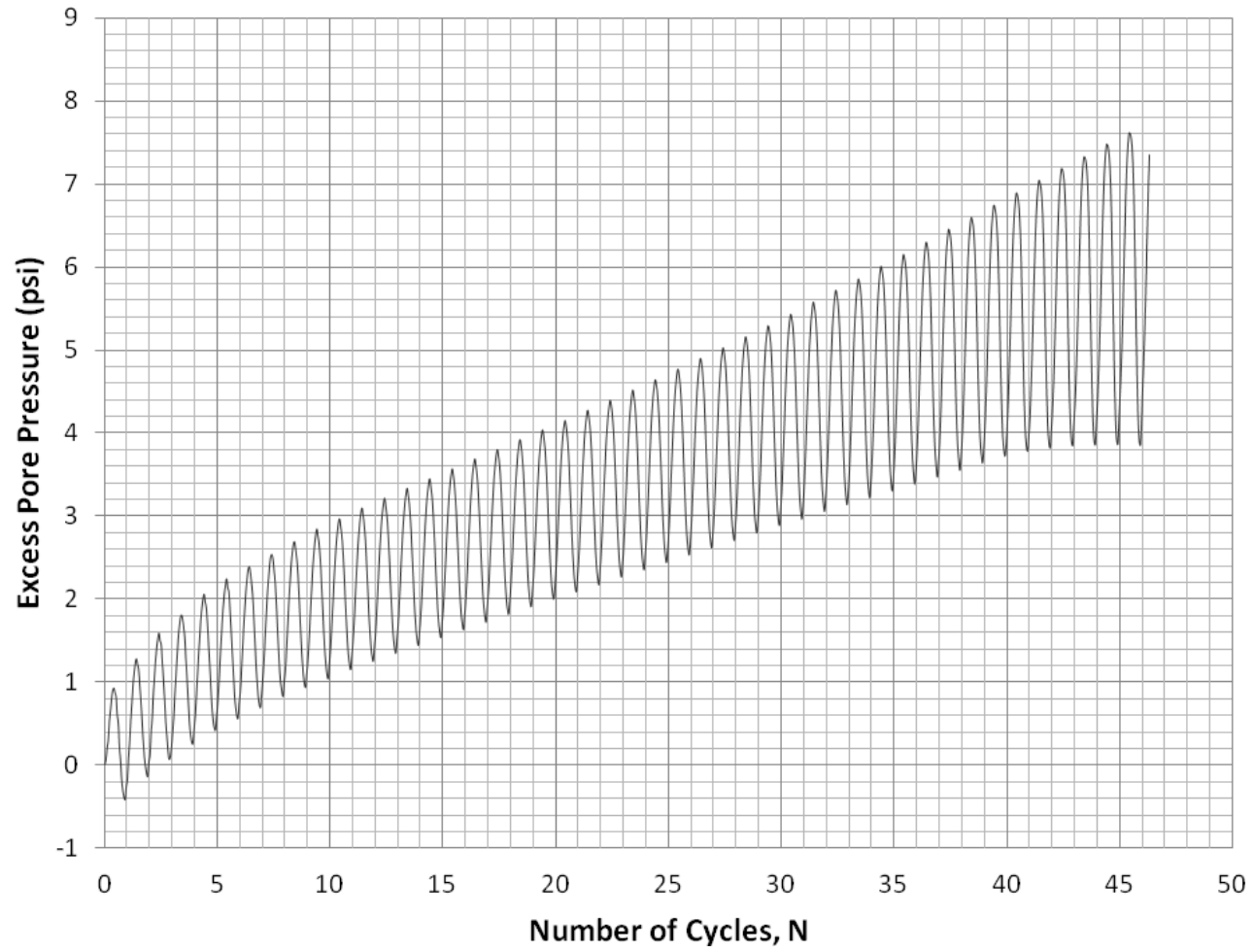
Figure A.23: Specimen F90P10 CSR 0.15 Excess Pore Pressure Versus Number of Cycles Graph
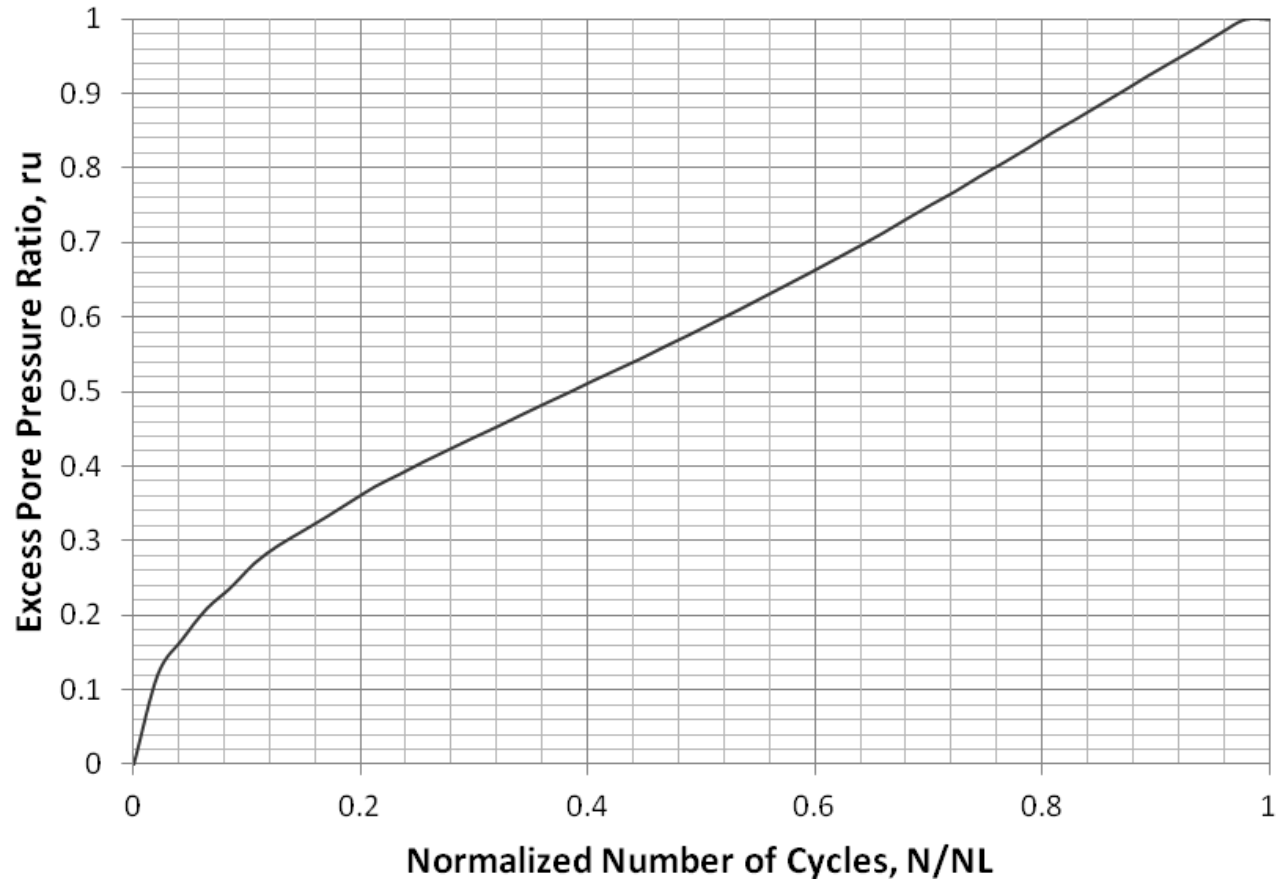
Figure A.24: Specimen F90P10 CSR 0.15 Excess Pore Pressure Ratio Versus Normalized Number of Cycles Graph
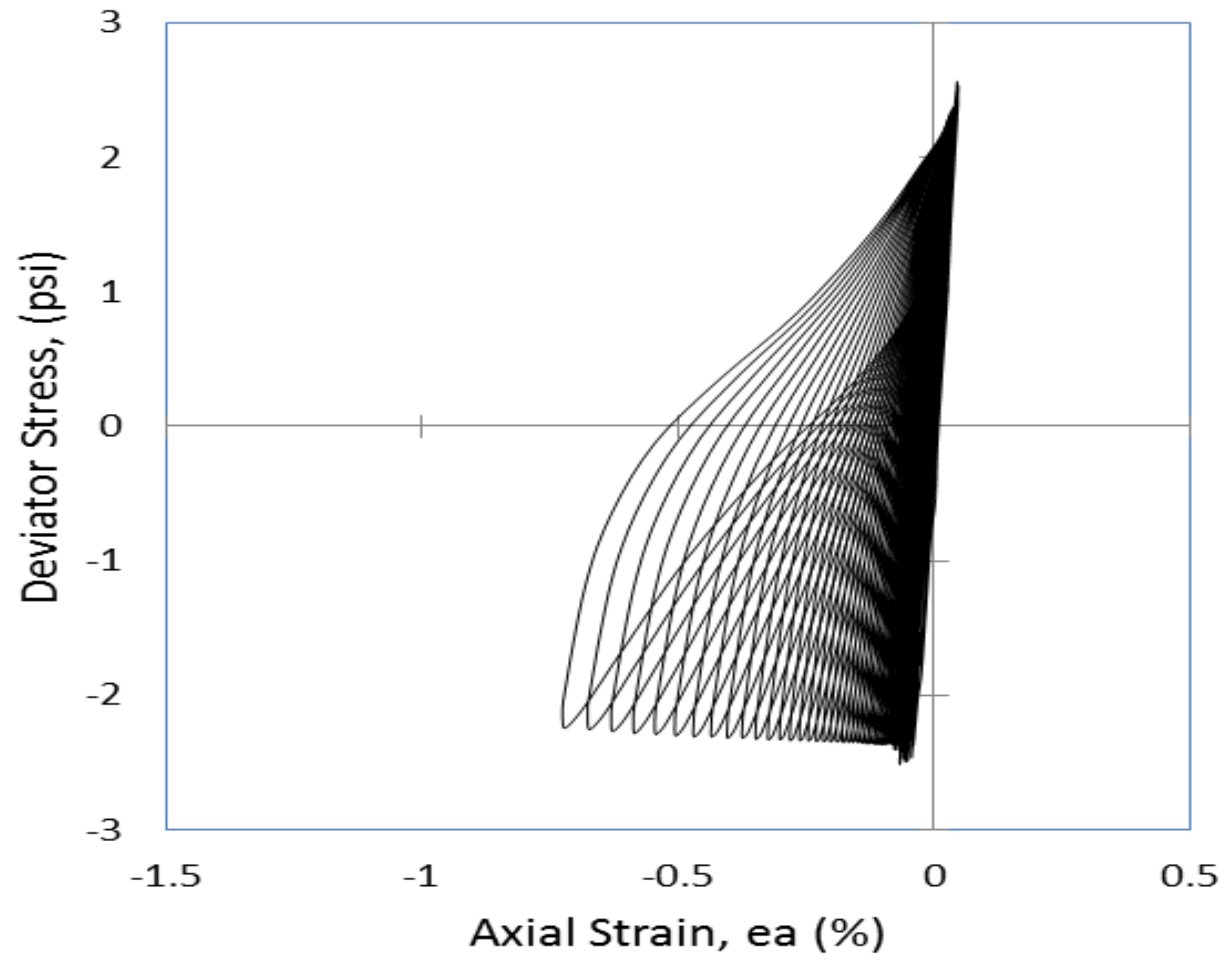
Figure A.25: Specimen F90P10 CSR 0.15 Deviator Stress Versus Axial Strain Graph

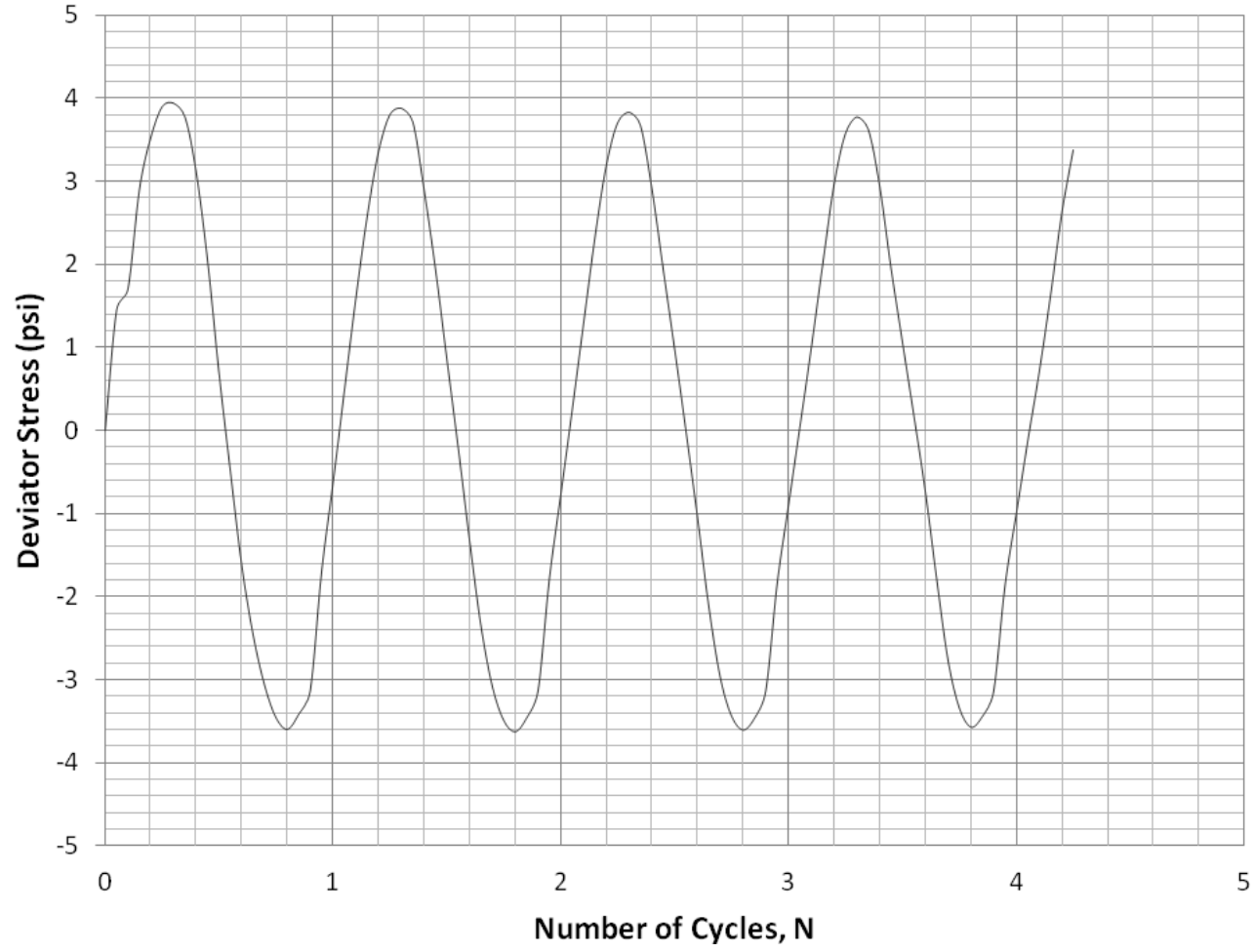Figure A.26: Specimen F90P10 CSR 0.30 Axial Strain Versus Number of Cycles Graph

Figure A.27: Specimen F90P10 CSR 0.30 Deviator Stress Versus Number of Cycles Graph

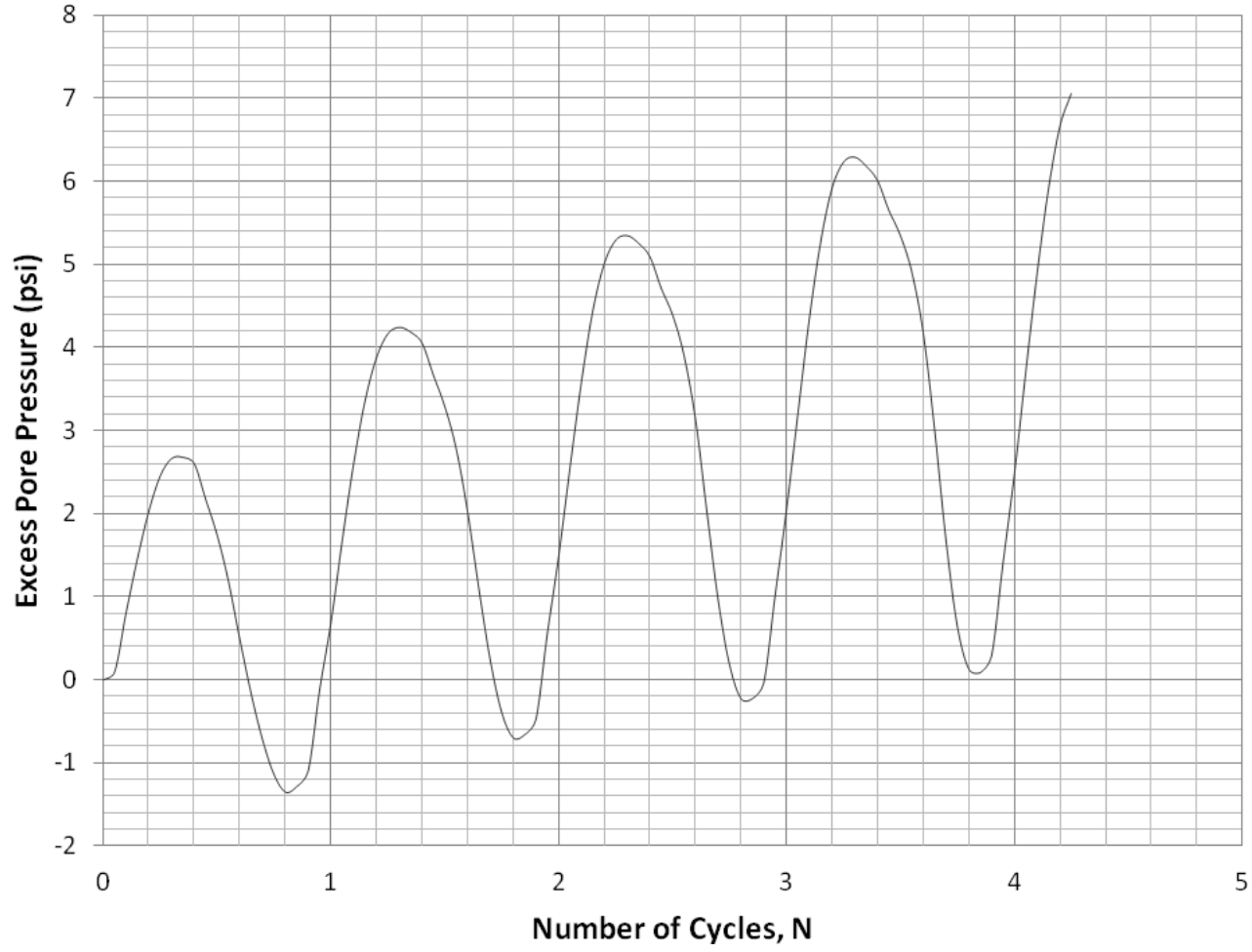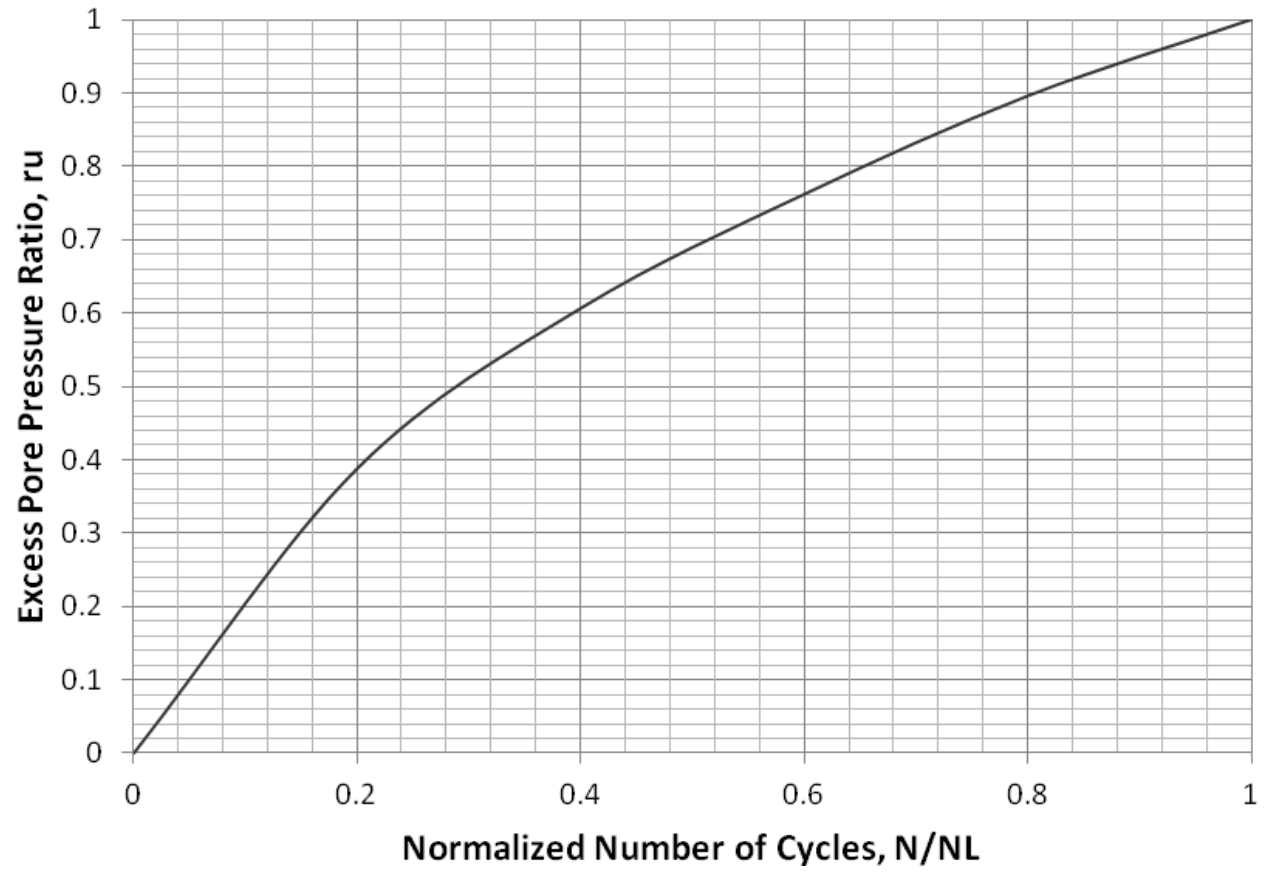Figure A.28: Specimen F90P10 CSR 0.30 Excess Pore Pressure Versus Number of Cycles Graph

Figure A.29: Specimen F90P10 CSR 0.30 Excess Pore Pressure Ratio Versus Normalized Number of Cycles Graph

Figure A.30: Specimen F90P10 CSR 0.30 Deviator Stress Versus Axial Strain Graph

Figure A.31: Specimen F90P10 CSR 0.50 Axial Strain Versus Number of Cycles Graph

Figure A.32: Specimen F90P10 CSR 0.50 Deviator Stress Versus Number of Cycles Graph

Figure A.33: Specimen F90P10 CSR 0.50 Excess Pore Pressure Versus Number of Cycles Graph

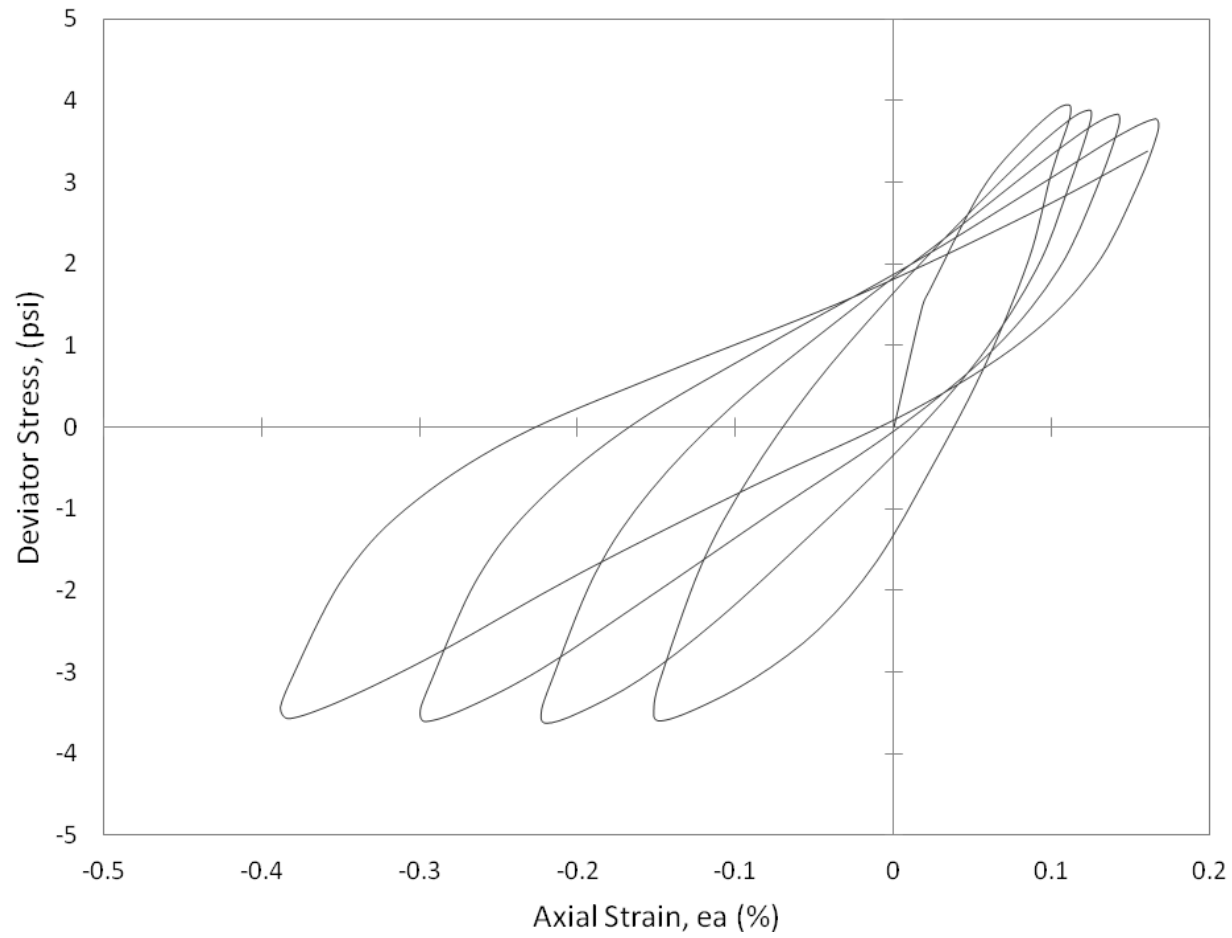Figure A.34: Specimen F90P10 CSR 0.50 Excess Pore Pressure Ratio Versus Normalized Number of Cycles Graph

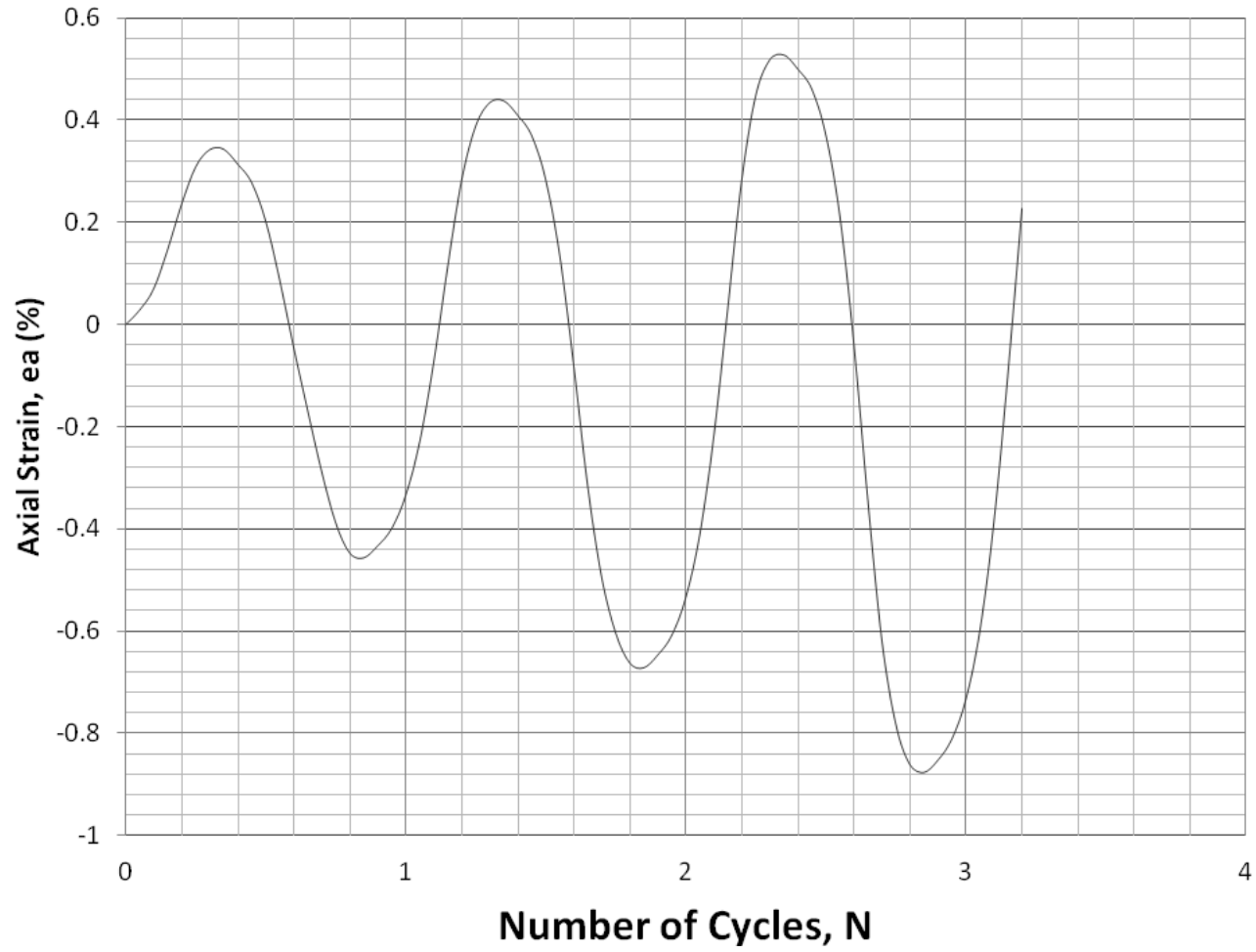Figure A.35: Specimen F90P10 CSR 0.50 Deviator Stress Versus Axial Strain Graph

Figure A.36: Specimen F80P20 CSR 0.30 Axial Strain Versus Number of Cycles Graph
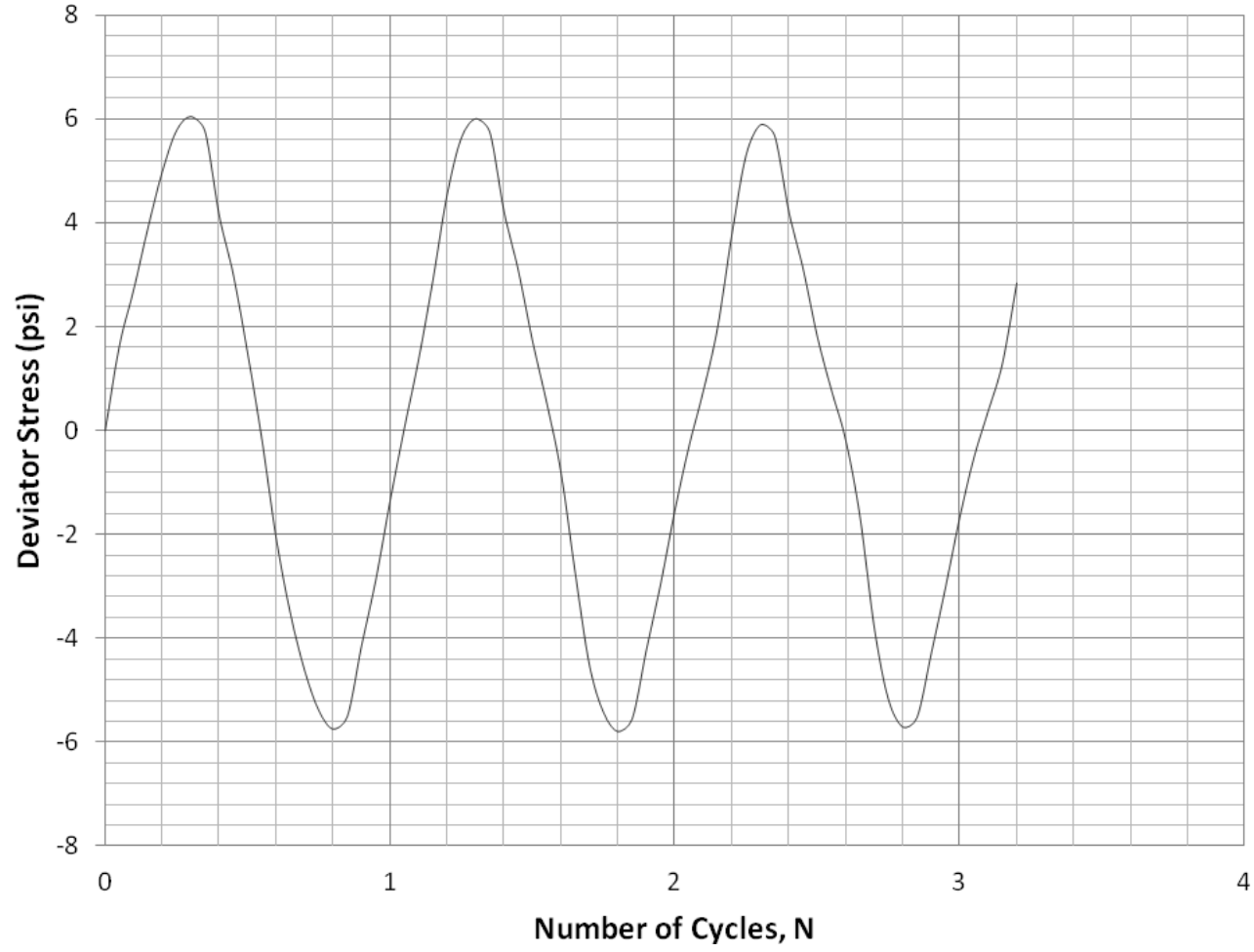
Figure A.37: Specimen F80P20 CSR 0.30 Deviator Stress Versus Number of Cycles Graph
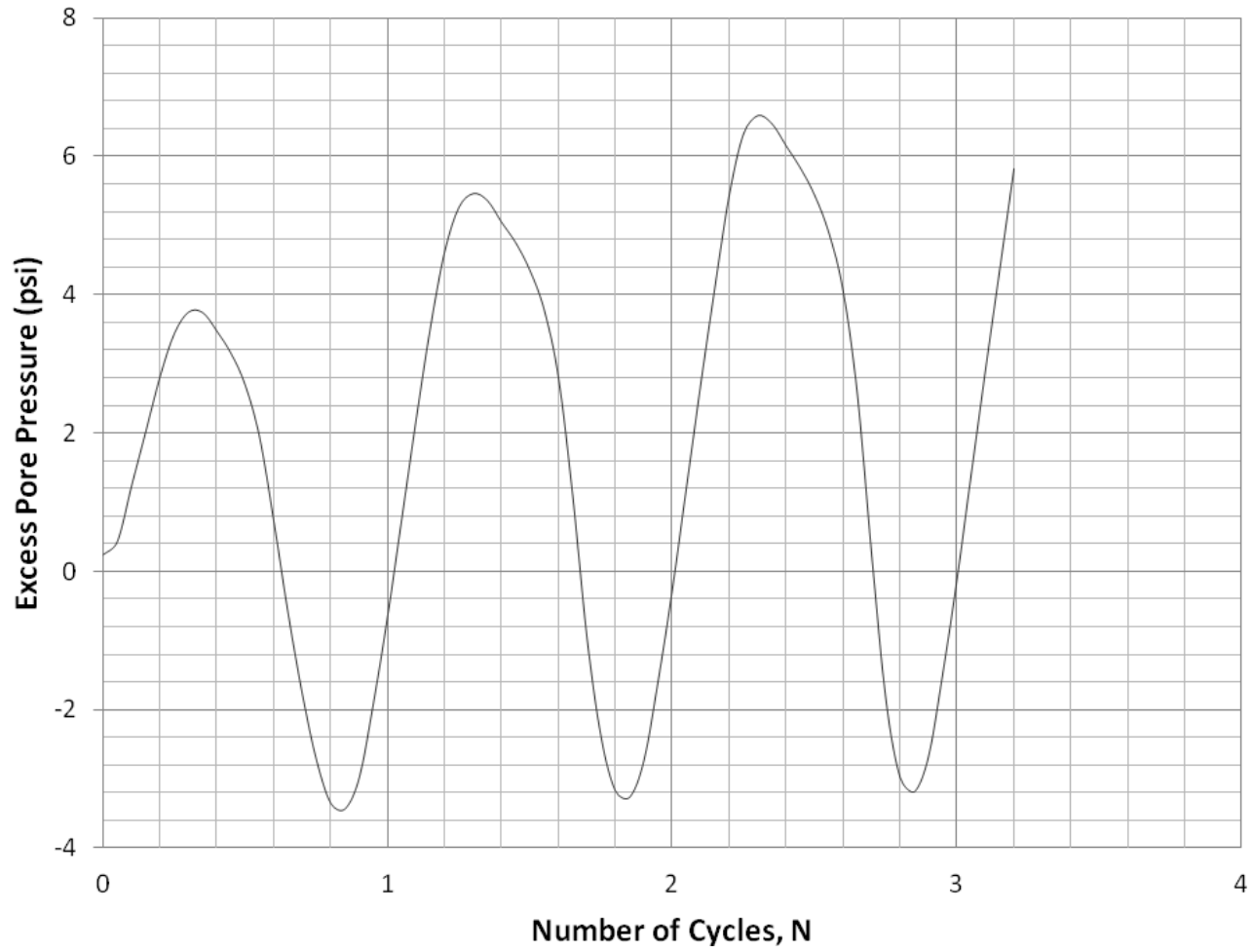
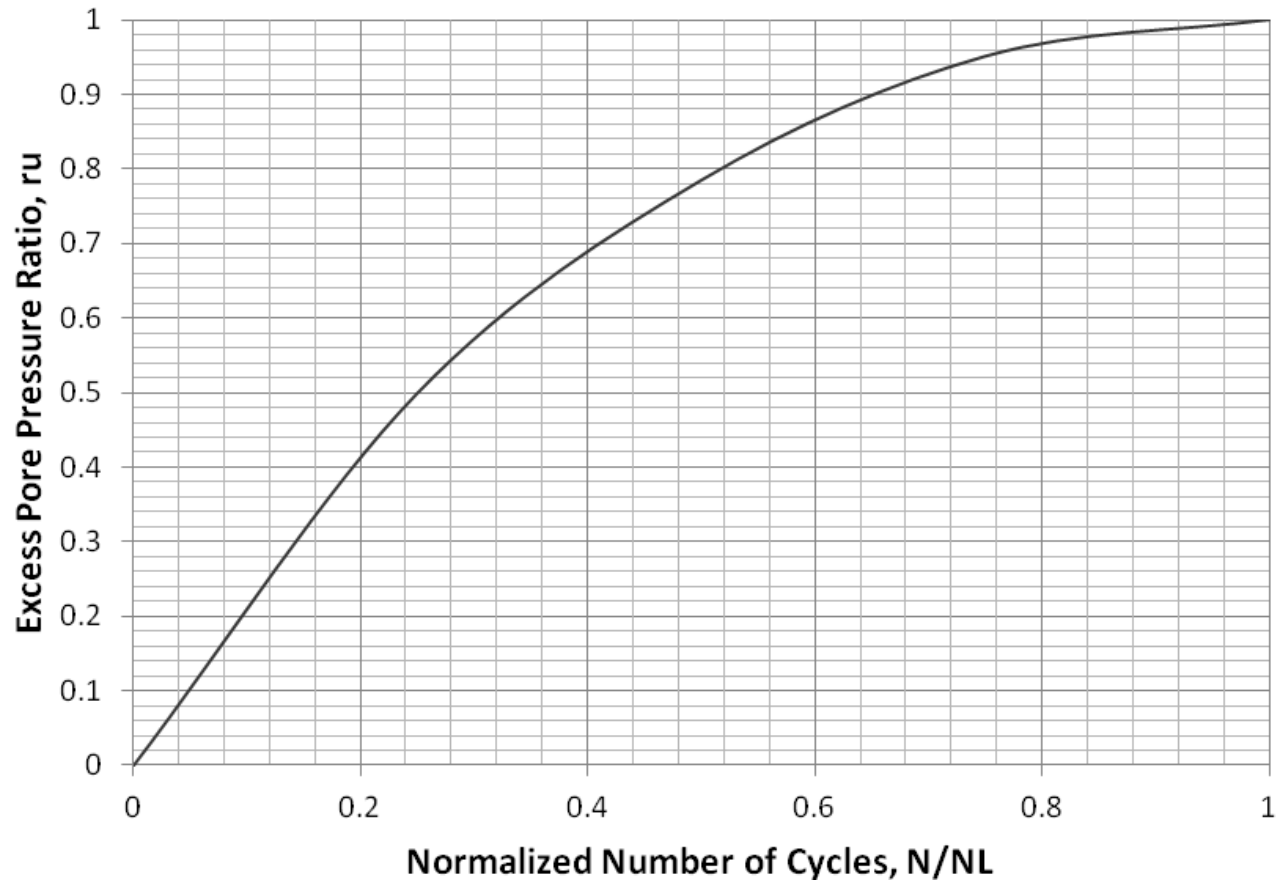Figure A.38: Specimen F80P20 CSR 0.30 Excess Pore Pressure Versus Number of Cycles Graph

Figure A.39: Specimen F80P20 CSR 0.30 Excess Pore Pressure Ratio Versus Normalized Number of Cycles Graph
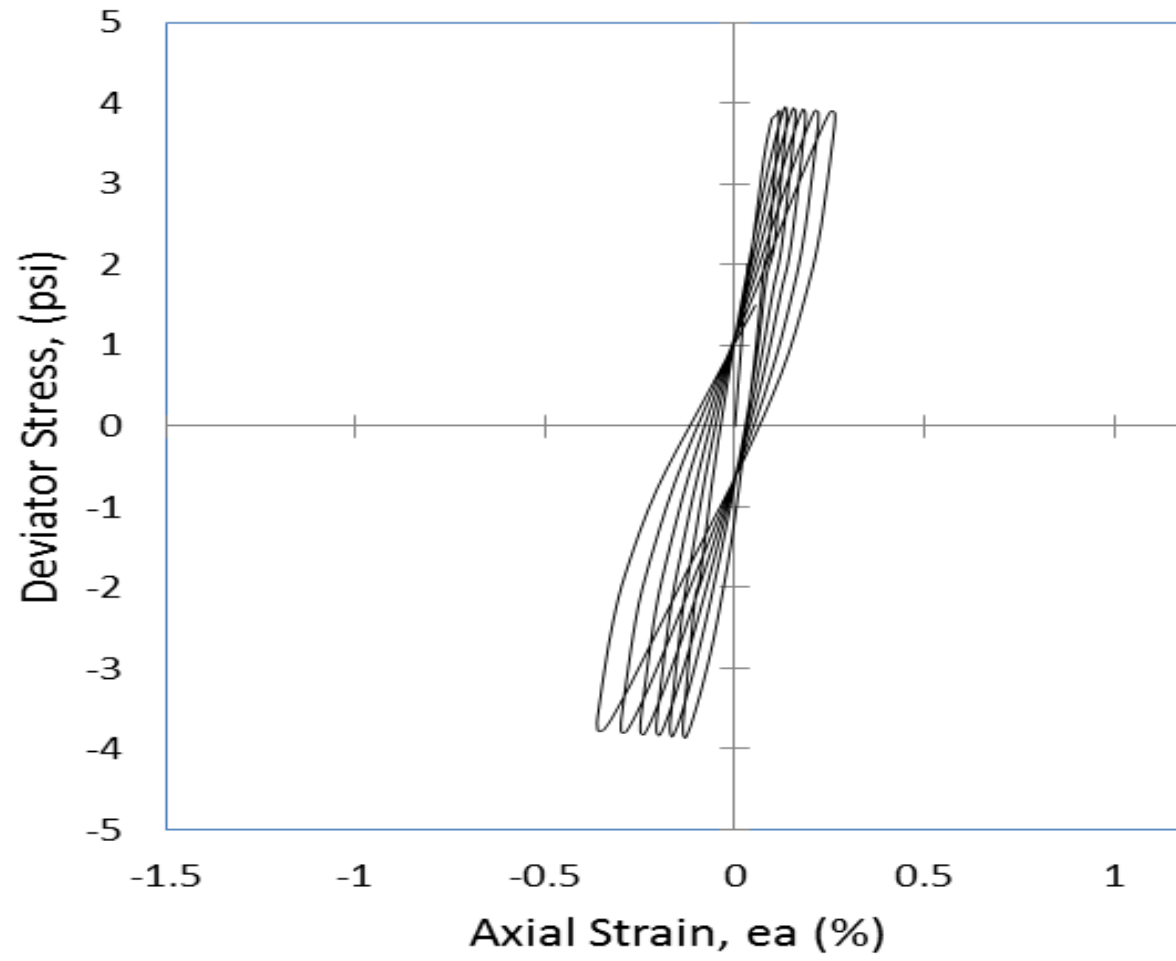
Figure A.40: Specimen F80P20 CSR 0.30 Deviator Stress Versus Axial Strain Graph

Table A.3: Specimen Information for Class F Fly Ash + Carpet Fiber

Sample Information:						
Specimen	F98.5C1.5	F98C2		F95C5		F80C20
Target CSR	0.30	0.50	0.50	0.30	0.15	0.30
Depth (Meter)	9.3	9.2	9.3	9.3	9.8	9.2
Depth (ft)	30.3	30.3	30.4	30.4	32.2	30.3
Preparation phase:						
Net. Solid weight (lb)	1.2642	1.1155	1.1155	1.1447	1.194	0.922
Diameter (inch)	2.7924	2.7793	2.7881	2.7887	2.7958	2.64
Height (inch)	5.8197	5.5848	5.782	5.7178	5.6	5.416
Ratio of height/diameter	2.08	2.01	2.07	2.05	2	2.05
Gs	2.15	2.15	2.15	2.15	2.15	2.15
Void ratio	1.19	1.36	1.46	1.37	1.38	1.5
γdry (pcf)	61.29	56.89	54.6	56.64	56.27	53.7
γsat (pcf)	95.18	92.83	91.61	92.69	92.5	91.12
Saturation phase:						
B-value (%)	97	98	98	95	96	97
Shear phase:						
Frequency (Hz):		0.5				
Period (Sec):		2				
Asked Deviator Stress (psi)	8.2	12.8	12.4	7.7	4.3	7.3
Confining Pressure (psi)	6.9	6.4	6.2	6.4	6.7	6.1
Actual CSR	0.274	0.462	0.442	0.288	0.162	0.272
Ncycle to liquefy	5	4	4	8	29	7

Definitions:

F = Class F Fly Ash

C = Carpet Fiber

98.5, 98, 95, 80, 20, 5, 2 and 1.5 = Percentage of Waste Material by Dry Weight

Figure A.41: Specimen F98.5C1.5 CSR 0.30 Axial Strain Versus Number of Cycles Graph
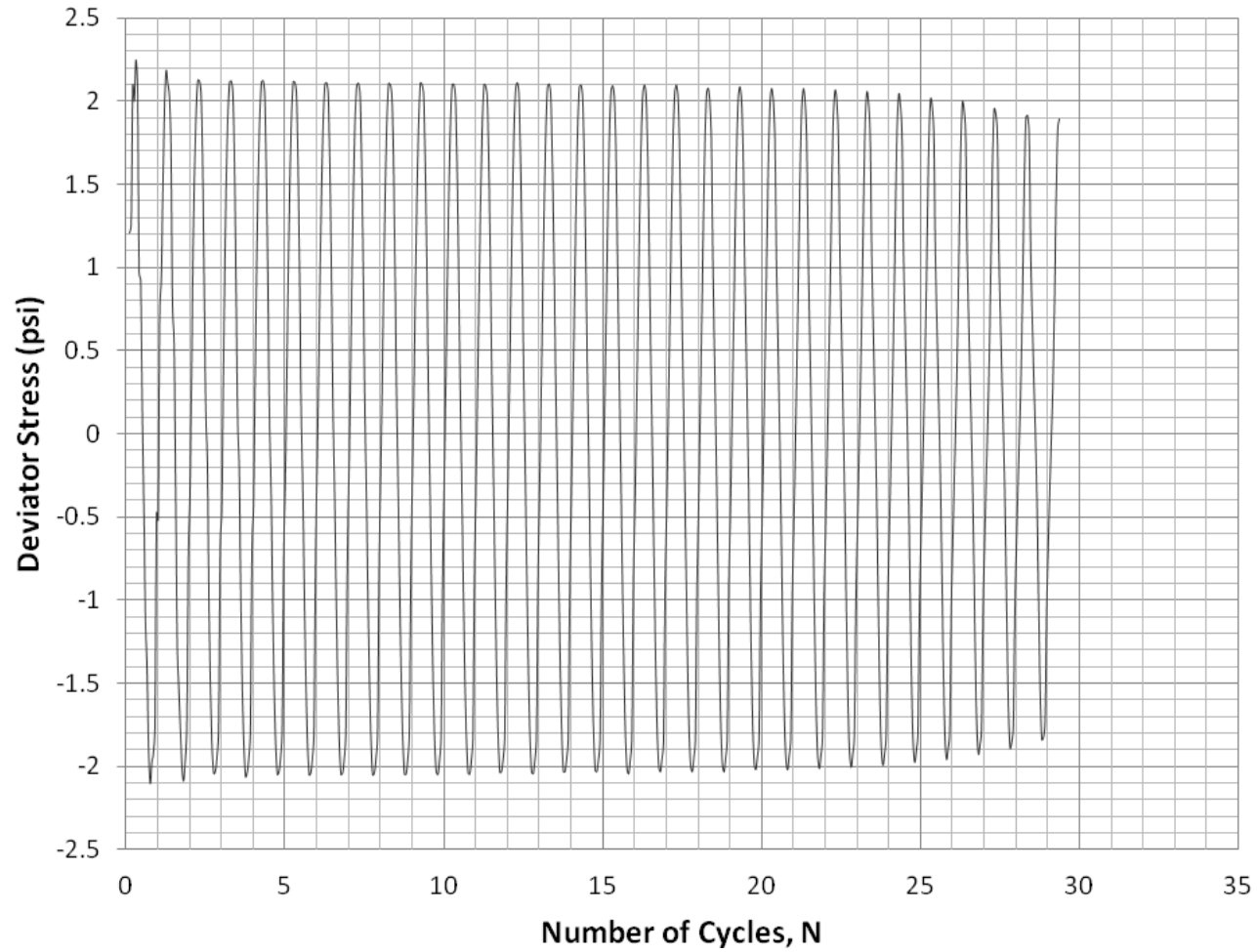
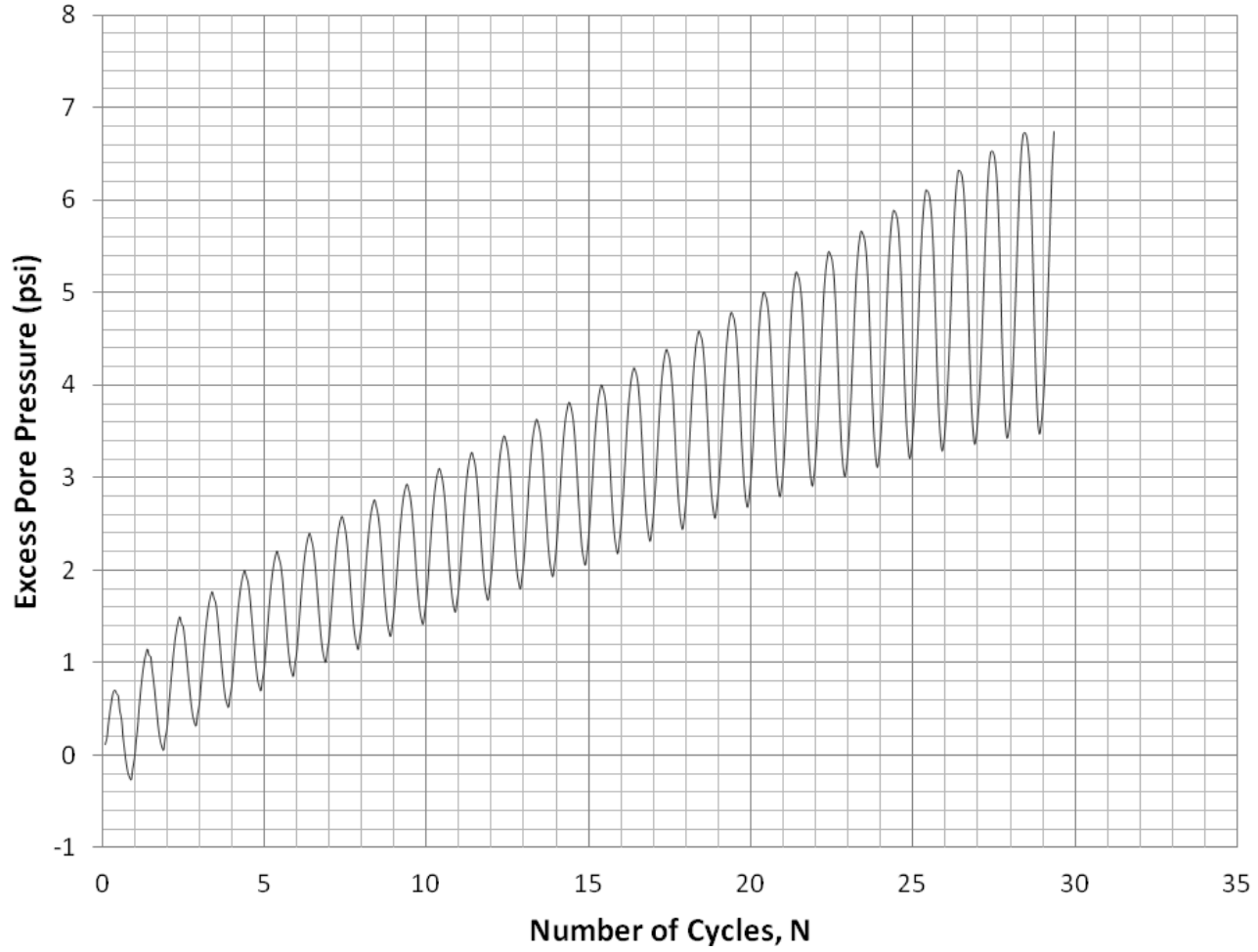Figure A.42: Specimen F98.5C1.5 CSR 0.30 Deviator Stress Versus Number of Cycles Graph

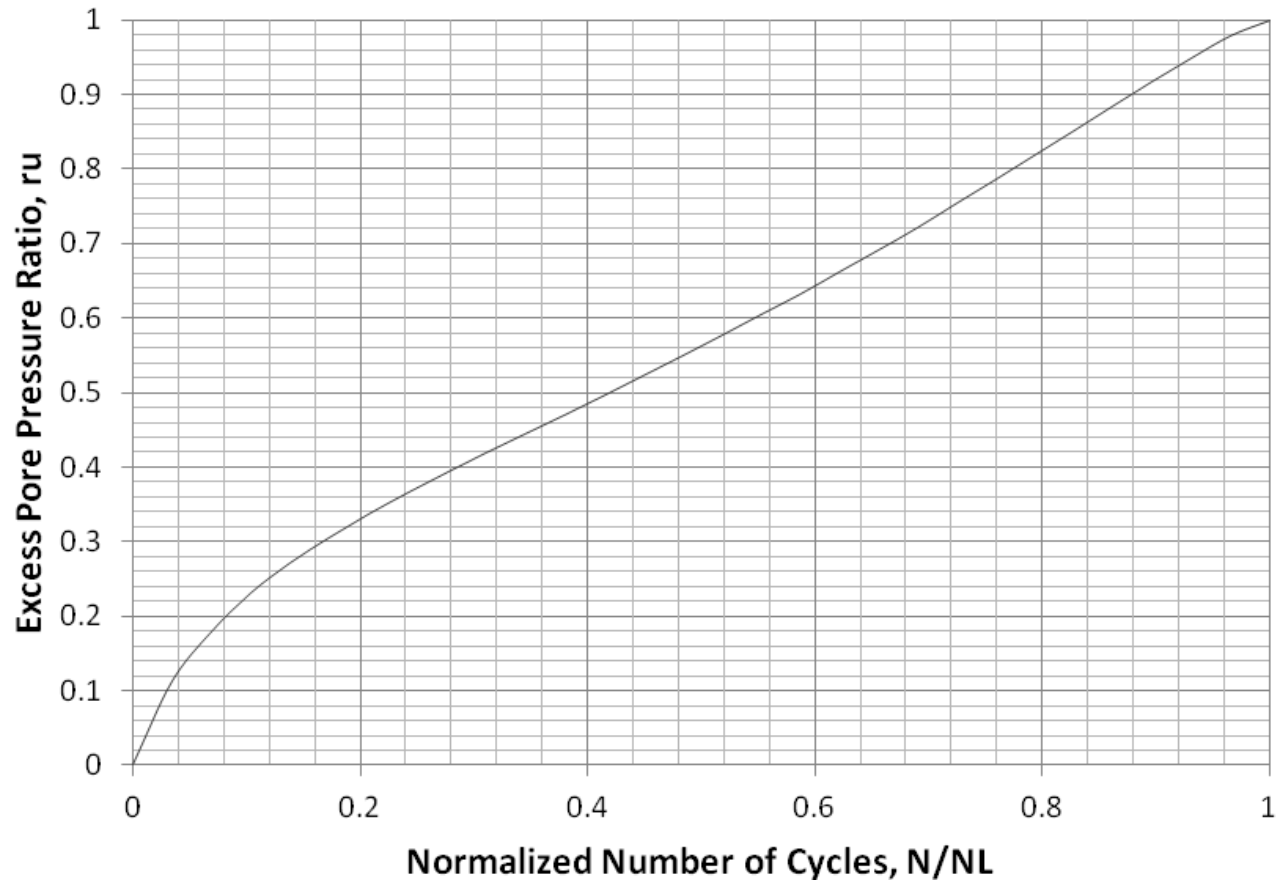Figure A.43: Specimen F98.5C1.5 CSR 0.30 Excess Pore Pressure Versus Number of Cycles Graph

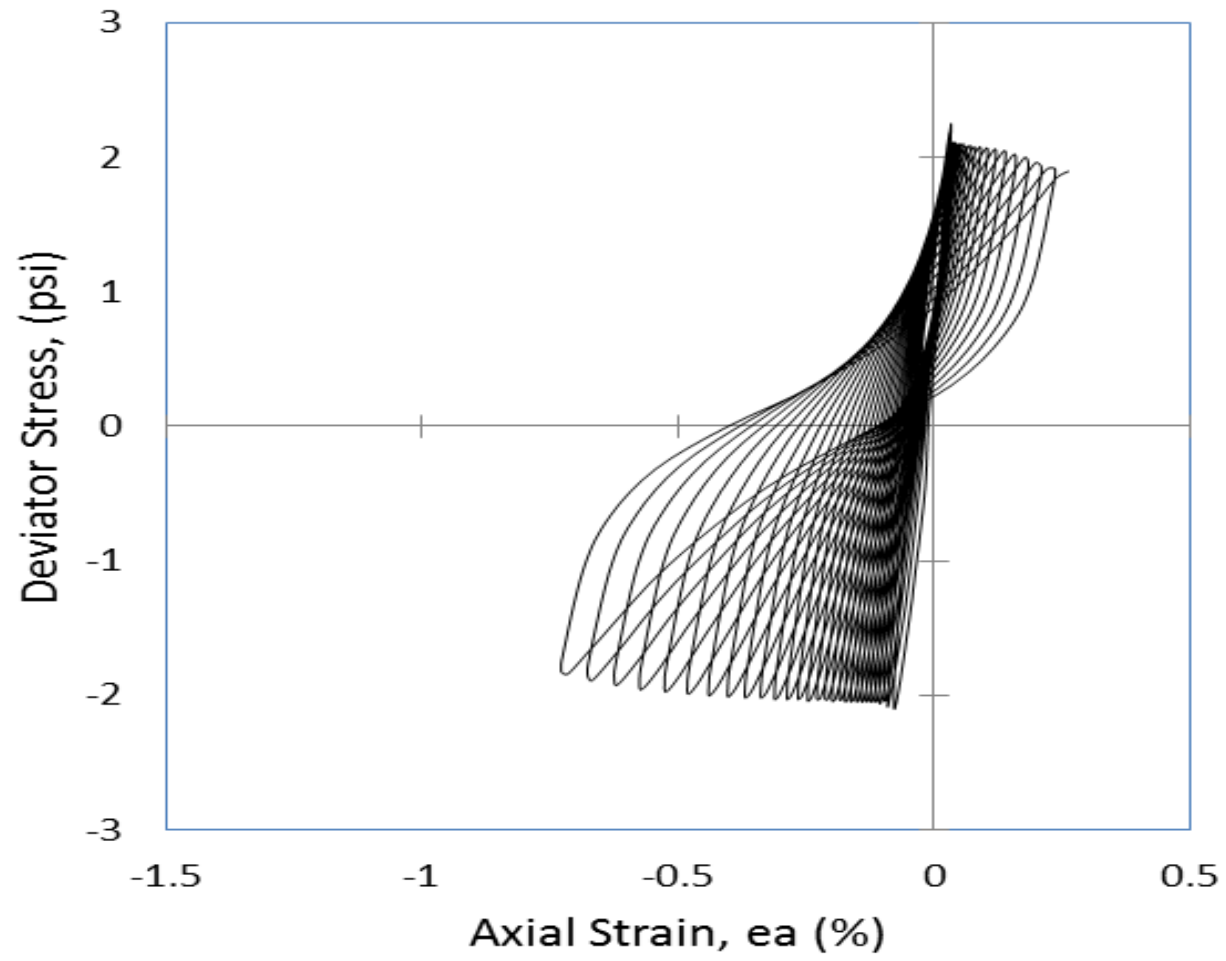Figure A.44: Specimen F98.5C1.5 CSR 0.30 Excess Pore Pressure Ratio Versus Normalized Number of Cycles Graph

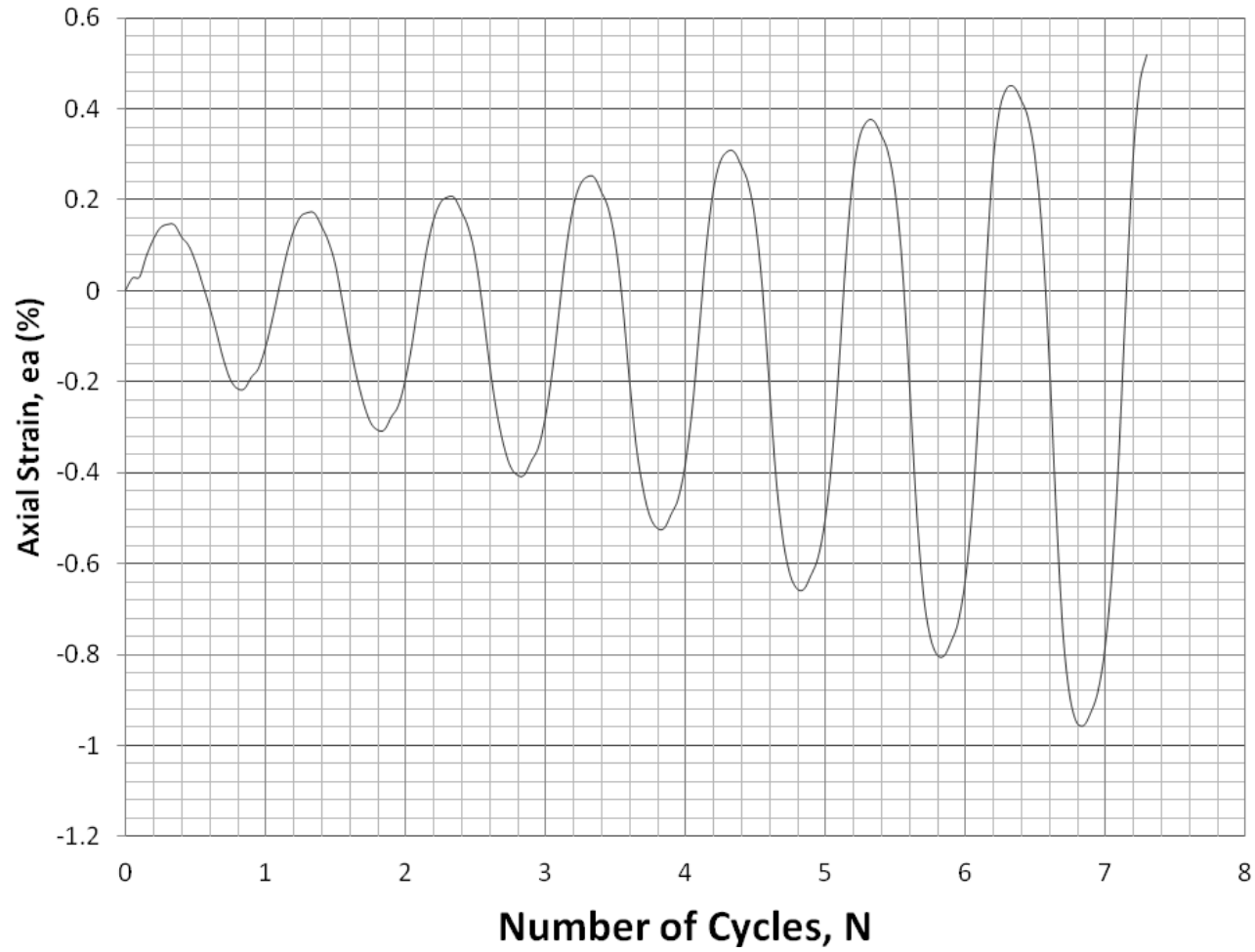Figure A.45: Specimen F98.5C1.5 CSR 0.30 Deviator Stress Versus Axial Strain Graph

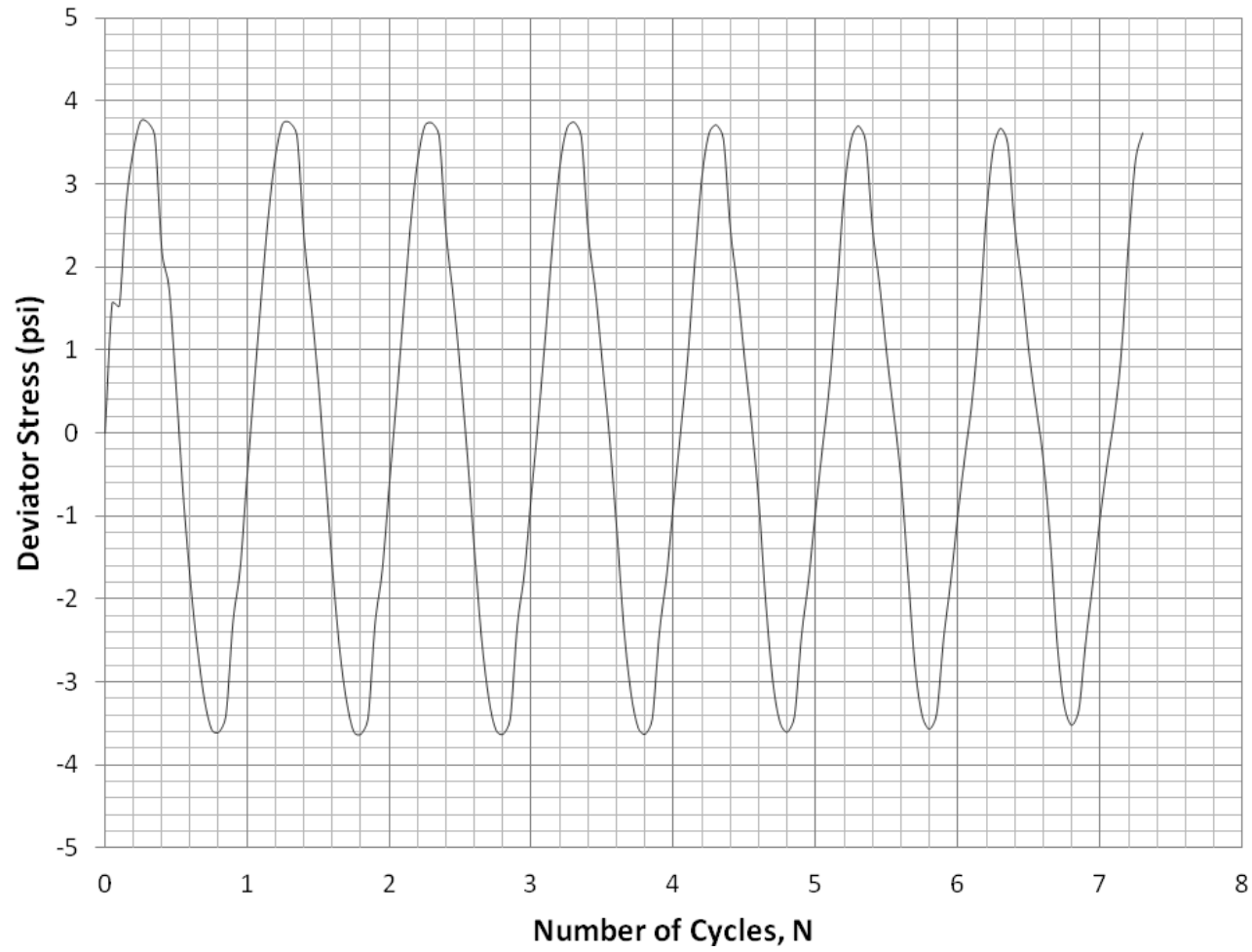Figure A.46: Specimen F98C2 CSR 0.50 Axial Strain Versus Number of Cycles Graph

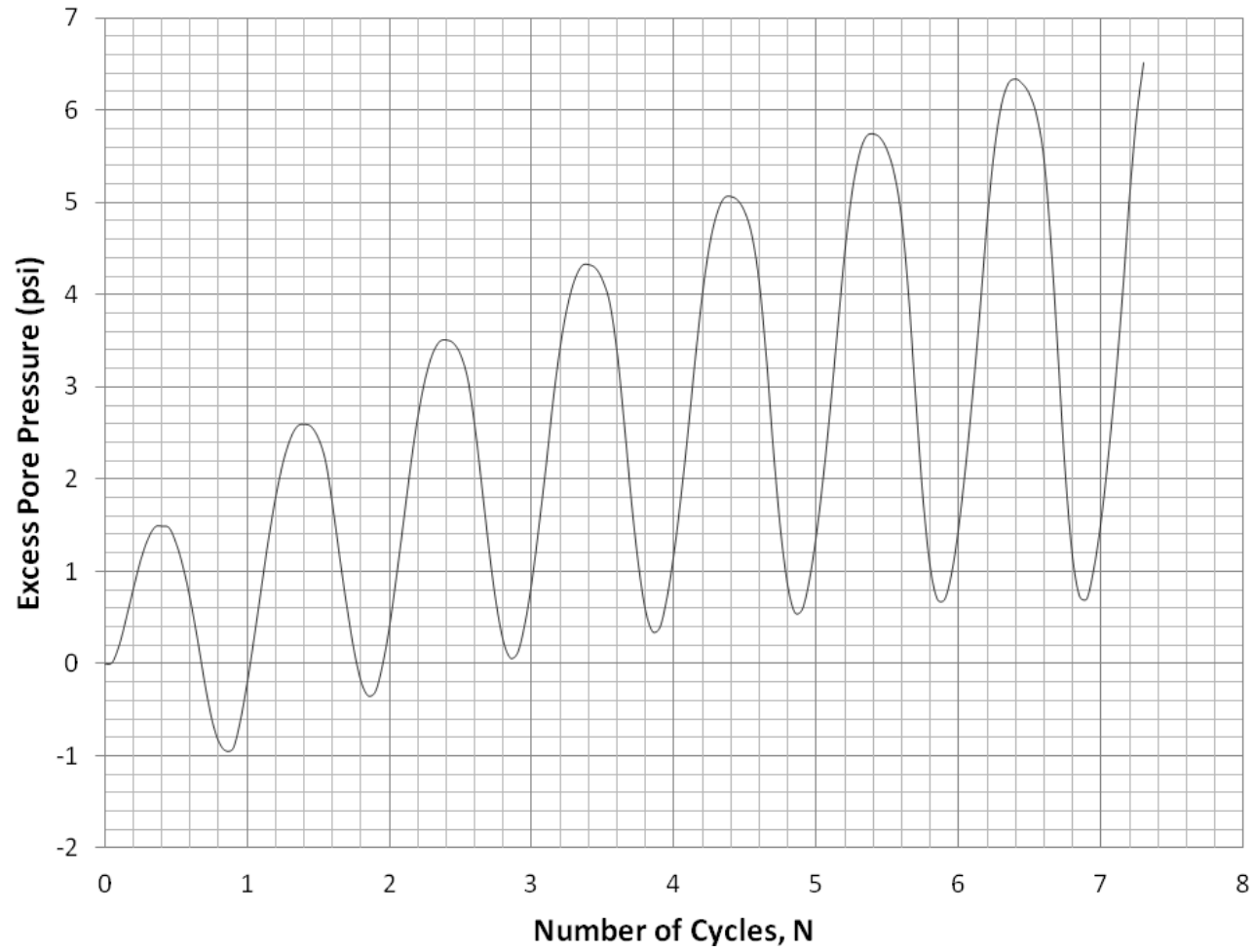Figure A.47: Specimen F98C2 CSR 0.50 Deviator Stress Versus Number of Cycles Graph

Figure A.48: Specimen F98C2 CSR 0.50 Excess Pore Pressure Versus Number of Cycles Graph

Figure A.49: Specimen F98C2 CSR 0.50 Excess Pore Pressure Ratio Versus Normalized Number of Cycles Graph
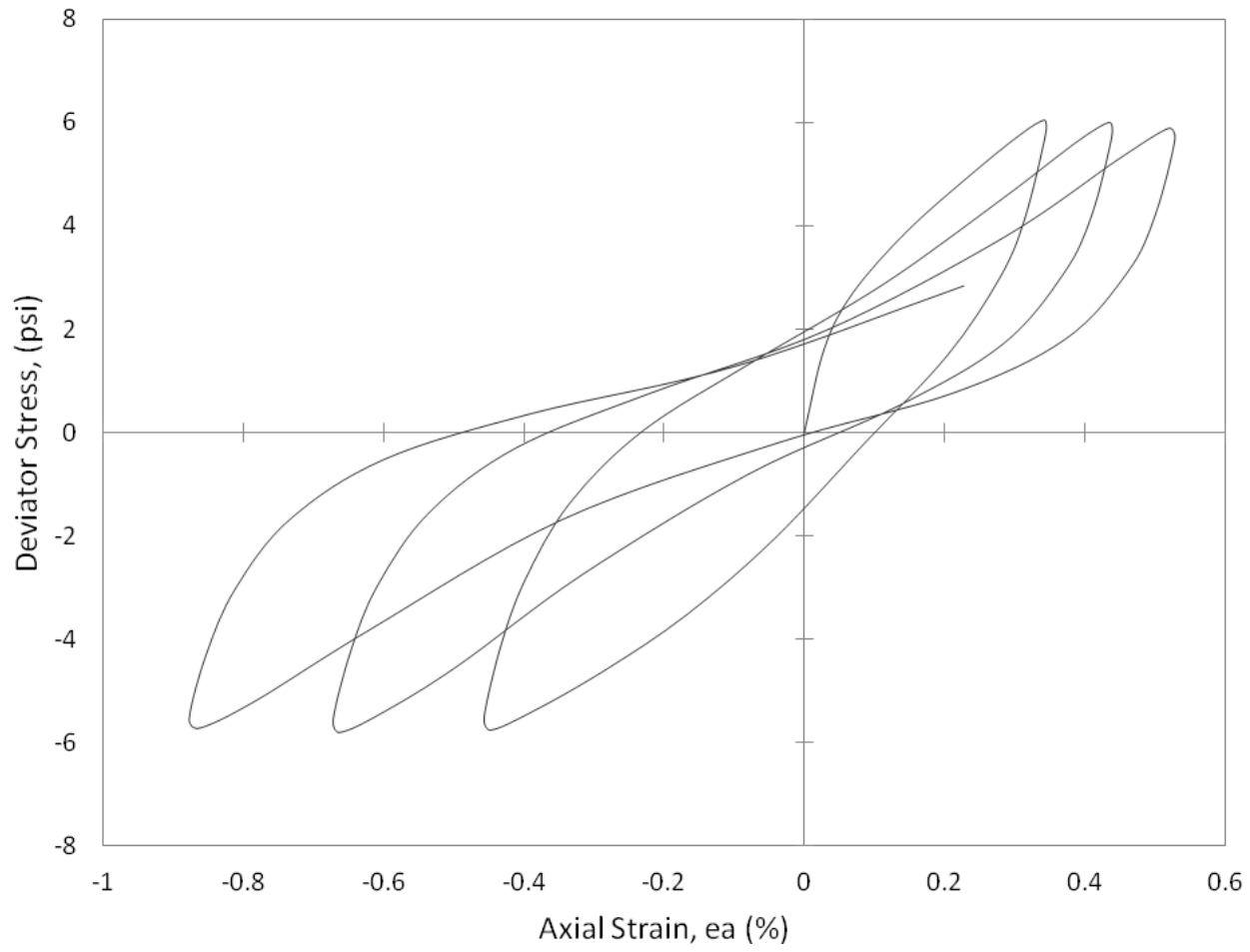
Figure A.50: Specimen F98C2 CSR 0.50 Deviator Stress Versus Axial Strain Graph
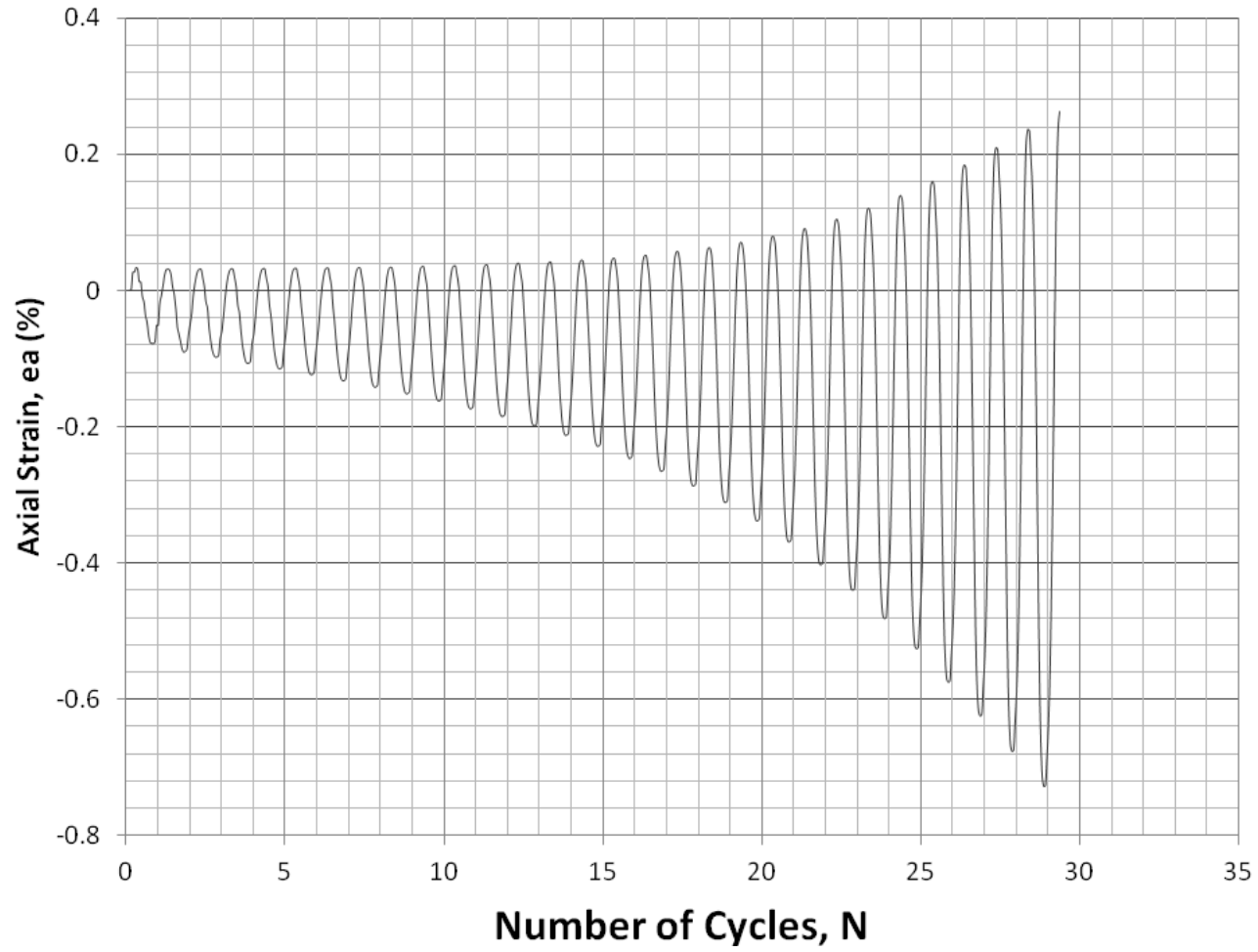
Figure A.51: Specimen F95C5 CSR 0.15 Axial Strain Versus Number of Cycles Graph

Figure A.52: Specimen F95C5 CSR 0.15 Deviator Stress Versus Number of Cycles Graph

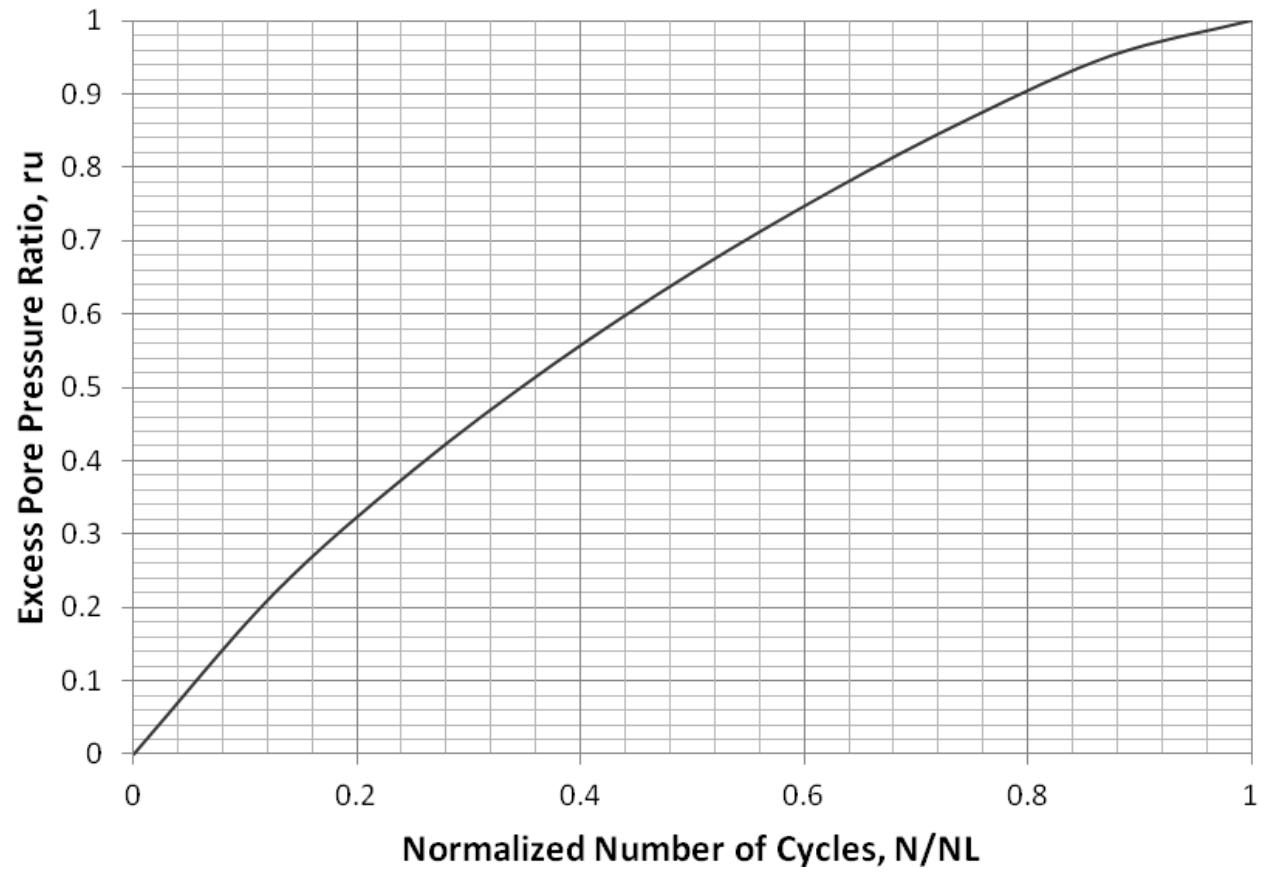Figure A.53: Specimen F95C5 CSR 0.15 Excess Pore Pressure Versus Number of Cycles Graph

Figure A.54: Specimen F95C5 CSR 0.15 Excess Pore Pressure Ratio Versus Normalized Number of Cycles Graph
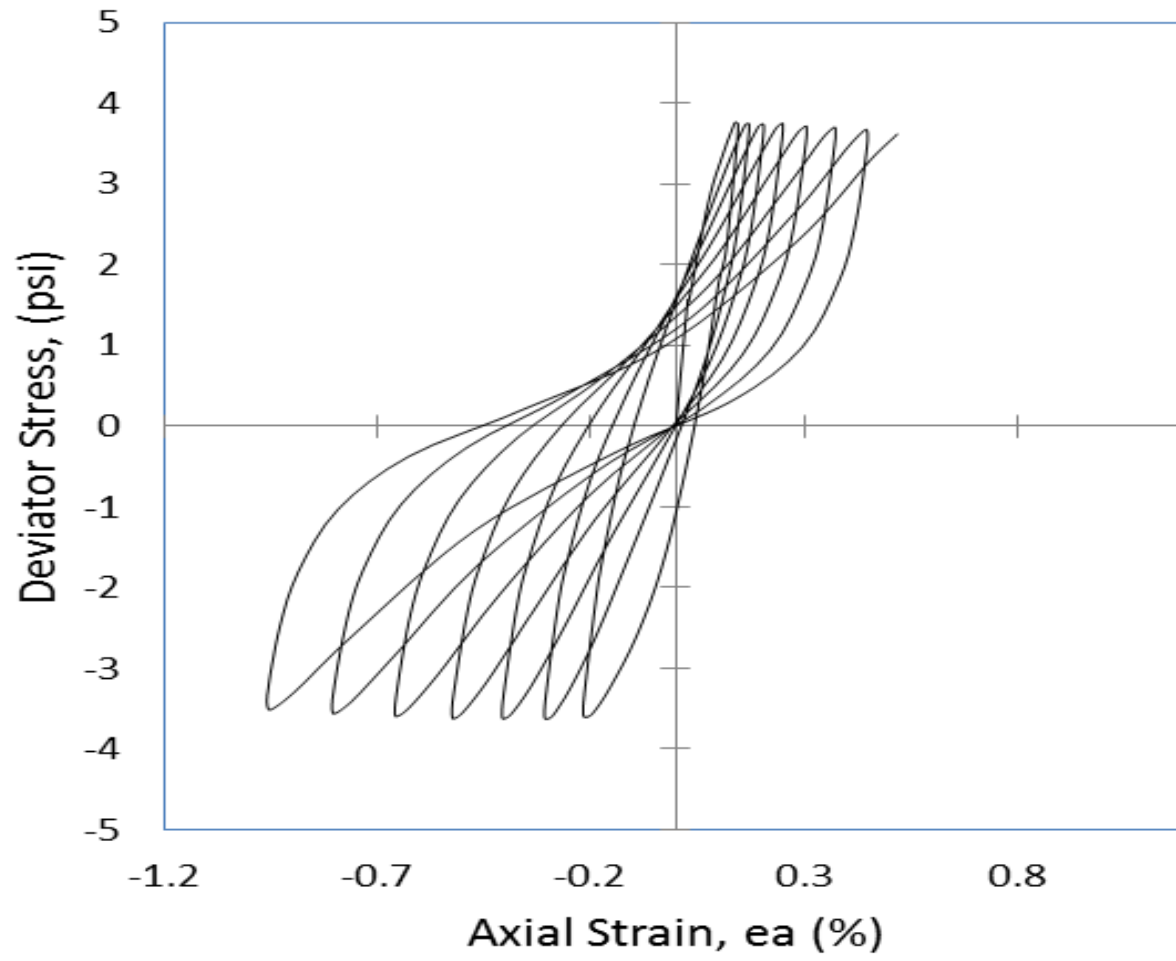
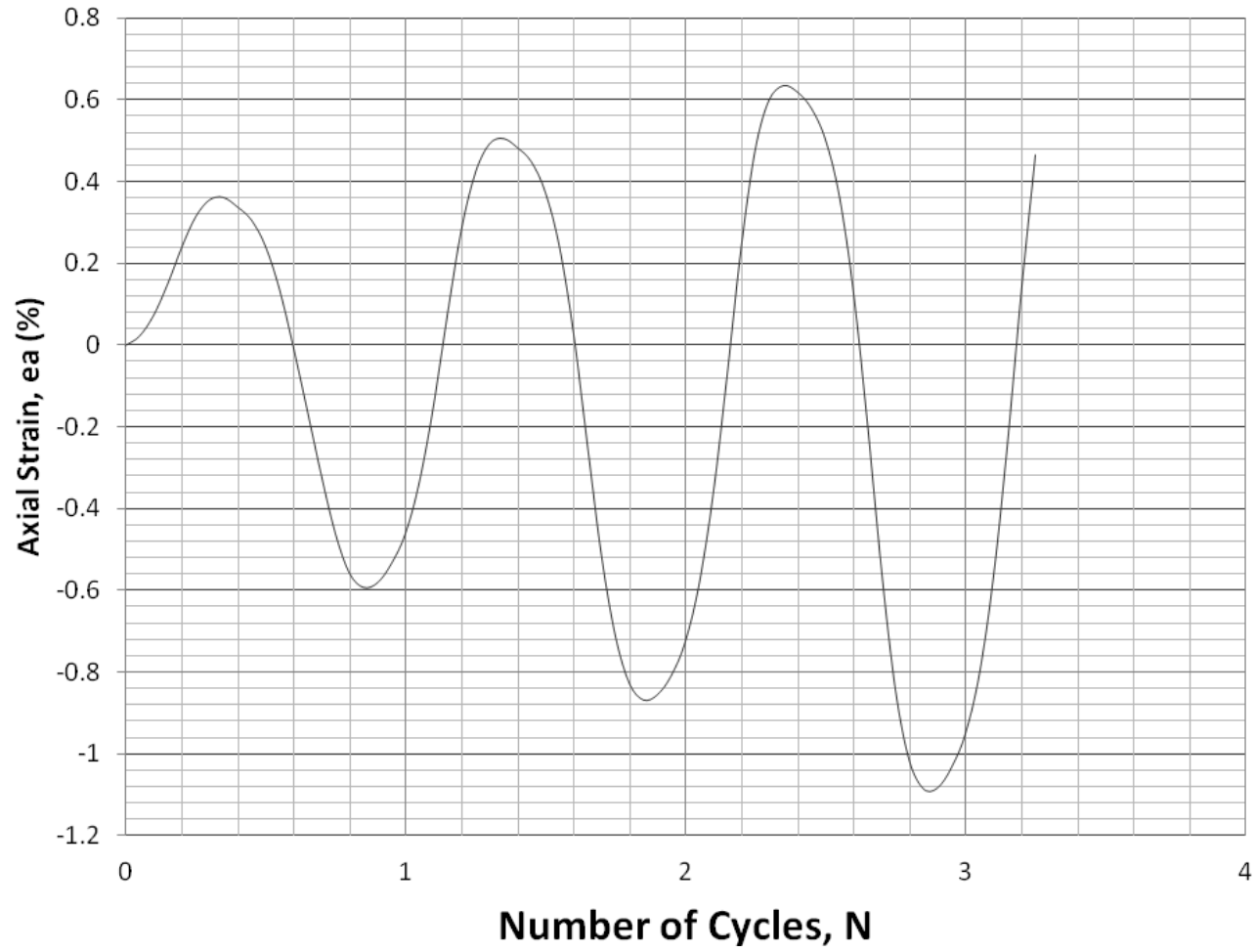Figure A.55: Specimen F95C5 CSR 0.15 Deviator Stress Versus Axial Strain Graph

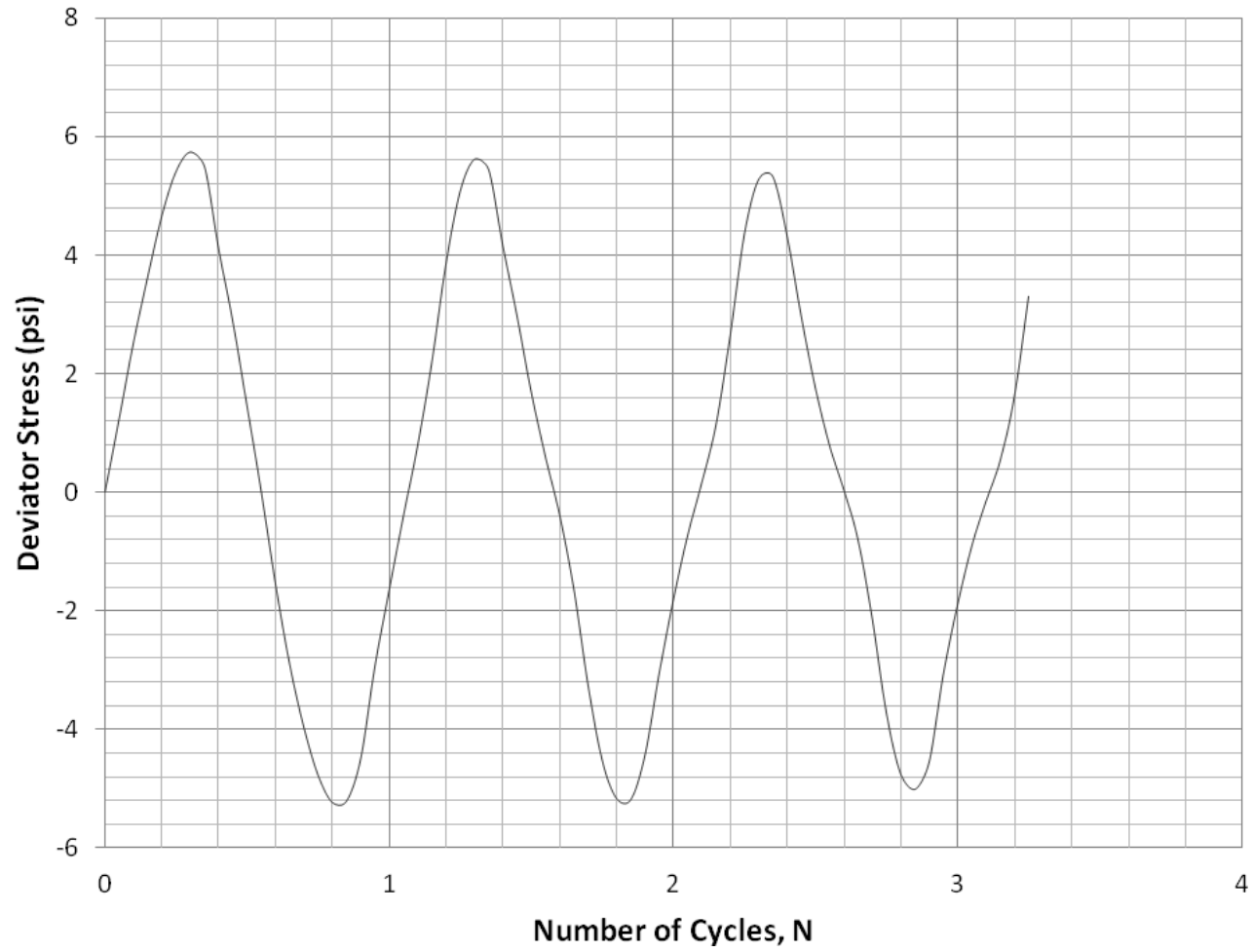Figure A.56: Specimen F95C5 CSR 0.30 Axial Strain Versus Number of Cycles Graph

Figure A.57: Specimen F95C5 CSR 0.30 Deviator Stress Versus Number of Cycles Graph

Figure A.58: Specimen F95C5 CSR 0.30 Excess Pore Pressure Versus Number of Cycles Graph

Figure A.59: Specimen F95C5 CSR 0.30 Excess Pore Pressure Ratio Versus Normalized Number of Cycles Graph

Figure A.60: Specimen F95C5 CSR 0.30 Deviator Stress Versus Axial Strain Graph

Figure A.61: Specimen F95C5 CSR 0.50 Axial Strain Versus Number of Cycles Graph

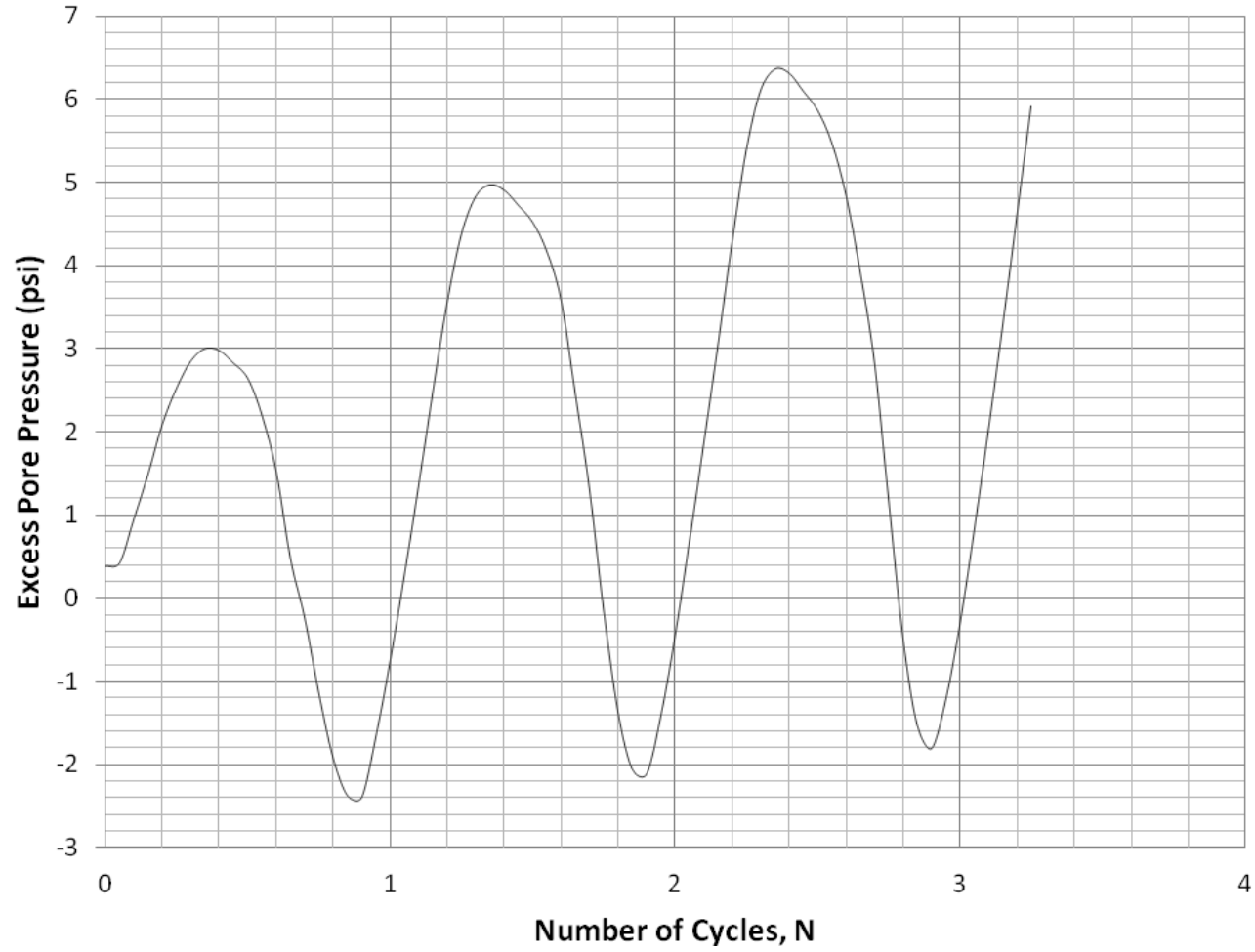Figure A.62: Specimen F95C5 CSR 0.50 Deviator Stress Versus Number of Cycles Graph

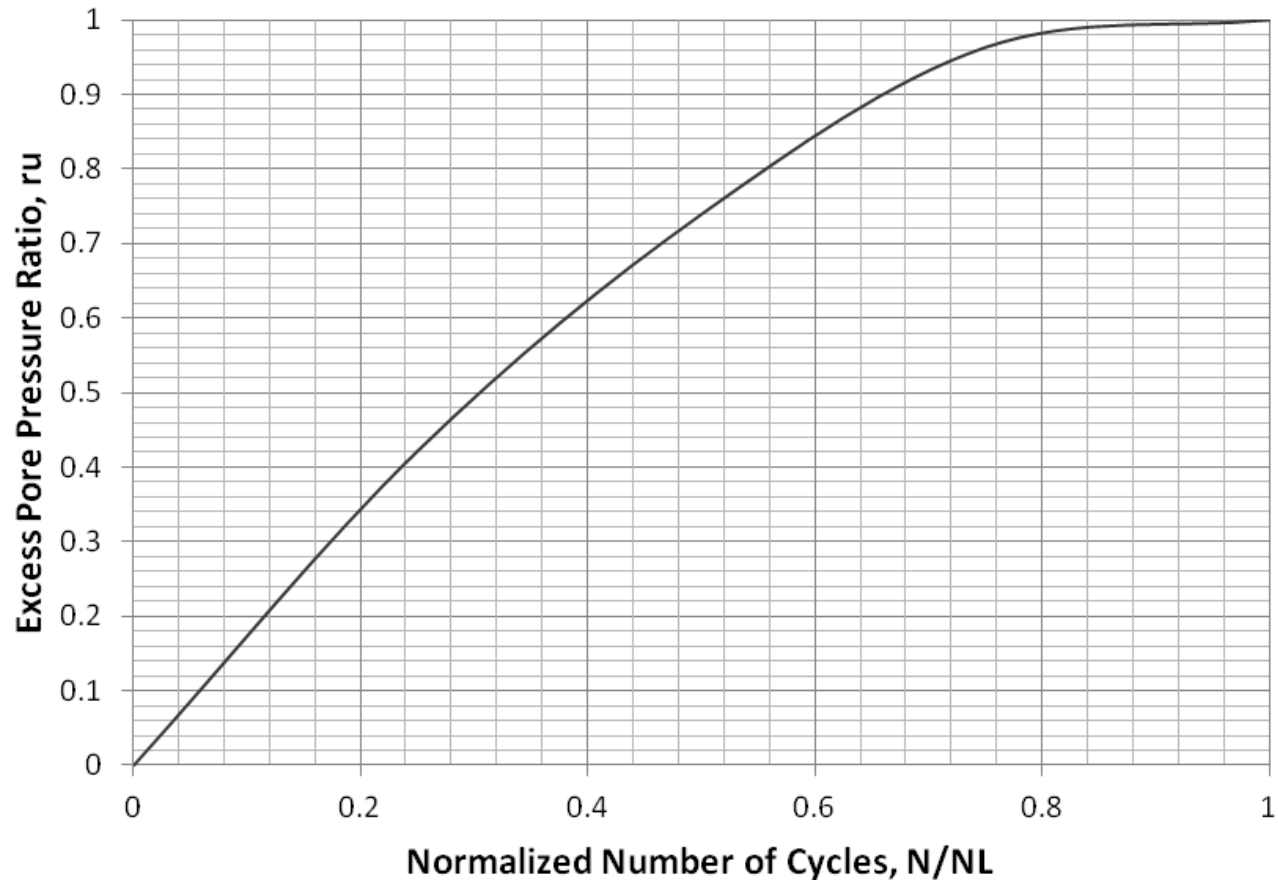Figure A.63: Specimen F95C5 CSR 0.50 Excess Pore Pressure Versus Number of Cycles Graph

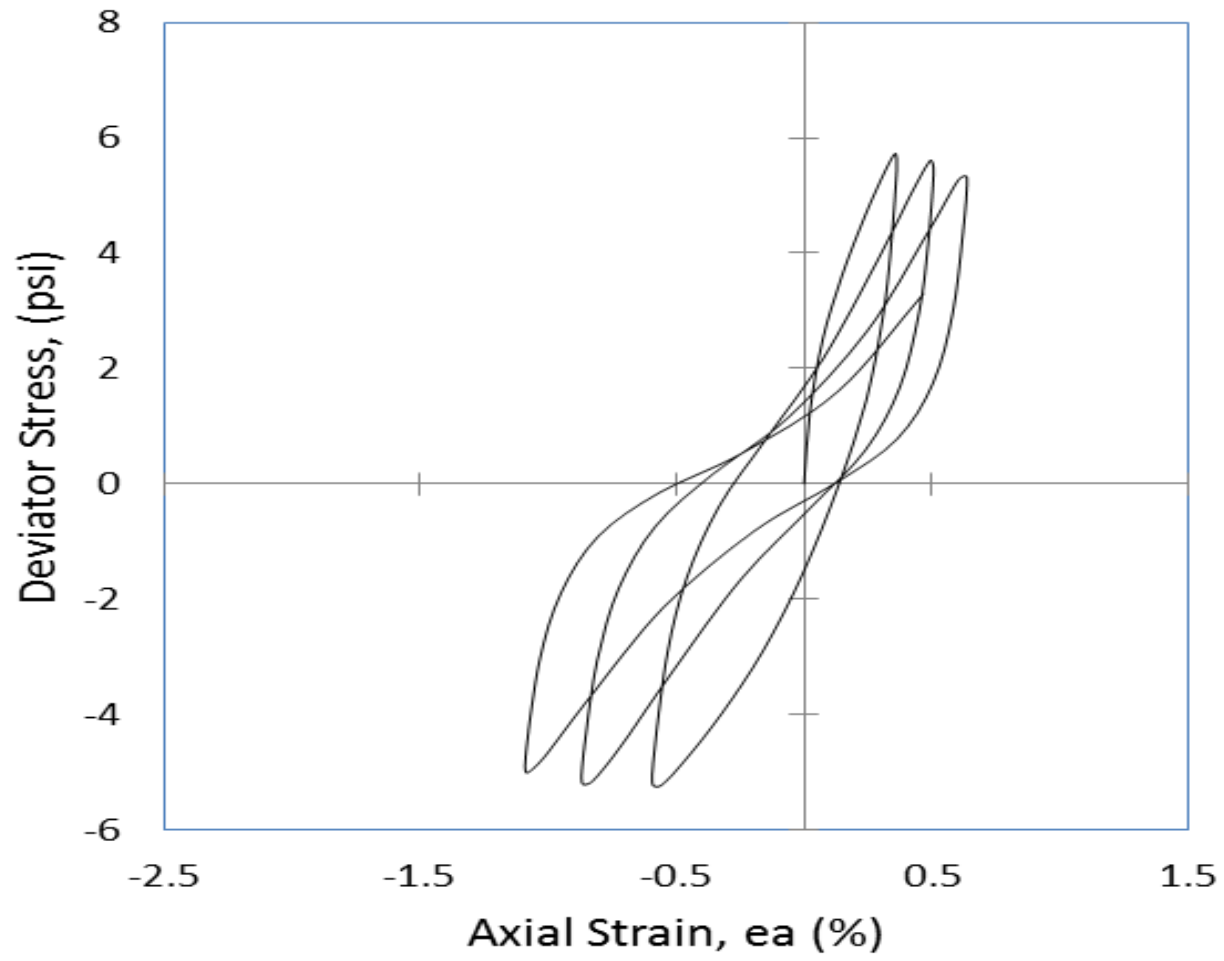Figure A.64: Specimen F95C5 CSR 0.50 Excess Pore Pressure Ratio Versus Normalized Number of Cycles Graph

Figure A.65: Specimen F95C5 CSR 0.50 Deviator Stress Versus Axial Strain Graph
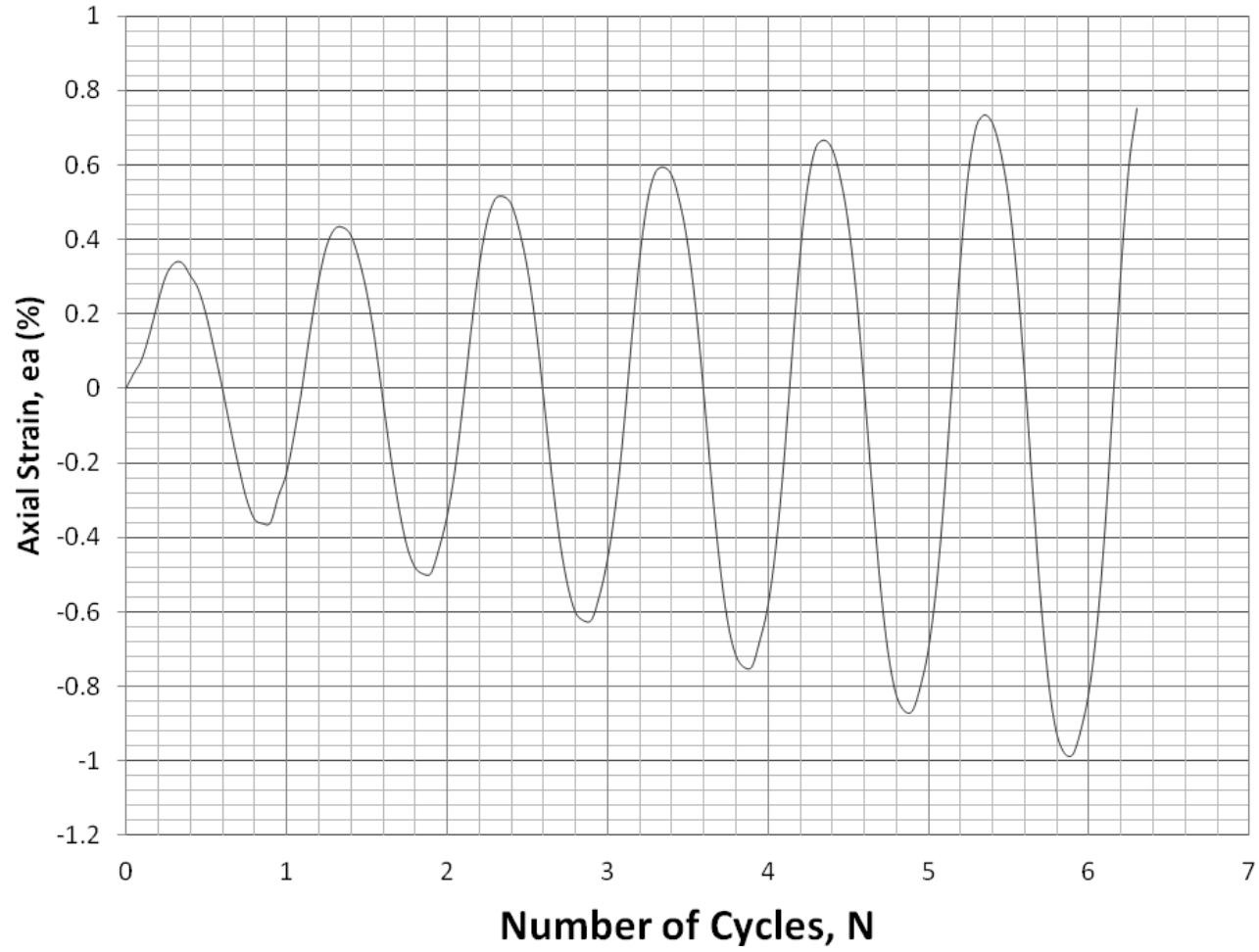
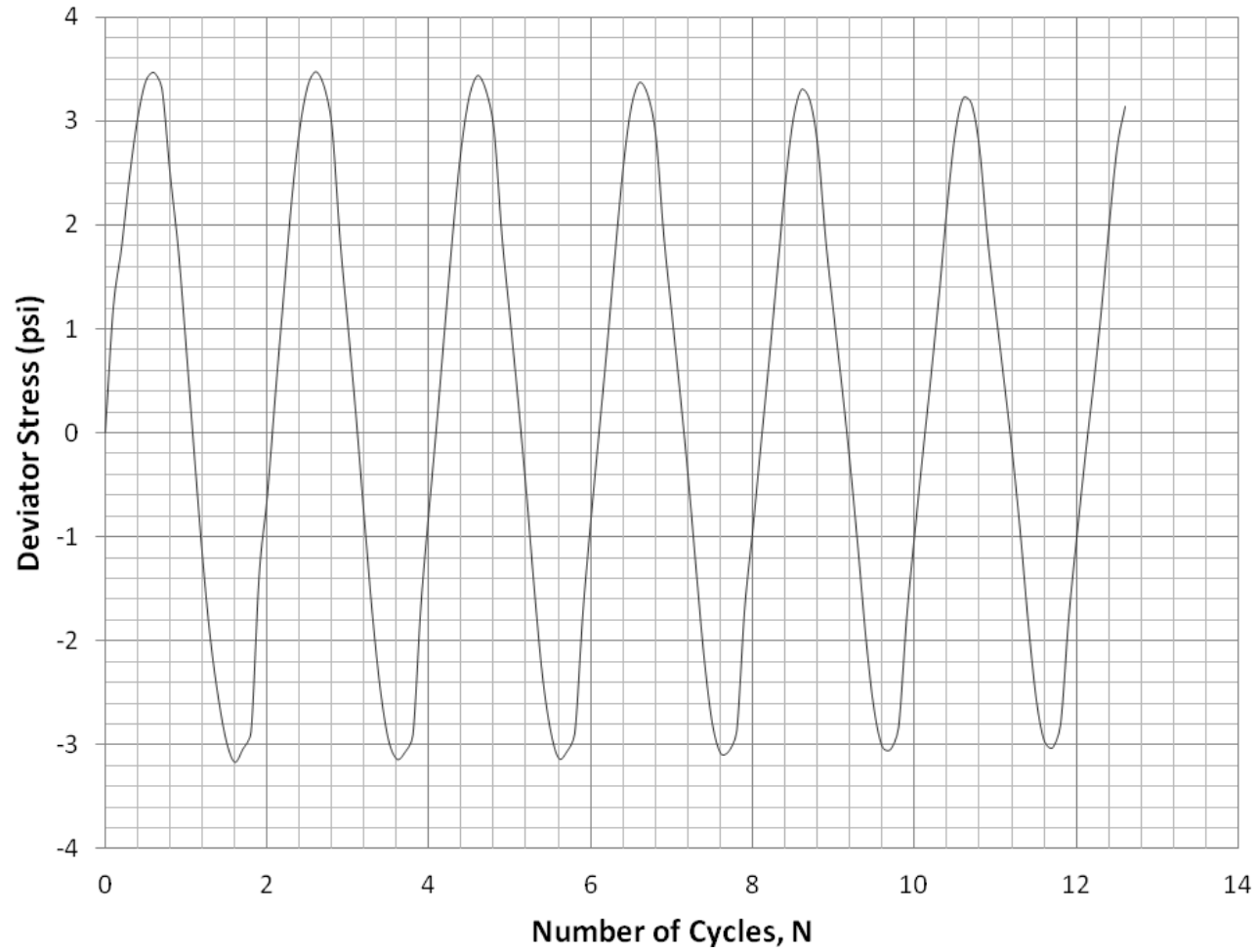Figure A.66: Specimen F80C20 CSR 0.30 Axial Strain Versus Number of Cycles Graph

Figure A.67: Specimen F80C20 CSR 0.30 Deviator Stress Versus Number of Cycles Graph
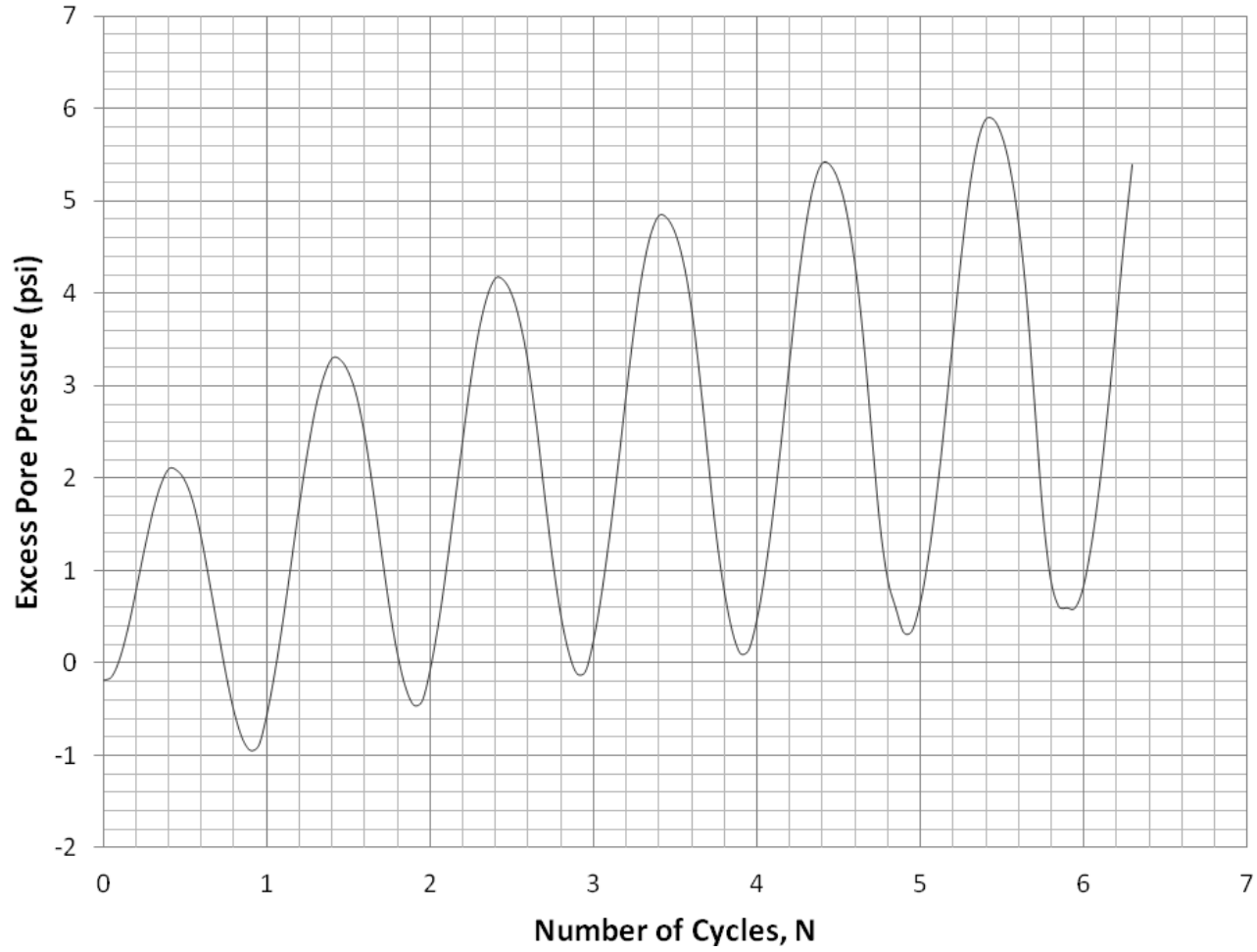
Figure A.68: Specimen F80C20 CSR 0.30 Excess Pore Pressure Versus Number of Cycles Graph
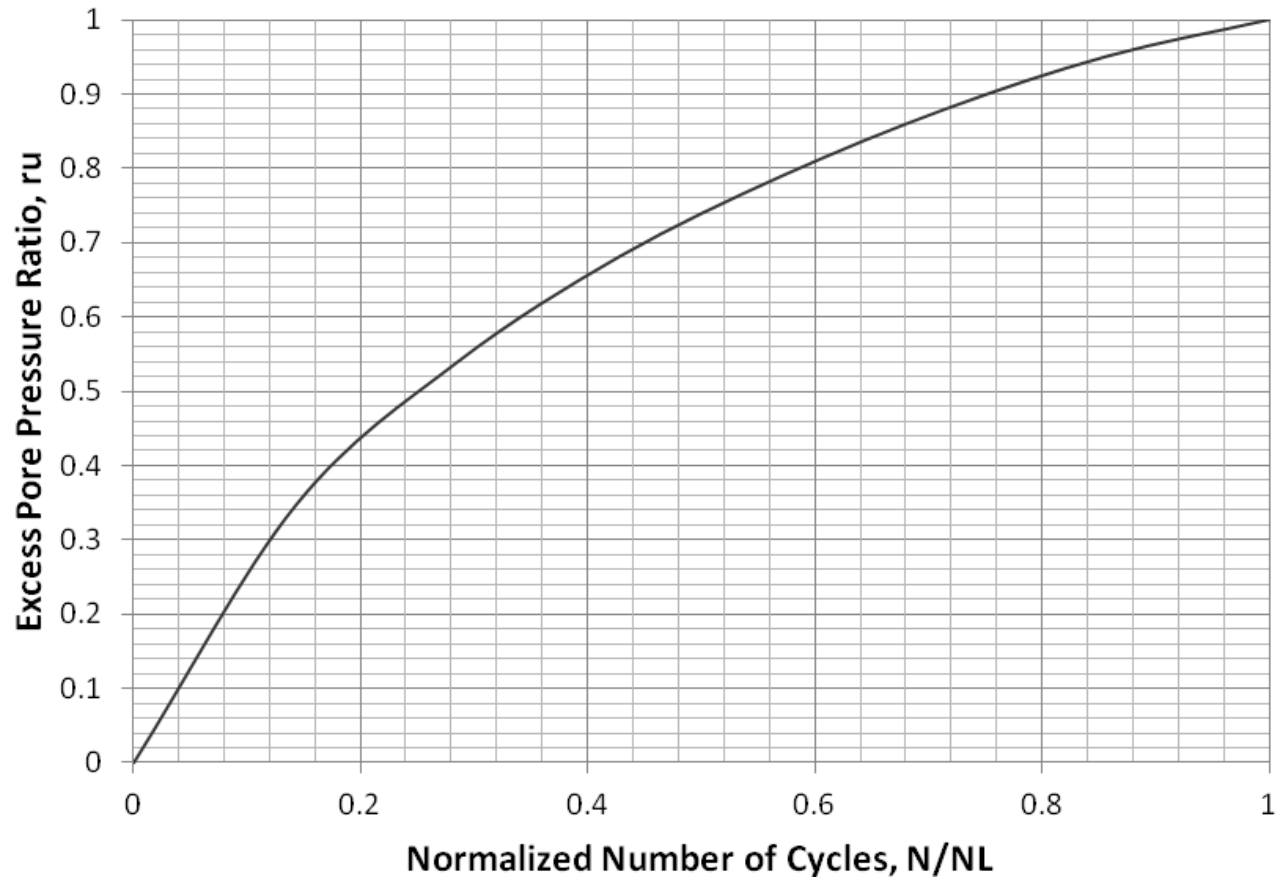
Figure A.69: Specimen F80C20 CSR 0.30 Excess Pore Pressure Ratio Versus Normalized Number of Cycles Graph
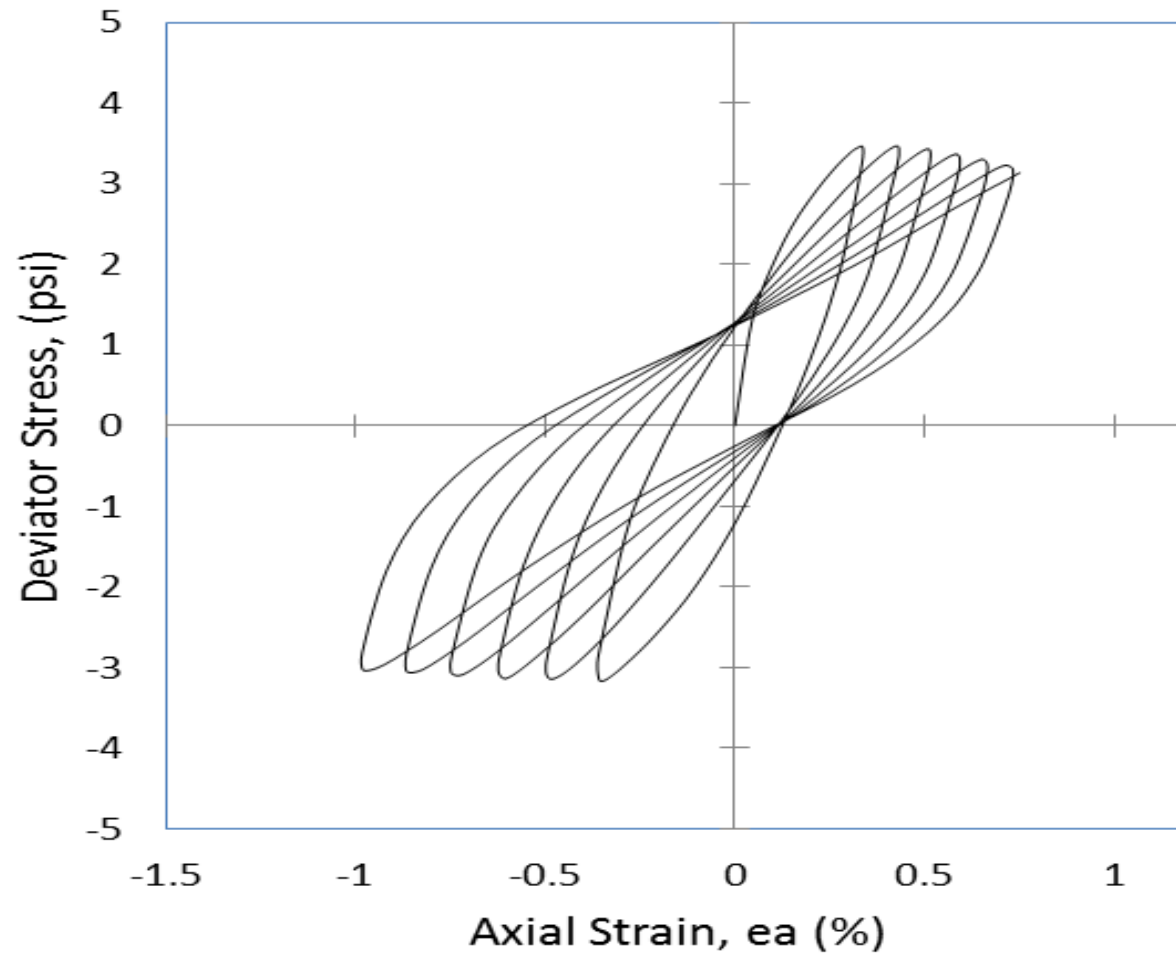
Figure A.70: Specimen F80C20 CSR 0.30 Deviator Stress Versus Axial Strain Graph

Table A.4: Specimen Information for Class F Fly Ash + Crumb Rubber

Sample Information:					
Specimen	F95R5	F90R10			F80R20
Target CSR	0.30	0.50	0.30	0.15	0.30
Depth (Meter)	9.8	9.8	9.8	9.2	9.8
Depth (ft)	32.1	32.2	32.2	30.0	32.2
Preparation phase:					
Net. Solid weight (lb)	1.2536	1.1986	1.1968	1.22	1.2919
Diameter (inch)	2.775	2.786	2.7805	2.787	2.772
Height (inch)	5.6377	5.5907	5.6465	5.6328	5.5573
Ratio of height/diameter	2.03	2.01	2.03	2.02	2
Gs	2.02	2.02	2.02	2.02	2.02
Void ratio	0.98	1.07	1.09	1.05	0.89
γdry (pcf)	63.52	60.76	60.32	61.34	66.53
γsat (pcf)	94.48	93.08	92.86	93.37	95.99
Saturation phase:					
B-value (%)	95	97	95	95	95
Shear phase:					
Frequency (Hz):		0.5			
Period (Sec):		2			
Asked Deviator Stress (psi)	8.6	13.7	8.2	4.2	9.0
Confining Pressure (psi)	7.2	6.9	6.8	6.5	7.5
Actual CSR	0.292	0.482	0.296	0.172	0.288
Ncycle to liquefy	4	4	11	86	7

Definitions:

F = Class F Fly Ash

R = Crumb Rubber

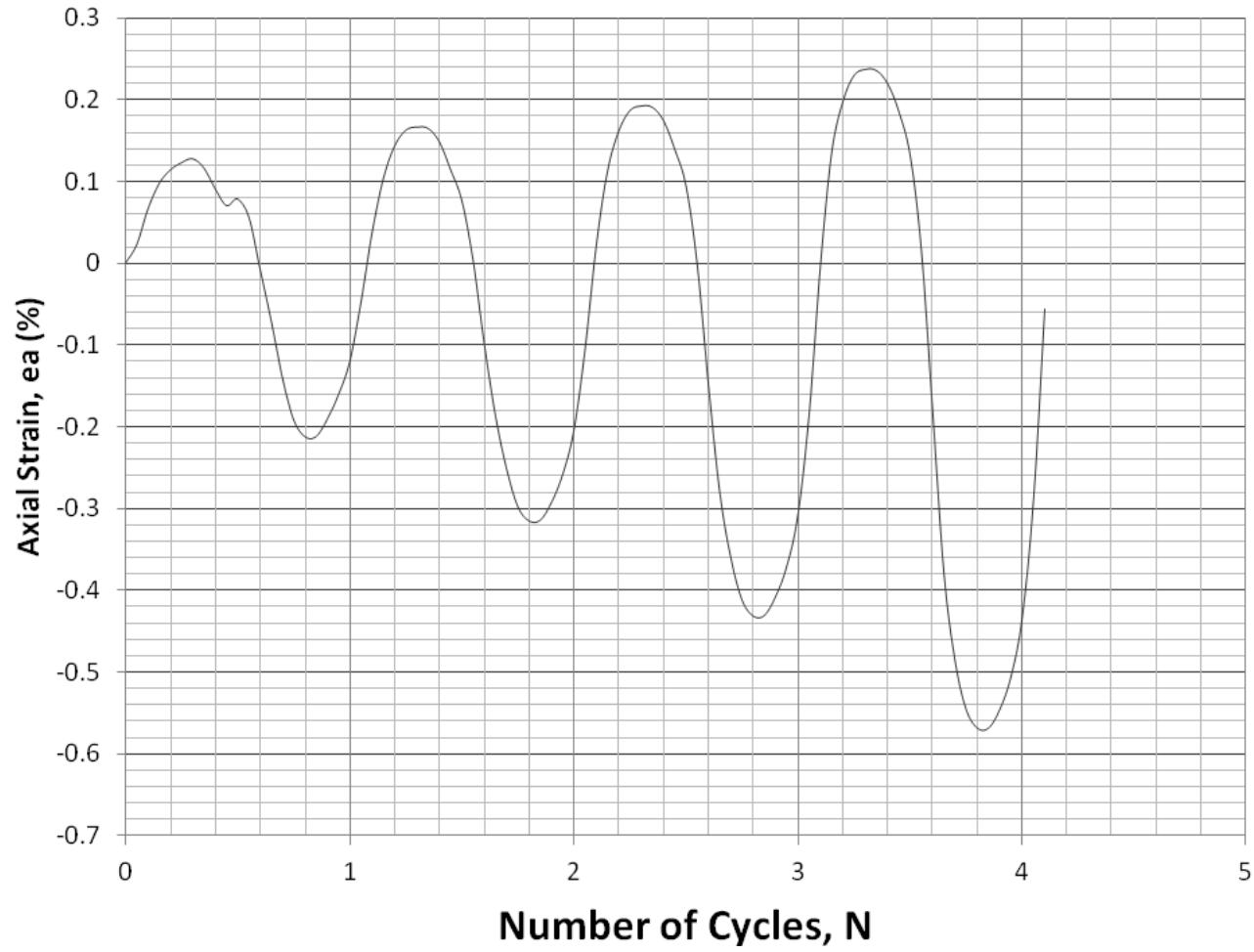95, 90, 80, 20, 10, and 5 = Percentage of Waste Material by Dry Weight

Figure A.71: Specimen F95R5 CSR 0.30 Axial Strain Versus Number of Cycles Graph
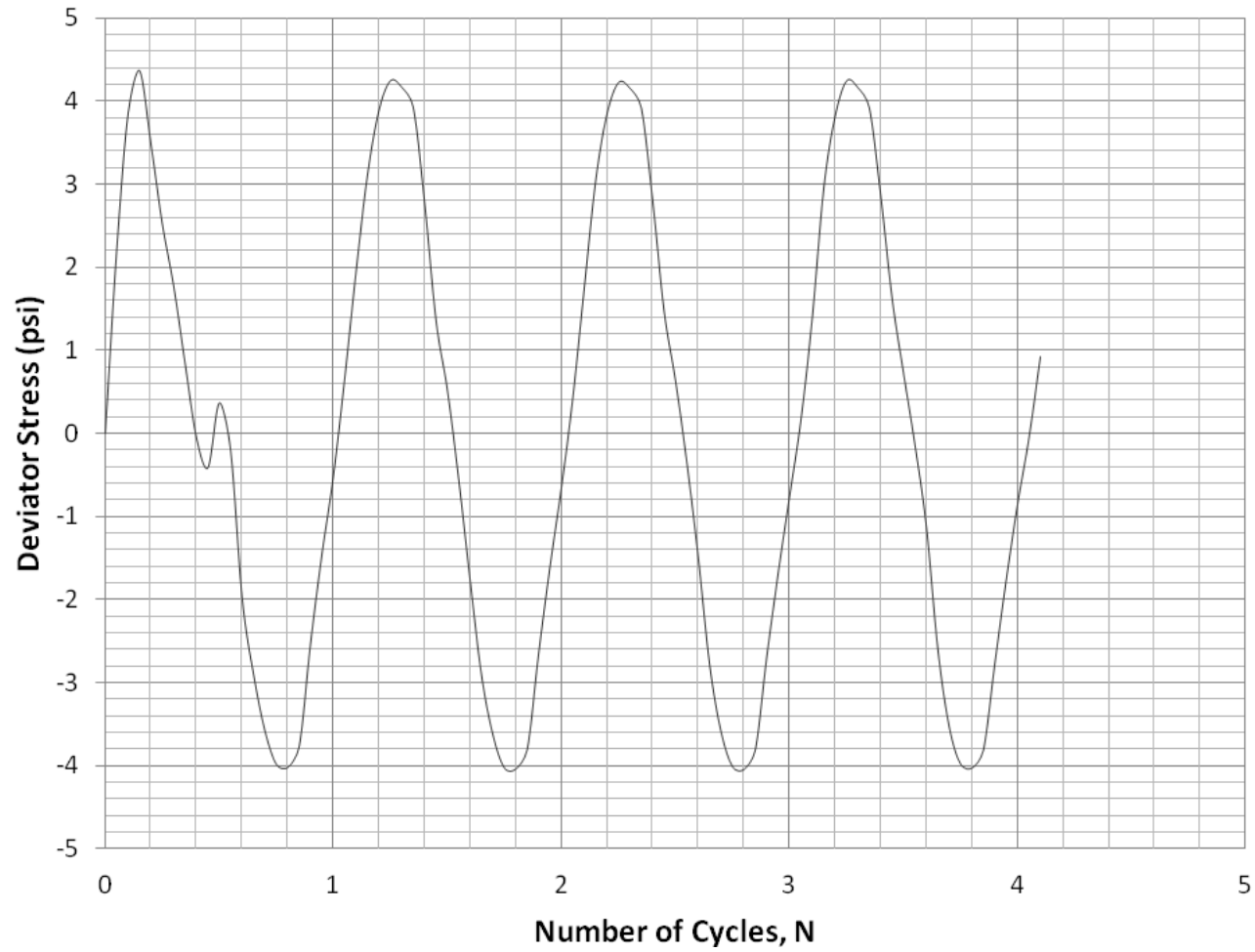
Figure A.72: Specimen F95R5 CSR 0.30 Deviator Stress Versus Number of Cycles Graph

Figure A.73: Specimen F95R5 CSR 0.30 Excess Pore Pressure Versus Number of Cycles Graph

Figure A.74: Specimen F95R5 CSR 0.30 Excess Pore Pressure Ratio Versus Normalized Number of Cycles Graph

Figure A.75: Specimen F95R5 CSR 0.30 Deviator Stress Versus Axial Strain Graph

Figure A.76: Specimen F90R10 CSR 0.15 Axial Strain Versus Number of Cycles Graph

Figure A.77: Specimen F90R10 CSR 0.15 Deviator Stress Versus Number of Cycles Graph

Figure A.78: Specimen F90R10 CSR 0.15 Excess Pore Pressure Versus Number of Cycles Graph

Figure A.79: Specimen F90R10 CSR 0.15 Excess Pore Pressure Ratio Versus Normalized Number of Cycles Graph

Figure A.80: Specimen F90R10 CSR 0.15 Deviator Stress Versus Axial Strain Graph

Figure A.81: Specimen F90R10 CSR 0.30 Axial Strain Versus Number of Cycles Graph

Figure A.82: Specimen F90R10 CSR 0.30 Deviator Stress Versus Number of Cycles Graph
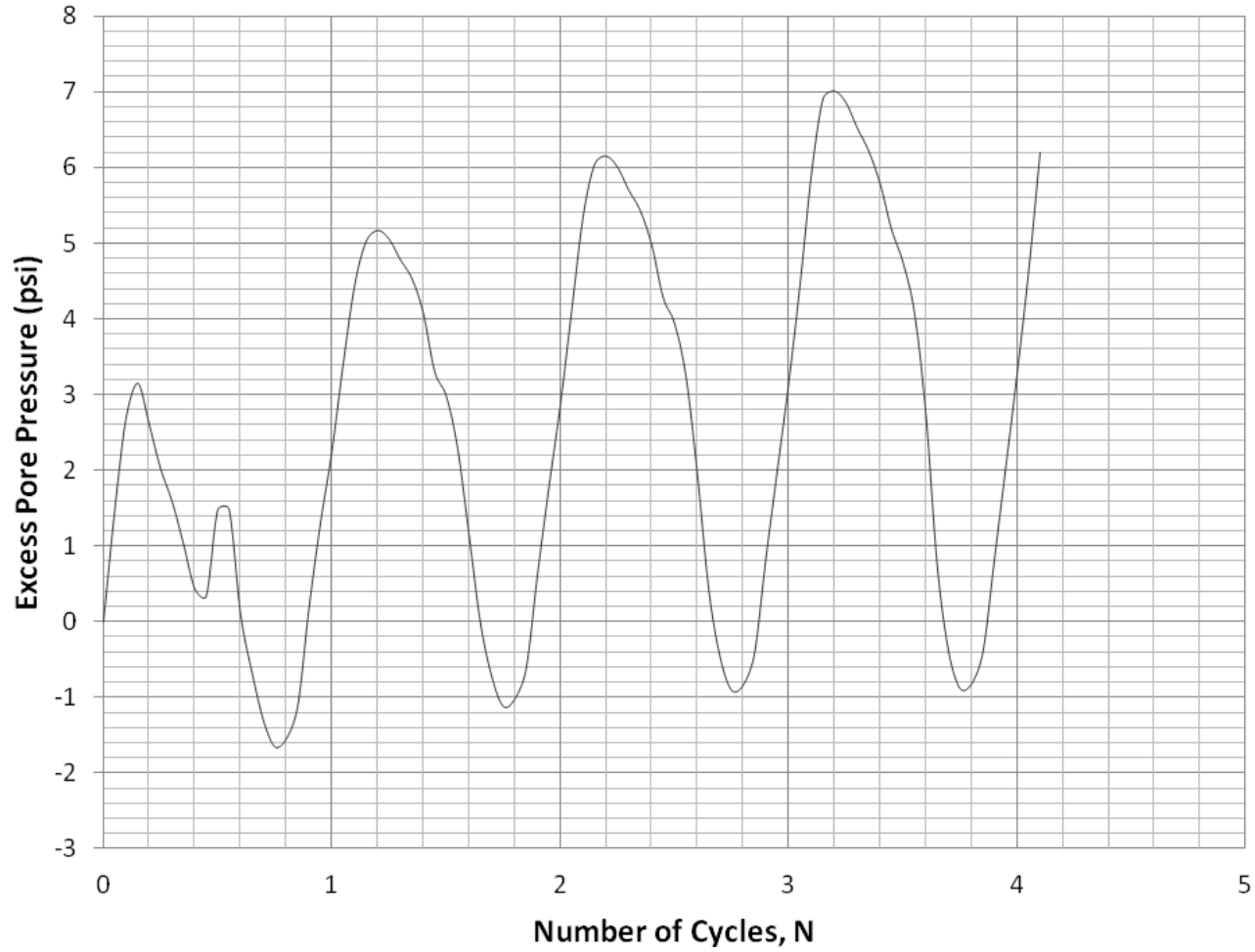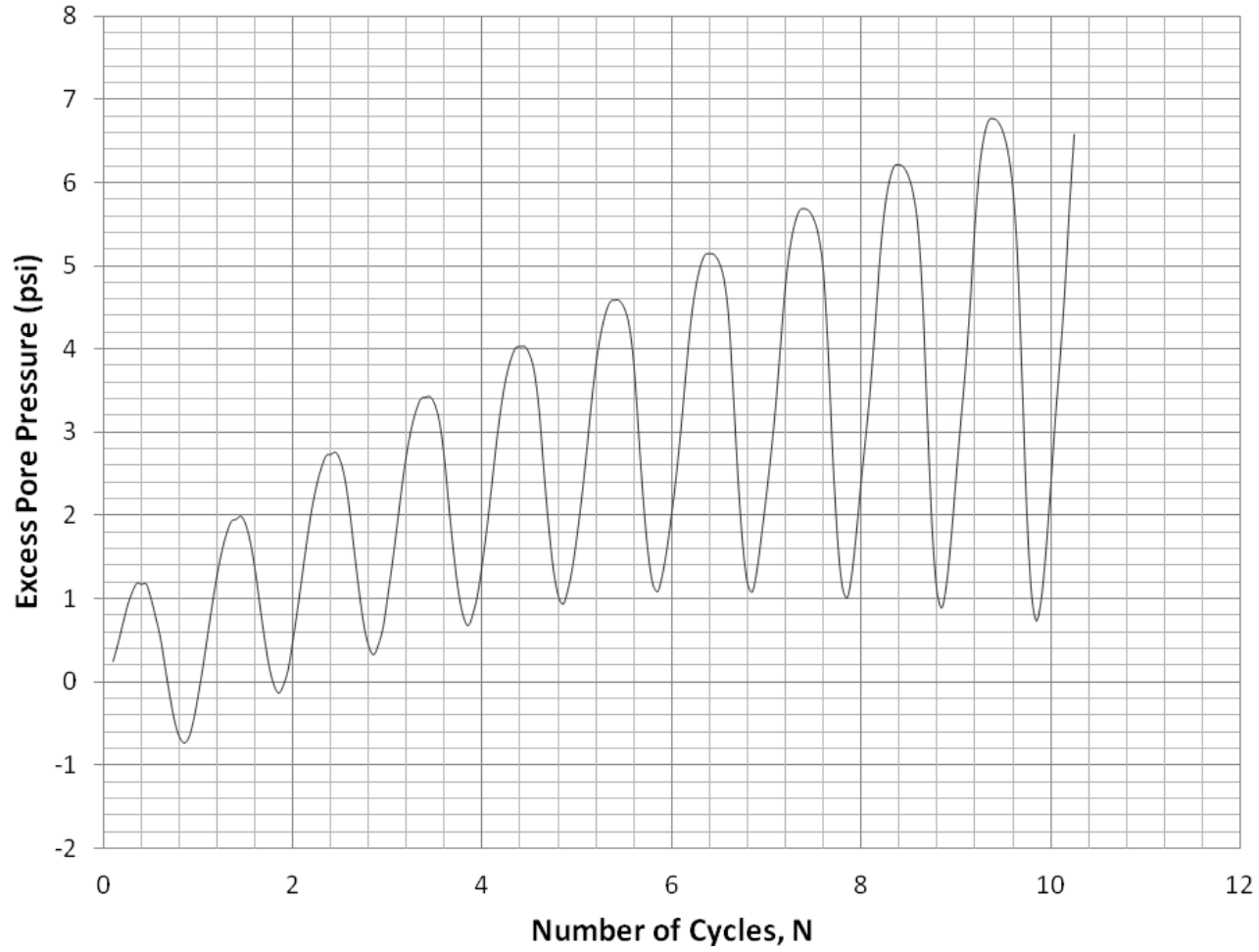
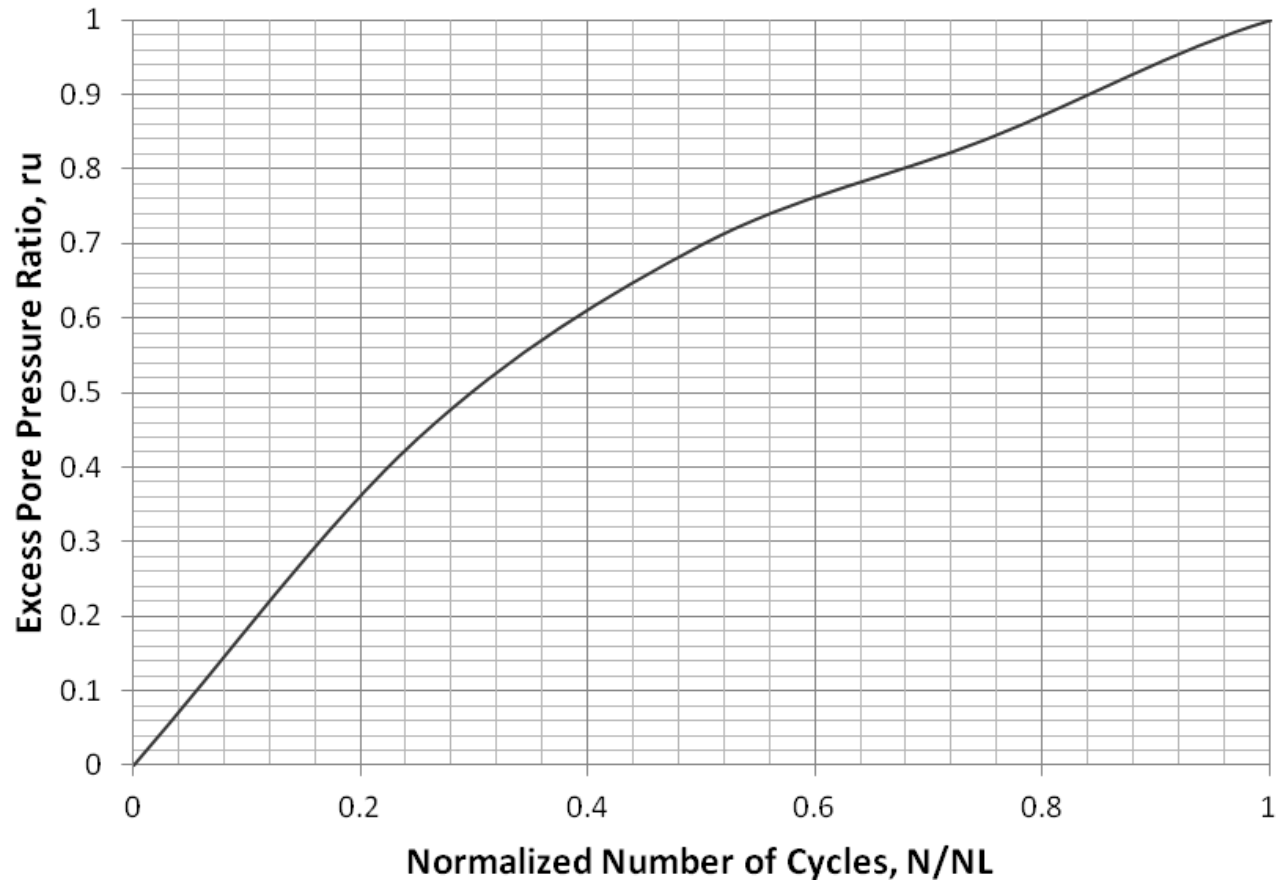Figure A.83: Specimen F90R10 CSR 0.30 Excess Pore Pressure Versus Number of Cycles Graph
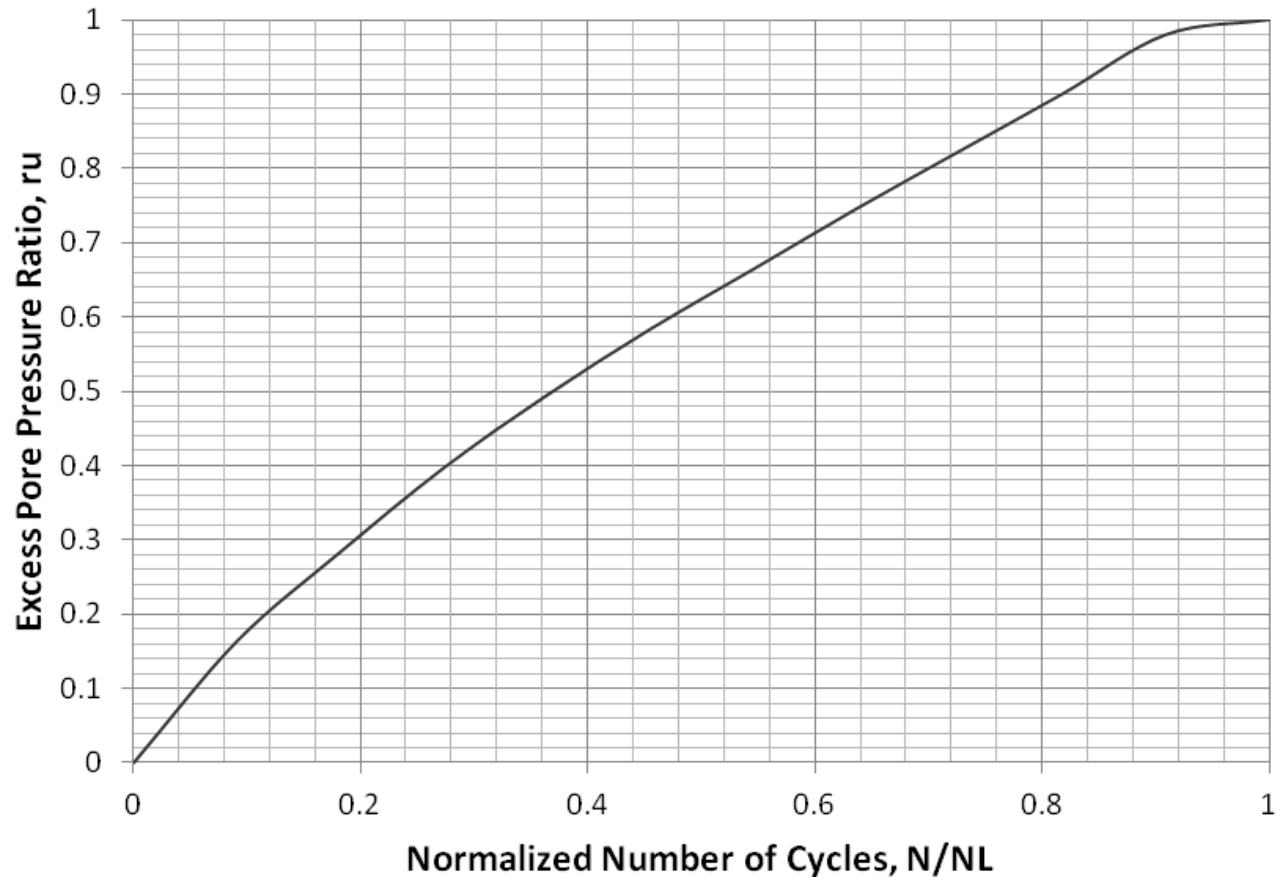
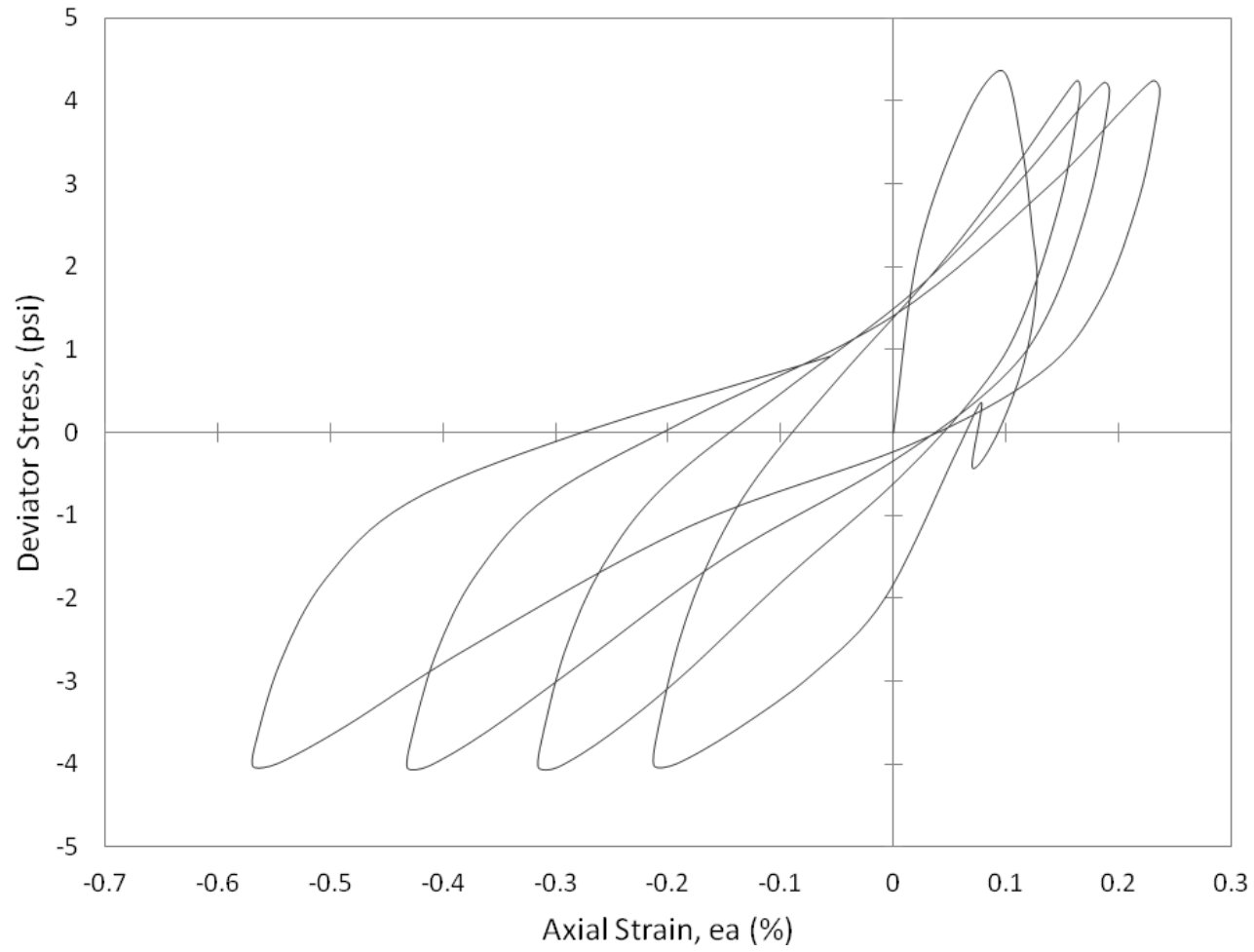Figure A.84: Specimen F90R10 CSR 0.30 Excess Pore Pressure Ratio Versus Normalized Number of Cycles Graph
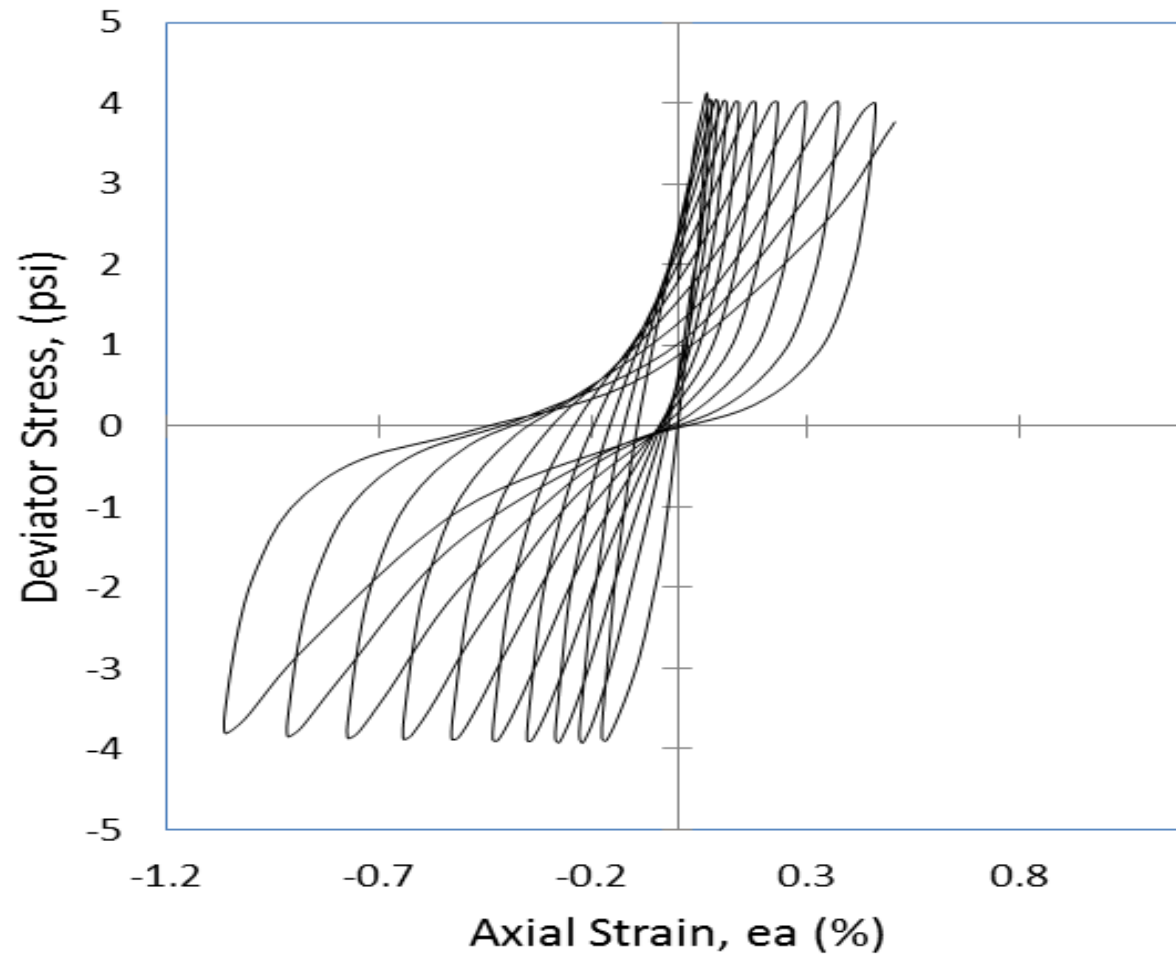
Figure A.85: Specimen F90R10 CSR 0.30 Deviator Stress Versus Axial Strain Graph
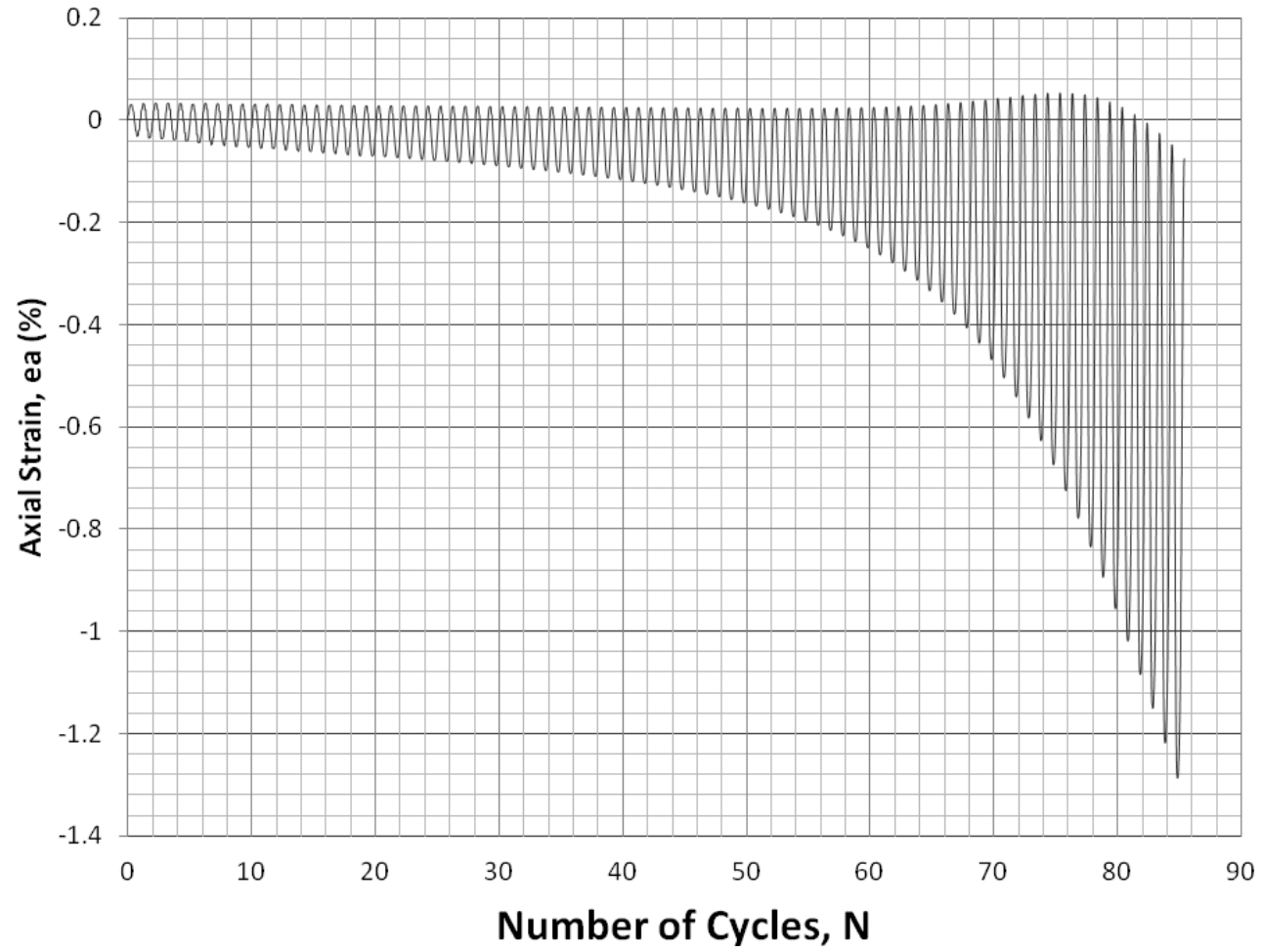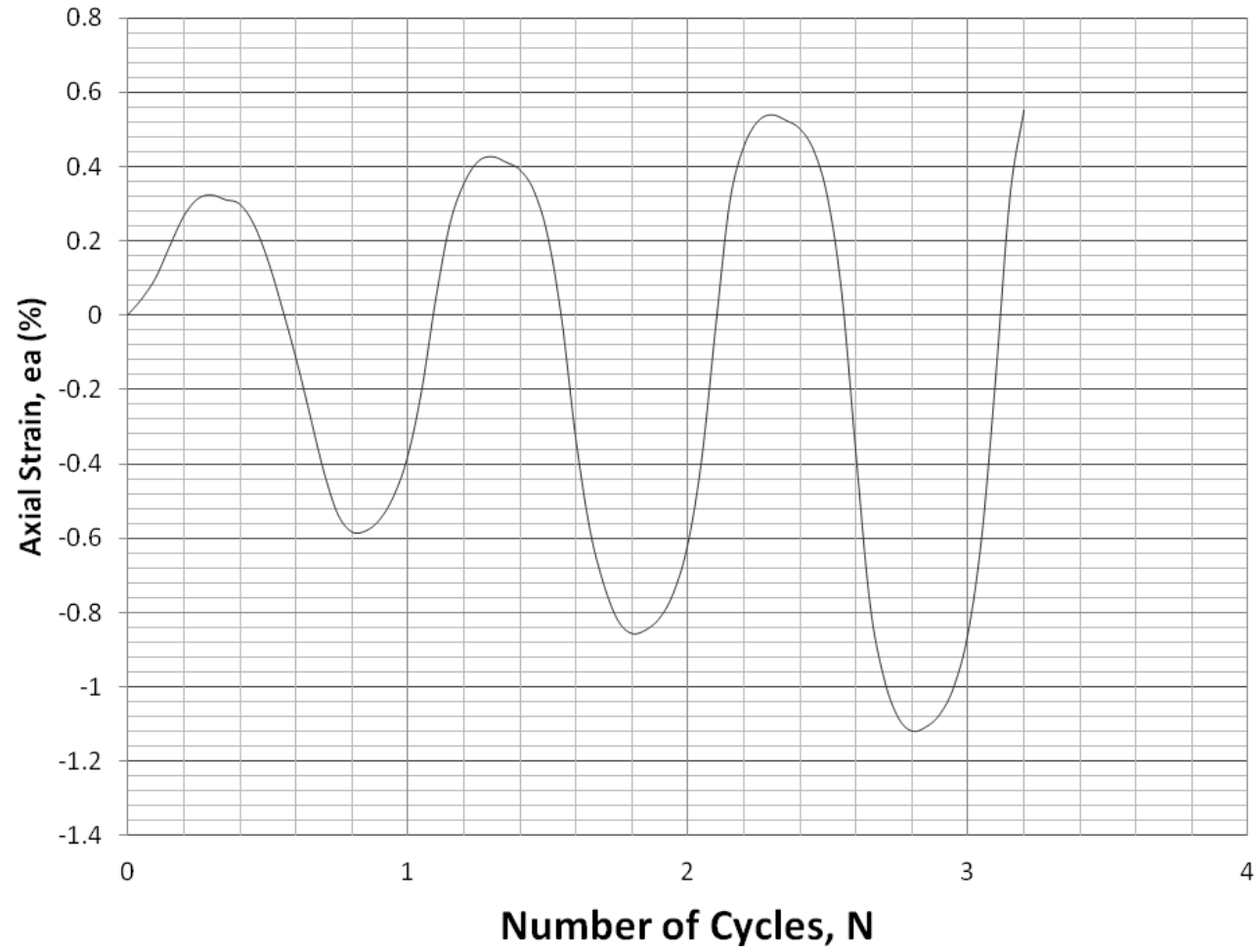
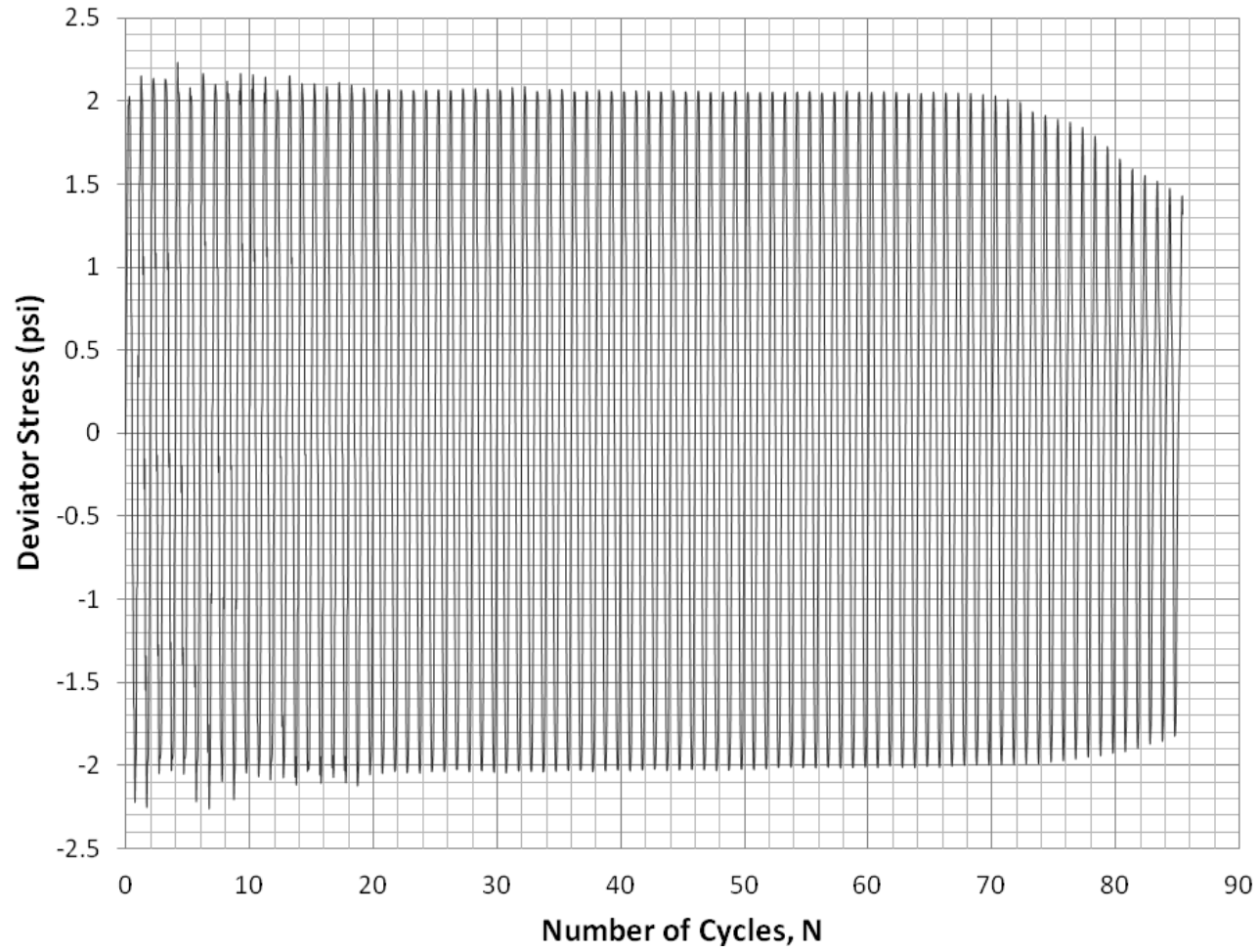Figure A.86: Specimen F90R10 CSR 0.50 Axial Strain Versus Number of Cycles Graph
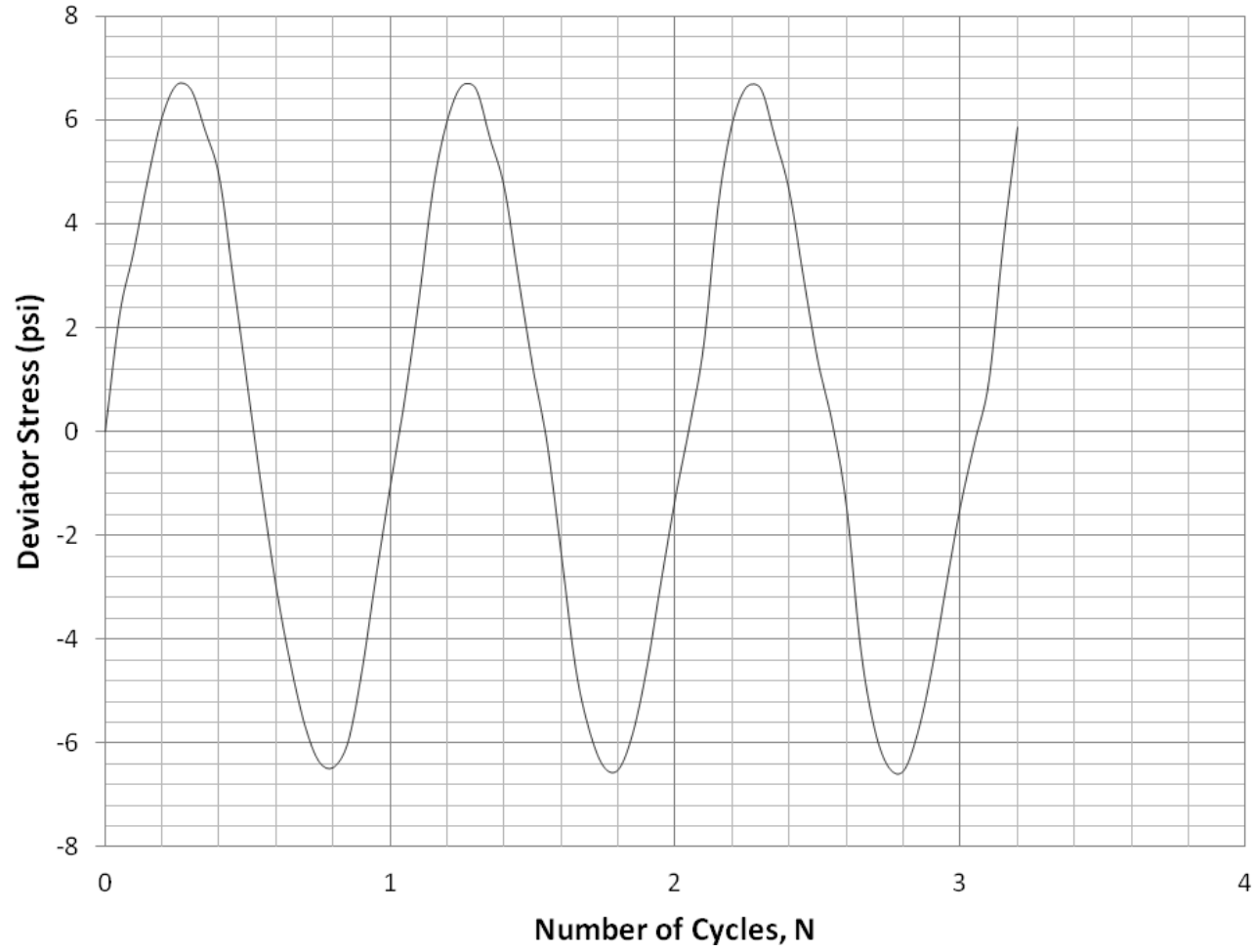
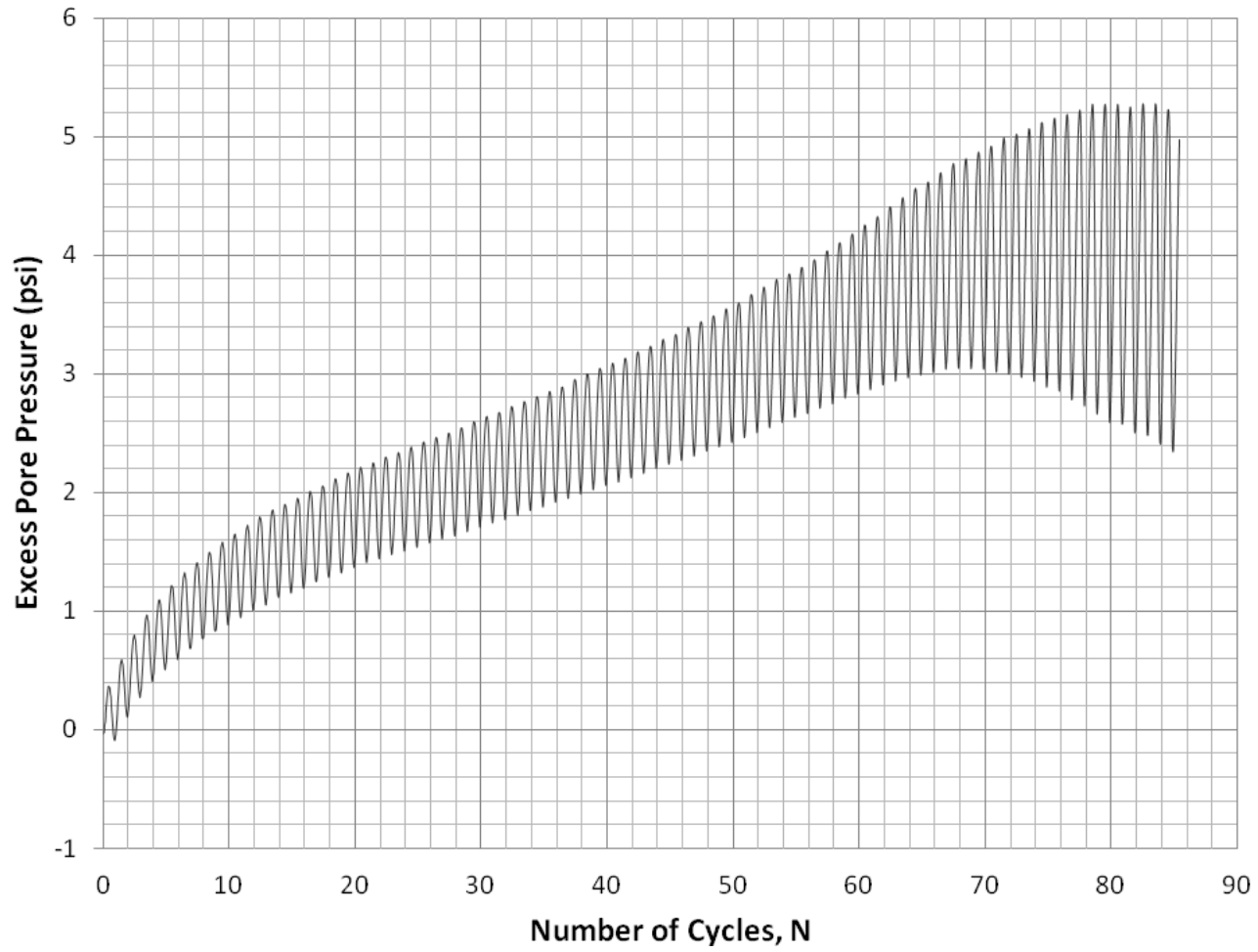Figure A.87: Specimen F90R10 CSR 0.50 Deviator Stress Versus Number of Cycles Graph
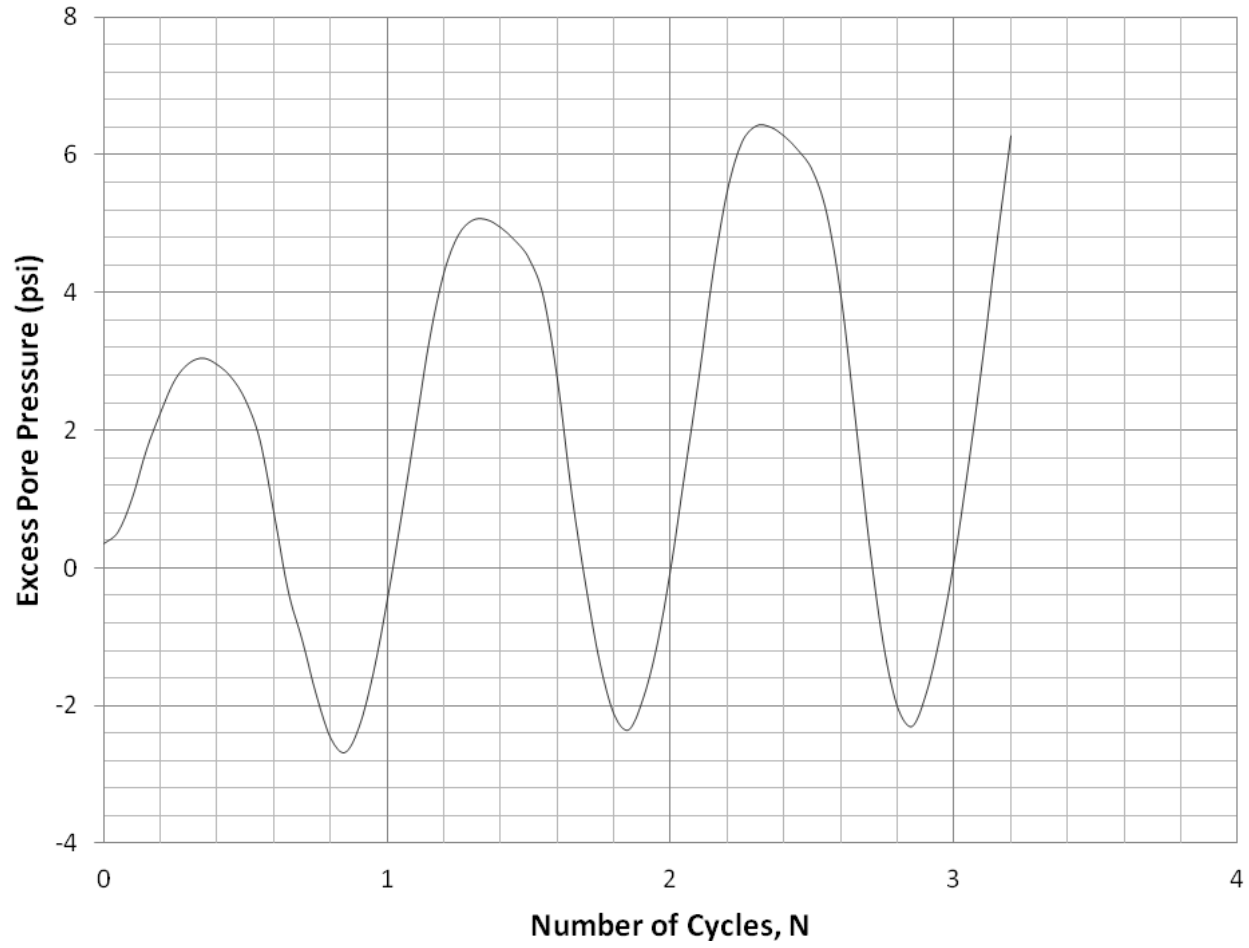
Figure A.88: Specimen F90R10 CSR 0.50 Excess Pore Pressure Versus Number of Cycles Graph
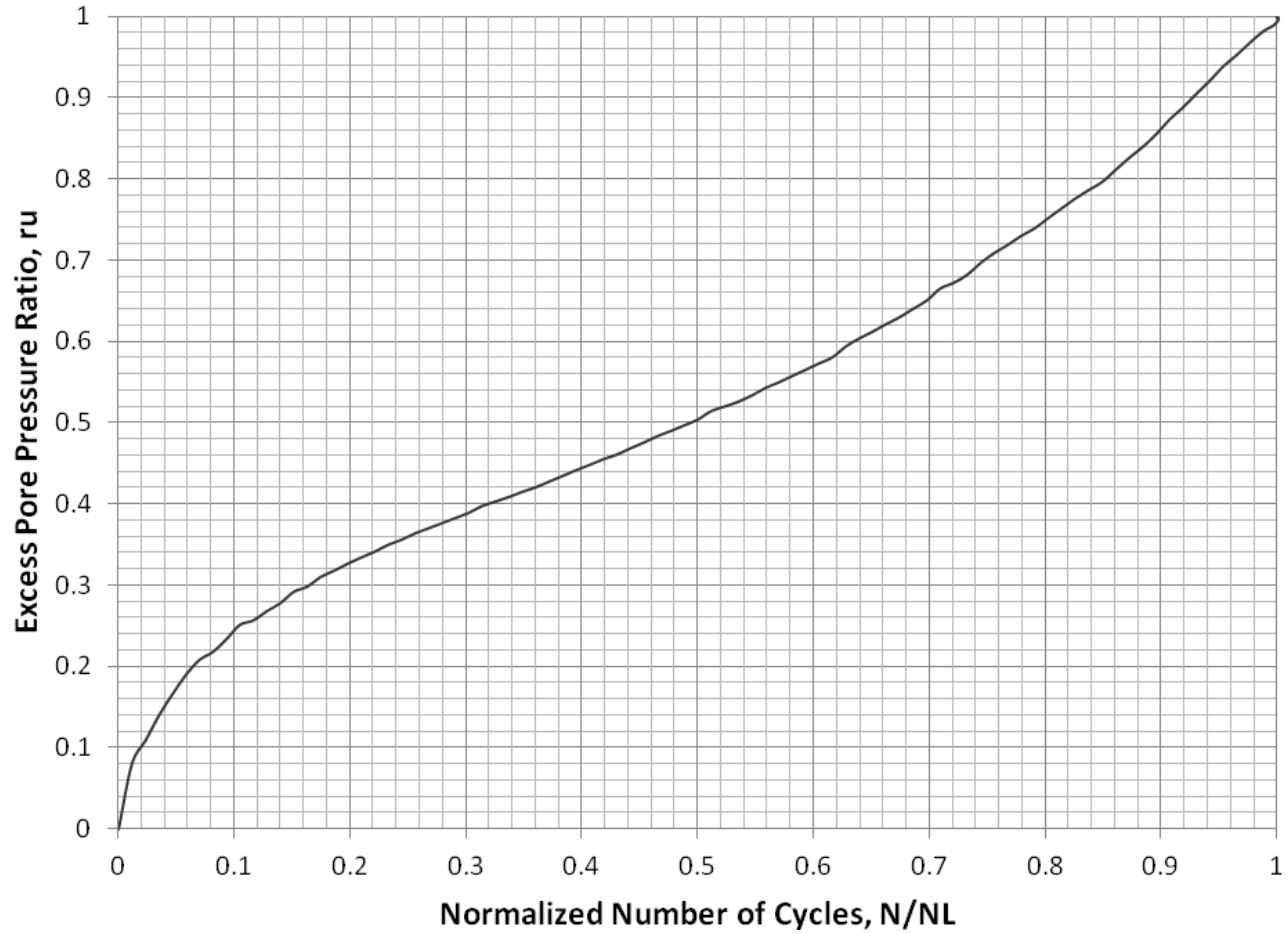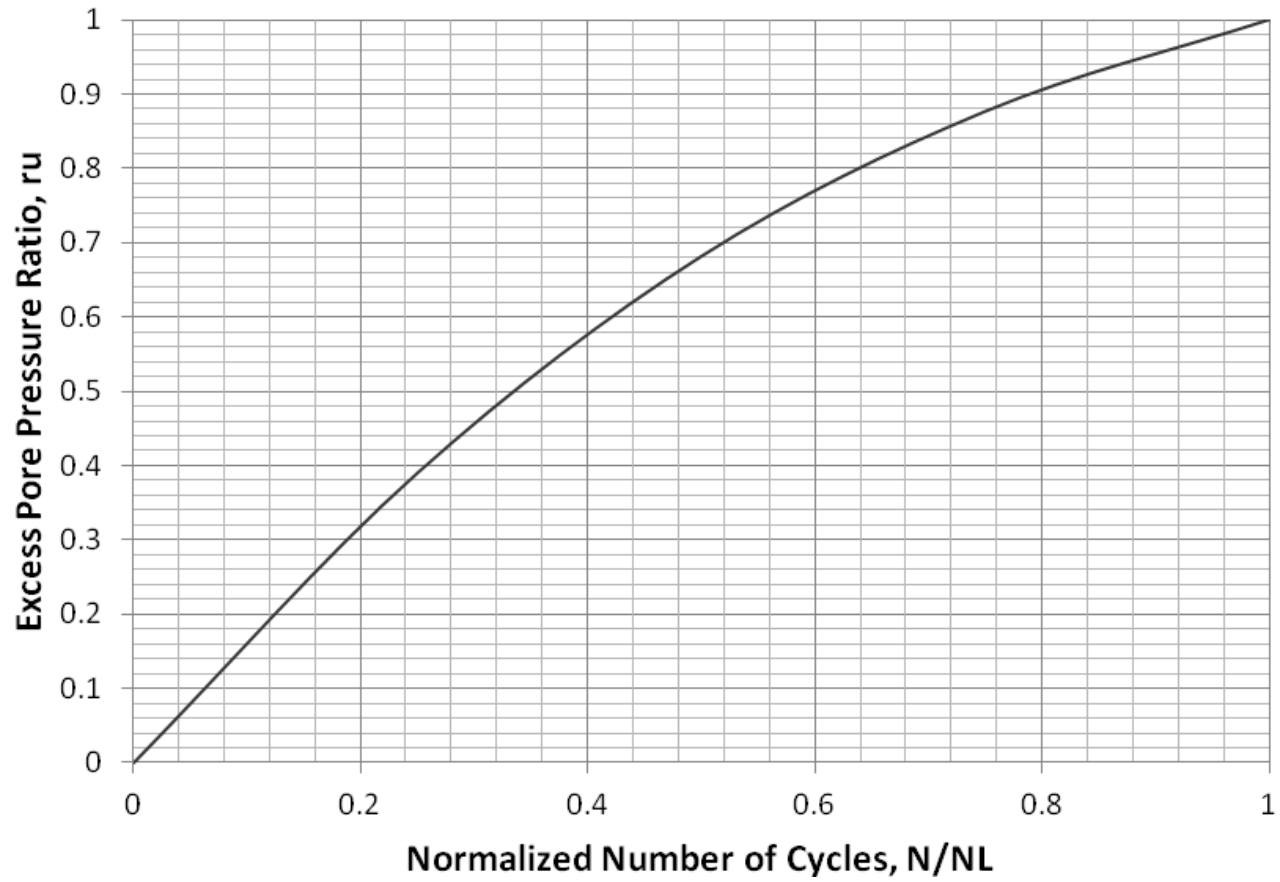
Figure A.89: Specimen F90R10 CSR 0.50 Excess Pore Pressure Ratio Versus Normalized Number of Cycles Graph
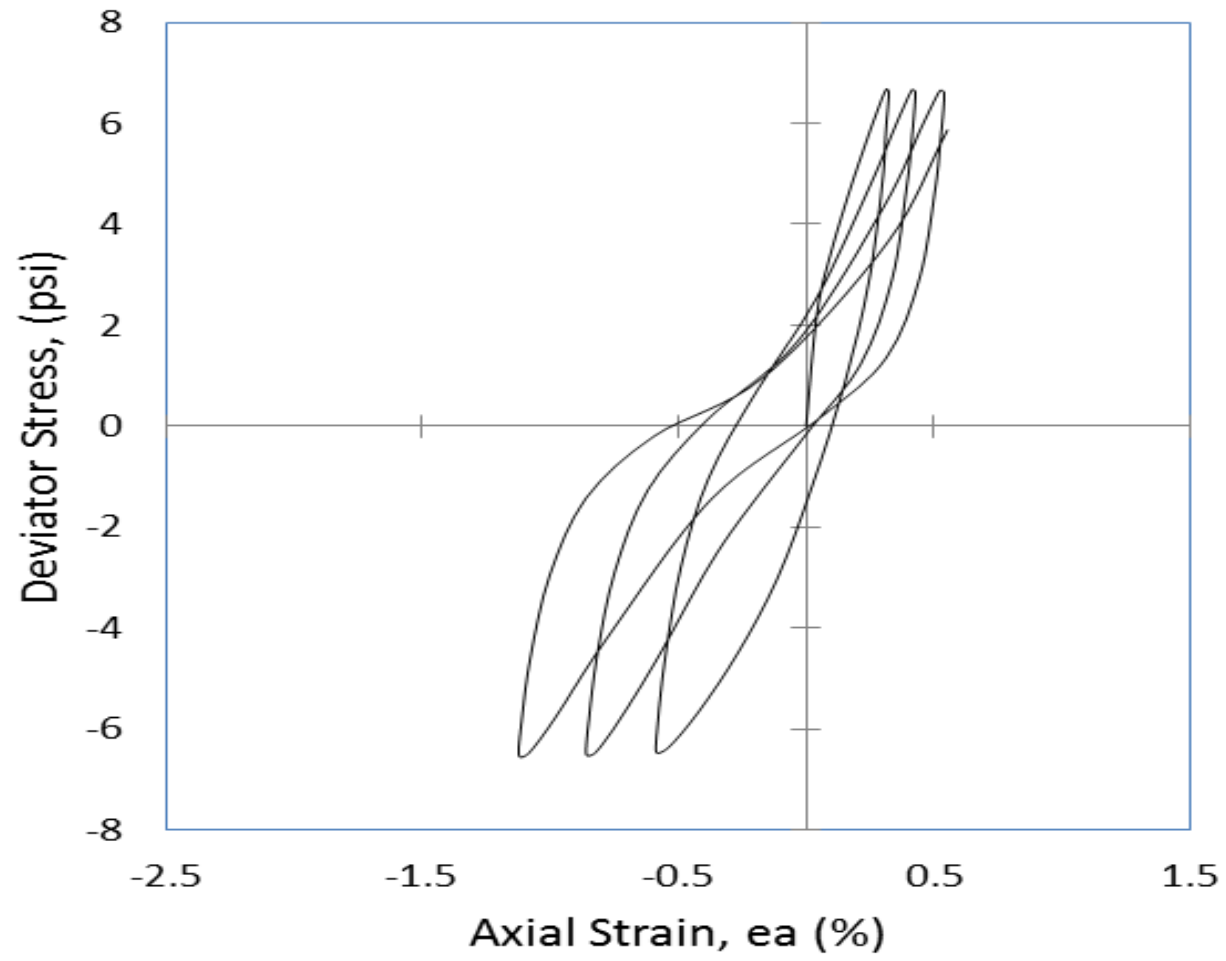
Figure A.90: Specimen F90R10 CSR 0.50 Deviator Stress Versus Axial Strain Graph
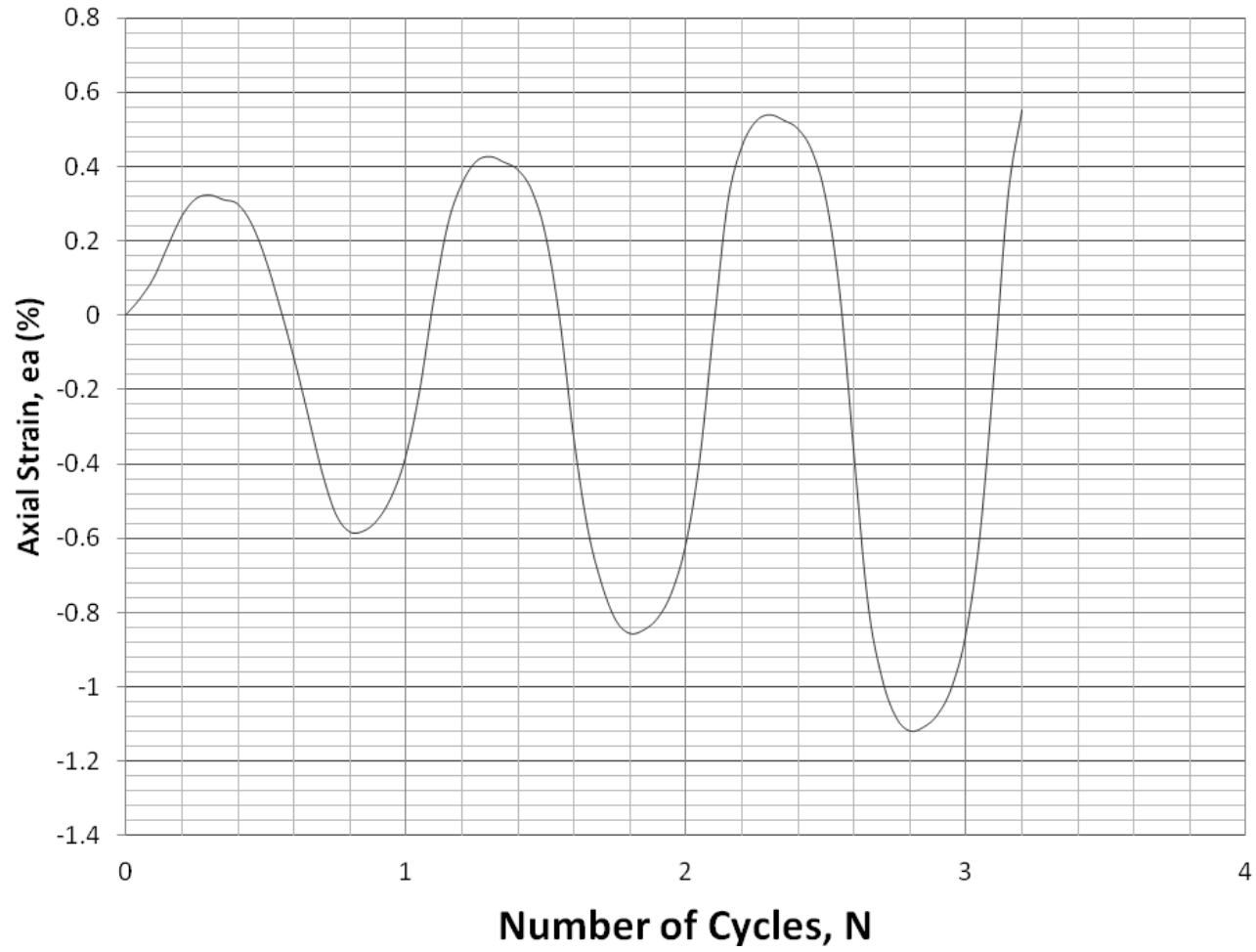
Figure A.91: Specimen F80R20 CSR 0.30 Axial Strain Versus Number of Cycles Graph
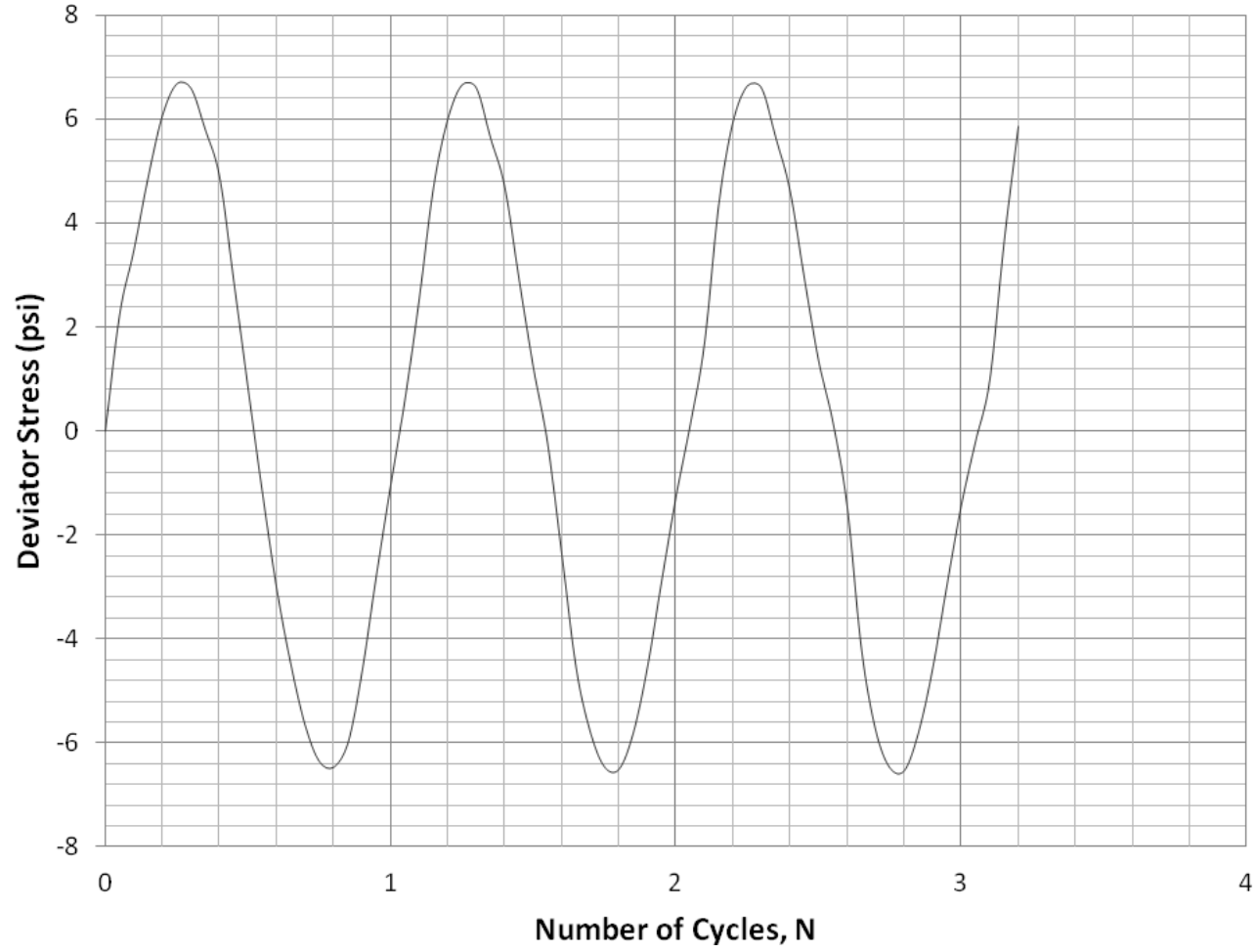
Figure A.92: Specimen F80R20 CSR 0.30 Deviator Stress Versus Number of Cycles Graph
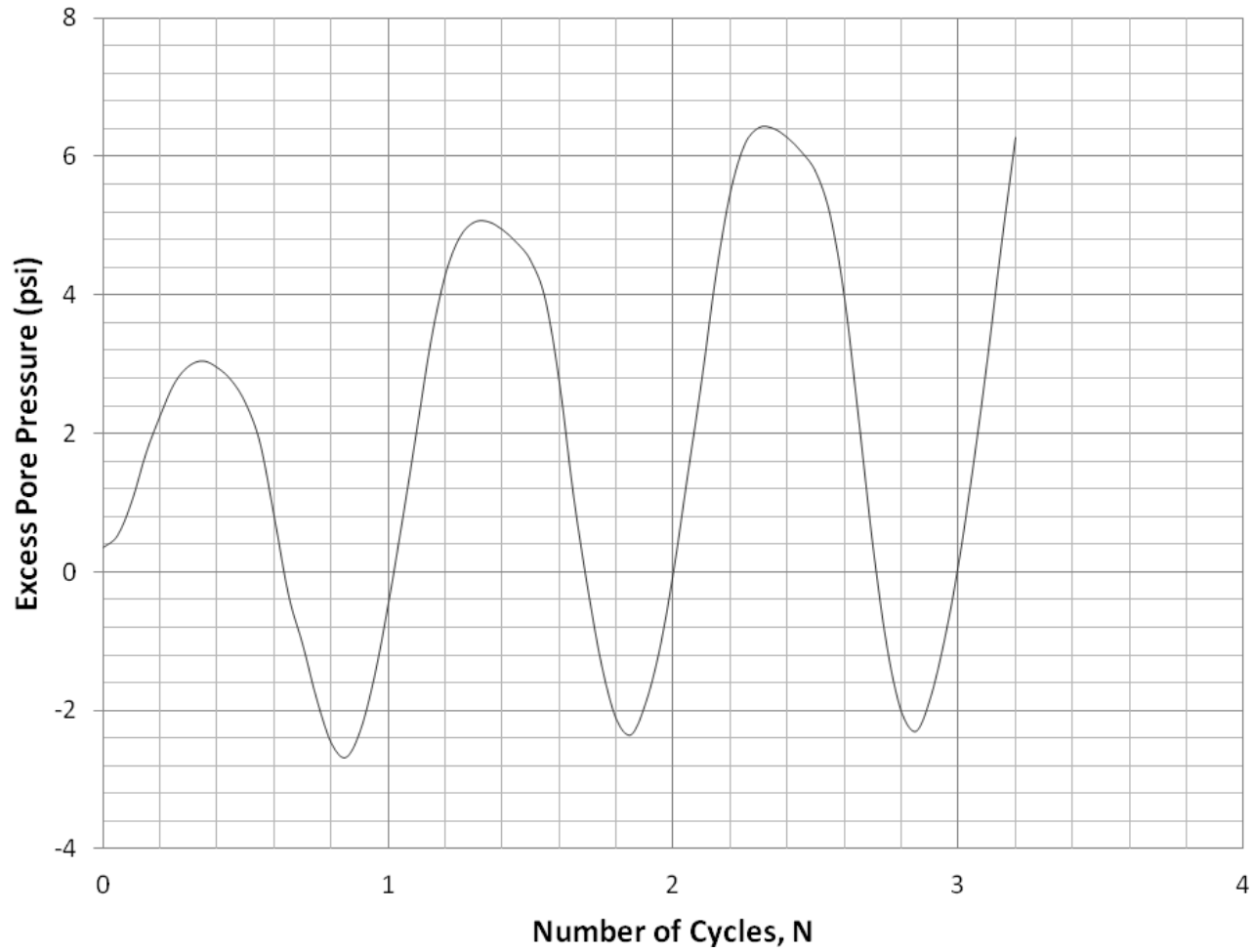
Figure A.93: Specimen F80R20 CSR 0.30 Excess Pore Pressure Versus Number of Cycles Graph
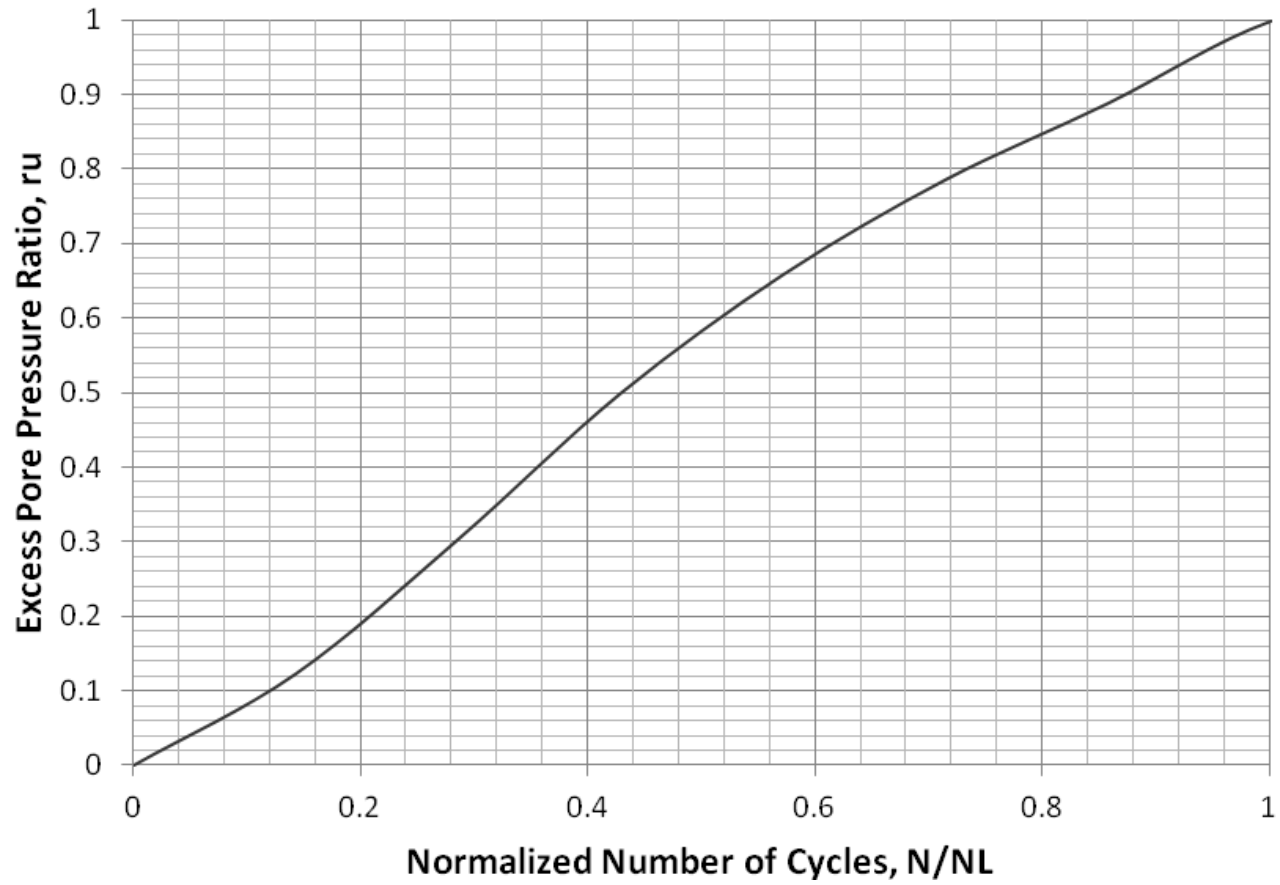
Figure A.94: Specimen F80R20 CSR 0.30 Excess Pore Pressure Ratio Versus Normalized Number of Cycles Graph
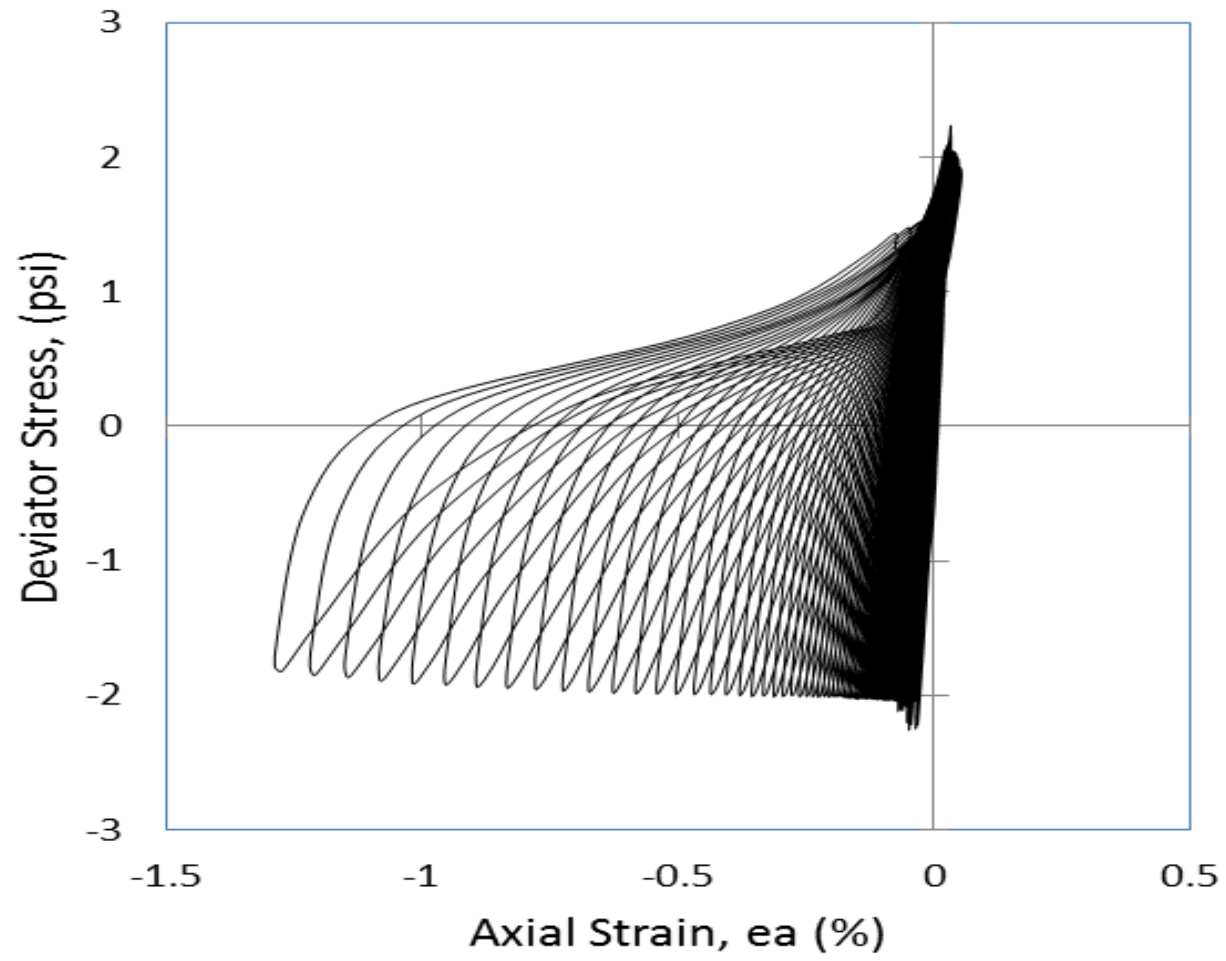
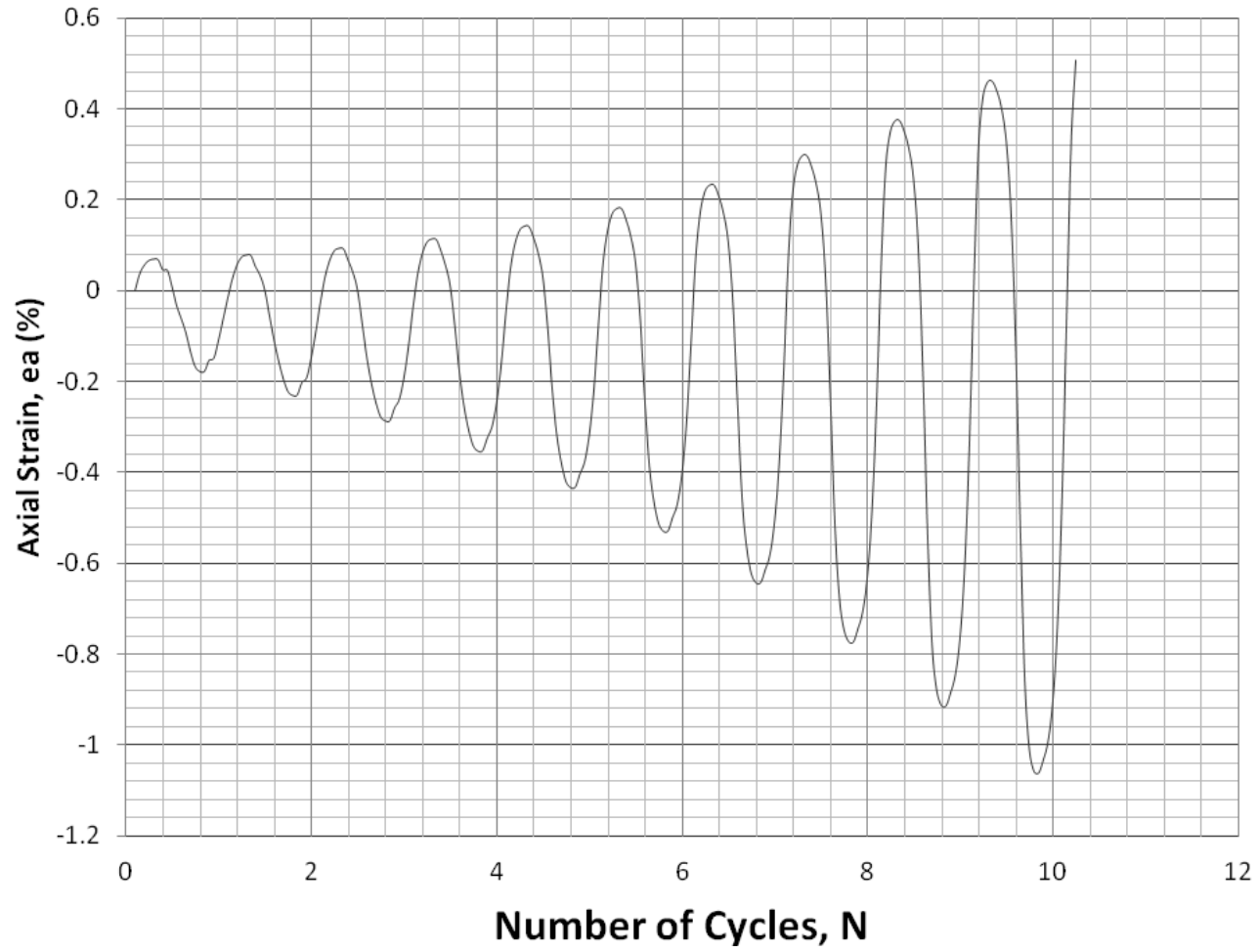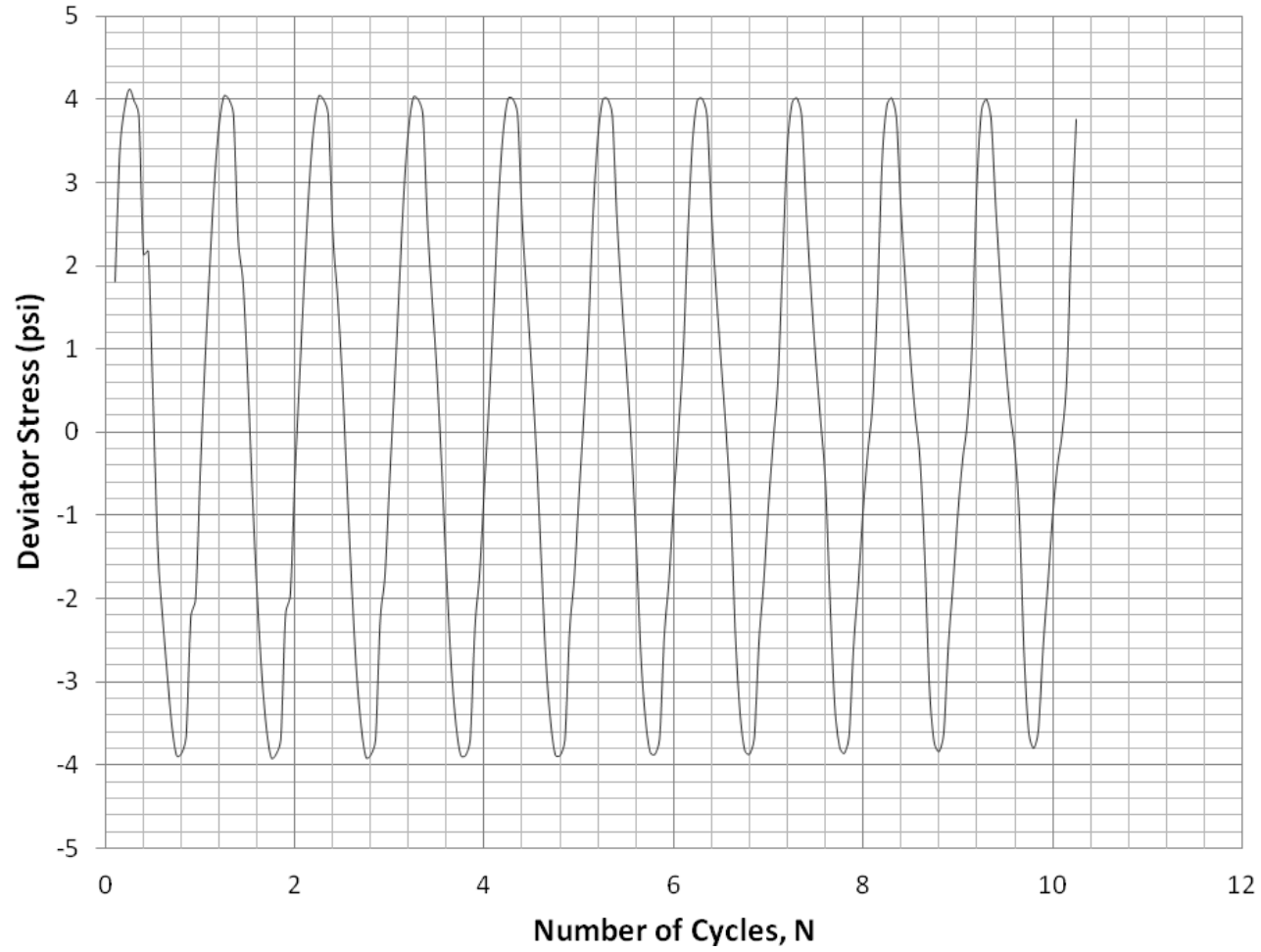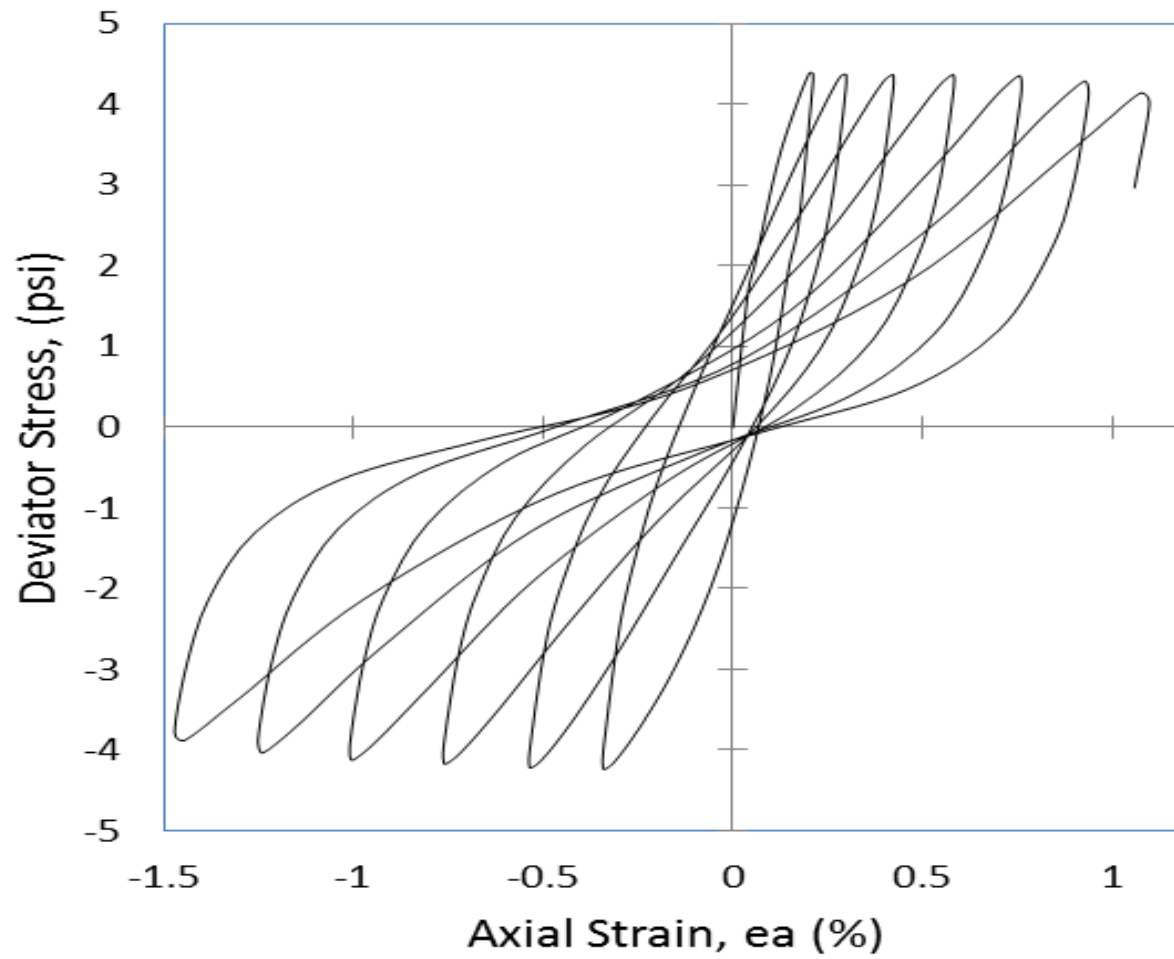Figure A.95: Specimen F80R20 CSR 0.30 Deviator Stress Versus Axial Strain Graph

APPENDIX B

Cyclic Triaxial Testing Procedure

B.1   Cyclic Triaxial Testing System

This chapter provides an introduction into the apparatuses and devices used and a step-by-step guide to perform experiments conducted in this research. There are four (4) main devices used to perform this research: resilient modulus testing system (Pressure board), hydraulic system (Gear Box), a cyclic triaxial system and a personal computer with GCTS Computer Aided Testing System (CATS) software installed. In Figure B.1, the main devices are shown.

Figure B.1: Pressure board, hydraulic system, cyclic triaxial system and a personal computer

B.1.1 Resilient Modulus Test System (Pressure Board)

There are three (3) separate switched, and knobs in the pressure board (Figure B.2). Fluid pressure, pore pressure and cell pressure, respectively from left to right. Each of the controls are equiped with burettes, regulators, valves and connections.
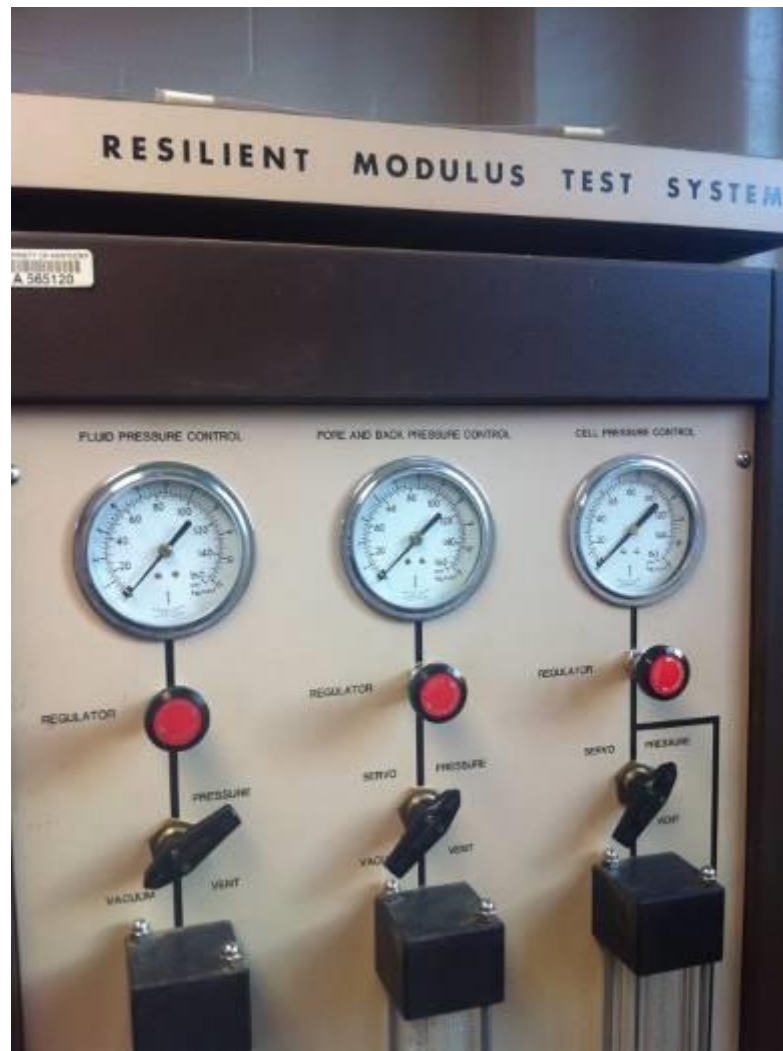
Figure B.2: Pressure board switches and knobs

The connection is illustrated by lines printed on top of the main board (Figure B.3). The water used in the storage tank inside the pressure board was medium grade

distilled that had been de-aired by connecting a hose from the pressure board to a vacuum source.

Figure B.3: Main board of a Pressure board

B.1.2 Cyclic Triaxial Machine

The cyclic triaxial machine consists of a plexiglas chamber with top and bottom platen, separately. There are five (5) connections on each platen. As illustrated on Figure B.4, the connection on the top platen consists of two (2) gear box connection, Lateral pressure connection, Vent connection, and LVDT sensor

.

Figure B.4: Top platen

Meanwhile as illustrated on Figure B.5, the connections on the bottom platen consists of top pedestal hose and sensor, bottom pedestal hose and sensor, Cell pressure sensor, Load cell sensor and liquid drain hose.
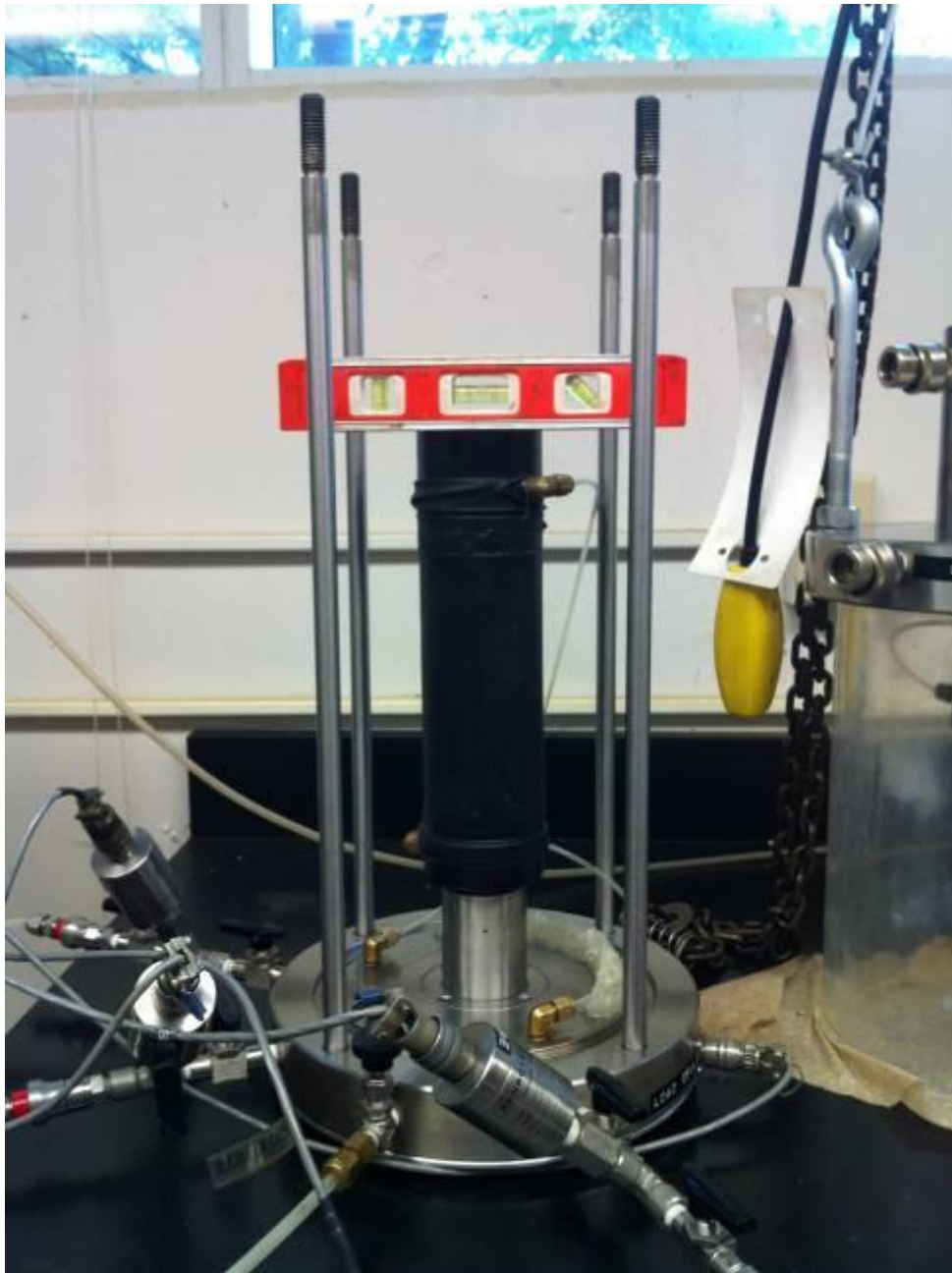
Figure B.5: Bottom platen

B.2   Reconstitute Test Specimen

Because fly ash has lower specific gravity compare to soils, a delicate handling

of reconstituting material should be applied to avoid the specimen from collapsing. To

help reconstitute the specimen, the tools needed are the following:

1.   Split mold with 2.8 inch in diameter

2.   Four (4) 2.8 inch rubber O-ring

3.   2.8 inch neoprene membrane

4.   Two (2) porous stone

5.   Two (2) filter paper

6.   Scale

7.   Ruler

8.   Caliper

9.   7/16" wrench

10.   1/4" diameter tube

11.   1/8" diameter tube

12.   Vacuum water trap (Figure B.6)

13.   Plastic funnel

Figure B.6: Vacuum water trap

First, cover the groove on the bottom pedestal with the membrane. Rolled down two (2) O-ring with one O-ring placed exactly on the groove, followed by placing porous stone and filter paper on top of bottom pedestal, in sequence.

Before pouring the sample inside the membrane, a spilt mold should be placed outside the membrane. The split mold has two 1/8" inch tube, connected together using T-connection and connected to vacuum source through vacuum water trap.

Start pouring the material inside the membrane by passing it through a plastic funnel. After getting the desired height, place the second filter paper, porous stone and the top pedestal, in sequence and get the weight of the whole system.

Next, mount the bottom pedestal on top of the bottom platen of the cyclic triaxial machine (Figure B.7) and secured by tightening the screw using an L-shape star driver. Connect both top and bottom pedestal hose with the connection on the bottom platen. Those connections are connected to vacuum source so a vacuum pressure can flow into the specimen. This pressure is important to prevent the specimen from slumping after the split mold removed.
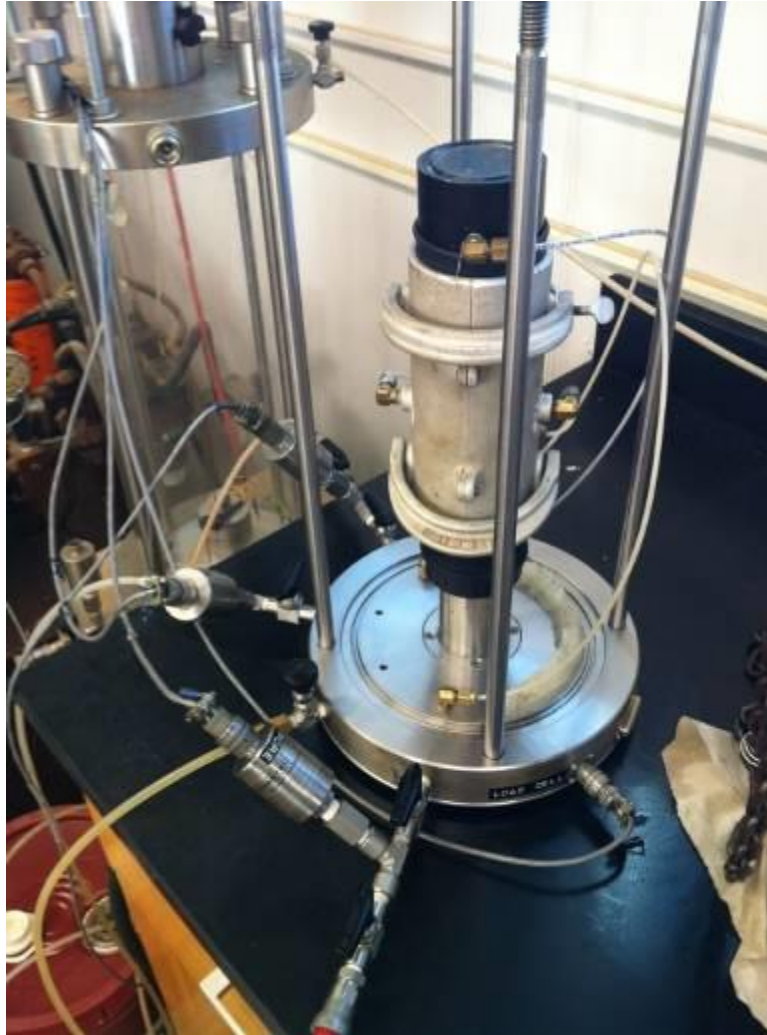
Figure B.7: Mounted specimen on top of bottom platen

B.3 Sealing the Chamber of Cyclic Triaxial Machine

Before sealing the chamber, the diameter and height of the specimen need to be recorded, load cell reading and pore pressure reading should be zeroed using the interface software and top pedestal should be leveled using a bubble level.

Tools and apparatus needed to seal the chamber are:

1. Two (2) Plexiglas chamber O-rings

2. Top pedestal O-ring

3.   Vacuum grease

4.   Plexiglas chamber

5.   500 lbs. crane (Figure B.8)

6.   Four (4) washers

7.   Four (4) nut caps

8.   Bubble level

Figure B.8: 500 Lbs. crane

First, take one Plexiglas O-ring, coated with vacuum grease and placed inside the

groove on the bottom platen. Cover both end of Plexiglas chamber with vacuum grease,

lift the Plexiglas chamber and place gently on top of Plexiglas O-ring of the bottom

platen.

Second, take top pedestal O-ring, coated with vacuum grease and mounted on the top pedestal. In the top platen, four (4) eye bolts with wire are installed and hooked to the 500 lbs. crane. This installment was made to help lifting and control the maneuver of top platen.

Lastly, lift the top platen, while in the air, take the second Plexiglas O-ring, coated with vacuum grease and placed inside the groove on the top platen. Now, the top platen can be place on top of the Plexiglas chamber and all the washers can be placed and all the nuts can be tightened (Figure B.9).

Figure B.9: Four washers and four nuts on top platen

B.4   Filling the Triaxial Chamber with Liquid

At this stage, the pedestal on top platen should be lowered until the gap with the top pedestal is closed (Figure B.10). To lower the pedestal, use the interface software and go to outputs function: set-point/function generation window and on the feedback option, set into system LVDT.

The LVDT range is 1000 mills with -500 mills as maximum limit or on upper position and 500 mills as minimum limit or at lower position.
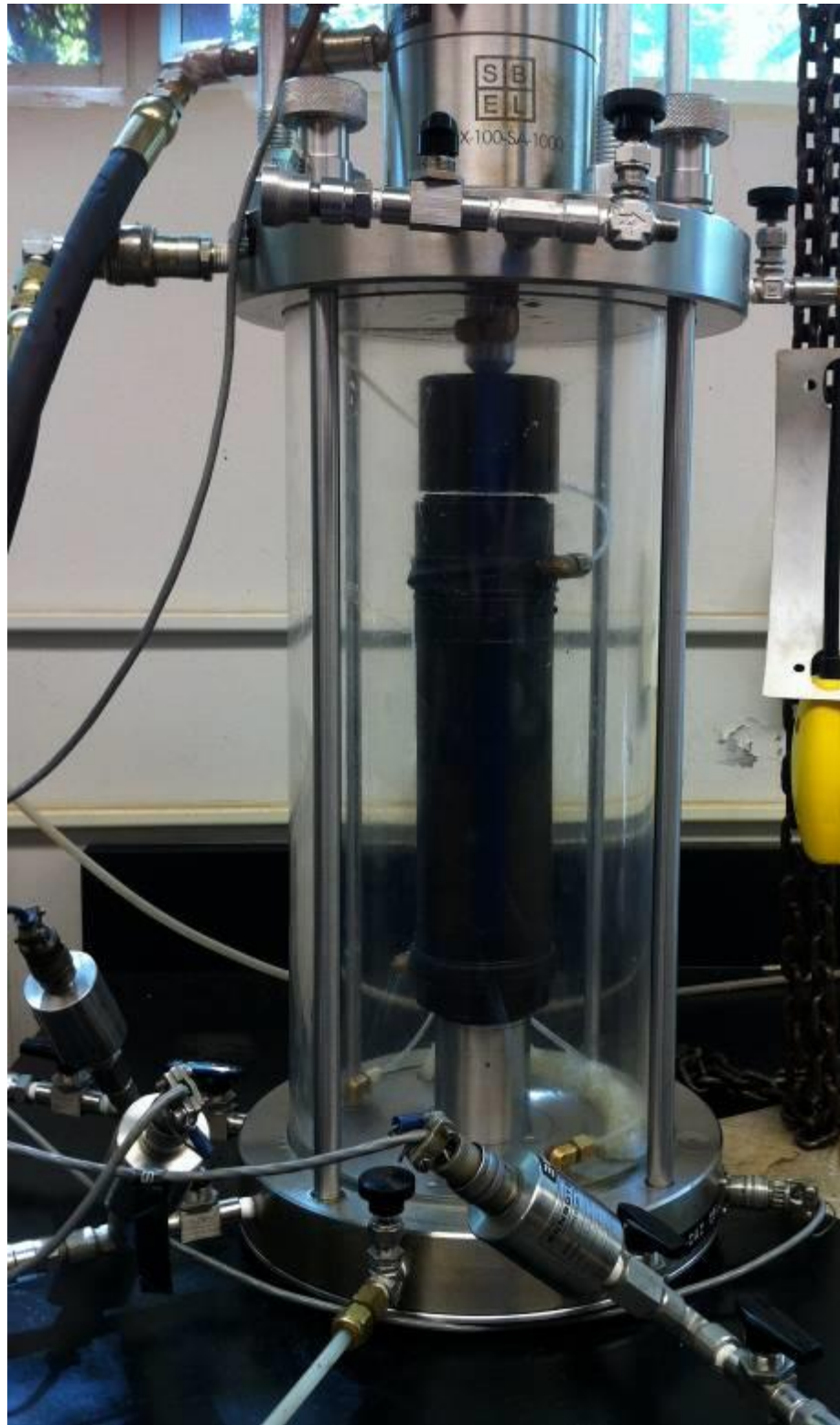
Figure B.10: Lowering pedestal of top platen to close the gap with top pedestal

To ensure the gap is sealed, connect vacuum source with vent connection and open the lateral pressure hose. No air suction flow on the lateral pressure hose means the gap is fully sealed. Vacuum source should be applied continuously, to hold the gap until the end of filling the chamber process.

After this stage until shearing process, the deviator stress should maintain at zero psi. To automate machine response with the changes at height of specimen due to variation on cell and pore pressure changes, re-setting the outputs function: set-point/function generation window and on the feedback option into standard deviator (Figure B.11).
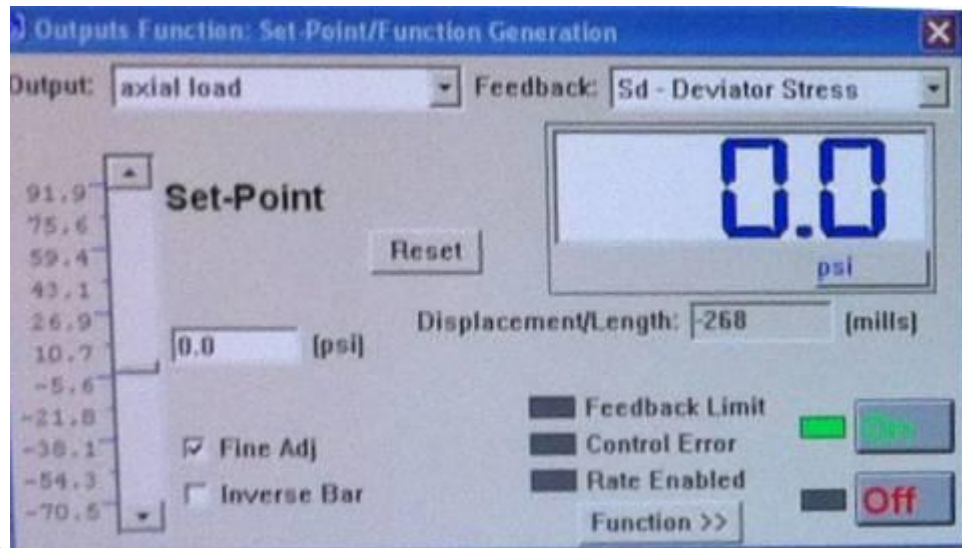
Figure B.11: Outputs function: set-point/function generation window with feedback option into standard deviator

To start the liquid flowing into the chamber (Figure B.12), connect lateral pressure hose into vacuum source and open liquid drain hose which submerged into

liquid source. The liquid used for this research was DTE25 Hydraulic oil produced by

Mobil (Figure B.13).
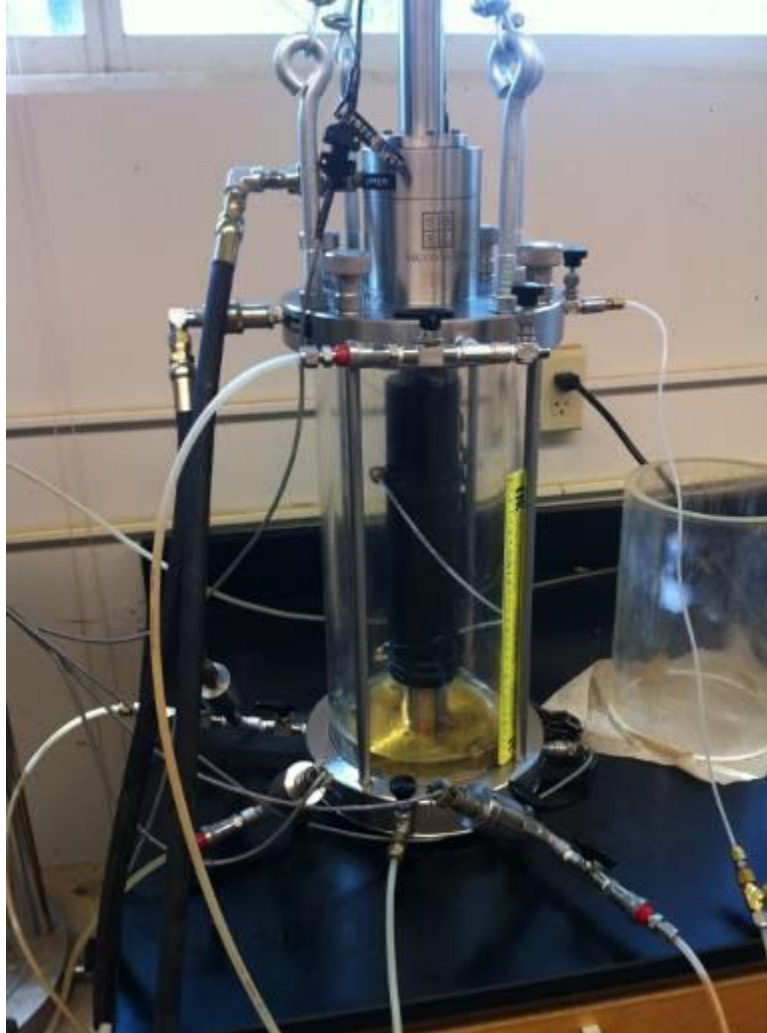
Figure B.12: Liquid flow into the chamber

Figure B.13: DTE25 Hydraulic oil produced by Mobile

There are two vacuum sources available; vacuum source from the building and Welch Dual Seal Vacuum pump (Figure B.14). Vacuum source from the building provides an 11 psi pressure and vacuum source from the pump can provides 14 psi pressure.

Figure B.14: Welch Dual Seal Vacuum pump

Should be noted that at any time, the vacuum pressure from the lateral pressure hose should not exceed vacuum pressure from vent connection and vacuum pressure given to the sample, the reason is to avoid the appearance of the gap between pedestal and the membrane from inflating, respectively.

Once the chamber is filled with oil, cell pressure can be applied into the specimen. The purpose of this pressure is to prevent the sample from collapsing and the maximum pressure is 5 psi which considers an appropriate pressure to maintain structural integrity of the specimen.

However, the pressure flow from pressure board is generated by air pressure that pushes water inside cell pressure burette and the chamber is filled with oil. To prevent water from getting inside the chamber, a chamber containing both water and oil was used (Figure B.15).

270

Figure B.15: Water oil separation chamber

B.5   Flooding and Saturating the Specimen

Prior to saturating the specimen, flooding phase was applied. The purpose of this phase is to push air bubbles out from the specimen for faster saturation. Before making any changes, parameters like: LVDT reading, pore pressure at the top and bottom of the sample, cell pressure, and burette reading should be recorded. The information is needed to monitor the volume changes in the sample from pressure variation.

Change the connection for bottom pedestal hose at bottom platen from applying vacuum pressure into fluid pressure connection at pressure board to flood the sample while the vacuum pressure at the top pedestal maintained.

The back pressure to flood the sample was set at 5 psi to maintain the structural integrity of the sample while the cell pressure set up slightly higher to 6.5 psi to keep maintaining the sample from slumping and not compressing the sample. This phase needs at least 24 hours, depend on the hydraulic conductivity and void ratio of the specimen.

After completing this phase, record LVDT reading, pore pressure at the top and bottom of the sample, cell pressure, burette reading and shut off the vacuum pressure apply to top pedestal hose.

A contamination separation chamber with rubber membrane in the middle separating two small chambers (Figure B.16) was used during saturation process to protect any contamination from going inside pressure board which can clog the halves.

Figure B.16: Contamination separation chamber

During this phase, the remaining air bubble will dissipate and the sample will start the saturation process. At this stage, the cell pressure should always be higher (+/- 1.5 psi) than pore pressure to avoid stress disturbance. To measure the saturation level, the Skempton's parameter (B) can be measured by following the guidelines recommended by ASTM D5311.

Saturation was determined by measuring the B-value. Once a specimen reached a B-Value of 95% or higher the cyclic triaxial test was performed. However, if the B-value did not reach this criterion within two days, the specimen was tested due to time constraints.

B.6   Consolidation Process

After achieving the minimum requirements for B-value, the consolidation phase can be executed. During the consolidation process, the specimen is allowed to drain. This process can be done by increasing the cell pressure to the desired confining pressure which is related to the in-situ effective stress of the sample. By increasing cell pressure and maintaining pore pressure, water inside the specimen will start flowing out which means consolidation process happened.

B.7   Applying Load-controlled Loading

After completing the consolidation process, cyclic load-controlled loading could be started. The applied pressure was determined in the form of cyclic stress ratio (CSR) and input as deviator stress in psi unit.

The specimen experienced a cyclic loading at frequency of 0.5 Hz or equivalent to a period of 2 seconds, and CSR ranged from 0.08 – 0.25. During the test, no drainage was allowed from the specimen.

This phase was set up to run for 120 – 300 seconds, depending on the CSR value, with lower CSR needing more time was needed and vice versa. Before starting the phase, shut off both pore pressure connections.

B.8   EMPTYING THE CHAMBER

The last phase is emptying the chamber and setting the machine in normal conditions to prepare for the next specimen. To drain the oil, connect lateral pressure connection with pressure source and open the drain hose.

Before unplugging all the connections and turning off the machine, make sure that the LVDT reading is back to original position or minus (-) 500, to assure that the next specimen will have enough space between the pedestals.

Remove and clean the specimen from bottom pedestal and put the end connection into both hoses to make sure that all the water will not drain during handling. Remove the specimen from neoprene membrane and measure the weight (Figure B.17) before putting inside the oven for moisture content measurement.

Figure B.17: Measuring the specimen weight after testing

APPENDIX C

CYCLIC TRIAXIAL TESTING SPREADSHEET

In this section, the spreadsheet to record all the information starting from specimen preparation until shear phase for cyclic triaxial testing are presented (Table C.1 – C.3).

To record all the reading during cyclic triaxial test, a spreadsheet was created to help organize and calculate all information needed for each specimen. The spreadsheet was used from the beginning of the test, to record the dimensions of sample, until the last phase to record the oven-dried weight of sample for moisture content measurement.

Table C.1: Spreadsheet (Page 1)

Record Data: Specimen Label

                                              Date
Preparation phase: Temperature

    Specimen, Mold and Tools :

Item		Unit		Unit
Total Mass:		gram		lb
Weight of 4 O-rings:		gram		lb
Weight of 2 filter paper:		gram		lb
Weight of membrane:		gram		lb
Weight of top pedestal:		gram		lb
Weight of bottom pedestal:		gram		lb
Weight of split mold and tubes:		gram		lb
Weight of porous stone:		gram		lb
Net solid weight of specimen:		gram		lb
Dia. of specimen + membrane:		cm		inch
Height of specimen:		cm		inch
Height/diameter ratio:				OK/Not OK

Flooding phase:

		Unit
LVDT:		mills
Pore:		psi
Cell:		psi

Burette reading:	Water	Oil

Saturation phase:

		Unit
LVDT:		mills
Pore:		psi
Cell:		psi

Burette reading:	Water	Oil

Consolidation phase:

		Unit
LVDT:		mills
Pore:		psi
Cell:		psi

Burette reading:	Water	Oil

Shear phase:

		Unit
LVDT:		mills
Pore:		psi
Cell:		psi

Burette reading:	Water	Oil

278

Table C.2: Spreadsheet (Page 2)

Specimen information:

		Specimen Label		
	Dia (in)			Height (in)
	B	M	T	
1				
2				
3				
	AVG	AVG	AVG	AVG
	Total AVG			

Total height Sample + Pedestal

_____ in

_____ cm

Gs: _____

Area: _____ cm3   _____ Inch3

Vol. : _____ cm3   _____ Inch3

Gamma Dry (Ws/V): _____ gr/cm3

_____ lb/in3

_____ pcf

Void ratio (Gs.gamma water/gamma dry) - 1 : _____

Gamma Sat (Gs + e) gamma water / (1 + e) : _____ pcf

Effective Pressure: _____ psf   _____ psi

(Gamma sat - gamma water) x depth or gamma' x Depth

Asked

CSR	Cell (psi)	Pore (psi)	p-p (psi)	Asked Dev. (psi)

Actual

CSR	Cell (psi)	Pore (psi)	p-p (psi)	Asked Dev. (psi)

Notes:

p-p = peak-to-peak

Table C.3: Spreadsheet (Page 3)

Input information :

Frequency:		Hz
Period:		Sec
Run time		Sec

Instrument settings

	Value	Peak&valley off
P		
I		
D		

B value Check

	Cell	Pore
	psi	psi
initial		
After		

B value [   ] %

Information to find actual CSR

Cell		psi
Pore		psi
Initial SD		psi
SD not P-P		psi

Comparison :

Asked		Actual Output	
σ'_0		σ'_0	
τ_d		τ_d	
CSR		CSR	

Water Content calculation:

Wt. of Pan:		g
Wt. Before Oven:		g
Wt. After oven:		g

w = [   ] %

Gamma (Gamma dry x (1 + w)): [   ] pcf

e   =   [   ]

Notes:
SD = Standard Deviator

REFERENCES

- *AECOM Technology Corporation (AECOM). (*2009*). Root Cause Analysis of TVA Kingston Dredge Pond Failure on December 22, 2008*.

- Alabama Earthquakes. (2016). Retrieved June 20, 2016, from http://gsa.state.al.us/gsa/geologichazards/Quakes_AL.htm

- American Coal Ash Association (ACAA). (2008). 2008 Coal Combustion Product (CCP) Production and use survey report. Retrieved from http://www.acaa-usa.org/Portals/9/Files/PDFs/2008_ACAA_CCP_Survey_Report_FINAL_100509.pdf

- American Coal Ash Association (ACAA). (2012). 1966-2012 Fly Ash Production and use charts. Retrieved from http://www.acaa-usa.org/Portals/9/Files/PDFs/1966-2012_FlyAsh_Prod_and_Use_Charts.pdf

- American Coal Ash Association (ACAA). (2012). "Frequently Asked Questions". Retrieved September 8, 2014, from http://acaa.affiniscape.com/displaycommon.cfm?an=1&subarticlenbr=5

- American Concrete Institute (ACI). (2010). "Fly ash Contribution to Sustainable Conrete Construction." *ACI-American Concrete Institute*. ACI, 21 March 2010. Web. 27 Aug 2010. <http://www.concrete.org/education/Webcasts/FlyAshIndex.html>.

- Associated Press; Samuel M. Simpkins/The Tennessean Retrieved from http://www.usatoday.com/story/news/nation/2013/12/22/coal-ash-spill/4143995/

- Assistant Secretary for Housing Federal Housing Commissioner. (1993). *HUD Building Product Standards and Certification Program for Carpet*. Tech. no. 44d. N.p.: Department of Housing and Urban Development, 1993. Print.

- ASTM C 618 Specification for Coal Fly Ash and Raw or Calcined Natural Pozzolan for Use as a Mineral Admixture in Portland Cement Concrete

- ASTM D422 - 63(2007) Standard Test Method for Particle-Size Analysis of Soils. American Society for Testing and Materials, Annual Book of ASTM Standards. Vol. 04.08.

- ASTM D854 - 10 Standard Test Methods for Specific Gravity of Soil Solids by Water Pycnometer. American Society for Testing and Materials, Annual Book of ASTM Standards. Vol. 04.08.

- ASTM D2216 - 10 Standard Test Methods for Laboratory Determination of Water (Moisture) Content of Soil and Rock by Mass. American Society for Testing and Materials, Annual Book of ASTM Standards. Vol. 04.08.

- ASTM D3999 - 11 Standard Test Methods for the Determination of the Modulus and Damping Properties of Soils Using the Cyclic Triaxial Apparatus. American Society for Testing and Materials, Annual Book of ASTM Standards. Vol. 04.08.

- ASTM D5311 - 11 Standard Test Method for Load Controlled Cyclic Triaxial Strength of Soil. American Society for Testing and Materials, Annual Book of ASTM Standards. Vol. 04.08.

- Boominathan, A., & Hari, S. (2002). Liquefaction strength of fly ash reinforced with randomly distributed fibers. *Soil Dynamics and Earthquake Engineering,* 1027-1033.

- Bray, J. D., Sancio, R. B., Riemer, M. F., and Durgunoglu, T. (2004). "Liquefaction susceptibility of fine-grained soils." Proc., 11th Int. Conf. on Soil Dynamics and Earthquake Engineering and 3rd Int. Conf. on Earthquake Geotechnical Engineering, D. Doolin et al., eds., Stallion Press, Singapore, 655–662.

- Castro, G. and Poulos, S. J. (1977). "Factors affecting liquefaction and cyclic mobility." *Journal of the Geotechnical Engineering Division, Proceedings of the ASCE*, 103(6), 501-516.

- Chen, Y., A. Gottesman, T. Aviad, and Y. Inbar. (1991). "The Use of Bottom-Ash Coal-Cinder Amended with Compost as a Container Medium in Horticulture," Acta Horticulturae 294: 173-I 8 1, 1991.

- Choudary, A., Jha, J., & Gill, K. (2011). *Shear strength characteristics of fiber reinforced fly ash*.

- Cunningham, J. A., Lukas, R. G., and Andreson, T. C. (1977). "Improvement of Fly Ash and Stage—A Case Study," *Proceedings, Conference on Geotechnical Practice for Disposal of Solid Waste Materials*, American Society of Civil Engineers, Ann Arbor, MI, 1977, pp. 227–245.

- Darendeli, M. (2001). "Development of a new family of normalized modulus reduction and material damping curves." *Ph.D. Thesis*, Dept. of Civil Eng., Univ. of Texas, Austin.

- Department of Ecology state of Washington "Waste Tires." Washington State Department of Ecology, 04 Apr. 2010. Retrieved from http://www.ecy.wa.gov/programs/swfa/tires/.

- Dey, Ashim, & Gandhi, S.R. (2008). Evaluation of liquefaction potential of pond ash. *Geotechnical Engineering for Disaster Mitigation and Rehabilitation,* Science Press Beijing and Springer-Verlag GmbH Berlin Heidelberg

- Engstrom, G. and R. Lamb. (2003). Using shredded waste tires as a lightweight fill material for road subgrades: a summary report. Minnesota Department of Transportation, Physical Research & Geotechnical Engineering Sections, Materials Research & Engineering. RMA. 2004b. U.S. scrap tire markets: 2003 edition. Rubber Manufacturers Association, Washington, DC.

- Environmental Integrity Project. (2013). *TVA's Toxic Legacy: Groundwater Contaminated by Tennessee Valley Authority Coal Ash*.

- Environmental Protection Agency (EPA). (2009). Fact Sheet: Coal Combustion Residues (CCR) - Surface Impoundments with High Hazard Potential Ratings, June 2009

- Federal Highway Administration (FHWA). (1999). "Fly ash facts for Highway Engineers." 3rd. 1. Washington, D.C.

- Gandhi, S., Dey, A., & Selvam, S. (1999). Densification of Pond Ash by Blasting. *Journal of Geotechnical and Geoenvironmental Engineering, 125*(10), 889-889. Retrieved September 8, 2014.

- Gandhi, S. R., Raju, V.S., and Vinal Kumar. (1997). "Densification of deposited ash slurry." Proc., 13th Int. Conf. on solid waste technol. And Mgmt., Vol. 1, 4C, 1-8.

- Garlisch, Nick. (2010). "Coal ash disposal" Retrieved from http://www.kentlaw.edu/faculty/fbosselman/classes/energyF10/Nick%20Garlisch.ppt

- Ghosh, A., & Subbarao, C. (1998). Hydraulic Conductivity and Leachate Characteristics of Stabilized Fly Ash. *JOURNAL OF ENVIRONMENTAL ENGINEERING,* 812-812.

- Gottlieb, B., Gilbert, S., & Evans, L. (2010). *Coal Ash the Toxic Threat to Our Health and Environment*. . Retrieved from http://www.psr.org/assets/pdfs/coal-ash.pdf

- Gray, D.H. and Lin, Y.K., (1972). Engineering properties of compacted fly ash. Journal of Soil Mechanics and Foundation Engineering, *ASCE, 98 (4),* 361–380.

- Guoxi, Zeng, Yaozhang, Gu, Jianping, Wu. (1985). Dynamic shear modulus of fly ash. Chinese Jounal of Geotechnical Engineering;1985-05

- Hardin, B. O. & Drnevich, V. P. (1972). "Shear modulus and damping in soils: Design equations and curves." *Journal of Soil Mechanics and Foundations Division, ASCE*. 98(7): 667-692.

- Health Canada. (1979). *Guidelines for Canadian Drinking Water Quality - Hardness.* Ottawa, Canada: Health Canada.

- Illinois Environmental Protection Agency (Illinois EPA). (2016). Used Tire Facts and Information. Retrieved June 20, 2016, from http://www.epa.illinois.gov/topics/waste-management/waste-disposal/used-res/facts/index

- Ishibashi, I. & Zhang, X. (1993) "Unified dynamic shear moduli and damping ratios of sand and clay". Soils and Foundations 33(1): 182-191.

- Kalinski, M. E., and Hippley, B. T., (2005). "The Effect of Water Content and Cement Content on the Strength of Portland Cement-Stabilized Compacted Fly Ash," Fuel, Elsevier, Vol. 84, No. 14-15, pp. 1812-1819.

- Kalinski, M. (2011). *Soil mechanics: Lab manual: 2nd edition* (Revised/Expanded ed.). Hoboken, NJ: Wiley.

- Kaniraj, Shenbaga, and V Gayathri. "Geotechnical behavior of fly ash mixed with randomly oriented fiber inclusions." *Geotechnical behavior of fly ash mixed with randomly oriented fiber inclusions* 21.3 (2003): 123-149. Web. 27 Aug 2010. <http://www.sciencedirect.com/science?_ob=ArticleURL&_udi=B6V3D-840TMK-1&_user=16764&_coverDate=06%2F30%2F2003&_rdoc=1&_fmt=high&_orig=search&_sort=d&_docanchor=&view=c&_searchStrId=1213993607&_rerunOrigin=google&_acct=C000001898&_version=1&_urlVersion=0&_userid=16764&md5=ccd25cd0a9630c4977009ce01072eff5>.

- Kennedy, Chloe. "TVA ash pond breach: Resident says area has 'changed forever'." *knoxvillebiz.com*. 23 Dec 2008. Knoxville Daily News, Web. <http://www.knoxnews.com/news/2008/dec/23/tva-ash-pond-breach-resident-says-area-has-changed/>, 14 Jun (2009).

- Kentucky Energy and Environmental Cabinet. (2012). *Kentucky Coal Facts - 12th Edition*.

- Kentucky transportation cabinet. (2015). 2015 Kentucky statewide rail plan, April 2015

- Kulkarni, S. (2003). Effect of filler-fiber interactions on compressive strength of fly ash and short-fiber epoxy composites. *Journal of Applied Polymer Science, 87*, 836-841.

- Kumar, Praveen, Mehndiratta, H C, Chandranarayana, S, & Singh, S P. (2006). Effect of randomly distributed fibers on flyash embankments. Vol. *86*, November 2005.

- Kumar, P., & Singh, S. (2010). Fiber-Reinforced Fly Ash Subbases in Rural Roads. *Journal of Transportation Engineering, 134*(4), 171-180.

- Lave L, Conway-Schempf N, Harvey J, Hart D, Bzee T and MacCracken C (1998). Recycling postconsumer nylon carpet: a case study of the economics and engineering issues associated with recycling post-consumer goods. J Ind Ecol 2: 117-126.

- Leather, T. (2010). Seas of Rubber: The Truth About Tire Recycling. Retrieved August 25, 2016, from http://recyclenation.com/2010/06/sea-rubber-truth-tire-recycling

- Lee, K. L. and Seed, H. B. (1967). "Cyclic stress conditions causing liquefaction of sand." *Journal of the Soil Mechanics and Foundations Division, Proceedings of the ASCE*, 93(1), pp. 47-70.

- Lemly, A. (2001). Symptoms and implications of selenium toxicity in fish: The Belews Lake case example. *Aquatic Toxicology,* 39-49.

- Leonards GA, Bailey B. (1982). Pulverized coal ash as structural fill. J Geotech Eng 108(GT4):517–531

- Marcuson,W. F., III. (1978). ''Definition of terms related to liquefaction.'' *J. Geotech. Engrg. Div.*, ASCE, 104(9), 1197–1200.

- Mohan, K.S.R., P. Jayabalan and A. Rajaraman, (2012). Properties of fly ash based coconut fiber composite. Am. J. Eng. Applied Sci., 5: 29-34.

- Nuttli, Otto W. (1974). *Earthquake Information Bulletin*. Volume 6.Number 2 (March-April 1974)

- Office of Research, Development, and Technology, Office of Safety, RDT. (2012). *User Guidelines for Waste and Byproduct Materials in Pavement Construction*. Publication. no. FHWA-RD-97-148, U.S. Department of Transportation Federal Highway Administration..

- Puppala, A., Hoyos, L., Viyanant, C., & Musenda, C. (2001). Fiber and Fly Ash Stabilization Methods to Treat Soft Expansive Soils. *Soft Ground Technology*, *112*, Pg. 136-145.

- Recycle Material Resource Center (RMRC). (2012). *Coal Bottom Ash/Boiler Slag - Material Description*. Retrieved from http://rmrc.wisc.edu/ug-mat-coal-bottom-ashboiler-slag/

- Right, R.J., Kemper, W.D., Millner, P.D., Power, J.F., Krocak, R.F., (1998). Agricultural uses of municipal, animal and industrial byproducts. USDA-ARS, Conversation Research Report. No. 44

- Rubber manufacturers association (RMA). (2004). U.S. Scrap tire markets 2003 edition. Retrieved from https://rma.org/sites/default/files/US_STMarkets2003-final.pdf

- Seed, H. B., and Idriss, I. M., (1971), Simplified Procedure for Evaluating Soil Liquefaction Potential, *Journal of the Soil Mechanics and Foundations Division, Proceedings of the ASCE*, Vol. 97, No. SM9, pp. 1249-1273.

- Seed, H. B., and Idriss, I. M. (1982). ''Ground motions and soil liquefaction during earthquakes.'' Earthquake Engineering Research Institute Monograph, Oakland, Calif.

- Seed, R. B., and Harder, L. F., (1990), SPT-Based Analysis of Cyclic Pore Pressure Generation and Undrained Residual Strength,. *Proceedings of the H. Bolton Seed Memorial Symposium*, University of California, Berkeley, Vol. 2, pp. 351-376.

- Seed et al. (2003). Seed, R B., Cetin, K.O., Moss, R.E.S., Kammerer, A., Wu, J., Pestana, J., Riemer, M., Sancio, R.B., Bray, J.D., Kayen, R.E., & Faris, A. 2003. Recent advances in soil liquefaction engineering: a unified and consistent framework. Keynote presentation, 26th Annual ASCE Los Angeles Geotechnical Spring Seminar, Long Beach, CA.

- Siuru, William D., (1993), Waste/energy: Turning tires and oil into alternative fuel, Retrieved from http://waste360.com/mag/waste_wasteenergy_turning_tires

- Southern Alliance for Clean Energy. (2013). *Coal Ash Storage Methods*. Retrieved from http://www.southeastcoalash.org/?page_id=78

- South Central Iowa Solid Waste Agency (SCISWA). (2016). Retrieved June 20, 2016, from http://www.sciswa.org/services/recycling/specialitem/tires.html

- Tsuchida, H., (1970). "Prediction and Countermeasure Against the Liquefaction in Sand Deposits," Abstract of the Seminar in the Port and Harbor Research Institute (in Japanese).

- U.S. Environmental Protection Agency (U.S. EPA). (1988). Wastes from the combustion of coal by electric utility power plants. USEPA Washington, DC. EPA/530-SW-88-002

- U.S. Environmental Protection Agency (U.S. EPA). (2010). Identifying Greener Carpet. Retrieved June 20, 2016, from https://www.epa.gov/greenerproducts/identifying-greener-carpet

- U.S. Environmental Protection Agency (U.S. EPA), (2016). Frequent Questions about Applicability of Other Regulations and Implementing the Final Rule Regulating the Disposal of Coal Combustion Residuals (CCR). (2016, June 7). Retrieved August 25, 2016, from https://www.epa.gov/coalash/frequent-questions-about-applicability-other-regulations-and-implementing-final-rule

- Viswanathan, R., Saylak, D., & Estakhri, C. (1997). Stabilization of Subgrade Soils Using Fly Ash

- Vucetic, M. and Dobry, R. (1991). "Effect of Soil Plasticity on Cyclic Response." *Journal of Geotechnical Engineering*, 117(1), 89–107.

- Wang W. (1979). "Some findings in soil liquefaction." *Water Conservancy and Hydroelectric Power Scientific Research Institute*, Beijing, China.

- Watson, T. (2006). The benefits of green carpeting, in any color. *The Seattle Times*.

- World health organization (WHO), (1984). Guidelines for Drinking-water Quality, volume 1 & 2.

- Yang, S., Lohnes, R. A., and Kjartanson, B. H., (2002). "Mechanical Properties of Shredded Tires," *Geotechnical Testing Journal,* GTJODJ, Vol. 25, No. 1, March 2002, pp. 44–52.

- Youd, T. L., Idriss, I. M., Andrus, R. D., Arango, I., Castro, G., Christian, J. T., Dobry, R., Finn, W. D. L., Harder, L. F., Hynes, M. E., Ishihara, K., Koester, J. P., Liao, S. C., Marcuson, W. F., Martin, G. R., Mitchell, J. K., Moriwaki, Y., Power, M. S., Robertson, P. K., Seed, R. B., and Stokoe, K. H., (2001), Liquefaction Resistance of Soils: Summary Report from the 1996 NCEER and 1998 NCEER/NSF Workshops on Evaluation of Liquefaction Resistance of Soils, *Journal of Geotechnical and Geoenvironmental Engineering*, American Society of Civil Engineers, Vol. 127, No. 10, pp. 817-833.

- Zand, B., Tu, W., Amaya, P., Wolfe, W., & Butalia, T. (2008). An experimental investigation on liquafaction potential and post-liquefaction shear strength of impounded flya ash. *FUEL, 88*, 1160-1166.

- Zand, Behrad, Wei Tu, Pedro J. Amaya, William E. Wolfe, and Tarunjit Butalia. (2007). "Evaluation of liquefaction potential of impounded fly ash." <u>World of Coal Ash</u>.

- Zhen, G.X., Gu, R.Z. and Wu, J.P. (1985). "Dynamic Shear Moduli of Flyashes", Chinese Journal of Geotechnical Engineering, Vol. 7, No. 5.

VITA

Alfred Jonathan Susilo was born in Jakarta, Indonesia. He graduated from Tarumanagara University, Jakarta, Indonesia in 2005 with Bachelor Degree in Civil Engineering. During his senior year, he worked as an assistant for surveying laboratory. After working as a full-time engineer for Consulting Engineering Company in Indonesia for Two (2) Years, he continued his study at McNeese State University (University of Louisiana System) in Lake Charles, LA from 2007 to 2009, and also worked as Graduate Assistant for Surveying and Soil Mechanics laboratories. The following year after earned his Master Degree in Civil Engineering, he continued his study at University of Kentucky, Lexington, KY and during his research he also employed as an instructor for the Undergraduate Soil Mechanics Laboratory

July 21, 2016